Jagiellonian University in Kraków
Faculty of Biochemistry, Biophysics and Biotechnology
Department of Medical Biotechnology

DOCTORAL THESIS

The novel mechanisms of the regulation of the endothelial cell functions and aortic pathology – focus on NRF2/KEAP1 axis and microRNA-34a

Aleksandra Kopacz

Supervisor: Anna Grochot-Przęczek, PhD, DSc

Kraków, 2022

Part of the results included in this doctoral thesis have already been published in:

Kopacz A, Werner E, Grochot-Przeczek A, Klóska D, Hajduk K, Neumayer C, Jozkowicz A, Piechota-Polanczyk A. *Simvastatin attenuates abdominal aortic aneurysm formation favoured by lack of Nrf2 transcriptional activity.* Oxidative Medicine & Cellular Longevity 2020.

Kopacz A, Klóska D, Cysewski D, Proniewski B, Personnic N, Piechota-Polanczyk A, Kaczara P, Zakrzewska A, Forman HJ, Dulak J, Jozkowicz A, Grochot-Przeczek A. *Keap1 controls protein S-nitrosylation and apoptosis-senescence switch in endothelial cells*. Redox Biology 2020.

The PhD student was supported by the scholarship obtained in the frame of the 20th edition of the Polish Edition of L'Oréal UNESCO For Women in Science Program and the 30th edition of START scholarship from the Foundation of Polish Science.

The PhD student was awarded Boehringer Ingelheim Travel Award to attend the EMBO Course "FISHing for RNAs: from classical to single-molecule approaches", which allowed the acquaintance with *in situ* hybridization techniques used in this thesis.

Acknowledgements

PhD is not only writing the thesis. For me, it was a few-year process which completely changed me and helped me to find my way in research. Therefore, this thesis is simply a small part of my scientific journey. Throughout 5 years of PhD studies, I got involved in many projects in several domains, which helped me to identify my main research interests, which I aim to continue during postdoctoral position. As I was given a lot of independence, I am not afraid to start a new part of my scientific odyssey. Throughout PhD studies, I had many difficult moments and many doubts. If there were not for some people, I am not sure I would succeed. Therefore, here I would like to thank all the people who helped me throughout this time and shaped who I am now.

My thesis supervisor, Anna Grochot-Przęczek, PhD, DSc

For accepting me as executor of her projects;
For constructive conversations and useful comments;
For trust and freedom to do the research, which impacted my scientific development.

Aleksandra Piechota-Polańczyk, PhD, DSc

For growing in me interest about aneurysms, teaching me methods
and supporting me in research and privately.

Prof. Alicja Józkowicz, PhD, DSc

For accepting me 10 years ago as her tutee and letting me join the lab from the very beginning, which helped me to grow my passion for science;
For constructive conversations and useful comments.

Prof. Józef Dulak, PhD, DSc

For accepting me as part of his team and valuable comments on my research.

Damian Klóska, PhD

For being with me on every step, for the support, for the help with the experiments, for the inspiration, for hours of conversation, and simply everything.

Izabela Kraszewska, MSc *(almost PhD)*

For the hours of conversations, for letting me speak my mind when I needed to, for making sure I am fine in all aspects, and everything else.

Nicolas Personnic, MSc, MD

For making me see another perspective in science, and our discussions, which were an immense inspiration;
For seeing in me a good researcher which helped me to go forward;
For trying to negate all my ideas to make them better.

Agnieszka Andrychowicz-Róg, MSc; Joanna Uchto-Bajołek, MBa

For an inestimable help with all the administrative struggles.

Marta Targosz Korecka, PhD, DSc;

For showing me the vast potential of physical approaches, very good advice in different fields, and successful collaboration in many projects.

Anna Bar, PhD; Prof. Stefan Chłopicki, PhD, DSc;
Kamil Awsiuk, PhD, DSc; Dominik Cysewski, PhD

For successful collaborations.

All members of the FBBB Animal Facility

For the help with the animal studies, and a friendly atmosphere.

My friends

For the understanding and being there for me when I needed.

My family

For the support, for making sure I can fully devote myself to science and for tolerance to my constant need for looking up the answers to scientific questions during rest days.

Therefore, I dedicate this thesis to my family, I hope to show them part of me, the way I think and I hope they will understand why science is fascinating.

It is through science that we prove,
but through intuition that we discover

Summary

The arterial system distributes blood throughout the body through a remarkable network characterised by vessel branching and bifurcation. Fluid dynamic patterns at these sites of flow division can be highly intricate compared to the flow in unbranching vessel segments. Arterial biomechanics governs cardiovascular fate and structure due to a reciprocal relationship between mechanical forces and cardiovascular remodelling. Besides, an abnormal mechanical strain with concomitant structural vulnerability conduces the permanent dilatation of the abdominal aorta - an abdominal aortic aneurysm (AAA). The occurrence of an aneurysm is associated with its expansion which may cause aortic wall rupture, leading to death in more than 80% of cases. The aetiology of AAA, although still not fully understood, is an orchestrated series of events that often start from small micro ruptures and end in the aortic wall bulging and rearrangements.

The research of the last decades overlooked the role of endothelial cells (ECs), which line all the blood vessels, in AAA development. Significantly, their role surpasses the sole establishment of a structural barrier between blood and surrounding tissues. It is a versatile and involute organ that keeps a tight rein on the proper functioning of the cardiovascular system. At the same time, ECs are very vulnerable, and exposure to adverse signals may trigger their premature ageing and dysfunction. It subsequently precipitates the impairment of the function of blood vessels and an increased risk of cardiovascular diseases. However, the endothelium involvement in the aetiology of AAA is vague. If postulated, it is mainly ascribed to the maintenance of healthy functional traits of ECs. They maintain a selectively permeable, anti-thrombogenic barrier, determine leukocyte migration to inflamed tissues, and secrete various paracrine factors to regulate vascular tone. All of them could play a significant role in AAA.

This research aimed to define the mechanisms underlying the development of AAA, focusing on endothelial cell function and ageing. The preliminary research and literature data indicate that the central modulator of the cellular response to stress - NRF2 and microRNA-34a, are crucial regulators of ageing, EC biology and aortic function. Thus, we hypothesised that they might have a decisive influence on the physiology of blood vessels and AAA development. In this thesis, we aimed to address the significance of age-related phenotypic, structural and functional features of the ECs and the aorta in the aetiology of AAA.

NRF2 transcriptional deficiency in mice leads to premature ageing of the aorta and predisposes to AAA compared to wild-type animals. Aneurysms that are formed in both genotypes share similar features: increased immune cell infiltration, robust aortic wall rearrangement and increased oxidation. In light of the importance of NRF2 transcriptional activity in harnessing oxidative stress, we propose it may be the susceptibility factor, rendering mice prone to AAA. Furthermore, in the quest to delineate the age-associated structural predilection factors to AAA, we observed that the structural stiffness depicted by atomic force microscopy could be significant. Moreover, we found a potential role of scanning electron microscopy-illustrated intimal aortic structural changes. They strongly correlate with the AAA incidence and may be caused by excessive vascularisation of the aorta and surrounding adipose tissue.

We efficiently rescued EC NRF2-dependent premature ageing and AAA formation in NRF2 transcriptional knockout mice using the EC-specific knockout of miRNA-34a, which implies the significance of intimal layer senescence in the susceptibility to AAA. Therefore, endothelial cells can be imperative regulators of AAA formation. However, contrary to previously postulated mechanisms, the maintenance of specialised functions of ECs is not the primary determinant of aneurysm formation. We propose instead that EC proliferation protects against AAA and can confer aneurysm stability.

To sum up, we conclude that EC ability to proliferate and tighten the arterial wall can be the primary determinant of the onset of AAA. Therefore, contrary to current opinions, the age-dependent proneness to AAA does not rely on the functional endothelium features but could instead stem from the cessation of EC proliferation.

Streszczenie w języku polskim

Krew rozprowadzona jest po całym ciele przez silnie rozgałęzioną sieć tętnic. Utrzymanie stałego dopływu krwi do tkanek wymaga od naczyń niemal natychmiastowej odpowiedzi na zmieniający się przepływ. Istnieje wzajemna zależność między siłami mechanicznymi a przebudową naczyń, zatem biomechanika tętnic może regulować los i strukturę układu sercowo-naczyniowego. Pojawienie się nieprawidłowego obciążenia mechanicznego w miejscach wrażliwych strukturalnie, może prowadzić do trwałego poszerzenia aorty brzusznej – tętniaka aorty brzusznej (TAB). Jego uformowanie i wzrost obarczone jest dużym ryzykiem pęknięcia, co najczęściej prowadzi do zgonu. Niestety, molekularne i komórkowe mechanizmy tej choroby są wciąż słabo poznane. Wiadomo, że w początkowych etapach dochodzi do mikropęknięć, które później prowadzą do znacznego wybrzuszenia i zmiany struktury aorty.

Dotychczasowe badania nad mechanizmami TAB niemal zupełnie pominęły znaczenie komórek śródbłonka. Komórki te wyścielają wszystkie naczynia krwionośne, jednak ich rola wykracza poza samo ustanowienie bariery strukturalnej między krwią a otaczającymi tkankami. Jest to wszechstronny narząd, który umożliwia prawidłowe funkcjonowanie układu krążenia. Niestety, szczególna lokalizacja na styku krwi i narządów sprawia, że komórki śródbłonka są silnie narażone na czynniki stresowe, które mogą prowadzić do ich przedwczesnego starzenia i utraty specjalistycznych funkcji. W efekcie dochodzi do zaburzenia funkcji naczyń krwionośnych i zwiększonego ryzyka wystąpienia chorób układu krążenia. Przypuszczalnie, rola komórek śródbłonka w mechanizmie powstawania TAB może być silnie związana z utrzymaniem ich zdrowego, w pełni funkcjonalnego, fenotypu. Stanowią one selektywnie przepuszczalną barierą przeciwzakrzepową, determinują migrację leukocytów do tkanek objętych stanem zapalnym i parakrynnie regulują napięcie naczyniowe. Każdy z tych procesów może mieć istotne znaczenie w TAB.

Badania prowadzone w ramach pracy doktorskiej mają na celu zrozumienie mechanizmów powstawania TAB, ze szczególnym uwzględnieniem funkcji i starzenia się komórek śródbłonka. Nasze wstępne badania oraz dane literaturowe wskazują, że główny regulator odpowiedzi komórek na stres - NRF2 oraz mikroRNA-34a są istotnymi modulatorami starzenia, biologii komórek śródbłonka oraz funkcji aorty. Stąd, podejrzewamy, że śródbłonek może mieć kluczowy wpływ na fizjologię naczyń krwionośnych i powstawanie TAB. Szczegółowym celem pracy jest określenie znaczenia

związanych z wiekiem fenotypowych, strukturalnych i funkcjonalnych cech komórek śródbłonka oraz aorty w etiologii TAB.

Niedobór aktywności transkrypcyjnej NRF2 u myszy prowadzi do przedwczesnego starzenia się aorty oraz predysponuje do TAB w porównaniu do myszy typu dzikiego. Utworzone tętniaki u obu genotypów myszy mają wspólne cechy charakterystyczne: nasilony naciek komórek odpornościowych, silne zmiany struktury ściany aorty i środowisko utleniające. W świetle kluczowego znaczenia aktywności transkrypcyjnej NRF2 w odpowiedzi na stres oksydacyjny, podejrzewamy, że jest to znaczący czynnik odpowiadający za podatność myszy na TAB. Co więcej, poszukiwania istotnych, związanych z wiekiem, strukturalnych czynników predysponujących do TAB, wykazały, że sztywność strukturalna obrazowana mikroskopią sił atomowych może być jednym z nich. Ponadto za pomocą mikroskopii elektronowej zaobserwowaliśmy istotne anomalie strukturalne w obrębie warstwy wewnętrznej aorty. Zmiany te silnie korelują z częstością występowania TAB i mogą być spowodowane nadmiernym unaczynieniem aorty oraz otaczającej tkanki tłuszczowej.

W dalszych badaniach, przy użyciu śródbłonkowo-specyficznego nokautu miRNA-34a, skutecznie odwróciliśmy przedwczesne starzenie się komórek śródbłonka oraz wrażliwość na TAB u myszy z nokautem transkrypcyjnym NRF2. Wskazuje to na kluczowe znaczenie starzenia warstwy wewnętrznej aorty w podatności na TAB, a komórki śródbłonka mogą być niezbędnymi regulatorami tej choroby. Jednak w przeciwieństwie do wcześniej postulowanych mechanizmów, utrzymanie wyspecjalizowanych funkcji komórek śródbłonka nie jest głównym wyznacznikiem powstawania tętniaka. Proponujemy, że to nasilona proliferacja komórek śródbłonka chroni przez TAB, a w przypadku jego utworzenia, może go stabilizować.

Podsumowując, uważamy, że zdolność komórek śródbłonka do proliferacji i uszczelnienia ściany aorty może być głównym czynnikiem chroniącym przed TAB. Ponadto, wbrew obecnemu stanowi wiedzy, zależna od wieku skłonność do występowania TAB nie opiera się na funkcjonalnych cechach śródbłonka, ale zamiast tego wynika z charakterystycznego dla starzenia, nieodwracalnego ustania podziałów komórek śródbłonka.

Table of contents

List of abbreviations

αSMA – alpha smooth muscle actin

AF – Alexa Fluor

AFM – atomic force microscopy

AGE – advanced glycation end products

Ang II – angiotensin II

ApoE – apolipoprotein E

BSA – bovine serum albumin

CA – carotid artery

CBP – cyclic adenosine monophosphate response element binding protein

CD31/PECAM-1 – cluster of differentiation 31/platelet endothelial cell adhesion molecule 1

CD41/ITGA2B – cluster of differentiation 41/integrin alpha-2b

CD45/PTPRC – cluster of differentiation 45/protein tyrosine phosphatase, receptor type C

CD64/FCGR1 – cluster of differentiation 64/F_c fragment of IgG, high affinity I receptor

CD144 – cluster of differentiation 144, cadherin 5, vascular-endothelial cadherin

CHD6 – chromodomain 6

CT – computed tomography

CV – cardiovascular

CVD – cardiovascular disease

CVS – cardiovascular system

DAPI – 4′,6-diamidino-2-phenylindole

EBM-2 – endothelial basal medium-2

EC – endothelial cell

EDTA – ethylenediaminetetraacetic acid

ECM – extracellular matrix

eGCX – endothelial glycocalyx

EGM-2MV – endothelial growth medium – 2 microvascular

eNOS – endothelial nitric oxide synthase

ERK – extracellular signal-regulated kinase

FAP – fibroblast activation protein

GAPDH - glyceraldehyde 3-phosphate dehydrogenase

GCLM – glutamate-cysteine ligase modifier

GCX – glycocalyx

GS – goat serum

HAEC – human aortic endothelial cells

HEPES - 4-(2-hydroxyethyl)-1-piperazineethanesulfonic acid

IF – immunofluorescence

IHC – immunohistochemistry

ILT – intraluminal thrombus

ISH – *in situ* hybridisation

ISZ – *in situ* zymography

LNA – locked nucleic acid

KO – knockout

MFS – Marfan syndrome

miRNA-34a^{EC-KO} – endothelial-specific knockout of miRNA-34a

miRNA/miR – microRNA

MLSP – mean lifespan

MMP2 – matrix metallopeptidase 2

MMP3 – matrix metallopeptidase 3

MMP9 – matrix metallopeptidase 9

MRI – magnetic resonance imaging

NO – nitric oxide

NOS – nitric oxide synthase

NQO1 – NAD(P)H quinone dehydrogenase 1

OCT – optimal cutting temperature medium

PDGF – platelet-derived growth factor

PDGFRA – platelet-derived growth factor receptor alpha

PDGFRB – platelet-derived growth factor receptor beta

PFA – paraformaldehyde

PVAT – perivascular adipose tissue

PWV – pulse wave velocity

RAGE – receptor for advanced glycation end products

RAS – renin-angiotensin system

RISC - RNA-induced silencing complex

ROS – reactive oxygen species

RXRα – retinoid X receptor alpha

SA-β-gal – senescence-associated beta-galactosidase

SASP – senescence-associated secretory phenotype

SBP – systolic blood pressure

SELE – E-selectin

SEM – scanning electron microscopy

SMC – smooth muscle cell

SSC – saline-sodium citrate (buffer)

TA – transcriptional activity

TBS(T) – tris-buffered saline (with Tween)

TFA – trifluoroacetic acid

TIMP – tissue inhibitor of metalloproteinases

TGFβ – transforming growth factor beta

tKO – transcriptional knockout

TNFα – tumour necrosis factor alpha

TrCP – beta-transducin-repeat-containing protein

US – ultrasound

VCAM1 – vascular cell adhesion molecule 1

VSMC – vascular smooth muscle cell

vWF – von Willebrand factor

WBC – white blood cell

WGA – wheat germ agglutinin

WSS – wall shear stress

WT – wild-type

Introduction

Biomechanical forces governing the arterial system

Following historical descriptions of Harvey and Malpighi, the vascular system is a pump mounted in series on vessels, assimilated to simple pipes. Its primary function is to conduct nutrients and oxygen to the peripheral tissues[1]. Unequivocally correct, yet comprehending the physical mechanisms governing blood movement in a compact and precise network of vessels is a scientific puzzle. This pertinent subject is also troublesome due to the complexity of the factors involved. To shine some light on this matter, we should first consider blood rheology, a complex fluid, as it is a suspension of somewhat deformable particles. We should remember that blood is subjected to divergent flow as it passes through the body, ranging from pulsatile and turbulent in arteries to continuous in smaller vessels. The size of vessels affects another crucial factor, the haematocrit. Finally, the model must include the geometry of the bifurcations and the wall elasticity. While large veins have flexible walls, capillaries are rigid and confine red blood cells in a small area, pushing them to deform[2]. These complex variables (vessel diameter, flow, velocity, viscosity, and haematocrit) should be taken into consideration when addressing two major cardiovascular (CV) fate-determining factors: wall shear stress (WSS) and circumferential strain (wall strain)[3].

Age-related cardiovascular diseases are associated with alterations in the vascular wall architecture and its physiological consequences, which are further manifested by the changes in the mechanical strength of the wall of blood vessels. The nanomechanical properties of large vessels, such as the aorta, are determined by the specific structure of their wall[4]. It consists of three distinct layers (Fig. I1). The interior elastic membrane supports the single layer of endothelial cells that compose the tunica intima (inner tunic). The *tunica media* (the middle tunic) takes in layers of elastic fibres and smooth muscle cells (SMCs). Finally, the *tunica adventitia* (external tunic) is mainly composed of collagen and contains the *vasa vasorum* (a network of microvasculature that supplies nutrients to the medial layer)[5].

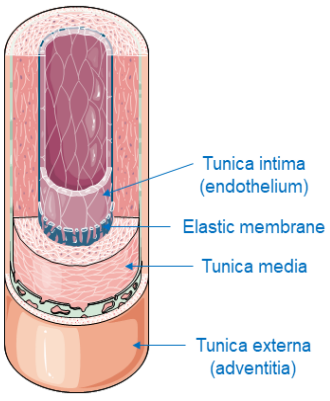

Figure I1. A scheme depicting structure of the aorta. Image was taken from Servier Medical ART images.

The vasculature's structure is flexible. The main arteries and veins have designated locations, but all blood vessels undergo considerable restructuring during development in response to evolving functional health demands and disease consequences. Genetic information could barely ensure the structural properties of the vast majority of vessel segments individually. Instead, the vasculature architecture must evolve due to each segment expansion and reshaping in response to environmental changes and stimuli encountered[6]. These are circumferential strain (forces acting on the vessel wall driven by blood pressure and flow) and wall shear stress (generated by blood flow)[7–9] (Fig. I2).

Intraluminal pressure induces forces perpendicular to the vessel wall triggering a stretch in all its parts (circumferential strain, also known as 'wall stretch')[10]. This pressure is the force per unit area exerted perpendicular to the vessel wall and triggers radial forces to widen the vessel wall, resulting in cellular elongation. The vessel wall changes shape in reaction to stretching imparted to it is called "wall strain", and it is a measure of deformation[11,12]. Vascular smooth muscle cells (VSMCs) and ECs are sensitive to wall strain and adapt structurally and functionally[13]. Physiological strains of 5 to 10% promote vascular stability and proper tone together with adjusted proliferation and rearrangements (Fig. I2).

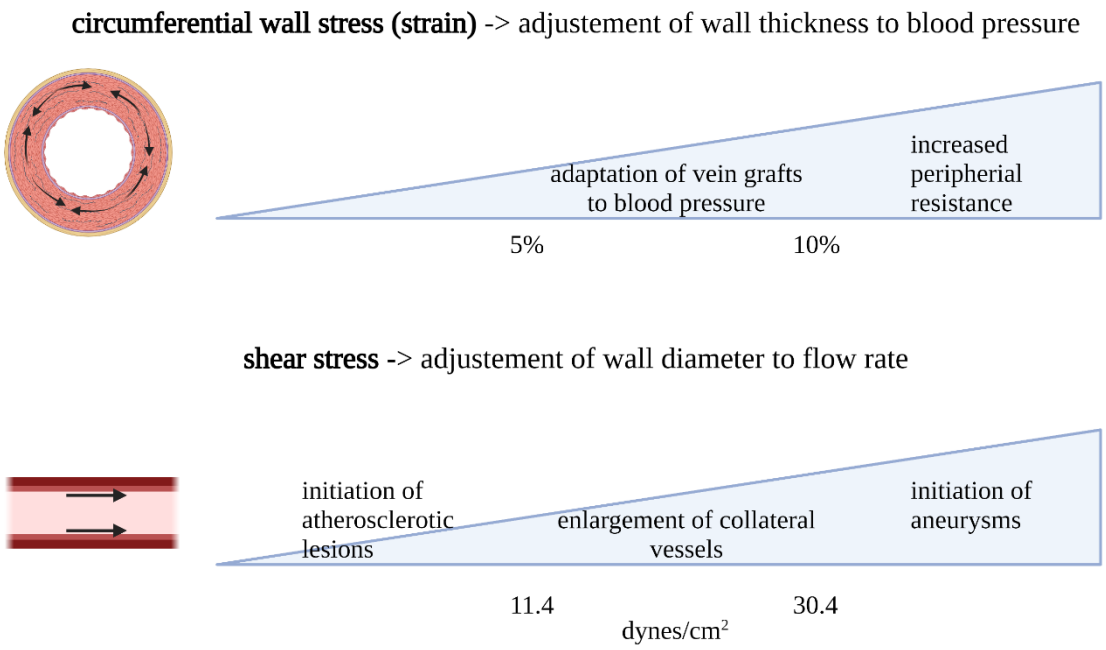

Figure I2. Physiological and pathophysiological adaptations to wall strain and shear stress. Image created with BioRender.com based on[10].

In these settings, wall stretch induces an elongated spindle-shaped VSMC phenotype (contractile phenotype). High magnitude spans of 20% or more are deemed abnormal. Under these circumstances, VSMCs develop a 'synthetic' phenotype characterized by poor contractility, hyperproliferative, promigratory, pro-inflammatory activity, and altered morphology with rhomboid shape and reduced length[10]. As for ECs, the excessive circumferential strain causes the production of vasoconstrictive angiotensin II (Ang II), which promotes their dysfunctional, pro-oxidative, and pro-inflammatory state[14]. Moreover, upon the pathophysiological stretch, they leave their basal low-proliferating state and start to divide[15].

There is shear tension anywhere fluid exists. Fluids operate on the cell surface in biology and vascular systems. Blood flow exerts a frictional force on the surface of the vessel walls, which is referred to as shear stress. This mechanical phenomenon has a prominent influence on tissue function and biological responses, modifying cell shape, proliferation, differentiation, metabolism, communication, and assisting in barrier development[7]. Shear stress is a force parallel to the tissue surface, induced by the shear flow of viscous fluids, and is affected by flow rate, blood viscosity, and tube geometry[10]. Compared to the venous system, the arteries and arterioles have significantly higher shear stress levels (11.4-30.4 dynes/cm^2 and 0.76-7.6 dynes/cm^2 for the arterial and venous systems, respectively)[16]. The vasculature responds to variations in shear stress by altering vascular tone and diameter. This capacity to react is conferred primarily by ECs in the process of mechanotransduction[3]. ECs face varying flow conditions in the vasculature. The intricate bifurcations, branch points, and curved portions of the vascular network considerably impact the shear stress characteristics and become a biochemical stimulus that affects endothelial function. Normal or slightly increased wall shear stress (10-30 dynes/cm^2) protects the endothelium by inhibiting endothelial proliferation, local inflammation and increasing antioxidant capacity[17]. However, lower wall shear stress, as found in some arterial bifurcations, promotes the pro-inflammatory state of the ECs, favouring the leukocyte recruitment to the intima. Lower wall shear stress may also trigger Ang II-driven signalling and oxidative stress[18]. On the other hand, the supra high wall shear stress has an abnormal effect on the EC morphology, cytoskeleton organisation, and on the production of extracellular matrix regulators[19].

The mechanical characteristics of arteries change with age and disease, mainly due to changes in the acellular components

The large arteries efficiently manage the pulsatile blood ejection from the left heart ventricle, delivering significantly less fluctuant, continuous blood flow to the smaller arteries. They also maintain organ perfusion during diastole. The complex characteristics of elastin, collagen, and SMCs maintain these critical mechanical qualities of the large arteries, commonly known as the Windkessel effect[20].

The mechanical properties of the large arteries deteriorate fairly rapidly, leading to arterial stiffness. It is defined as diminished arterial compliance and distensibility, which assesses an artery ability to dilate and contract in response to pressure changes[21]. Paradoxically, in most situations, it is not the artery that takes the brunt of the damage; instead, the unfavourable effects predominantly target the pump (ventricles) and the supply destinations (organs). The loss of arterial compliance triggers an increase in arterial pulse pressure, heightening the impact on the left ventricle. Simultaneously, the impaired conversion of pulsative to continuous flow results in strong flow pulsations being conveyed further until the blood reaches organs[22,23].

Artery stiffness is one of the few biological factors that doubles with age. Age-related cardiovascular diseases mainly occur in large vessels. They are associated with vascular wall architecture and mechanical strength alterations, which impact the (patho)physiological outcomes[4,24]. The blood flows through arteries, which have capacitance and resistance based on their shape, constituent composition, and activity. It is a composite material made up of structural (elastin, collagen) and functional (endothelial and smooth muscle cells) components that affect the load-bearing capacity of the wall[25]. Structurally, water makes up more than 70% of the artery wall, which explains its mean Poisson ratio of 0.5 (so that of an incompressible substance)[26]. However, because of the anisotropy of the vessel wall, Poisson's ratio fluctuates with the axis of stress. Similarly, the artery elastic modulus is nonlinear due to the multi-layered, inhomogeneous wall of these blood vessels[24]. Therefore aorta defies Hooke's law of a completely elastic material. As it is an elastomer, there is a curvilinear connection between the modulus of the artery wall and applied stress, depending on which different extracellular matrix (ECM) proteins are involved in the mechanical response of the aorta (Fig. I3)[27].

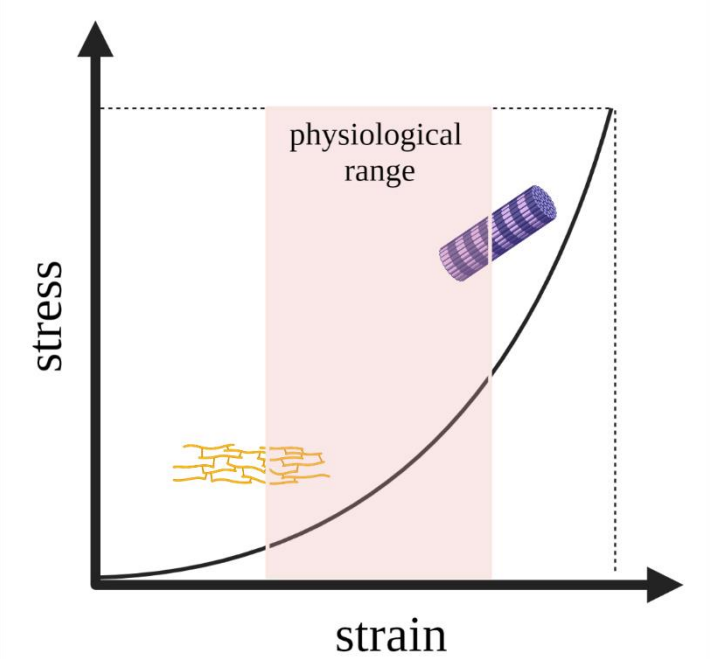

Figure I3. A typical curvilinear stress to strain relation for the arterial wall with stress applied circumferentially. The load is carried by elastin and collagen fibres at low and high strains, respectively. Physiologically both types of fibres are recruited. Image created with BioRender.com.

Out of these proteins, collagen and elastin make up approximately half of the dry weight of the vessel and govern the mechanics[28]. Type I and type III collagens make up 60% of the arterial wall in this group, whereas elastin accounts for 30%[29]. The responsive elastin fibres dominate the mechanics at low degrees of stretch, whereas helically-oriented collagen fibres are engaged at greater levels of deformation[30]. Because collagen fibres are 100-1000 times stiffer than elastin, the incremental elastic modulus increases dramatically at greater degrees of circumferential deformation[31] (Fig. I3).

The relative number, alignment, and slackness of these components dictate the mechanical characteristics of the vascular wall. The aorta is the largest and most malleable artery, thanks to its elastin content and size[32]. Due to the slow turnover of elastic fibres *in vivo* (approx. 70 years[33]), age-related alterations in its continuity, structure, or amino acid chemistry may occur, impacting its functionality[34,35]. Even though the elastin content remains the same with age, it loses the functional load-bearing capacities, which are then transferred to collagen. Consequently, the inhibition of elastin modifications hampers collagen deposition and counteracts blood pressure rise[36]. Elastin fragmentation may also occur due to pulsatile wall stress fatigue[37,38] or hyperactivity of ageing-induced proteases[34]. Moreover, with time, the calcium levels rise in the arterial wall, allowing calcium ions to directly bind to elastin fibres and cause their calcification (elastocalcinosis) and further fragmentation[39].

Substantiating elastin importance, its deletion (elastin knockout) causes uncontrolled SMC proliferation and perinatal mortality in mice due to elevated blood pressure, arteries thickening and stenosis[40]. In comparison, elastin haploinsufficiency promotes the incidence of aortic supravalvular stenosis. Interestingly, unlike the increased blood pressure, the arterial compliance in these animals remains unchanged compared to wild-type counterparts. It is probably due to significant hypertension-related thickening of the wall caused by increased elastic lamellae and the content of disorganized SMCs[41]. Moreover, the treatment with anti-hypertensive captopril impedes the premature death of elastin knockout mice[42].

Unlike elastin, collagen concentration rises with age in all constituents of the arterial wall, affecting the elastin:collagen ratio orchestrating artery mechanics. Collagen is mainly produced by medial SMCs and adventitial fibroblasts[43–45]. However, ageing promotes the acquisition of mesenchymal-like phenotype by ECs. They start to express alpha smooth muscle actin (αSMA) and collagen I, which contributes to arterial stiffening and intimal thickening[46]. Collagen crosslinking *via* non-enzymatic glycation, in conjunction with the increment in collagen concentrations, increases arterial stiffness with age. Glycation is a phenomenon that occurs between reducing sugars and proteins that directly stiffens tissues while also releasing harmful end products (AGE – advanced glycation end products). *In vivo* AGE crosslinking occurs mostly between lysine residues on collagen and the AGE N-carboxy-methyl-lysine[47]. Furthermore, a specific receptor for AGE (RAGE) affects cellular signalling, promoting the pro-oxidative and pro-inflammatory phenotype. It may trigger EC hyperpermeability and diminish the nitric oxide availability[48,49].

The different makeup of each arterial layer allows for layer-specific mechanical qualities that can vary across individuals and depend on the size of the arteries[50]. The media is less compliant than the adventitia during the axial stretch and non-axisymmetric deformation. Under circumferential and longitudinal pressures, the media carries around 60% and 25% of the load, with the rest taken by adventitia[51–53]. Because each layer's mechanical characteristics change, it is vital to remember that each layer's cells are exposed to and perceive the qualities of the layer they dwell in (Fig. I4). As a result, measurements and analysis of each particular layer are critical when addressing cellular level mechanobiology[29].

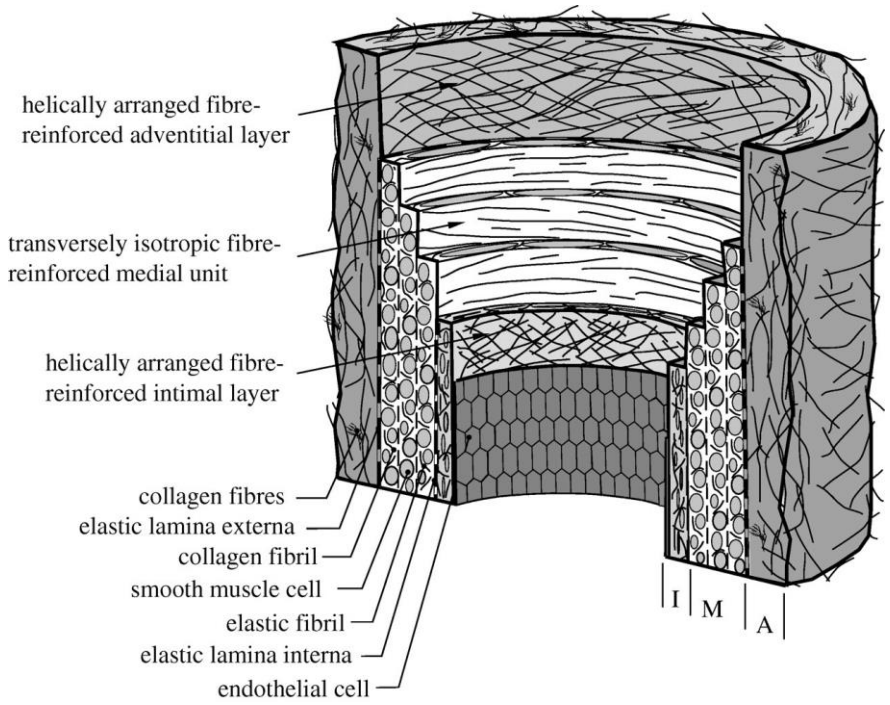

Figure I4. Structural features of an aged aorta with intimal thickening. The aorta is composed of three layers: intima (I), media (M), and adventitia (A). Intima is formed by a single layer of endothelial cells and lies on the elastic lamina interna, which thickens with age due to the accumulation of collagen fibres. Media is formed of smooth muscle cells, an elastic and collagen fibril network, and elastic laminae that divide media into several transversely isotropic fibre-reinforced units. The outermost layer is adventitia, which is bordered by loose connective tissue. Adventitia is mostly composed of thick bundles of collagen fibrils organized in helical patterns (image from[54]).

The intimal layer is the deepest layer of the artery wall. The luminal layer, also known as the basal membrane, is a thin foundation membrane with a proteoglycan-rich matrix and little collagen[54]. The luminal layer has a single layer of ECs that govern vascular homeostasis (described in more detail below). Elastin and collagen fibres bind the EC layer to the internal elastic lamina in the subendothelial layer (second intima layer). In the intima, collagen fibres (mainly collagen IV) are dispersed, whereas intimal elastin forms a three-dimensional network of elastic fibres[54]. The intima gradually thickens with age; in neonates, the intima is relatively thin, and the endothelial lining is tightly attached to the first elastic lamella of the media. ECs lining the aorta lumen become uneven in form as they age. SMCs migrate from the media, causing the intima to thicken. Collagens, proteoglycans, and VSMCs constitute the subendothelial space[55].

The medial layer involves structural and functional arterial units called medial lamellar units, which orchestrate the vascular mechanics[51,56]. They contain around half (47%) of collagen (mainly I and III), and the rest is elastin, and SMCs (29% and 24%, respectively)[28]. Layer-by-layer elastin lamellae are joined by thick elastic fibres sandwiched and reinforced by a dense network of finer elastin fibres and

circumferentially-oriented SMCs. As most of the artery wall is composed of the distinctive medial lamellae, tunica media is recognized as playing a significant role in arterial mechanical behaviour[51]. It is primarily responsible for the elastic rebound that keeps blood pressure stable during diastole, and its unique structure permits withstanding significant circumferential loads. Thus, the number of lamellar units is connected to the artery resistance to strain. The artery walls with increased wall tension have more elastic layers and wider diameter[37,57].

SMCs are active and functional components of arteries, which localize in bundles of approx. 100 μm in diameter[24,58]. They directly impact arterial stiffness as their contraction and relaxation alter lumen diameter. In addition, they affect the loading state of elastin and collagen fibres, indirectly influencing arterial compliance. However, unlike the latter, SMCs contribute to wall viscoelasticity and modulate the artery's damping, viscous properties[24]. Their mechanical characteristics vary significantly with the contractile state. Their Young's modulus ranges from 10 kPa during relaxation to 100 kPa during contraction[59]. The aorta loses medial SMCs in the course of physiological[60] or premature ageing[61]. With age comes a decline in cell proliferation, which reduces the number of cells inside the vascular wall[38,62]. This can be further augmented by excessive inflammation and calcification, which enhance VSMC apoptotic death[60]. Collagen redistributes within the media to unstructured and chaotic bundles near lamellae units and replaces VSMCs in the course of medial fibrosis[63,64]. Glycans can also supersede SMCs in a process called cystic medial necrosis or degeneration, which weakens the aortic wall[65].

The exterior elastic lamina separates the media and adventitia. This is a poorly structured collagen-rich connective tissue that is highly vascularized and innervated. It fuses with the surrounding connective tissue. The adventitia contains a lot of fibroblast-produced collagen type I, offering mechanical support to the vessel and increasing the circumferential load-bearing strength and longitudinal tethering[66]. Adventitia is highly irrigated by blood vessels (*vasa vasorum*), which deliver oxygen and nutrients to the media and nerve endings to maintain sympathetic innervation of the vessel wall. Contrary to media, the adventitia thickens with age, owing to the higher deposition of collagen. Furthermore, adventitia-exiting inflammatory cells enter the artery wall *via* the *vasa vasorum*[67].

The summary of age-related changes in the aorta is depicted in Fig. I5. These alterations are also present in cardiovascular diseases (CVD)[66,68,69]. However, the direct causality mechanisms have not been clearly defined.

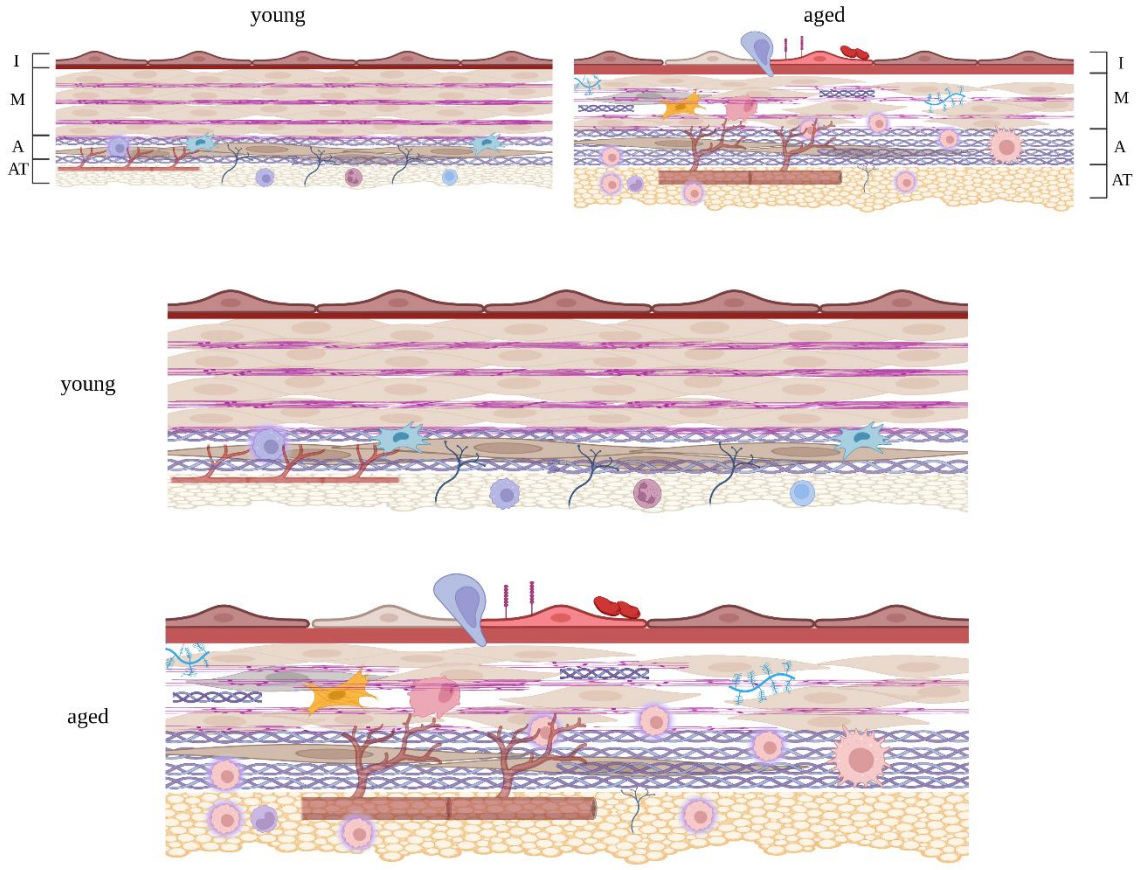

Figure I5. Age-associated arterial wall alterations. The arterial wall is composed of endothelial cells (intima layer - I) and concentric SMC layers associated with elastic fibres, generating lamellar units in the medial layer (M). The adventitial layer (A) contains fibroblasts, mesenchymal (progenitor) cells, collagen fibres, and vasa vasorum. As endothelial cells age, they become pro-thrombotic and more permeable, permitting inflammatory cell infiltration. In the medial layer, elastic fibres calcify and break as collagen production rises, stiffening the vessels. The medial layer thins; on the contrary, the adventitia thickens due to intense collagen deposition. Moreover, the primarily adventitial cell subtypes migrate to the media, augmenting the pro-inflammatory phenotype. Similarly, the higher inflammation in the adventitia and adipose tissue (AT) triggers expansion of the *vasa vasorum*. Image created with Biorender.com.

Aortic aneurysm – a disease linked to impaired biomechanical adaptation

In vivo, blood artery walls are subjected to a variety of mechanical forces. In the case of the artery wall, its intraluminal surface is subjected to mean pressure of ~13.3 kPa (100 mmHg, systolic) and ~5.3 kPa (40 mmHg, diastolic)[32]. Furthermore, owing to the blood flow, cardiac cycle-oscillating WSS of a few Pa is applied to the intraluminal surface.

In the longitudinal direction, arterial walls are stretched by 30–50%, artery diameter changes by ~10% and its length by a few % during the cardiac cycle[70]. In general, the artery adapts well to blood flow and pressure variations, taking advantage of complicated, interrelated physics-law-driven and biological mechanisms. It is undeniable that these interactions constitute a tightly controlled loop that supports adequate vascular tone and structural management (Fig. I6). The fine-tuning of this mechanism is pivotal, as the changes in any of the loop components may weaken the arterial wall, triggering the permanent dilatation of the arterial wall – an aneurysm[71].

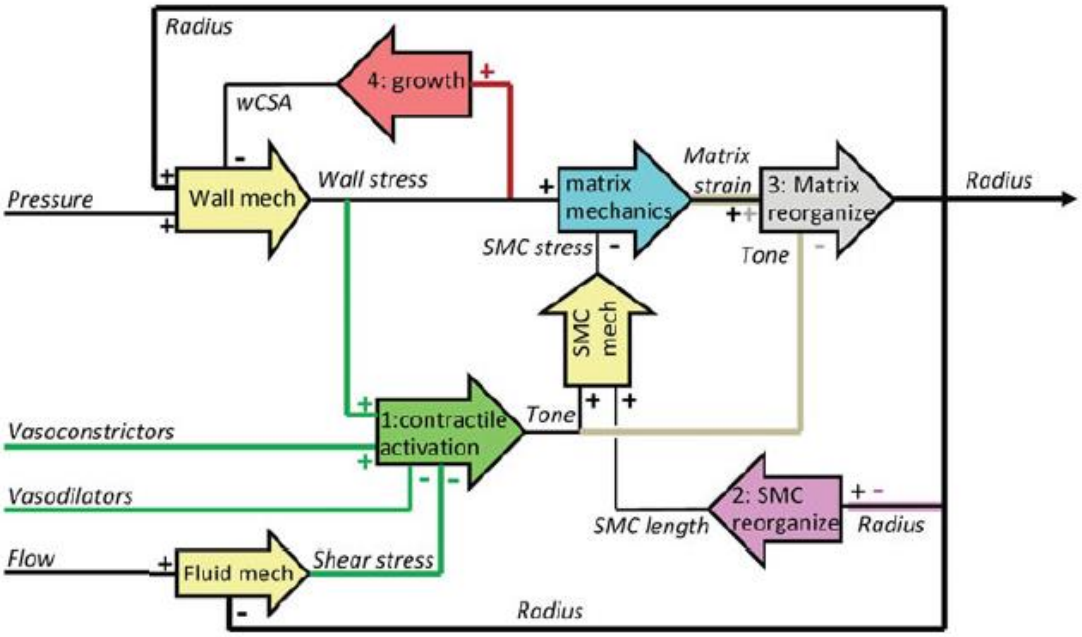

Figure I6. Schematic model representation of a series of events leading to aortic diameter enlargement. The factors involved are mechanical (Laplace law-driven vascular wall mechanics, fluid mechanics, the concept of wall stress-bearing matrix and cells), with additional biological outputs (regulation of tone, organization of smooth muscle cells and matrix, and cellular hypertrophy) (image from[72,73]).

Mechanically, the formation of an aneurysm is similar to the engineering-encountered problem of fatigue-driven plastic deformation or permanent bulging (of a pipe or a tire), which, when uncontrolled, can result in the rupture triggered by oscillatory internal pressure. That usually happens due to the weakening of the object, or the arterial wall for aneurysms[74]. However, the problem is significantly more involved and challenging to analyse in the case of arteries because their walls are composed of a complex structure of living cells and a structural network of cells and proteins capable of not only actively modifying their mechanical properties in response to changes in mechanical stimuli but also undergoing permanent remodelling.

In physiology, transmural pressure is the gauge pressure (the pressure variation across the walls of a blood vessel). The transmural pressure causes a diseased weak point on an artery wall to enlarge, increasing the radius of the wall. A larger radius demands a stronger wall to retain the pressure, which sometimes exceeds the wall capacity[75]. According to Laplace law, the pressure distributes equally in every direction. Therefore, if we imagine a part with lower load-bearing capacities, this part may not resist this pressure.

An artery behaves much like a long cylindrical balloon. When attempting to blow up such a balloon, the initial blow is rather tough; but, after the balloon reaches a certain radius, it typically becomes much easier to expand the balloon. That is, less pressure is required to raise the size of the balloon. If this happens to an artery, we have an aneurysm, and even the relatively constant blood pressure will keep it expanding[76]. According to Laplace's rule, luminal dilatation causes increasing wall tension, resulting in a vicious cycle of growing dilation and higher wall stress.

Using the balloon analogy, the inflation makes it thinner, and thus easier to enlarge. Similarly, if the balloon is not uniformly made, old or lightly damaged (ex. by a light nick or prolonged exposure to sun radiation), it or its parts would easily inflate. Hence, the weakening of ‘the wall’ could alter its load-bearing capacities and result in localized enlargement (Fig. I7). The same happens in the case of an artery. Healthy vascular tissue heals faults continuously, which enables the preservation of tissue integrity. Individual host response flaws or incomplete healing under supraphysiological stress levels or in diseased tissues leads to the accumulation of weak links, irrevocably reducing its strength[77].

Blood vessel formation and maintenance include complex biological processes, events, and feedback to the vascular tree. Genetically programmed and managed hemodynamic or metabolic needs maintain and modify artery structural integrity. Vascular remodelling is a dynamic and adaptive process of structural change that includes cell growth, death, and migration, and extracellular matrix (ECM) synthesis or breakdown[78–81]. ECM is a noncellular component of the aortic wall that, in addition to providing structural support, regulates the bioavailability of a variety of growth factors and cytokines, influencing cell function and behaviour and ultimately determining physiological or pathological aortic wall remodelling[82].

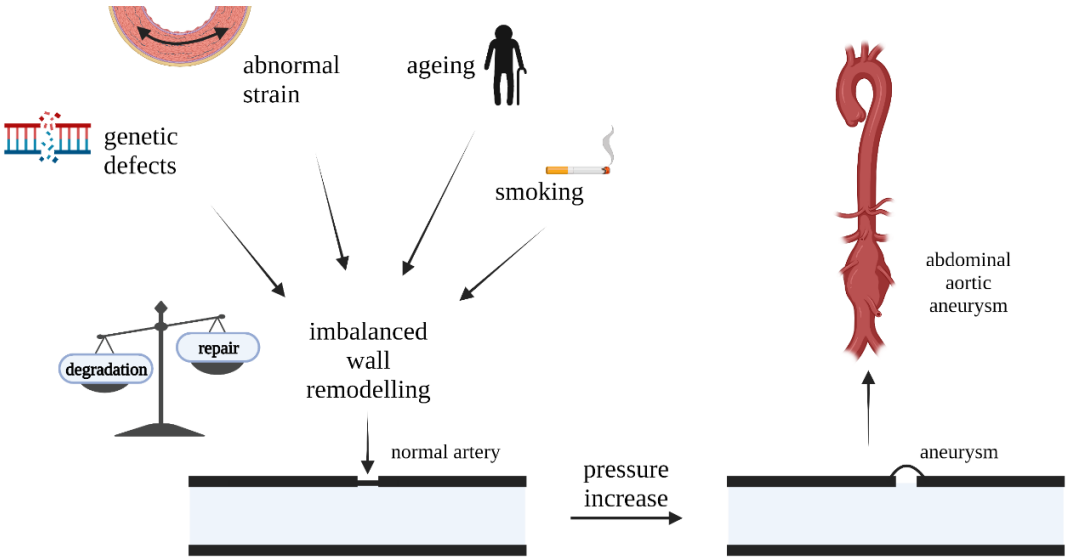

Figure I7. **Weakening of the part of the arterial wall may result in aneurysm formation.** This disease is considered multifactorial and primarily degenerate, emerging from a complex interplay of various biological variables and particular alterations in hemodynamic stimuli on the artery wall, which may destabilize the regulatory system. Once an aneurysm occurs, pulsatile blood flow causes progressive enlargement of the compromised artery wall. As the wall geometry, composition, and strength decrease during growth, the aneurysm ruptures when the distended artery wall cannot withstand blood flow strains. An aneurysm rupture causes death or disability. Image created with BioRender.com.

At normal blood pressure levels, the aorta resilience is attributable to the reversible expansion of elastic lamellar units in the media, which account for the aorta stretchiness. When mechanical strain exceeds the capacity of medial elastic fibres, the aorta tensile strength is transferred to its collagen fibre meshwork[54]. Physiologically, the elastin becomes gradually inefficient, triggering the coordinated synthesis of collagen fibres, with a mild increase in the proteases to ensure proper orientation and shape of collagen fibres[54,77]. Moreover, the wall undergoes constant rearrangements to sustain the needs, responding to the increase in blood pressure or wall strain. These changes are often imperceptible and rely on balanced vessel wall destruction and synthesis of needed components[82].

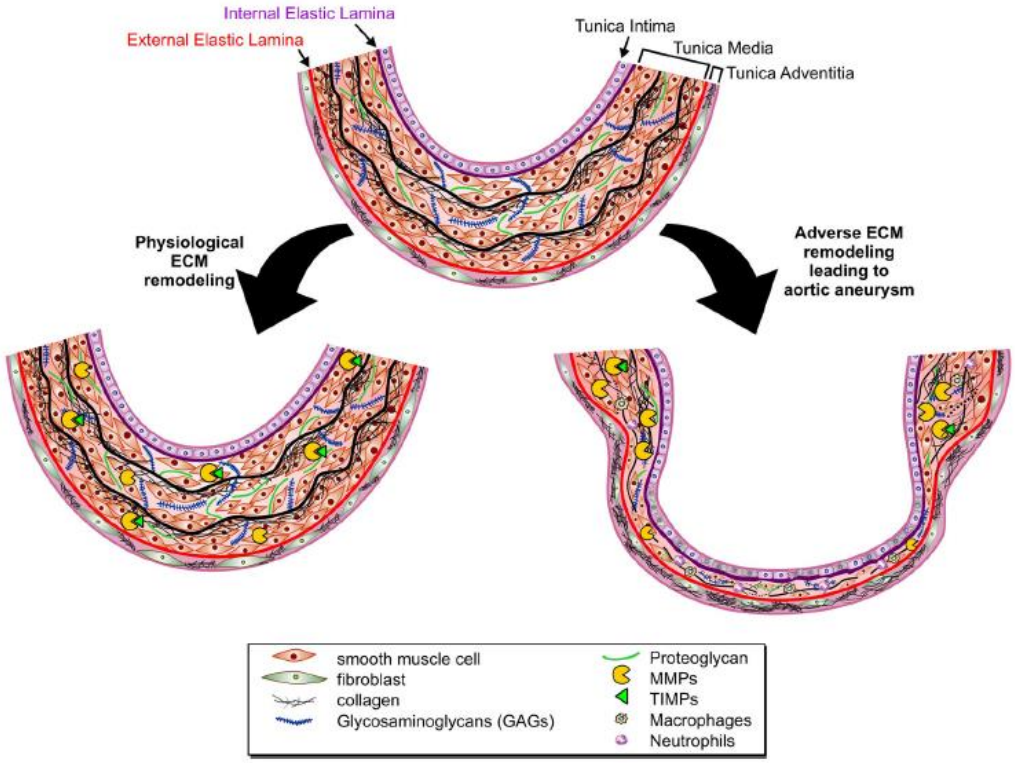

Figure I8. Aortic wall cross-section and its healthy and pathological remodelling. The tunica medium comprises interspersed layers of elastic fibre and smooth muscle cells and is rich in proteoglycans and glycoproteins. During physiological remodelling, MMPs (and other proteases) degrade ECM proteins, which are balanced by newly produced ECM proteins, while tissue inhibitors of proteases (TIMPs) keep MMP proteolytic activity under control. Excess ECM breakdown or poor ECM renewal production, along with smooth muscle cell death, result in adverse ECM remodelling, as seen in aortic aneurysms (image from[82]).

On the other hand, upon strong inflammation and oxidative stress, which can be induced, for example, by tobacco[83], the balance between shifts towards the degradation and significantly longer aortic components synthesis cannot recompensate for the considerably faster destruction processes[84]. The mutations in the load-bearing components or the regulators of proper mechanosensing result in the predilection towards aneurysm formation (Table 1). These two features are intertwined: mechanosensing necessitates intact load-bearing structures, and load-bearing structure assembly necessitates intact mechanosensing[85]. Congenital changes in these programs can cause variable, faulty, or absent vessel wall rebuilding. The connection between arterial variations and aneurysms suggests insufficient arterial wall development and rearrangement[86]. These clinical observations were replicated in experimental aneurysm models mimicked using elastase infusion, demonstrating that increased segmental aortic stiffness, creating at the same time weaker segments, may be a trigger

for the malformation[87]. Moreover, the increased mechanical load can be considered an inherent feature of the aneurysm[88].

Gene	Function	Disease	
FBN1	Myofibril, elastogenesis, TGFβ bioavailability, and smooth muscle phenotype	Marfan Syndrome	AA, TA
EFEMP2	Fibulin 4, elastic fibres	Cutis laxa autosomal recessive IIA	AA
TGFBR1, TGFBR2, TGFB	Signalling of TGFβ receptor	Loeys-Dietz syndrome	TA
MYH11	Smooth muscle contractions	Familial TA with patent ductus arteriosus	TA
ACTA2	Smooth muscle contractions	Familial TA	TA
COL3A1	Type III collagen, altered extracellular matrix fibres	Ehler-Danlos vascular type IV	TA
SLC2A10	Decreased GLUT10 protein in the TGFβ pathway	Arterial tortuosity syndrome	aorta, arteries
SMAD3	Impaired TGFβ signal transduction	Syndromic form of AA and dissection	aorta

Table 1. The link between the mutations in structural and mechanical signalling proteins with the occurrence of aortic aneurysms (table prepared based on[89]). AA – abdominal aneurysm, TA – thoracic aneurysm.

The proper regulatory systems ensuring the aortic wall stability can be largely affected by another biomechanical stimulus – shear stress. The flow patterns in the proximity of the aneurysm are complicated and undergo constant modification. As an aneurysm shape evolves, its initially high wall shear stress (WSS) lowers as the shape of the aneurysm changes[90].

However, to fully emphasize the role of hemodynamic alterations, human studies show a significant susceptibility to aneurysm formation in people after a leg amputation. Physiologically, the aortic bifurcations (mainly renal and iliac arteries) divide ‘aortic blood’ and decrease by four. The amputation reduces iliac artery size asymmetrically. If the flow pattern becomes asymmetrical, both the impulse and counterimpulse are directed laterally, enhancing the mechanical stress on the aortic wall and degenerative changes. Flow asymmetry in the infrarenal aorta causes high shear stress zones with local dilatation at the convexity and low shear stress areas along the concavity, leading to an aneurysm of the abdominal aorta[91].

Abdominal aortic aneurysm – an ageing-associated disease

The abdominal aorta exceptional architecture, with many arterial branches and lower support by the skeleton, renders it significantly prone to dilatation. An abdominal aortic aneurysm (AAA) is a complicated and fatal vascular disease affecting a large proportion of the world's population[92]. It is a permanent dilation of the aorta that exceeds the standard diameter by at least 50%, most often developing in the infrarenal aorta. The occurrence of an aneurysm is associated with its expansion which may cause aortic wall rupture, leading to death in more than 80% of cases providing 150,000–200,000 annual deaths worldwide[93].

Although AAA may be suspected based on risk factors, abdominal palpation, or clinical manifestations, a definitive diagnosis requires abdominal imaging studies that demonstrate a focal aortic dilation meeting the criteria for an aneurysm. Abdominal ultrasound and computed tomography of the abdomen are both highly sensitive and specific for diagnosing AAA. AAA does not typically cause symptoms unless the aneurysm is expanding rapidly, has become large enough to compress surrounding structures, is an inflammatory or infectious aneurysm, or has ruptured. AAA may be seen incidentally on plain films of the abdomen, abdominal computed tomography (CT), and magnetic resonance imaging (MRI). Both CT and MRI are highly accurate and specific tests for AAA[92]. They are recommended under differing clinical circumstances, depending on the presence of symptoms and the patient's hemodynamic status. Abdominal CT provides additional anatomic detail which identifies ruptured, infected, or inflammatory aneurysms and other important features in the subsequent management of symptomatic AAA[94].

The main risk factors for the development of AAA are age, sex, hypertension, smoking, and family history. Aneurysmal degeneration is more frequent in the elderly population. The age-related changes in the arterial wall composition increase the risk of pathological remodelling. Moreover, the protease activity correlates with age. The degenerative effect can be augmented by the loss of viscoelastic SMCs, which are replaced by proteoglycans, significantly decreasing the load-bearing capacity of the arterial wall. Shear stress forces activate (genetically determined) steps that modify the balance of remodelling mediators (metalloproteinases, nitric oxide synthase, platelet-derived growth factor (PDGF), and transforming growth factor β (TGFß)). This increased collagen degradation, combined with inadequate collagen deposition, has been associated

with the progression and ultimately rupture of AAA[95]. Moreover, ageing reduces the vessel wall ability to react to hemodynamic changes and stress. This progressive ageing process causes vessel wall fragility that varies by gender and age.

Although still not fully understood, the aetiology of AAA is an orchestrated series of events that often start from small micro ruptures and end in the aortic wall bulging and rearrangement[92,96]. Animal models, including mice, have become irreplaceable in cardiovascular research since they offer a representative, time-efficient model to study the pathologies such as aortic aneurysm, which takes decades to develop in humans. Around 20 years ago, a model of AAA based on the infusion of angiotensin II (Ang II) was presented, and it has been used until now. Ang II is a short peptide, present endogenously, with hypertensive and pro-inflammatory properties. It may be delivered by small osmotic pumps. Infusion of Ang II causes an abrupt increase in blood pressure (hypertension) and may result in the formation of AAA. The incidence of AAA varies between mice strains and can give insights into the mechanisms of the disease[97]. This model is considered a gold standard for pre-clinical AAA research, as it replicates many features of human AAA, including dilatation, aortic wall destruction, and subsequent rearrangement[98] (Fig. I9). Another advantage of this model is the lack of necessity for complicated surgical interventions as in other AAA models[99]. On the other hand, the main drawback is the low incidence of intraluminal thrombus, which is usually present in humans, and plays an essential role in wall rearrangement[98].

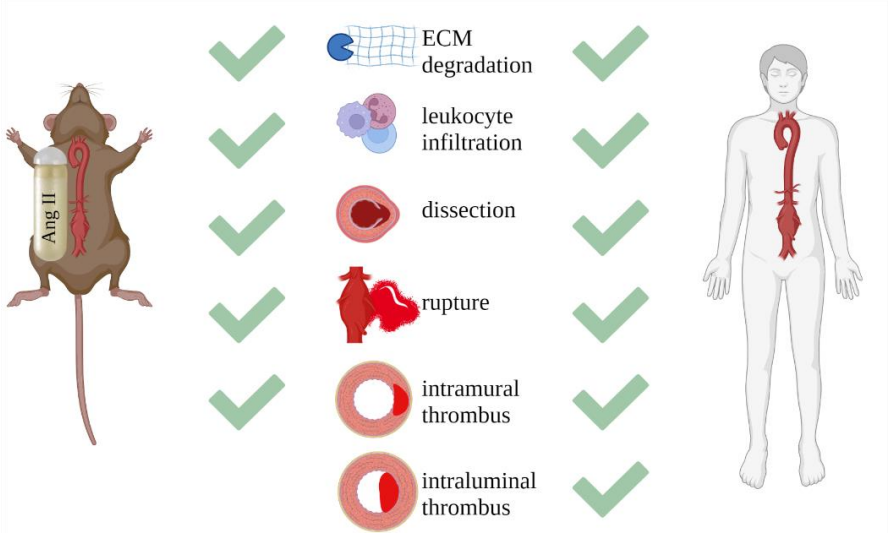

Figure I9. Features of aneurysms in the Ang II-based model replicate the human disease. Image created with BioRender.com[100].

This model relies on the hypertensive and pro-inflammatory features of Ang II. It is a component of the renin-angiotensin system (RAS) and is adaptable due to its multidimensional nature directly affecting the fate of CVS. Ang II, a complex member of the RAS family, has many recognized actions. After decades of diligent investigation, our understanding of this peptide has vastly improved. Numerous studies have established that the bulk of Ang II-regulated activities in the system is mediated by the Ang II receptor 1 (AT1R). It has been found that functional crosstalk exists between AT1R-mediated signal transduction cascades and other signalling pathways, mainly redox and inflammatory signalling[101], which can be even more exacerbated in the atherosclerosis-prone hyperlipidaemic mice[97]. Not only is there an increase in blood pressure upon treatment with Ang II, but it also affects vascular inflammation and endothelial function[102]. Moreover, there is an increased activity of Ang II with age[103,104]. Inhibition of Ang II signalling is considered protective, leading to an increase in the lifespan[105–107]. On the other hand, Ang II action through Ang II receptor 2 (AT2R) or some of Ang II metabolites, like angiotensin 1-7 (Ang 1-7), play a protective, vasodilatory role. Hence, the RAS pathway has a multimodal impact on the cardiovascular system, largely dependent on the favoured metabolite or used receptor (Fig. I10).

While the AngII-driven signalling and inflammatory response have been the subject of AAA research for years[108], the structural changes only begin to be explored[109]. As rising data points out to AngII-based AAA model as a dissection one[96,110], it heightens the influence of endothelial layer integrity and plausible structural alterations in the disease aetiology.

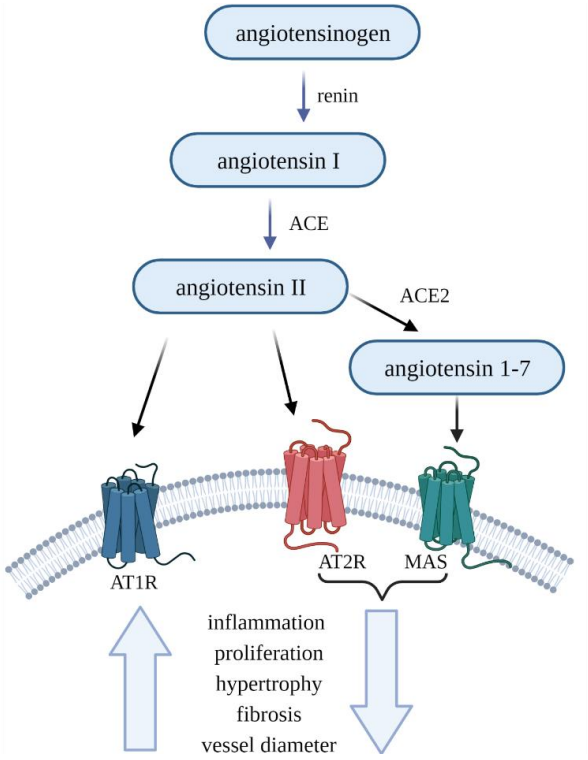

Figure I10. The complexity of renin-angiotensin signalling regulation. Angiotensin (Ang) peptides and receptors have been identified to govern cardiovascular regulation. Angiotensinogen is converted to angiotensin I by renin. Angiotensin-converting enzyme (ACE) converts Ang I to Ang II, which can activate the AT1R and AT2R. Ang II can be further split into Ang (1–7) *via* ACE2. The functional role of angiotensin family peptides is exerted by specific receptors, which have an opposite impact on the CVS. Image created with BioRender.com.

ECs – the overlooked players in AAA?

The formation of AAA is accompanied by substantial activation of proteolysis, severe inflammation, and oxidative stress, which result in the death of smooth muscle cells (SMC) and the rearrangement of the aortic wall. Nonetheless, the detailed activation pathways and initiating stimuli are not yet well understood[92]. The last 20 years of research into the Ang II-based model mechanisms mainly elucidated the role of SMCs, which are considered important regulators of AAA, due to cell-specific mutation sensitizing to aortic aneurysms. Moreover, loss of normal aortic SMCs with a concomitant increase in non-SMC mass may correlate with the significant increase in aortic aneurysms[111]. Similarly, as robust immune cell infiltration accompanies AAA formation, the main research was directed toward immunological pathways. The primary evidenced mechanisms of AAA formation are depicted in Fig. I11.

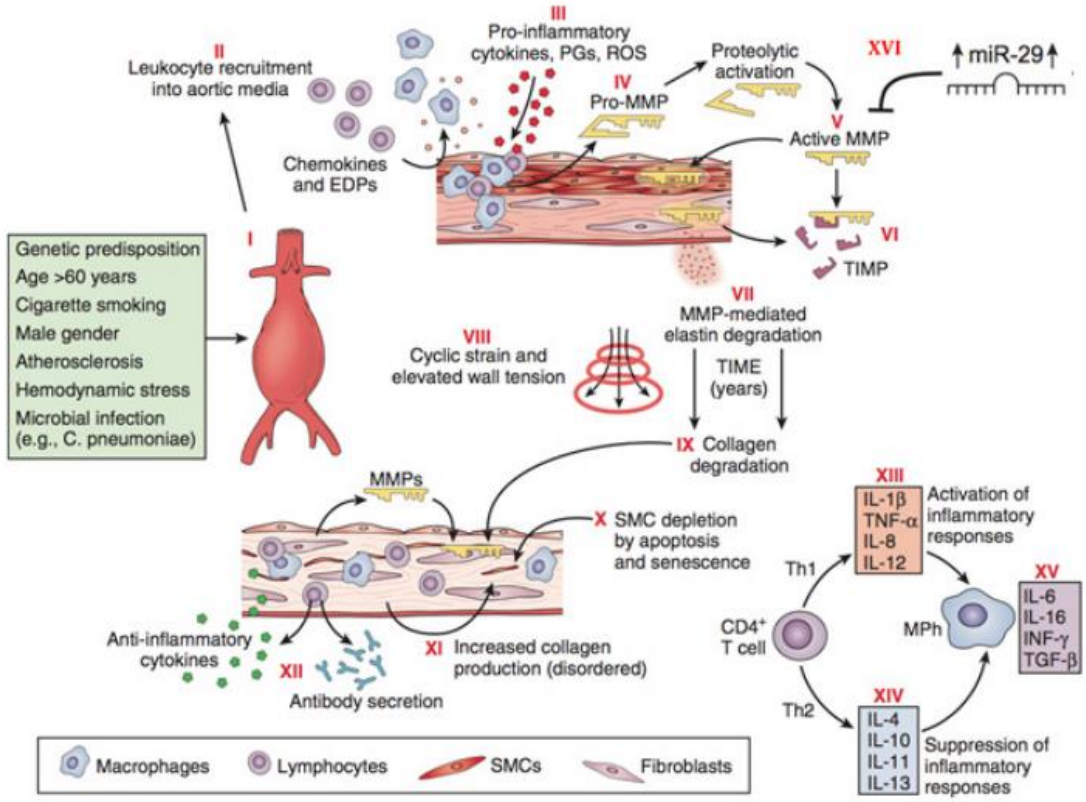

Figure I11. An outline of the central mechanisms governing the AAA formation in the mice models, on the example of miR-29 regulation. Please note that the EC-related pathways are not depicted (image from[112,113]).

On the other hand, one of the main drawbacks of the murine model is the scarcity of intraluminal thrombus, which is often accompanied by excessive atherosclerosis. Asymptomatic plaque ruptures and intraluminal/intramural clots that may or may not heal *via* intimal healing are caused by the terminal aorta unique hemodynamics (reflection on the iliac bifurcation, increased convection and collision, and decreased wall withstanding capacity due to fewer elastic lamina units). Mural thrombotic events combined with aortic dilatation create an intraluminal thrombus (ILT)[92,114]. It exhibits spatiotemporal hemorheology, including luminal renewal at the circulating blood contact, intermediate compaction from fibrin transglutamination, and abluminal lysis at the artery wall interface. This morphology emerges from several sequential stages of transformation. It is scarlet due to RBCs. It also contains aggregated platelets, which aid in activating prothrombin and fibrin. Circulating leukocytes, primarily neutrophils, degranulate and die during tissue retention, releasing proteases. Plasmin-activated proteolytic activation of matrix metalloproteinases by intraluminal thrombus can directly intervene in the course of AAA. Furthermore, thrombus formation can compromise aortic wall oxygen transport, resulting in relative hypoxia and SMC death[92,114,115] (Fig. I12).

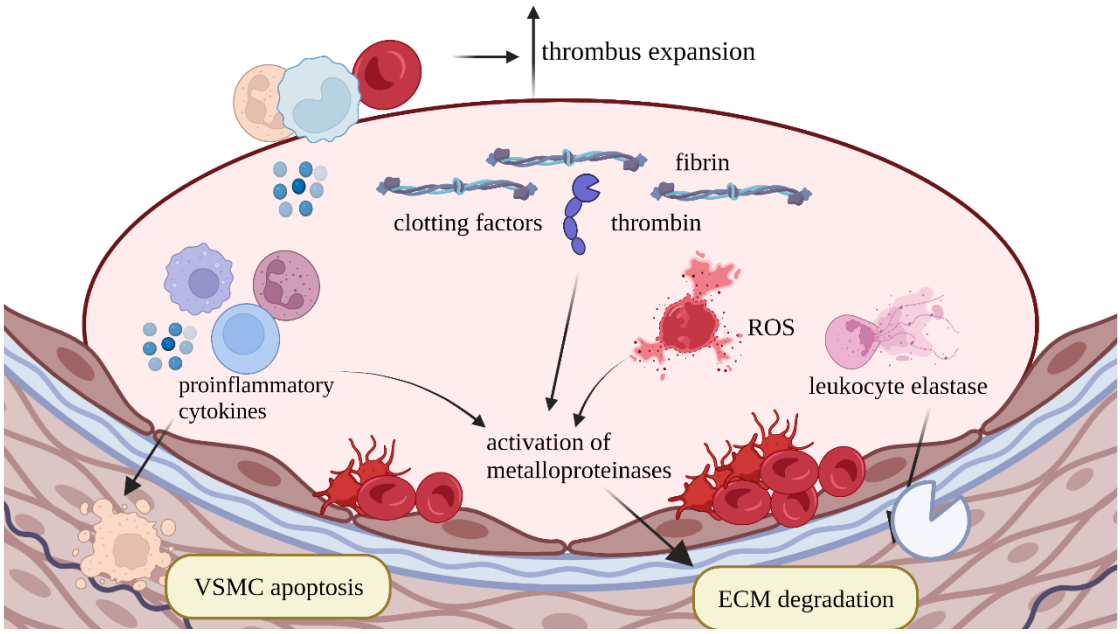

Figure I12. The intraluminal thrombus is a source of proteases capable of aortic wall rearrangement. Description in the text. Image created with BioRender.com.

The formation of thrombi largely depends on the anticoagulant properties of endothelial cells[116], implying there could be the functional relevance of ECs in AAA formation. Moreover, if endothelial involvement is considered in AAA, it is postulated in review papers that it mainly relies on endothelial function[117–119]. It is primarily substantiated by the protective effect of endothelial layer reestablishment in the stability of AAA[120]. The scarce research addressing the role of endothelial-specific protein function in AAA shows that the deletion of endothelial nitric oxide synthase (eNOS) exacerbates the AAA formation[121]. Accordingly, its recoupling, thus, increasing NO production, protects against AAA[122]. Similarly, the deletion of KLF11 in ECs predispose to AAA in the murine model, implying the inhibition of the dysfunctional phenotype as the mechanism[123]. However, the authors considered and correlated the oxidative stress or activation of metalloproteinases to dysfunction without providing unequivocal proof.

On the other hand, peering closer at recent single-cell analyses from murine AAA, we can identify several EC populations, which may respond to paracrine signals to proliferate and form new vessels[124]. Functionally, they were attributed to regulating ECM production, lipid metabolism, and angiogenesis[125]. Given this discrepancy, it would be of utmost importance to elucidate the significance of EC function unambiguously. Especially as the KFL family and eNOS are regulators of endothelial proliferation[126,127], thus the protective effect could be related to the latter.

The endothelium – the maestro of circulation

Endothelial cells constitute the thinnest part of the arterial or venous wall and the only one in the capillaries. The endothelium is a specialised epithelium, which creates a semipermeable barrier between two body compartments: the blood plasma and the interstitial tissue fluid. Histologically, endothelial cells vary in form across the vascular tree but generally are squamous, polygonal, and elongated with the long axis in the direction of blood flow, measuring 50–70 μm long, 10–30 μm wide, and 0.1–10 μm thick[128]. Endothelium, supported by its basal lamina, is highly differentiated to mediate the bidirectional exchange of molecules by simple and active diffusion, receptor-mediated endocytosis, or transcytosis[129,130]. As it is subjected to various tissue environmental cues and is influenced by multiple metabolites, growth factors, cytokines, oxygen tension, and mechanical forces, it varies significantly across the circulatory system. ECs are now regarded as more than a barrier-forming cell population acting as a responsive interface. Their microenvironment is the gatekeeper of organ development, homeostasis, and tissue regeneration[131]. Endothelial cells are a very heterogeneous cell population that differs not just across organs but also between vessel calibres within an organ[132]. They differ in permeability, which translates to function. A distinction is made between continuous, fenestrated and discontinuous endothelia (Fig. I13).

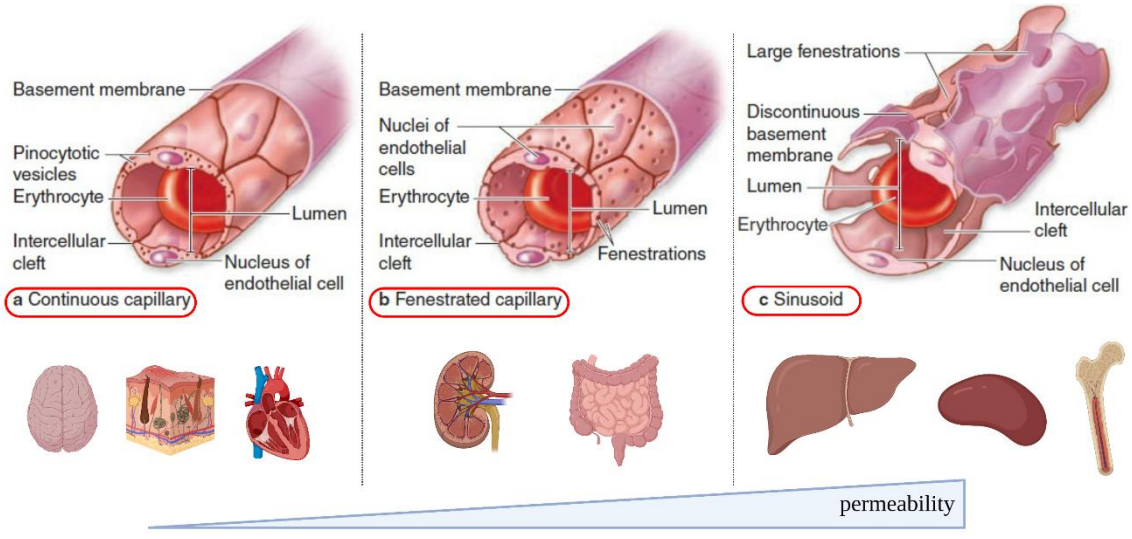

Figure I13. Endothelial cells exert diverse functions, which translate into a high morphological heterogeneity. Image created with BioRender.com based on images from[133].

Besides permeability, organ-specific vasculature can supply nutrients to tissues differently, mainly through tissue-specific transporters/channels, adjusted to specified

nutritional or functional needs of the organ[131]. Capillary ECs are more than simply passive conduits for oxygen and nutrients; they also aid in organ development and adult organ regeneration by releasing tissue-specific paracrine growth hormones known as angiocrine factors[134].

It is critical for ECs to have direct contact with both the liquid phase, plasma, and the solid structure, the basal membrane extracellular matrix. They may swiftly modify their shape and function in response to physical or chemical stimuli. *In vitro*, until confluence, ECs have a cubic form. When exposed to shearing forces, such as in a perfusion chamber, they take on an elongated shape in the sense of flow, with significant cytoskeleton remodelling[135–137]. Furthermore, coronary artery bypass grafting is an excellent example of how mechanical limitations impact the endothelium. After being exposed to arterial flow, human saphenous graft ECs change shape, elongating with the central axis parallel to the flow[138]. It outlines significant endothelial plasticity. Furthermore, endothelium regularly interacts with the ECM of the basement membrane and alters phenotype accordingly. For example, attachment on the fibronectin promotes the formation of fenestrations[139]. Moreover, the amount and location of adhesion molecules broadly vary with matrix type[140]. Depending on the location, endothelial cells may start to express atypical proteins, which were assumed to be expressed only in the tissue parenchyma, implying previously unknown organ-specific endothelial plasticity and adaptability[141].

The arteriovenous destiny of endothelial cells is determined by genetic factors early in embryogenesis[142]. Arteries are mostly lined with non-fenestrated continuous endothelium characterised by specific transcriptional networks (AP1, ETS, GATA, SOX), distinguishing it from other types[143]. ECs extend and align in the direction of blood flow, thanks to tight junctions, which are also critical in mechanotransduction[71]. Hence, they help to regulate blood pressure by secretion of physiological mediators capable of modulating vascular tone. Arterial branches and large curvatures are subjected to a nonlinear, damaging flow that poses a risk of inflammation, coagulation, or uncontrolled bleeding[144–146]. Therefore, the proper function of ECs is of utmost importance.

Glycocalyx - a determinant of the EC function

In a nanometric scale, endothelium turns out neither smooth nor uniform but instead covered with brush-like sprouting polymers. This structure is called endothelial glycocalyx (eGCX) - a negatively charged set of macromolecules: sugar, proteins and lipids. It is a delicate structure that is often overlooked as it is challenging to visualise and easily degradable. It was identified during the 1960s with the advent of electron microscopy[147]. The thickness of this negatively-charged layer is comparable to the endothelial cell body and varies from 0.1 μm to 5 μm[148]. Moreover, its diameter is less than 10% of the tiniest capillaries. With these dimensions, the glycocalyx protects the vessel walls without obstructing the outflow[149]. The main components of the endothelial glycocalyx are: proteoglycans, glycosaminoglycans and glycoproteins, as well as absorbed plasma proteins (Table 2).

Group	**Examples**	**Features**
proteoglycans	syndecan	Main components of GCX; core protein associated with glycosaminoglycans; Bridge the glycocalyx to the actin cytoskeleton, impacting mechanotransduction.
glycosaminoglycans	heparan sulphate, dermatan sulphate chondroitin sulphate hyaluronic acid (HA)	Create a protective layer disturbing the interaction with blood components; Thanks to their hypo- or hypersulphated domains, interact with circulating proteins, impacting the anticoagulant capacities; HA binds to CD44 and affects the actin cytoskeleton; HA exerts space-filling and hydratation roles.
glycoproteins	integrins selectins	Mediators of cell adhesion signalling, recruitment of immune cells, interaction with platelets; they are located inside the glycocalyx.

Table 2. Endothelial glycocalyx components and their features related to endothelial function. GCX – glycocalyx.

The glycocalyx, which forms a tangled and thick network (Fig. I14), acts as the first barrier in front of the endothelium and regulates cellular and macromolecular flow[150]. The eGCX plays an important role in small and large vessels. It acts as a mechanotransducer, regulates capillary wall adsorption and permeability, and influences haematocrit and blood viscosity (Table 3). Therefore, we can consider

its size as a marker of EC function, defined as the maintenance of anti-thrombogenic, anti-inflammatory and VSMC regulatory phenotype.

The thickness of eGCX differs between the areas of laminar and turbulent flow[151]. Its degradation, induced by oxidative stress and enhanced activity of metalloproteinases, correlates with the onset of cardiovascular diseases (CVD), such as diabetes, haemodialysis or ischemia-reperfusion injury. If damaged, it releases the circulating components, which serve as a marker of EC dysfunction and increased risk of CVD[152,153].

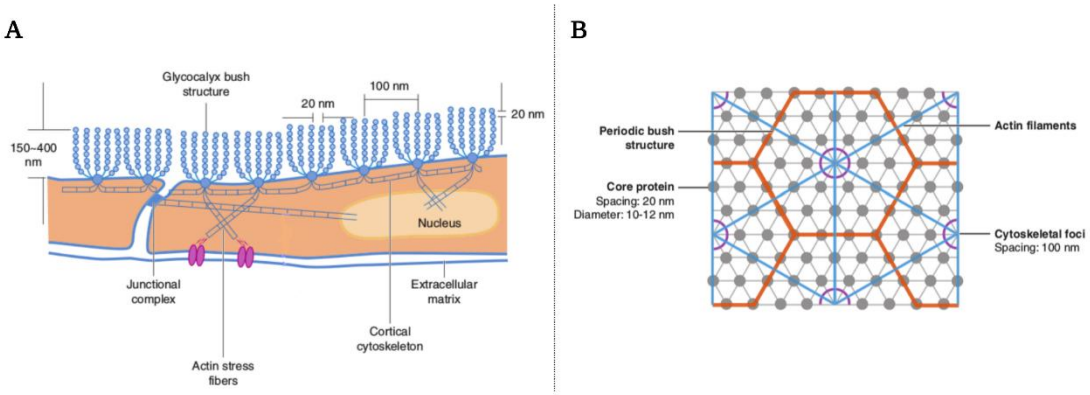

Figure I14. The complexity of endothelial glycocalyx structure. The GCX has a precise geometry, with anchor points of the bush-like bundles drawing a 6-fold pattern on the endothelium. The average distance between neighbouring anchors is 100 nm, although the brush-like structure of filaments causes a thickening, with a spacing of roughly 20 nm in all directions. The monomer diameter is also approximately 20 nm, rendering the GCX an extremely dense matrix. Modified images from[154].

Importantly, the state of ECs highly determines exerting their versatile functions. In the majority of adult tissues, ECs are in a non-cycling, quiescent state, which is required for their barrier and signalling interface functions. Quiescence is defined as a condition in which ECs are not activated but rather rest and await activating signals, which essentially changes their features. Loss of quiescence triggers the expression of pro-coagulant, pro-adhesive, and vasoconstricting markers and facilitates the immune cell transmigration[155].

	Glycocalyx function	Impact of shedding	Ref
Vascular permeability	GCX is an effective protein osmotic barrier and thus regulates osmotic pressure.	Less protein (mainly albumin) is retained in GCX, which leads to water escape from the intraluminal sector.	[141, 142]
	HA, through the interaction with its receptor CD44, enhances the expression of stabilising actin filaments in the cell cortex (ex. S100 family, annexin II); Moreover, HA inhibits cytoskeleton destabilisers.	Increased level of RhoA-GTP leads to strong actin polymerisation and formation of stress fibres, which can impact tight junctions coherence.	[158]
	Expression of tight junction components (CD31 and CD144).	Weakening of endothelial tight junctions.	[159]
Leukocyte adhesion	GCX components (mainly GAGs) create a protective layer which vastly surpasses the height of cell adhesion molecules (in capillaries: 0.4-0.5 μm vs 0.02-0.04 μm for selectins), which disrupts the interaction with the leukocytes.	The interaction between immune cells and adhesion molecules accrues.	[160]
Thrombosis	GCX maintains the anticoagulant positively charged phospholipids in contact with blood and masks the pro-coagulant substances. GCX components are cofactors of anti-coagulant proteins (ex. anti-thrombin, thrombomodulin).	Enhanced thrombi formation.	[161]
Shear stress sensing	GCX, and mainly HA and HS (but not chondroitin sulphate), are the mechanoreceptors responsible for shear stress sensing and NO production through PI3K/AKT/NOS3 pathway, permitting smooth muscle relaxation.	Removal of HA and HS abolishes flow-triggered NO production and impedes vasodilatation.	[162]
Hampering oxidative stress	Antioxidative enzyme extracellular superoxide dismutase (EC-SOD) locate within glycocalyx due to affinity to heparan sulphate; sialic acid impacts antioxidative signalling.	Impaired antioxidant response, which may damage the endothelium.	[163]

Table 3. The glycocalyx is a crucial regulator of EC function and the proper functioning of CVS. HA – hyaluronic acid, HS – heparan sulphate.

Contrary to previous beliefs, stating that the ECs have dampened capacity to perceive signals in the quiescent state, we now know that they are awake. They consistently receive and originate functionally significant signalling inputs, and this condition is actively controlled[155]. They can transition between the activated and quiescent state or irreversibly undergo senescence (Fig. I15). Signalling mechanisms involved in preserving functionally quiescent endothelia are being discovered, including endocrine, autocrine, paracrine, and mechanical inputs[155]. The relevance of this control is underlined in vascular diseases induced by abnormal activation of the critical mitogenic signalling pathways PI3K–AKT and RAS–MAPK, which results in vascular malformations[164]. On the other hand, irreversible loss of proliferative phenotype (senescence) contributes to CVD diseases[165–167].

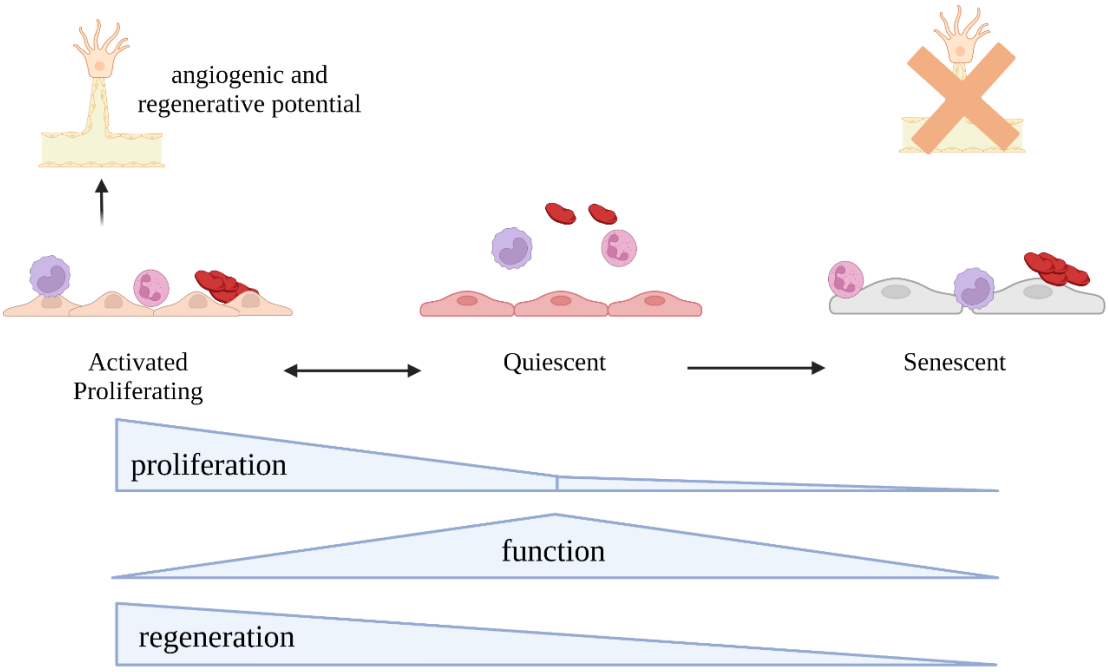

Figure I15. Endothelial cells can transition between three fates differing in function, regenerative capacity and proliferation. Image created with BioRender.com

Of importance, shear stress is one of the pivotal factors in the establishment of EC fate. Blood flow-mediated biophysical forces are central in the maintenance of fully functional, differentiated, quiescent endothelial cells, mainly through the regulation of metabolic glycolytic state[168].

ECs – integrators of biochemical and biomechanical stimuli to orchestrate proper functioning of the CVS

Shear tension exists anywhere fluid exists. Fluids operate on the cell surface in biology and vascular systems. The blood flow exerts a frictional force on the surface of vessel walls, referred to as shear stress. This mechanical phenomenon has a prominent influence on tissue function and biological responses, modifying cell shape, proliferation, differentiation, metabolism, communication, and assisting in barrier development[7]. The diameter of blood vessels is adjusted to maintain fluid shear stress. This reaction is absent when endothelial cells are eliminated[32]. Endothelial cells promote blood vessel dilatation in response to increased flow. They detect shear stress in the fluid and produce chemicals (mainly nitric oxide) that cause blood vessel dilatation.

The endothelium is subjected to interconnected stresses of two sorts: substrate characteristics-induced contact stress and blood flow-related stress. The contact stress on endothelial cell basal surface is driven by substrate topography, curvature, and stiffness. On the other hand, the viscous blood flow, the compressive blood pressure, and circumferential and axial tensile stress from transmural pressure, differential and tissue movement create shear stress on the EC apical (luminal) surface (the fluid-derived stress)[169]. These factors are all dynamic but on distinct time scales. While the substrate physical properties remain relatively stable over time, shear, pressure, and tensile stresses are highly variable owing to blood flow pulsatility. Moreover, the kind and degree of these mechanical cues vary depending on the organ and its vasculature[169].

The aorta is nourished from the outside, and the internal endothelium-lined aortic layer has to remain impermeable, which is ensured by tight junctions connecting the endothelial cells. Such connections, together with strategic location, enable the endothelial cells to be integrators of biochemical and biomechanical stimuli to orchestrate the proper functioning of the CVS[170]. Stiff endothelium syndrome predisposes hypertension and atherosclerosis, both associated with AAA[171].

EC sensing and mechanical force response rely on converting mechanical surface stimuli into intracellular biochemical reactions (mechanotransduction). It requires the existence of mechanosensors localised on the apical, basal surface and at cell-cell junctions (Fig. I16). They detect blood flow-induced hemodynamic forces such as shear stress, hydrostatic pressure, and circumferential stretch. They are linked to intracellular

proteins, often by actin cytoskeleton[172], thus permitting the modulation of cellular response to sustain their needs.

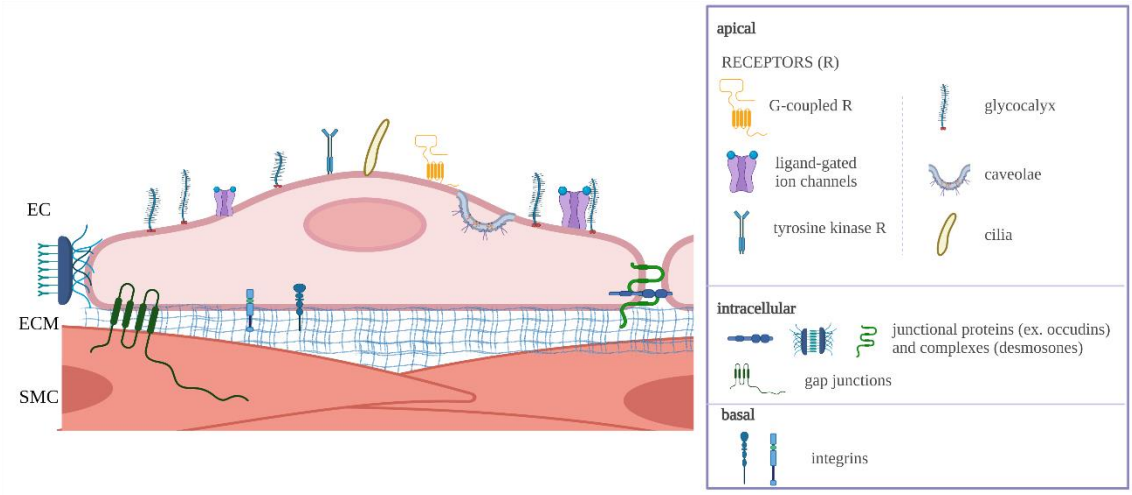

Figure I16. Endothelial mechanosensors. This image depicts major mechanosensitive proteins located apically (at the lumen side) and basally (at the proximity of elastic lamina), and at the cell-cell junctions. Image created by Biorender.com**.**

The close functional connection between ECs and surrounding VSMCs regulates vascular tone and cell response to biochemical and mechanical bloodstream stimuli. The mechanical properties of ECs rely on flow-mediated forces and dictate VSMC contraction status. This well-described process is predicated on the EC ability to secrete nitric oxide (NO) in a shear stress-dependent manner, where it promotes vasodilation *via* cGMP-dependent pathways[173]. Increased amounts of reactive oxygen species (ROS) created by NAD(P)H oxidase, xanthine oxidase, or uncoupled eNOS in the vascular wall cause NO scavenging and disruption of several signalling pathways that mediate its production[174]. ECs and VSMCs govern vascular function and vessel tone. Endothelium ability to adjust to altering stiffness is a critical physiological trait. Dysfunctional endothelial cells are stuck in persistent stiffening[175]. The dysfunction significantly augments with age, which may be related to significant glycocalyx shortening[153], thus diminishing the EC function, including the mechanotransduction[162]. Intracellularly, the altered mechanical response can be related to diminished NO production during ageing[176] or upon oxidative imbalance[177]. Notably, the reduced NO availability triggers premature endothelial ageing[178], which represents one of the CVD risk factors[165–167]. A general mechanism of how the apical mechanosensors can modulate the EC response is shown in Fig. I17.

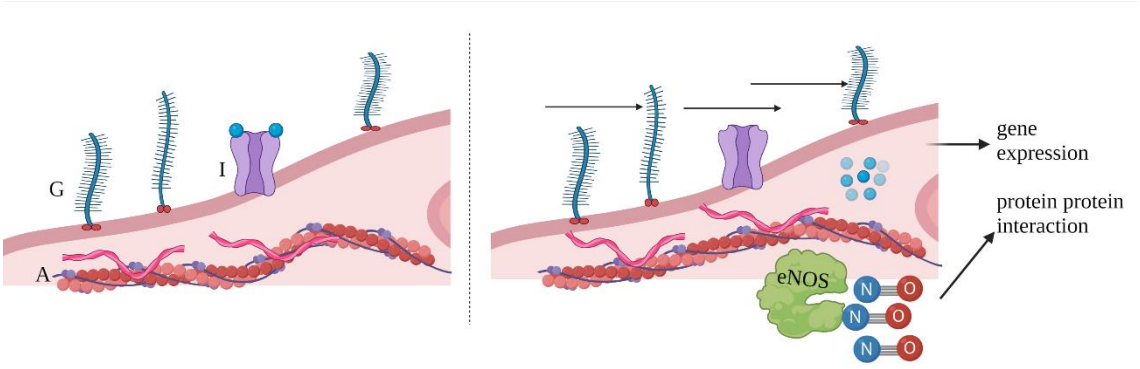

Figure I17. The simplified and exemplary mechanisms linking the apical mechanosensors to intracellular signalling. In this image, the flow is sensed by glycocalyx (G) and the ion channels (I). Upon flow, the glycocalyx-transduced signal triggers the remodelling of the actin cytoskeleton (A) and the production of nitric oxide by endothelial nitric oxide synthase (eNOS). Also, the influx of ions through the channels can alter the signalling pathways. Image created with BioRender.com.

NRF2 - a multifaceted CVS regulator counteracting ageing

Since the 1950s, one of the most recognized theories explaining the mechanisms of ageing has been Harman's free radical theory[179], which states that ageing results from accumulated damage caused by excessive oxidative stress. Consolidating cellular responses to stress is an important role of defensive mechanisms. Using a series of well-coordinated steps, the cell attempts to restore homeostasis and protect itself against internal perturbations while minimizing acute damage. It has been found that the NRF2/KEAP1 axis is a crucial node in the cross-talk between cellular defence and survival pathways[180–182].

NRF2 (nuclear factor (erythroid-derived 2)–like 2) is a transcription factor transactivating the expression of hundreds of protective genes[183,184], which comprise more than 1% of the human genome[185]. NRF2 was reported for the first time in 1994[186]. It is expressed in all human tissues[187] and is a master regulator that mediates the adaptive response to cellular stress. It belongs to the cap'n'collar (CNC) subfamily of basic-leucine-zipper (bZIP) transcription factors[188]. A number of genes that encode detoxifying enzymes (glutathione S-transferase (GST), NAD (P) H: quinone oxidoreductase (NQO1)), stress-responsive proteins (heme oxygenase-1 (HO-1)) and reactive oxygen species (ROS) scavenging enzymes (glutathione peroxidase (GxP), superoxide dismutase (SOD)) are directly regulated by NRF2 *via* its consensus sequence – antioxidant redox element (ARE)[184,189].

The NRF2 transcriptional activity is tightly regulated by KEAP1. NRF2 is retained in the cytoplasm under basal conditions and undergoes constant proteasomal degradation,

regulated by KEAP1-associated Cullin 3 complex. Upon stress, the cysteine residues of KEAP1 are modified, which triggers conformational change and abolishes NRF2 ubiquitination and degradation. Then, newly translated NRF2 can translocate to the nucleus, where it can regulate the transcription of genes[185] (Fig. I18).

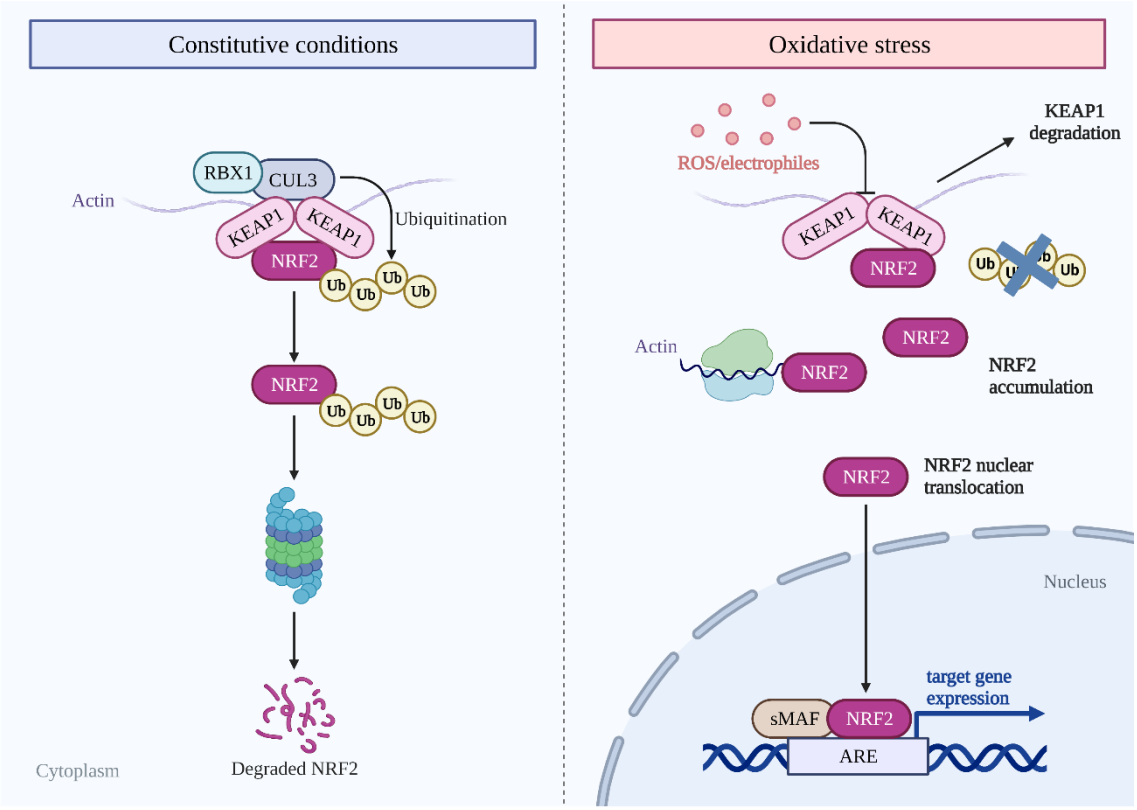

Figure I18. Schematic regulation of NRF2 activity. Description in the main text. Image created with BioRender.com.

The tight regulation of the activity of NRF2 is ensured by the presence of 7 distinctive Neh (NRF2-ECH) domains (Table 4, Fig. I19).

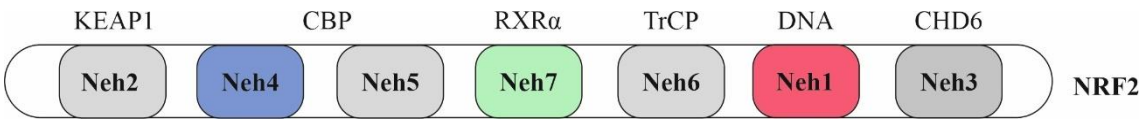

Figure I19. Domain structure of NRF2. The organisation of Neh domains in the order of NRF2 amino acids with their major interactors (image from Kloska, Kopacz et al., Vasc Pharm[190]). CBP – cyclic adenosine monophosphate response element binding protein; RXRα – retinoid X receptor alpha, TrCP – beta-transducin-repeat-containing protein; CHD6- chromodomain 6; DNA – deoxynucleic acid.

Domain	Amino acids	Description	Ref.
Neh1	435-562	Consists of CNC and bZIP regions; essential for DNA binding, contains nuclear localization and export signals, impacting the cellular localization of NRF2	[191]
Neh2	16-86	Contains ETGE and DLG motifs responsible for interaction with KEAP1	[192,193]
Neh3	563-602	C-terminal domain; enables interaction with transcriptional regulators	[194]
Neh4	112-132	Transcription activation domains, facilitate the recruitment of transcription regulators	[195,196]
Neh5	183-201		
Neh6	338-388	Contains DSGIS and DSAPGS motifs responsible for the interaction with β-transducing repeat-containing protein (β-TrCP), and the proteasomal degradation	[197]
Neh7	209-316	Can be bound by nuclear receptors to repress NRF2 activity	[198]

Table 4. The functions and the amino-acid location of NRF2 domains in human. The amino acid division is based on[199].

The fine-tuning of the redox balance seems to be pivotal for the well-functioning of CVS. The activity of NRF2 has already been described in the context of many disorders and mainly relies on the NRF2-related enhancement of the expression of detoxifying and cytoprotective genes. Its role has been mainly studied using chemical activators rather than genetic approaches. However, the reported data point to a protective impact of NRF2 in many cardiovascular settings. Furthermore, NRF2 can decrease the detrimental effects of acute injuries, such as myocardial infarction. On the other hand, the exact role of NRF2 in atherosclerosis is still controversial and strongly dependent on the cell type (Fig. I20, reviewed in Kloska, Kopacz et al., Vasc Pharm[190]).

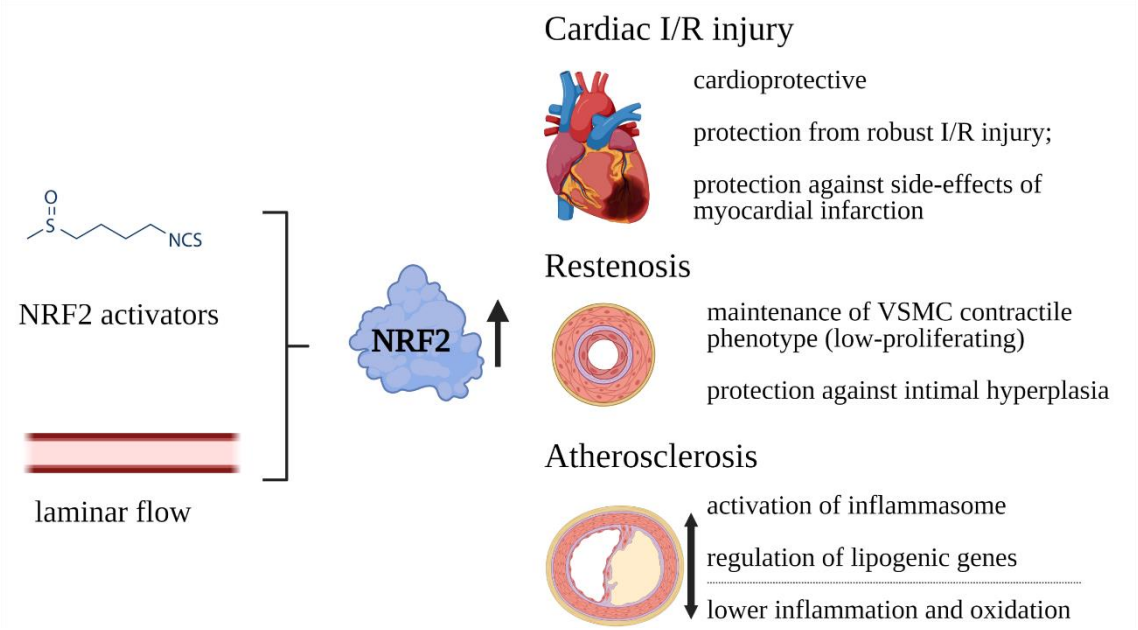

Figure I20. The summary of the impact of NRF2 enhancement on the CVD. NRF2 is induced either by laminar flow or by chemical activators and was shown protective in cardiac I/R injury and restenosis. In atherosclerosis, a dual role was observed (image created with BioRender.com based on information from Kloska, Kopacz et al., Vasc Pharm[190]).

The impact of NRF2 on the aneurysmal disease was studied using chemical activators, which were shown protective in aortic[200] and intracranial aneurysms[201]. As for plausible mechanisms, NRF2 activity decreased ROS level, affected SMCs phenotype, prevented their death, and decreased immune cell infiltration to the aortic wall. However, the NRF2-protective mechanisms in AAA settings may reach beyond the ROS-harnessing properties. NRF2 is a mechanosensitive transcription factor[202], activated only by laminar shear stress, which is considered to be protective[203]. Therefore, NRF2 is activated in several models, characterized by significantly altered biomechanics: hypertension[204], chronic pressure overload[205] and aortic constriction[206]. Moreover, Ang II induces NRF2 nuclear translocation[207].

As evidenced in models of other CVDs, NRF2 has a protective, function-enhancing impact on ECs and VSMCs (Fig. I21), which could alleviate vascular injury and prevent AAA formation. It can mitigate the inflammation by direct repression of transcription of interleukin 6 and 1β[208], or inhibition of mRNA stability of STING[209], a known innate immunity response regulator, which was recently reported as a trigger of AAA-related inflammatory response[210]. Furthermore, it emerges as a crucial regulator of extracellular matrix[211], hence could prevent vessel weakening, central to AAA formation. Still,

the exact NRF2 involvement and the responsible mechanisms in AAA have not been elucidated.

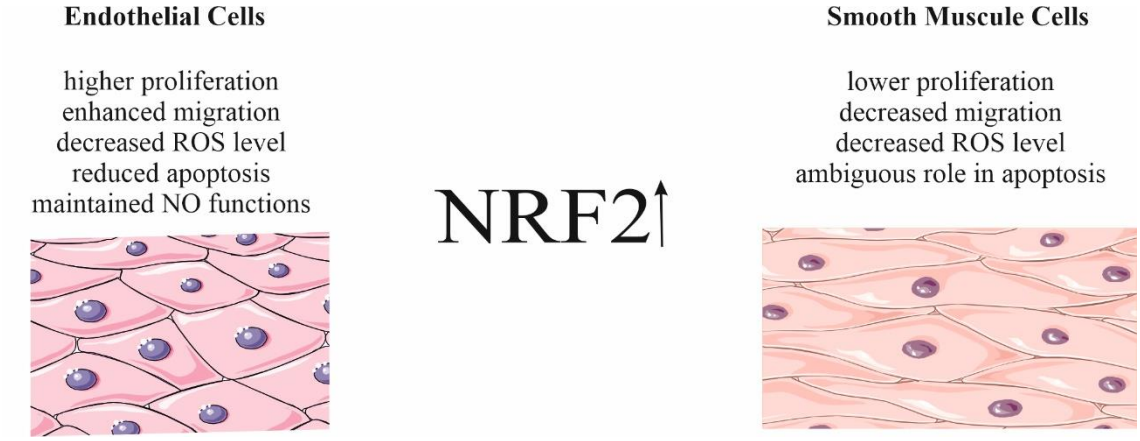

Figure I21. The summary of the influence of NRF2 on aortic endothelial and smooth muscle cells. (image from Kloska, Kopacz et al., Vasc Pharm[190]).

Furthermore, the last decade of research revealed the significant role of NRF2 in combatting ageing. NRF2 activity correlates with maximum lifespan (MLSP) in rodents[212], and in the most-long lived species (naked mole-rat), the expression of NRF2 at mRNA level is 6-fold higher in comparison to wild-derived mouse[213]. Importantly, the association between NRF2 signalling and ageing are universal between species: from worms to humans[214–219]. Although the extent of the deterioration of NRF2 signalling differs between tissues[190], for the cardiovascular system, there is a concise age-dependent decrease, as shown in rat aortas, monkey carotid arteries[220,221], and also human-derived primary aortic endothelial cells[222]. Notably, NRF2 activity rose 1.4-fold for every 10-year increase in longevity. Surprisingly, the researchers discovered that NRF2 protein levels did not correlate with MLSP. Instead, processes regulating NRF2 activity, such as KEAP1 expression, were strongly connected to MLSP[212].

KEAP1 - a moonlighting NRF2 regulator impacting ageing

KEAP1, encoded by the *KEAP1* gene, was discovered in 1999 as sensitive to electrophiles, NRF2-repressing protein[223]. Later studies defined it as an intracellular sensor of oxidants[224], which is executed by highly reactive cysteines surrounded by positively-charged, basic amino acids[225]. KEAP1 represents a sensor of environmental stress[226], creates an adaptive interface between the exposome and genome[227], and is a target for pharmacological modification as it has been comprehensively reviewed in[180,224]. These switching modifications are localized to many of 27 cysteines of (human) KEAP1. Mindful of the particular significance of the cysteine proteome in the adjustments of cellular response[227], KEAP1 grows into a conceivable critical governor of cellular fate.

Structurally, KEAP1 is a member of the BTB-Kelch protein family. The characteristic feature of this subset is the presence of two canonical domains in their structure: BTB (Broad-Complex, Tramtrack and Bric a brac) and Kelch domain[228,229].

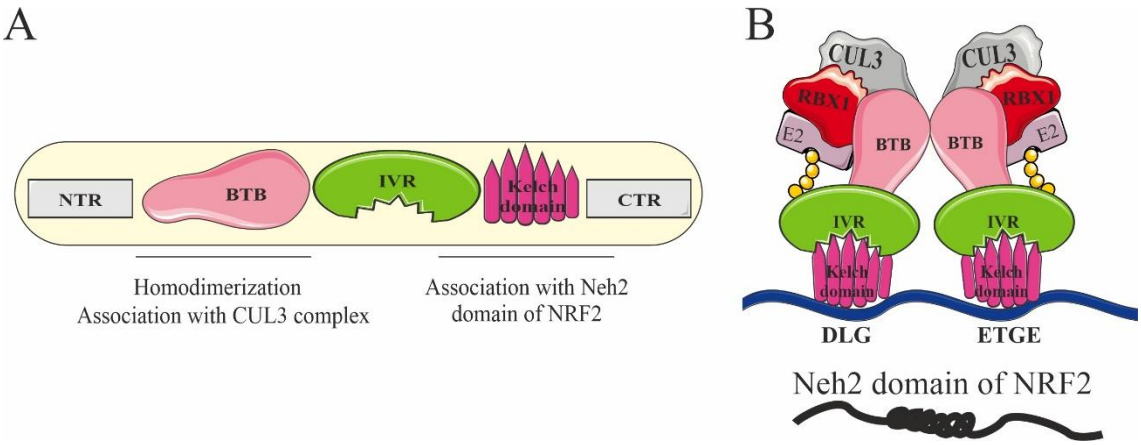

Figure I22. Domain structure and spatial organization of the KEAP1 protein. (A) domain organization of KEAP1, outlining the NRF2-related functions **(B)** spatial organization of KEAP1 dimer binding Neh2 domain of NRF2 (modified image from Kopacz et al., FRBM[230]).

Five distinct regions can be distinguished in the structure of KEAP1 (Fig. I22A), and the middle ones exhibit diverse functions (Table 5). The X-ray and cryogenic electron microscopy permitted the elucidation of KEAP1 spatial organization. KEAP1 resembles a cherry bob, where BTB domains form a stem, whereas IVR and Kelch domains are closely located and form the spherical "cherry" part"[231–235] (Fig. I22B).

Domain	a.a.	Description	Ref
BTB	61-179	Canonical domain; mediation of KEAP1 homodimerisation (crucial for NRF2 interaction); enables the interactions with the Cullin-3-RBX1-E3 ligase complex; involved in sensing electrophilic compounds, and nitric oxide (C151).	236
IVR	180-314	Cysteine-rich region; C273 and C288 are required for the repression of NRF2 nuclear accumulation and are responsible for sensing alkenes; C257, C272, C288, and C297, which are the direct redox sensors and targets for pharmacological activation of the pathway.	180,224,226,237–239
DGR, Kelch	315-598	Canonical domain; contains six repeats of the Kelch motif, which form a six-bladed β-propeller structure. Each blade of this structure (I-VI) is built of four-stranded antiparallel ß-sheets (A-D), which enable KEAP1 interactions with diverse proteins.	233

Table 5. The function of major domains of human KEAP1 with their amino acid location. The amino acid division is based on[199].

KEAP1 is expressed widely in various cell types and tissues[223] and mostly locates in the perinuclear region of the cytoplasm, the nucleus, endoplasmic reticulum and inclusion bodies[240–242]. Due to its reactive nature, KEAP1 undergoes many post-translational modifications, which serve as an alternative way of non-canonical NRF2 activation. Curiously, one of them, S-nitrosation, not only modifies the KEAP1 cysteine residues by attachment of NO moiety but is also directly dependent on KEAP1. KEAP1 directly interacts with nitric oxide synthase (NOS) and transnitrosating protein GAPDH (glyceraldehyde 3-phosphate dehydrogenase) to regulate S-nitrosation in mammalian cells. Deleting any protein of this complex inhibits protein S-nitrosation (Kopacz et al., Redox Biology[243]). When this modification is present on KEAP1, it modifies the interaction of NRF2 and KEAP1, resulting in the nuclear translocation of *de novo*-synthesised NRF2[226,244–246].

KEAP1 signature interacting protein is NRF2. Many approaches were used to explore this interaction, and it was discovered over time that NRF2 binds to KEAP1 in the stoichiometry 1:2. ETGE and DLG motifs recruit the NRF2 Neh2 domain to KEAP1[247]. Both motifs interact with the identical KEAP1 dimer residues (DGR/Kelch) but with

distinct binding affinities, most likely owing to variable acidic residue composition. ETGE has a 100-fold greater affinity than DLG[235,248]. Importantly, the binding of ETGE-containing proteins to KEAP1 can displace NRF2, preventing its degradation and allowing it to translocate to the nucleus[249,250]. Such interaction may also be possible when in the amino acid sequences of a given protein, two glutamic acid residues are separated by two other amino acids (EXXE) (Kopacz et al., Redox Biology[222]).

Over 25 KEAP1 interactors were verified by biochemical methods and further confirmed by mutations and the exchange of amino acids. Up to now, KEAP1 has an established role in the regulation of the cytoskeleton, proteostasis, mitochondria, and cell cycle progression. Moreover, it possesses a broad interactome and functions beyond NRF2 repression (Kopacz et al. FRBM[230]).

Recent studies have found that unregulated KEAP1 is deleterious to cellular homeostasis and highlighted the function of NRF2 as a regulator of KEAP1[222,243,251,252], suggesting that NRF2 and KEAP1 mutually inhibit each other. Notably, the absence of either NRF2[222,243,251,252] or KEAP1[253] seriously affects cellular and organismal homeostasis. The dysfunctions of cells lacking NRF2 can be entirely restored by deleting KEAP1 concurrently[222,243,251,252]. In line with this, the adverse consequences of KEAP1 depletion are reversed in NRF2/KEAP1 double knockout animals[253]. These results evidence that NRF2/KEAP1 balance is central in maintaining cellular well-being (discussed in [230]).

KEAP1 is reported to increase during ageing or in the models of premature senescence[222,243,254]. In accordance, KEAP1 overabundance and related massive S-nitrosation are responsible for the NRF2 deficiency-related senescence[243] and physiological ageing[222]. However, the exact role of KEAP1, in contrast to that of NRF2, in ageing has not been thoroughly addressed yet. The non-canonical functions of KEAP1 have a tremendous potential to be explored further, for example, in the context of age-related dysfunctions, when an imbalance between NRF2 and KEAP1 occurs[222].

miRNA-34a – a hallmark ageing-associated non-coding RNA

Contrary to the impact of KEAP1 on ageing, the involvement of microRNA-34a has already been widely studied, constituting it as a hallmark noncoding RNA (ncRNA) induced by senescence[255–258]. MicroRNAs (miRNAs) are non-coding RNAs that regulate gene expression by partnering with target mRNAs. MiRNAs can come from protein-coding gene introns or polycistronic gene transcript[259]. Transcribed by RNA

Polymerase II, pri-miRNAs are lengthy polyadenylated double-stranded precursors with a cap and stem/loop motifs. A complex consisting of Drosha endonuclease and its cofactor DGCR8 cleaves this pri-miRNA into pre-miRNA. The stem/loop shape product is 65-70 nucleotides long and is further transported to the cytoplasm by RanGTP-dependent exportin 5. There, Dicer endonuclease processes the stem/loop structure, forming an 18-24 miRNA duplex consisting of miRNA-5p and complementary miRNA-3p[260]. The targeted set of mRNA can be overlapping or distinct between these two complementary miRNA. For miRNA-34a, there is only a subset of overlapping genes. One of the strands is combined with a multiprotein complex called RISC (RNA-induced silencing complex), which contains an endonuclease Ago2, stabilising the miRNA:target mRNA complex. The recognition of target mRNA is based on the nucleotide. RISC, directed by miRNA, engages with the 3′-UTR or, in certain cases, the coding region of target mRNAs, blocking protein translation or decaying the mRNA target[261] (Fig. I23).

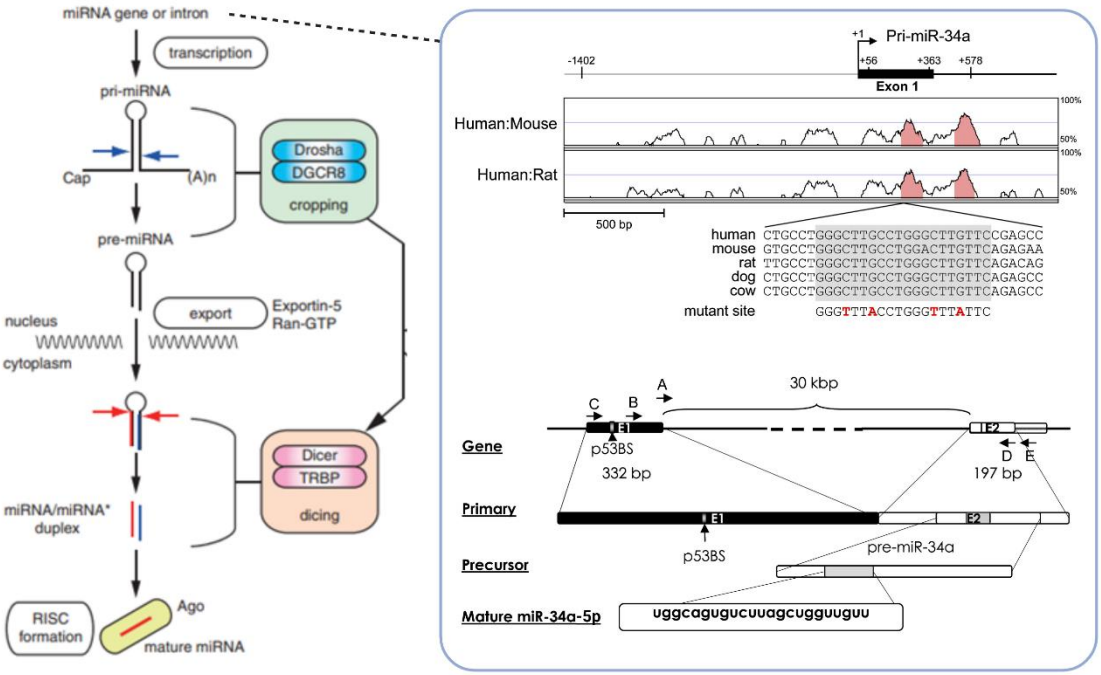

Figure I23. The general miRNA biogenesis pathway and the genomic location of miRNA-34a. Description in the text (images from[262–264]).

The main transcript encoding *MIR34A* has two exons, the second containing the *MIR34A* precursor. A p53-binding site is located inside a CpG island about 30 kb upstream of the mature *MIR34A* sequence in the first exon. Before processing the mature *MIR34A*, the main transcript undergoes splicing to remove the 30-kb intron[262,263]

(Fig. I23). This miRNA functions as an effector and amplifier of the p53 pathway[265], being induced by p53 and sharing similar targets. The transcription of *MIR34A* is also regulated by ELK1, SNAIL, ZEB1, STAT3, and HSF1[266]. Notably, miRNA-34a (1p36) genetic locus is frequently mutated in diverse human cancers. However, as for CVS, it leads to left-ventricular non-compaction cardiomyopathy, manifesting in, apart from heart defects, developmental delay and intellectual disability[267]. Loss of this genetic loci indirectly increases the level of precancerous MYCN[268].

miRNA-34a has been extensively studied in the context of tumorigenesis[269]. However, the mounting data indicates it may be a crucial regulator of CVS. The involvement of miRNA-34a in CVD has spurred a surge of interest. While its level is the highest in brain[270], it is also highly expressed in endothelial cells[257]. It is approximately 2-fold induced in the models of premature senescence[271]. Although there are many reports showing the miR-34a-related impact on CVS, if any possible mechanism is acknowledged, it is through the regulation of SIRT, its canonical target (Fig. I24). Moreover, its expression can be decreased by typical drugs used to treat vascular diseases, including metformin[272,273] and statins[274].

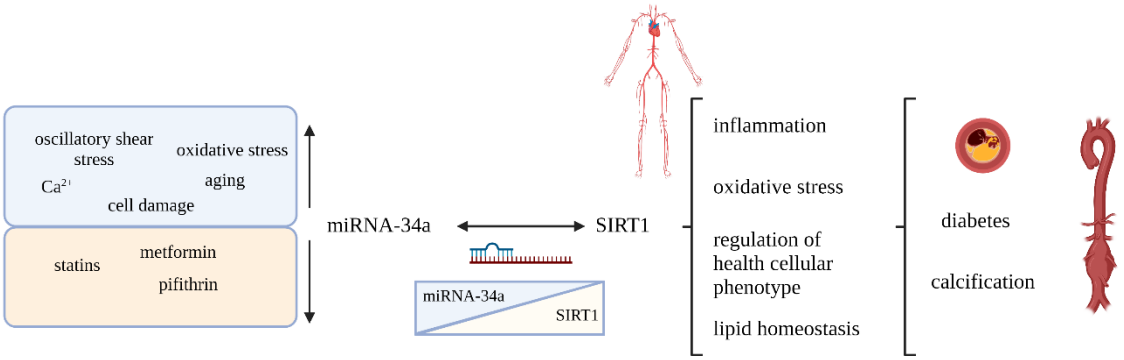

Figure I24. The interrelation of miRNA-34a and SIRT1 in the governance of the cardiovascular system. Image created with BioRender.com based on the papers cited in the text.

Moreover, miRNA-34a significance in endothelial cells is emphasised by its regulation by oscillatory shear stress, possibly contributing to increased inflammation in these conditions[275]. Interestingly, its level is regulated by NRF2 upon proatherogenic stimuli[276]. Although the global deletion of miRNA-34a does not trigger any obvious vascular developmental defects[277], the detailed histological analysis outlines some changes. The lack of miRNA-34a in young animals results in significantly thicker and more cellularly packed media. Accordingly, miRNA-34a knockout-derived SMCs proliferate more rapidly than the ones from wild-type animals, implying that miR-34a

may restrict cell division to maintain proper vascular homeostasis[278]. Conversely, the increase in miRNA-34a triggers senescence. In aged mouse aortas, miR-34a levels increase along with p16 and p21 expression and the SASP factor IL6[258]. The impact on proliferation mainly results from the vast number of miRNA-34a targets participating in the cell growth regulation through ERK and Raf[279].

MiRNA-34a expression is higher within the aneurysm compared to healthy human aorta[280]. It is also induced in the murine models of AAA[281]. Accordingly, its inhibition abrogates the formation of AAA in the hyperlipidaemic ApoE knockout mice[282]. Importantly, this research did not point out the exact cellular type conferring the protection. For instance, miRNA-34a is a regulator of smooth muscle phenotype in intracranial aneurysm[283]; however, given the alleged and likely protective impact on EC function[266], we cannot discard the potential role of ECs in the regulation of AAA[117,118]. Still, in light of the available data, we should suspect that maintaining a healthy EC phenotype will confer protection.

Aim

This research aims to define the mechanisms of ageing and dysfunction of endothelial cells underlying the development of cardiovascular diseases, particularly the abdominal aortic aneurysm - AAA. Based on our preliminary research and literature data, the central modulators of the cellular response to stress, NRF2 and microRNA-34a, are crucial regulators of ageing, endothelial cell biology and aortic function. Thus, they may have a decisive influence on the physiology of blood vessels and AAA.

In the frame of this doctoral dissertation, I would verify the following hypotheses:

- The NRF2-related premature ageing leads to significant structural changes in the aorta, which predispose to the development of AAA.
- The susceptibility of NRF2 tKO to AAA results from the overabundance of miRNA-34a in endothelial cells.
- The deficiency of miRNA-34a in endothelial cells facilitates the maintenance of their healthy phenotype and therefore protects against AAA.

Materials and methods

In vivo studies

Animals. The animals were maintained under a constant 14/10 h light/dark cycle at an environmental temperature of 22 ± 2°C. They were provided with food and water *ad libitum*, except for special procedures indicated in the detailed method description. For all animals studies, mice were handled in strict accordance with good animal practice, following the guidelines from Directive 2010/63/EU of the European Parliament on the protection of animals used for scientific purposes, local ethical committee approvals (mentioned in the procedure description), and the institutional recommendations. The age of the animals which were used in the study is indicated in the results section. They were genotyped prior to the study.

The following strains of animals were used:

1) Global NRF2 transcription knockout mice (C57Bl6/J NRF2 tKO)

NRF2-transcriptional knockout (tKO) mice, initially developed by Prof. Masayuki Yamamoto (Tohoku University, Japan)[183], were kindly provided to our Department by Prof. Antonio Cuadrado (Universidad Autonoma de Madrid, Spain). In these mice, the NRF2 DNA binding domain is replaced by LacZ gene, which abrogates NRF2 transcriptional activity[183].

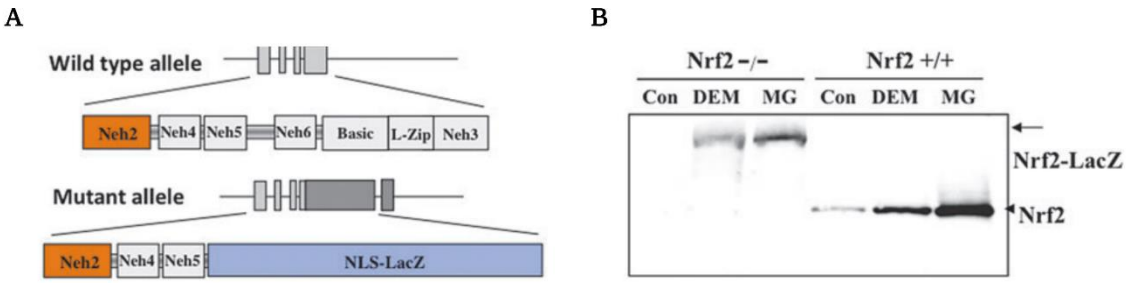

Figure M1. The occurrence of a fusion protein NRF2-LacZ in NRF2 transcriptional knockout mice. (**A**) To develop NRF2 transcriptional knockout mice, the carboxyl 280 amino acid residues of NRF2, including the DNA binding domain, were replaced by LacZ, thus resulting in the ability to express the remaining N-terminal 301 amino acids of NRF2 being linked to LacZ protein. (**B**) The presence of fusion protein in NRF2 tKO ($NRF2^{-/-}$) mice upon stimulation with known NRF2 stabilizers diethylmaleate (DEM) and proteasome inhibitor MG-132 (MG) (image from[284], data in B confirmed by our team in[251]).

Although worldwide these mice are referred to as NRF2 knockout mice (or NRF2 null mice), in fact this genetic manipulation leads to the appearance of fusion protein NRF2-β-galactosidase, which lacks transcriptional activity (TA) but still contains N-terminal fragment of NRF2, responsible for its repression by KEAP1[190,284,285] (Fig. M1).

The presence of NRF2-LacZ fusion protein has no effect on the detection of senescence-related β-galactosidase (Kopacz et al., Redox Biology[243]).

In order to maintain these mice on C57Bl6/J background, they were crossed back to the C57BL6/J strain every 10 generations in our animal facility. After obtaining homozygotic knockout mice, they were crossed between homozygotes for another maximal 5 generations. Such handling permits the generation of mice of comparable body weights in relation to wild-type counterparts.

2) miRNA-34a floxed mice (*Mir34a*$^{tm1.2Aven}$/J)

This strain was purchased from Jackson laboratory (strain: #018545). Originally the mice were created by Andrea Ventura (Memorial Sloan Kettering Cancer Center). A targeting vector was created with a loxP site upstream of the pre-miRNA-34a sequence and an frt-flanked neomycin resistance (neo) cassette downstream of the sequence, followed by the second loxP site. The neo cassette was deleted by the Flp-mediated recombination, leaving the pre-miRNA-34a sequence floxed. These mice were maintained on a mixed background (Fig. M2). Upon arrival to JAX, mice were bred to C57BL/6J inbred mice for at least one generation to establish the colony. In our hands, the mice were maintained as homozygotes and crossed with Cre recombinase-bearing strain for the targeted deletion of pre-miRNA-34a.

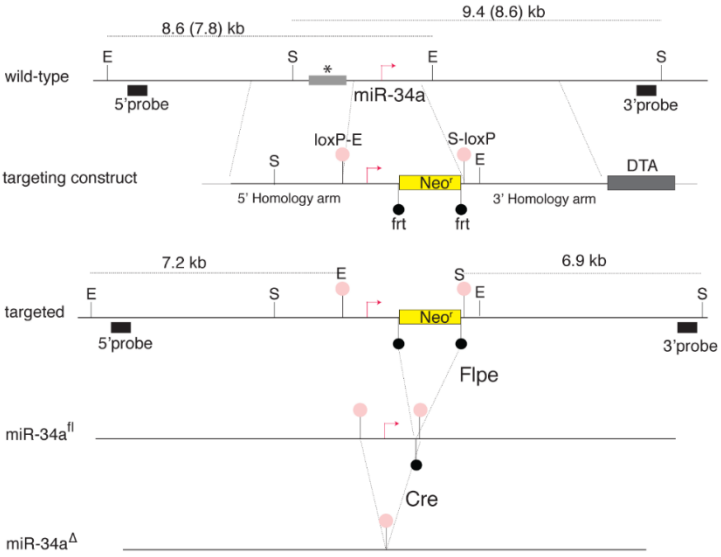

Figure M2. Scheme of generation of miRNA-34a floxed mice, the description in the text body (image from[277]).

3) Inducible endothelial specific Cre recombinase bearing mice (*Cdh5*(PAC)-CreERT2 mice)

These mice contain a tamoxifen-inducible Cre recombinase under the control of the vascular endothelial cadherin (VE-cadherin, *Cdh5*) promoter. The *Cdh5*(PAC)-CreERT2 mice were developed in the laboratory of Ralf Adams at the London Research Institute[286] and purchased from Taconic (strain 13073). Microinjecting a transgene comprising a genomic *Cdh5*(PAC) promoter region linked to a CreERT2 cDNA into C57BL/6 zygotes permitted the generation of the model. For at least five generations, the progenies were backcrossed to C57BL/6. In the FBBB animal facility, these mice were crossed between the progeny to maintain the presence of CreERT2 and, if needed, were crossed with other strains for the generation of inducible deletion models.

4) ROSA-Rainbow mice (R26VT2/GK3)

The Rainbow construct is introduced into the Rosa26 locus. The expression construct contains a ubiquitous CAG promoter, lox2272 site, loxN site, loxP site, EGFP, lox2272 site, mCerulean, loxN site, mOrange, loxP site and mCherry (Fig. M3). While EGFP expression is constitutive, the remaining reporters are only expressed following Cre-mediated recombination. The mice were generated in the laboratory of Irving Weissman (Stanford)[287].

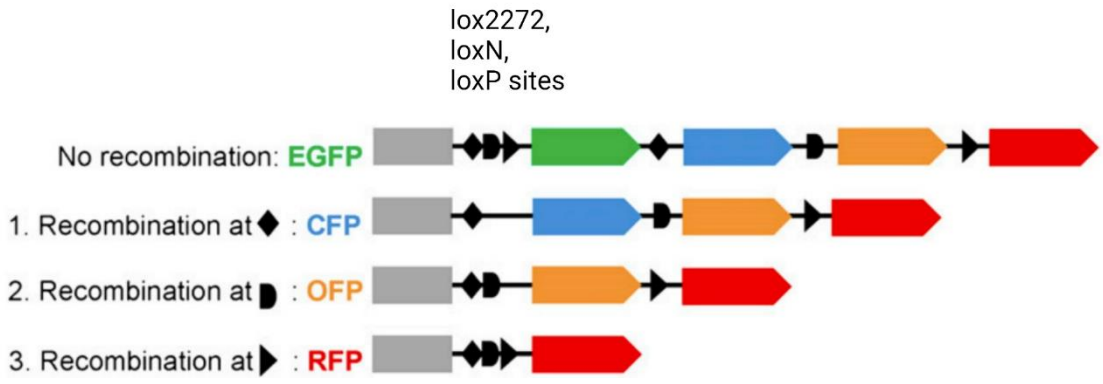

Figure M3. Schematic representation of the Rainbow construct and recombination-driven possible outputs depending on the lox site (image from[288]).

These 4 basic strains were used for further crossing to establish:

1) NRF2 transcriptional knockout mice with inducible EC-specific knockout of miRNA-34a (NRF2 tKO x miRNA-34a floxed x *Cdh5*-CreERT2)
2) EC-specific knockout of miRNA-34a (miRNA-34a^{EC-KO}, miRNA-34a floxed x *Cdh5*-CreERT2)

3) Inducible EC-specific lineage tracing Rainbow mice (ROSA Rainbow x *Cdh5*-CreERT2)

For breeding and experimental purposes, we followed several rules. The donor of Cre recombinase was always a male, and if mice were crossed further, it was possible up to the fifth generation (F5) (Fig. M4). For the final comparisons, we always compared Cre-bearing mice, which differed at the floxed gene site, to diminish the effect of tamoxifen on the aortic function[289].

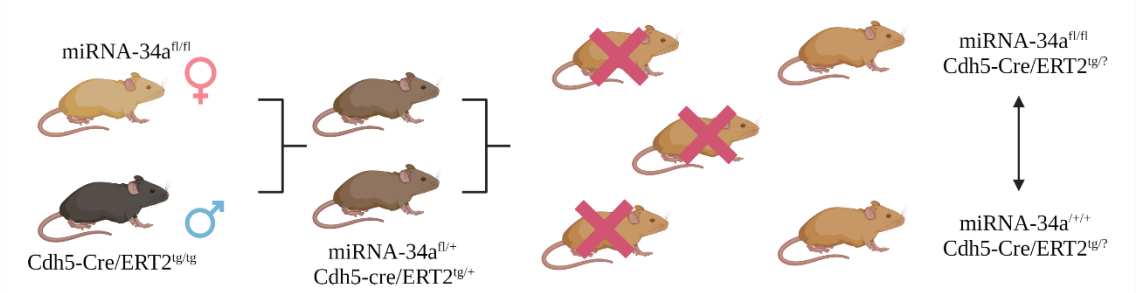

Figure M4. Example of the breeding strategy permitting the creation of inducible EC-specific knockout mice. As described in the text, the males were donors of Cre recombinase. Having obtained from one litter miRNA-34a$^{fl/fl}$ *Cdh*5-CreERT2^{tg} and miRNA-34a$^{WT/WT}$ *Cdh5*-CreERT2$^{tg/+}$, the mice were used for the experiments. Upon tamoxifen-induced recombination, EC-specific knockout of miRNA-34a was created from miRNA-34a$^{fl/fl}$ *Cdh5*-CreERT2^{tg} mice; as a control, we used miRNA-34a$^{WT/WT}$ *Cdh5*-CreERT2$^{tg/+}$.

Specific *in vivo* procedures

The animals of the aforementioned strains were used in the following procedures. The specific doses of used compounds are noted in Table 6.

Compound	Dose	Vehicle	Route of delivery
Angiotensin II (Bachem)	1000 ng/kg/min	Saline	osmotic pumps
Simvastatin (Sigma)	20 mg/kg/day	Saline	intragastric gavage
Rapamycin (Selleckchem)	5 mg/kg/day	EtOH in 5% Koliphor (Sigma) and 5% Tween-80 (Bioshop)	intraperitoneally
Tamoxifen (Sigma)	75 mg/kg/day	Corn oil (Sigma)	intraperitoneally
Rhodamine 6G (Sigma)	50 µg	saline	intravenous through retroorbital sinus
TNFa (R&D)	2 µg/kg	saline	intraperitoneally
Collagen type I (R&D)	75 µg/kg	saline	intraperitoneally
Epinephrine (Sigma)	30 µg/kg	saline	intraperitoneally
$FeCl_3$ (PoCh)	3%	water	topically
Ketamine (Bioketan, Vetoquinol)	10 mg/kg	saline	intraperitoneally
Xylasin (Sedazin, Biowet)	5 mg/kg	saline	intraperitoneally
Isoflurane (Isoflurin, Geulincks)	2-5%	air	inhalant
Paraformaldehyde (Santa Cruz Biotechnology)	1% or 4%	PBS	perfusion
Heparin (Polfa)	10 U/ml	PBS	perfusion

Table 6. The compounds used in the *in vivo* assays performed in the frame of this thesis.

Induction of Cre recombinase. In order to induce Cre-loxP recombination, the mice were injected intraperitoneally with tamoxifen for the subsequent 5 days. The mice were analysed 10 days after the last dose of tamoxifen, except for aneurysm studies, when the withdrawal period lasted 30 days. This procedure was accepted by II Local Ethical Committee in Kraków and used in approvals no.: 283/2020, 320/2020, 16/2021, 171/2021, 249/2021, 349/2021 and annexes to these approvals.

Induction of abdominal aortic aneurysm. The mice were infused *via* osmotic minipumps (Alzet) with angiotensin II or saline for up to 28 days. Osmotic pumps were placed subcutaneously under isoflurane anaesthesia, and the wound was closed with metal clips. Osmotic pumps were filled the day before and left overnight in saline at 37°C. This procedure was accepted by II Local Ethical Committee in Kraków and used

in approvals no.: 76/2016, 320/2020, 16/2021, 44/2021, 249/2021, and annexes to these approvals.

Blood pressure measurement. All mice underwent non-invasive blood pressure measurement by tail-cuff plethysmography (BP-2000 series II, Visitech Systems) after a period of adaptation and before the commencement of the treatment protocol. The results were presented as a percentage change compared to day 0 (after adaptation time and before the administration of any drugs). This procedure was accepted by II Local Ethical Committee in Kraków and used in approvals no.: 74/2016 and 249/2021.

***In vivo* ultrasound (US) imaging of abdominal aorta.** Changes in the abdominal aorta diameter were monitored using the high-frequency ultrasound imaging system (Vevo 2100, FUJIFILM VisualSonics). Two-dimensional (B-mode) imaging was done using a 22-55 MHz linear-array transducer (MS550D) synchronised to the electrocardiographic signal. The animals were placed in a supine position on a heated table under inhalation anaesthesia with isoflurane. The abdominal cavity was shaved, and a pre-warmed ultrasound gel was applied to the area of interest. Longitudinal images of the suprarenal and infrarenal aorta and transverse images at the level of the abdominal aorta between the diaphragm and the outlet of the left renal artery were acquired in the B-mode to assess the maximum cross-sectional diameter [mm] in real-time for each mouse at each time point (Fig. M5). This procedure was accepted by II Local Ethical Committee in Kraków and used in many approvals, e.x.: 74/2016, 249/2021, and 249/2021.

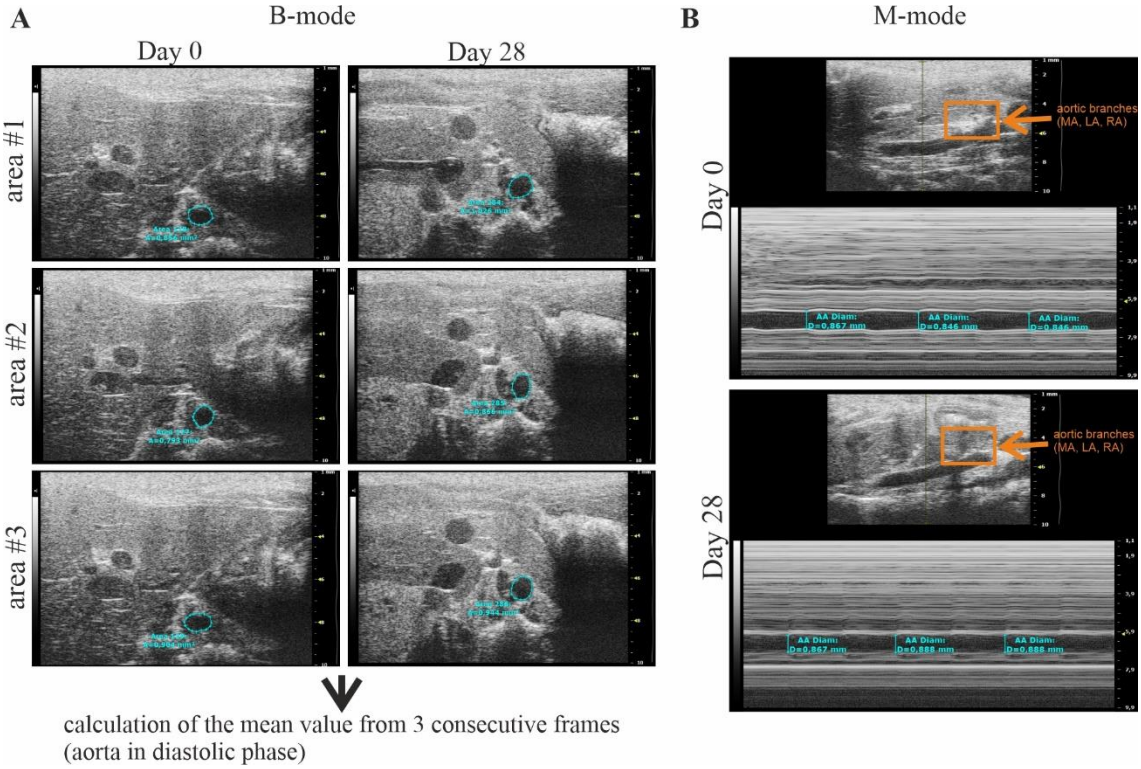

Figure M5. Example of US analysis. The description in the body text (image published in Kopacz et al., OMCL[290]).

Intravital assessment of leukocyte adhesion. The analysis was performed according to the previously used protocol[80]. 4 h before the experiment, the mice were injected with TNFα. After that time, the mice were anaesthetized with ketamine and xylazine. Upon confirmation of loss of pedal reflex, the mice were injected intravenously with rhodamine 6G. After 1 min, the abdominal cavity was opened, and the mesenteric venules were visualized gently using cotton buds. The mice were placed in the microscope, and the flow of leukocytes was recorded for 1 min in at least 3 parts of the mesentery using a fluorescent microscope (Nikon) (Fig. M6).

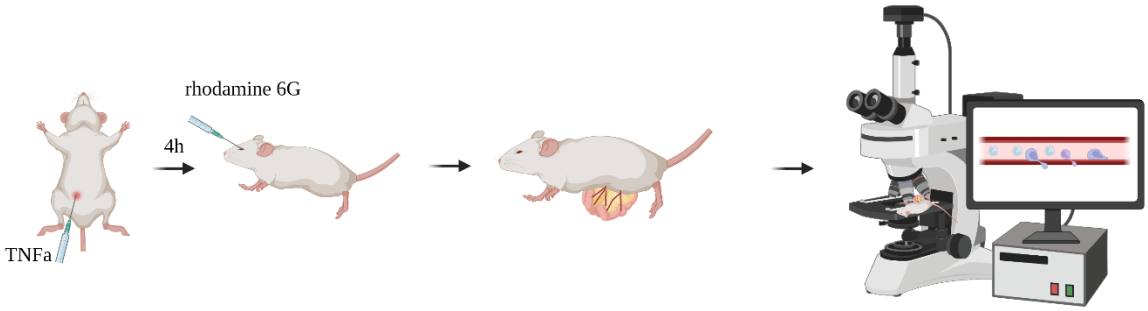

Figure M6. Schematic representation of the experimental setup for the assessment of leukocyte adhesion. Image created with BioRender.com.

After the procedure, the mice were euthanized by cervical dislocation. This procedure was accepted by II Local Ethical Committee in Kraków and used in approval no. 171/2021 and the annexe to this approval.

Induction of thrombosis by extrinsic pathways (collagen – epinephrine). The analysis was performed according to[292,293]. 4 h before the experiment, the mice were injected with TNFα. After that time, they were anaesthetized with ketamine and xylazine. Upon confirmation of the loss of pedal reflex, the mice were injected 10 µg of AF488-labelled anti-CD41 antibody into the retroorbital sinus. After 5 min, the mice were injected with collagen and epinephrine to induce thrombosis. After exactly 5 min, the mice were euthanized by cutting the spinal cord, and the vasculature was perfused through the right ventricle with 10 ml of 4% PFA. The lungs and aortas were collected for subsequent analyses (Fig. M7). This procedure was accepted by II Local Ethical Committee in Kraków and used in approval no. 171/2021 and the annexe to this approval.

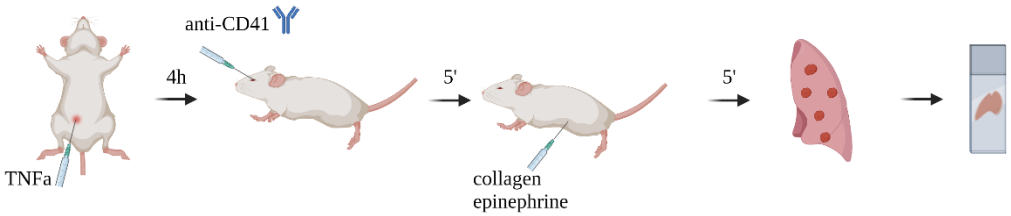

Figure M7. Schematic representation of the experimental setup for the assessment of prothrombotic phenotype. Image created with BioRender.com.

Ferric chloride ($FeCl_3$) induced thrombosis. The mice were anaesthetized with ketamine and xylazine. Upon confirmation of loss of pedal reflex, the carotid arteries (CA) were exposed and prepared for easy removal (sutures were placed on both sides of CA). The Whatman paper soaked in $FeCl_3$ was put on the left carotid artery for precisely 3 min. Upon that time, the flow to CA was abrogated, and CA was rapidly removed and immediately soaked in the 4% formaldehyde. The blood from the inferior vena cava was collected in the ratio of 9:1 to 3.8% sodium citrate to assess coagulation factors. The CA were fixed for 20 min, and then the remaining perivascular tissues were removed. The thrombus inside the CA was photographed under binoculars, and then the CA was frozen in an OCT medium for further histological analyses (Fig. M8). This procedure was accepted by II Local Ethical Committee in Kraków and used in approval no. 171/2021 and the annexe to this approval.

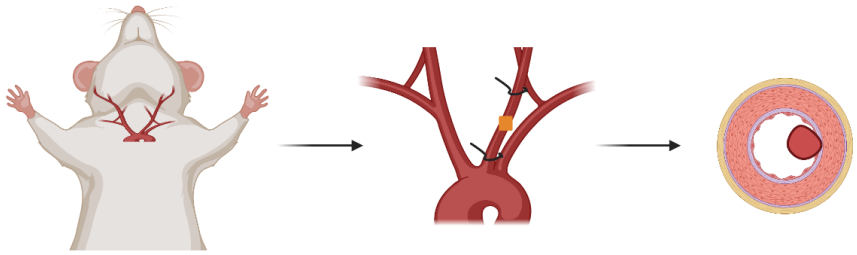

Figure M8. Scheme of the experimental setup for the analysis of ferric chloride-induced thrombosis in the carotid artery. Image created with BioRender.com.

Pulse wave velocity. Pulse wave velocity (PWV) measurements were performed in collaboration with Dr. Anna Bar and Prof. Stefan Chłopicki (Jagiellonian Center for Experimental Therapeutics), using a Doppler flow velocity system (Indus Instruments, Scintica Instrumentation) as described previously[294]. During Doppler measurements, the mice were anaesthetized using isoflurane. PWV was measured using two 20 MHz Doppler probes, simultaneously recording velocity signals from 2 sites, representing the thoracic and abdominal aorta. Aortic PWV was calculated by dividing the separation distance by the difference in arrival times of the velocity pulse timed with respect to the ECG. Signal analysis was performed using a Doppler signal processing workstation (version 1.625, Indus Instruments). This procedure was accepted by II Local Ethical Committee in Kraków and used in approval no. 166/2021.

Microvasculature assessment. For this terminal procedure, the mice were anaesthetized with ketamine and xylazine. Upon loss of pedal reflex, the abdominal aorta (just before the iliac arteries) was cannulated with a 22G catheter, perfused for 1 min with PBS with heparin, and then for 5 min with 4% PFA. Then aorta with perivascular fat was excised and used for further analyses. For the vasculature integrity assessment, 1 µg of Rhodamine-conjugated Wheat Germ Agglutinin was injected into the retroorbital sinus 3 min before the aorta cannulation and mice perfusion. This procedure was accepted by II Local Ethical Committee in Kraków and used in approval no. 172/2021.

Euthanasia and material collection. The mice were euthanised mainly by overdosing carbon dioxide. If needed, the blood was collected from either retroorbital sinus to tubes containing EDTA (for blood cell count assessed by ABC Vet Blood, Horiba) or from inferior *vena cava* (for serum). The organs were collected and either snap-frozen or further preserved in OCT freezing medium for histological staining or RNAlater (Sigma-Aldrich) for gene expression analysis.

Ex vivo studies

Subsequent analyses were performed on the collected material from the animals:

Immunofluorescent stainings. Immunofluorescent stainings were performed on frozen slides, cut on a cryostat (Leica) for specimens of variable thickness depending on the subsequent stainings. The samples were fixed as indicated in Table 7 (4% PFA or ice-cold acetone or ice-cold methanol for 10 min, washed 3 times with PBS, if needed, permeabilised (0.1% Triton X-100 for 10 min), and then blocked in 10% goat serum (GS) in PBS with 0.05% Tween-20, for 1 h at room temperature. After washing in PBS, the samples were incubated overnight (4ºC) with antibodies (Table) diluted in 1% GS in PBS with 0.05% Tween. On the next day, the samples were washed and, if needed, incubated with the host-specific antibodies conjugated with Alexa Fluor (AF) fluorophores (dilution 1:1000; IgG H+L, Life Technologies) and DAPI or Hoechst 33342 (1 μg/ml, Sigma-Aldrich) for 1 h at RT. The samples were analysed under a meta-laser scanning confocal microscope (LSM-880; Carl Zeiss).

Target	**Thickness**	**Fixation+ permeabilisation**	**Primary antibody**
CD31	10 μm	PFA+Triton	1:100, Biolegends, clone MEC 13.1, AF647 conjugated
αSMA	10 μm	PFA+Triton	1:500, Abcam, AF488-conjugated
CD45	40 μm	no	1:100, BD, clone 30-F11, APC-conjugated
CD64	40 μm	no	1:100, BD, Clone X54-5/7.1, PE-conjugated
Collagen I	20 μm	acetone	1:250, Abcam
Collagen III	20 μm	acetone	1:250, Abcam
P-ERK	20 μm	methanol	1:100, CST
MMP-9	8 μm	acetone	1:100, CST

Table 7. The details of the immunofluorescent staining protocol, including the thickness of the sample, fixation/permeabilisation method and the antibodies used.

En face **immunofluorescent stainings**. For *en face* immunostaining (Fig. M10), the mice were perfused with 4% PFA. The whole aorta was removed, gently cleaned of perivascular fat and fixed for 15 min with 4% PFA. Next, aortas were incubated for 3 h in blocking (5% goat serum, 1% BSA in PBS) or blocking permeabilising buffer (0.3% Triton X-100, 5% goat serum, 1% BSA in PBS) and then incubated overnight with the antibodies diluted in 3% BSA. After that, the aortas were washed 3 times and, if needed, incubated with the host-specific antibodies conjugated with AF fluorophores (dilution 1:1000; IgG H+L, Life Technologies) and DAPI (1 μg/ml, Sigma-Aldrich)

for 2 h at RT (Tab. 8). After 3 series of washing, the aortas were opened, intima facing up and mounted with Dako Fluorescence Mounting Medium (Dako). High-resolution images were taken using a meta-laser scanning confocal microscope (LSM-880; Carl Zeiss). By modulating the Z-axis, we could focus on different types of cells. The final distinction was based on the nuclear shape, round for endothelial cells and significantly elongated for smooth muscle cells (Fig. M10).

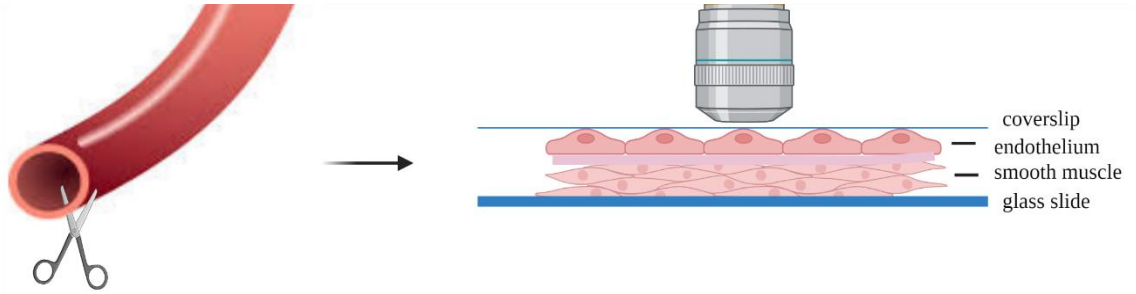

Figure M10. Schematic representation of the aorta preparation and imaging in case of *en face* stainings. The aorta is cut longitudinally, opened and put on the slide with intima opposing the coverslip. Image created with BioRender.com

Staining	**Blocking/permeabilisation buffer**	**Antibody/Detection compound**
CD31	blocking	AF647-conjugated; anti-CD31 antibody, clone MEC 13.3, Biolegends
AT1R	blocking	ATTO-550- conjugated anti-AT1R antibody, allomone labs
actin	blocking+permeablisation	Phalloidin-iFluor647 Reagent (Abcam)
Glycocalyx (its components N-acetyl-D-glucosamine and sialic acid)	blocking	Wheat Germ Agglutinin, Rhodamine conjugate (Vector Labs)

Table 8. The *en face* immunofluorescent staining protocol details, including the permeabilisation method and the used detection reagents.

Histological stainings. They were performed on frozen slides embedded in OCT medium (Leica), which were cut on a cryostat (Leica) for specimens of variable thickness depending on the subsequent stainings (Tab. 9). After staining, the specimens were dehydrated by subsequent incubations for 1 min in increasing concentrations of ethanol (70%, 96% twice, 99.8% twice) and xylene (twice). After that, the samples were mounted in Histofluid (Marienfeld). The samples were analysed under a light microscope (Nikon) with NIS elements BR software (Canon).

Staining	Thickness	Procedure
HE	8 µm	1. Staining for 14 min in Mayer's Haematoxylin (Sigma-Aldrich). 2. Washing for 5 min with tap water. 3. Staining with eosin (Sigma-Aldrich) for 90 s.
Trichrome	8 µm	1. Incubation in preheated Bouin's Solution (Sigma-Aldrich) at 56°C for 15 min. 2. Washing in running tap water for 5 min. 3. Staining in Mayer's Hematoxylin for 5 min. 4. Washing with tap water for 5 min followed by immersion in distilled water. 5. Staining in Biebrich Scarlet-Acid Fuchsin (0.9% Biebrich Scarlet, 0.1% acid fuchsin in 1% acetic acid; Sigma-Aldrich) for 5 min. 6. Rinse in deionized water 7. Differentiation in 2.5% Phosphotungstic/2.5% Phosphomolybdic Acid Solution for 5 min. 8. Staining in 10% Aniline Blue Solution for 5 min. 9. Incubation in 1% Acetic Acid for 2 min.
Elastin (Verhoeff - van Gieson)	5 µm	1. Staining in Verhoeff's solution (3% hematoxylin, 2.5% ferric chloride, 0.5% potassium iodine, 0.25% iodine) for 1 h. 2. Rinse in tap water for 5 min. 3. Differentiation in 2% ferric chloride for 1 min. 4. Washing in tap water for 5 min. 5. Incubation with 5% sodium thiosulfate for 1 min. 6. Washing with running tap water for 5 min. 7. Staining in Van Gieson's solution (1% aqueous acid fuchsin in saturated picric acid) for 3-5 min.

Table 9. The detailed protocols, including the specimen thickness, of the histological analyses.

Detection of SA-β-gal activity. Aortas were fixed for 3 min with 4% formalin, washed twice with PBS and incubated overnight with a staining solution (5 mM potassium ferricyanide, 5 mM potassium ferrocyanide, 150 mM NaCl, 2 mM $MgCl_2$, 1 mg/ml X-gal in citrate buffer pH 6). The next day, the aortas were washed with PBS and photographed as a whole mount and in *en face* projection (under the binocular). To depict the vascular layer, the aortas were embedded in OCT freezing medium, frozen, and the aortic specimens were cut on cryostat for further immunofluorescent staining with CD31, αSMA antibodies as indicated above. The images were taken in the brightfield and fluorescence using a confocal microscope LSM 880 (Zeiss).

***In situ* zymography (ISZ).** *In situ* gelatinolytic activity was performed in frozen abdominal aorta cut into 8 μm specimens as described previously[295]. Aortic sections of 8 μm were incubated in a dark-wet chamber for 2 h at 37ºC with a 20 μg/ml stock solution of fluorescein-conjugated, dye-quenched gelatin from pig skin (DQ™-gelatin, Thermo Fisher) diluted in gelatinase reaction buffer (150 mM NaCl, 5 mM $CaCl_2$, 0.2 mM NaN_3, 50 mM Tris-HCl, pH 7.6). Next, slides were washed three times in water and used for subsequent immunofluorescent detection of MMP-9 following the regular immunofluorescent staining protocol as indicated above. The specificity of the ISZ protocol was confirmed through two types of negative controls. In the first control (gelatinase activity blockage), samples were preincubated for 1 h at 37ºC with 1 mM 1.10-phenanthroline dissolved in gelatinase reaction buffer, then washed with PBS, and incubated with the working solution for DQ-gelatin and stained for MMP-9 as described above. The second negative control (autofluorescence control) was prepared by covering unfixed samples with the working solution for DQ-gelatin, which was immediately frozen at -20ºC and kept there for 2 h.

***In situ* hybridization (ISH).** The aortas (or aortic specimens cut on a cryostat to 10 μm) were fixed in 4% PFA for 10 min, washed with PBS, digested for 8 min with 20 μg/ml Proteinase K in Digestion buffer (50 mM Tris HCl pH 7.4, 1 mM EDTA pH 8.0), followed by 5 min wash with 0.2% glycine in PBS. After PBS wash, the aortas were refixed for 10 min with 4% PFA and then washed twice with PBS. For the acetylation step, the aortas were treated for 10 min first with 0.1 M Triethanolamine pH 8 (Sigma-Aldrich), then with 0.1 M triethanolamine with 0.25% acetic acid, which was followed by PBS wash twice. For the hybridization step, the stock 3'DIG-labelled probes (scrambled (included in miRCURY LNA Control Set - Qiagen); miRNA-34a custom probe YD00618250-BEG)) were diluted to 25 μM in Hybridisation buffer (50% formamide, 5x SSC (saline-sodium citrate salts, Thermo Scientific), 5x Denhardt's solution (Thermo Scientific), 500 mg/ml salmon sperm DNA (Thermo Scientific), 250 mg/ml tRNA (Thermo Scientific)), denatured for 5 min in 85°C, and then, after cooling, placed on the aortas for the overnight hybridization at 50°C. On the next day, the aortas were washed for 5 min at RT with 5xSSC, followed by a 30 min wash with 20% Formamide/0.5x SSC at the hybridization temperature. Afterwards, the aortas were washed for 5 min with TBST buffer (0.1% Tween in TBS), then blocked with Blocking Buffer (10% sheep serum in TBST) for 1 h. Then the next steps of the protocol

differed depending on the used aortic samples. Whole mount aortas were used for fluorescent staining and thus incubated overnight with Rhodamine-conjugated anti-DIG (digoxygenin) antibody (Roche, 1:500) and AF647-coupled anti-CD31 antibody (clone MEC13.3, Biolegends, 1:100) diluted in Blocking Buffer. The following day, the aortas were counterstained with DAPI, washed with PBS, opened longitudinally and mounted with Dako Fluorescence Mounting Medium (Dako). For the conventional miRNA ISH protocols, the aortic sections were incubated overnight at 4ºC in a water-humidified chamber with anti-DIG-AP antibody (anti-digoxygenin antibody coupled with alkaline phosphatase) diluted in Blocking Buffer (Roche, 1:500), followed by 3 washes with TBST (5 min each) on the next day. Then the slides were incubated in staining solution (175 µg/ml BCIP (5-bromo-4-chloro-3-indolyl-phosphate), 338 µg/ml NBT (4-nitro blue tetrazolium chloride)) at 32ºC for 4 h, followed by a wash in TBST and final fixation in 4% PFA for 10 min. If not specified, all the reagents were from Sigma-Aldrich.

Total RNA isolation, reverse transcription and quantitative PCR. RNA from 5 mm of abdominal aortic tissue was extracted with the RNeasy Mini Kit (Qiagen) according to the manufacturer's instructions. cDNA was synthesised using a High-Capacity cDNA Reverse Transcription Kit (Thermo Fisher Scientific), and then the cDNA concentration was adjusted. RT-qPCR was conducted on 30 ng of cDNA Step-One Plus Real-Time PCR Systems using a Power SYBR® Green PCR Master Mix according to the manufacturer's instructions (Thermo Fisher Scientific). Eukaryotic mouse translation elongation factor 2 (*Eef2*) was used as a reference gene. Relative expression was calculated using the ΔΔCt method. Primer sequences are gathered in Table 10.

Serum miRNA isolation. miRNA was isolated from 400 µl of mice serum using miRNeasy Serum/Plasma Kit (Qiagen) according to the attached protocol. Reverse transcription reaction was carried out using Mistiq microRNA and cDNA Synthesis mix (Sigma-Aldrich) and following the vendor's instructions. Quantitative RT-PCR was performed in a StepOnePlus real-time PCR system (Applied Biosystems) using SYBR Green PCR Master Mix (Sigma). Primer sequences: miR-34a: 5'- GCCTGGCAGTGTCT TAGCTGGTTGT -3', U6: 5'- CGCAAGGATGACACGCAAAT -3'.

Gene	Primer sequence
Mouse *Eef2*	Forward: 5'- GACATCACCAAGGGTGTGCA -3' Reverse: 5'- TCAGCACACTGGCATAGACC -3'
Mouse *Vcam1*	Forward: 5'- CCGGCATATACGAGTGTGAA -3' Reverse: 5'- GATGCGCAGTAGAGTGCAAG -3'
Mouse *Sele*	Forward: 5'- ATGCCTCGCGCTTTCTCTC -3' Reverse: 5'- GTAGTCCCGCTGACAGTATGC -3'
Mouse *Col1α1*	Forward: 5'- ACTACCGGGCCGATGATGCTAACG -3' Reverse: 5'- CGATCCAGTACTCTCCGCTCTTCC -3'
Mouse *Col1α2*	Forward: 5'- GCCACCATTGATAGTCTCTCC -3' Reverse: 5'- CACCCCAGCGAAGAACTCATA -3'
Mouse *Col3α1*	Forward: 5'- ATCTATGAATGGTGGTTTTCAGTT -3' Reverse: 5'- TTTTGCAGTGGTATGTAATGTTCT -3'
Mouse *Col4α1*	Forward: 5'- CAGATTCCGCAGTGCCCTA-3' Reverse: 5'- GGAATAGCCGATCCACAGTGAG -3'
Mouse *Mmp2*	Forward: 5'- ACAGGACATTGTCTTTGATG -3' Reverse: 5'- TACACAGCGTCAATCTTTTC -3'
Mouse *Mmp3*	Forward: 5'- CTAAAAGCATTCACACCCTG -3' Reverse: 5'- TTTCTTCTCATCAAACCTCC -3'

Table 10. The primer sequences used in the study.

Atomic force microscopy (AFM) nanoindentation. After cleaning from perivascular fat, the abdominal aorta was cut into small patches to expose the inner wall of the aorta. The aortas were prepared like for en face staining and glued to the glass using Cell-Tak (BD Biosciences). After preparation, the samples were placed in Krebs-HEPES buffer pH 7.4 (100 mM NaCl, 4.7 mM KCl, 1.2 mM $MgSO_4$, 1 mM KH_2PO_4, 2.5 mM $CaCl_2$, 25 mM $NaHCO_3$, 5.6 mM glucose, 20 mM HEPES) for 1 hour. Then the buffer was changed to Hanks' balanced salt solution (HBSS) supplemented with 1% fetal bovine serum (EURx), 1% penicillin/streptomycin, and 5 mmol/L glucose. If not specified, all the reagents were from Sigma-Aldrich. AFM nanoindentation experiments were performed with a NanoWizard III system (JPK, Germany). We used a spherical colloidal (4.5 μm diameter, NovaScan), attached to a cantilever with a spring constant of 0.01 N/m. The indentation curves were recorded for a maximal loading force of 1 nN at a velocity of 1.5 μm/s. For each aorta sample, spatial maps of indentation curves were recorded at many random positions of the sample. Typically, each region of interest comprised 100 curves that were recorded on a 20×20 μm area. If needed, for the better resolution, the size of grids was increased. The analysis was performed following the published protocol by Dr. Marta Targosz-Korecka[296]. For the analysis of glycocalyx

Krebs-HEPES buffer was supplemented with 2% serum of collected form analysed mouse. The extraction of different parameters (corresponding to different parts and layers of the aorta) was based on the range of nanoindentation.

Assessment of Endothelial NO production in the isolated aorta using Electron Paramagnetic Resonance. NO measurements were carried out on the abdominal aorta by EPR spin-trapping with diethyldithiocarbamic acid sodium salt (DETC). Krebs–HEPES buffer pH 7.4 (100 mM NaCl, 4.7 mM KCl, 1.2 mM $MgSO_4$, 1 mM KH_2PO_4, 2.5 mM $CaCl_2$, 25 mM $NaHCO_3$, 5.6 mM glucose, 20 mM HEPES) was deoxygenized by bubbling argon. 10 mM DETC and 1 mM $FeSO_4$ were separately dissolved under argon gas bubbling in ice-cold Krebs–HEPES buffer. One half (upper segment) of freshly harvested aortas was cleaned from adherent tissue, opened longitudinally, and placed in a place filled with Krebs–HEPES buffer and preincubated for 30 min at 37°C. DETC and $FeSO_4$ solutions were mixed 1:1 (v/v) and added to the well in 2.5x higher volume than the preincubation one (it was not removed). Then immediately 1 μM calcium ionophore (eNOS stimulator) A23187 (Sigma-Aldrich) was added to well with aortas and subsequently incubated at 37°C for 90 min. After incubation, each aorta drained on a piece of kimwipe, and weighted. Then, they were frozen in liquid nitrogen in Krebs–HEPES buffer and stored at -80°C until the measurements. They were performed using an EMX Plus Bruker spectrometer (Bruker). The resulting spectra were collected and analyzed with WinEPR Processing software (Bruker BioSpin GmbH). The NO-$Fe(DETC)_2$ signal was a clear triplet centered at g = 2.039 and was quantified as the amplitude normalized to the weight of tissue[297]. If not specified, all the reagents were from Sigma-Aldrich. The analysis was done in cooperation with Dr. Anna Bar and Prof. Stefan Chłopicki from the Jagiellonian Center for Experimental Therapeutics.

Scanning electron microscopy (SEM) imaging of aorta ultrastructure. 40 μm unfixed specimens of OCT-frozen abdominal aortas were used to assess the changes in their ultrastructure. SEM high-resolution pictures were taken by FIB / (E)SEM Dual Beam Microscope Quanta 3D FEG in environmental mode (pressure 100 Pa). Images were collected by GSED detector using 5 keV energy-bearing electrons, while the specimen was kept at RT at pressure of 100 Pa of water vapor. The occurrence of intimal SEM-depicted alteration was quantified by macroscopic scoring ranging from 1 to 10, where each incremental number reflected a steeping percentage of intimal cells

with alterations by 10%. SEM imaging was done in cooperation with Dr. Konrad Szajna and Prof. Franciszek Krok from the Institute of Physics, Jagiellonian University.

Assessment of aortic proteome by mass spectrometry. Abdominal aortas were disrupted mechanically and with sonication (Bioruptor, 30 cycles 30s/30s on/off, 8 °C) in in 600µl of lysis buffer (6M guanidine chloride, 100mM Tris, 10mM TCEP (tris(2-carboxyethyl)phosphine), 50mM CAA (chloroacetamide), and protease inhibitors (MSSAFE-1VL)). After centrifugation (20 min, 16 000g), the supernatant was collected (named soluble fraction). Then the pellet was resuspended in 200 µl of lysis buffer II (6M guanidine chloride, 300mM NaCl, 100mM Tris), incubated at 96°C for 10 minutes with shaking (1000 rpm). After centrifugation (20 min, 16 000g) the supernatant was collected (named insoluble fraction), and the pellet was discarded. 100µl of each fraction was taken and submitted to cold acetone precipitation. Four volumes (400µl) of acetone were added to the samples and incubated for 60 min at -20°C, followed by centrifugation (10 min, 16 000g). The pellet was resuspended in 50 µl of digestion buffer: (6M urea, 100 mM ammonium bicarbonate, 1 µg of LycC/Trypsin mix (Promega V5071)), vortexed (800 rpm, 37°C, 4h), then 300 µl of 25mM ammonium bicarbonate was added and samples were vortexed one more time (800 rpm, 37°C, overnight). Samples were acidified with 10 µl of 5% TFA (trifluoroacetic acid). The resulting peptide mixture was purified at Oasis HLB 10 mg sorbent (Waters) 96-well plates, vacuum-dried, and suspended in 40 µl of 2% acetonitrile, 0.1% TFA. Samples were measured in an online LC-MS setup of EvosepOne (Evosep Biosystems) coupled to an Orbitrap Exploris 480 (Thermo Fisher Scientific) mass spectrometer following a previously published protocol[298]. If not specified, all the reagents were from Sigma-Aldrich. Raw data were analyzed with PEAKS X Studio and searched against mouse reference proteome, taking into account preparation methodology (digestion: trypsin semispecific, maximum two missed cleavages, fixed modification: carbamidomethylation, FDR 1%). Proteins identified as differing groups have been analyzed in terms of belonging to individual pathways with the Reactome platform. To get more insight into the oxidative stress environment of each biological condition, the normalized intensity level of oxidized peptides identified with Peaks_PTM mode was compared.

Analysis of cholesterol content by Time-of-flight secondary ion mass spectrometry (TOF-SIMS). The analysis of the dried *en face* abdominal aorta specimen placed on a

silica plate was carried out using the ToF-SIMS V instrument (ION.TOF GmbH, Munster, Germany) equipped with a 30 keV bismuth (Bi_3^+) primary ion gun. A dual-beam mode was used for the determination of the depth distribution of the components in the aortas. The samples were sputtered with a C60 ion beam (10 keV eV, 0.6 nA) rastered over a 500 μm × 500 μm area and the positive ion spectra were collected from crater center using a focused bismuth beam (Bi_3^+, 0,5 pA) rastered randomly over a 150 μm × 150 μm area. The data analysis was performed for the signals collected from 50 sequential cycles, each consisting of 2 frames of analysis with $Bi3^+$, followed by a 1 frame of sputter. The assessment of cholesterol was based on $C_{27}H_{45}^+$ peaks.

Assessment of the angiogenic capacity of aortic explants. For this assay, the mice were euthanised by carbon dioxide. Afterwards, fibrinogen solution (2 mg/ml, Sigma-Aldrich) was prepared in Endothelial Basal Medium (EBM-2) containing 2% FBS and 15 μl of thrombin (50 U/ml, Sigma-Aldrich) solution. The fibrin gel was left for a partial polymerization for 5 min in the RT, and then the aortic explants were mounted on it. The fibrin gel was allowed for a final polymerization for 15 min at 37°C, with 5% CO_2. 0.5 ml of EBM-2 medium containing stimulants was added to the top of the fibrin clot and incubated for 3 days. On day 3, the pictures of aortic explants were taken using a Nikon Eclipse TE 2000-U microscope fitted with a camera.

In vitro studies

Cell culture. Human aortic endothelial cells (HAECs) isolated from a 21-year-old female donor (Gibco, Life Technologies) were used in the study. HAECs were grown in EBM-2 (Lonza) supplemented with EGM-2MV SingleQuot Kit Supplements & Growth Factors without antibiotic (Lonza) and 10% foetal bovine serum (FBS) (EURx). Cells were cultured at 37°C in a humidified incubator in a 5% CO_2 atmosphere. The cells used in all experiments were between passages 5 and 14 to exclude the impact of senescence caused by prolonged cell culture.

Stimulation of cells. The cells were stimulated with 500 nM Ang II for 6 h in EGM-2MV medium.

Transfection. HAECs were transfected either with 20 nM siRNA (against human *NFE2L2* (Life Technologies, s9493), *TP53* (Life Technologies, s605), *PDGFRA* (Life Technologies, s10236), *PDGFRB* (Life Technologies, s10242) or scrambled siRNA (Life

Technologies 4390846)) or 10 nM anti-miRNA-34a-5p (AM11030), pre-miRNA-34a-5p (AM17100) or negative anti-miR (AM17010) using Lipofectamine™ RNAiMAX Transfection Reagent (Life Technologies) in Opti-MEM I Reduced Serum medium (Life Technologies). The experiments were performed 48 h after transfection. The transfections of more than one target were performed concomitantly.

Detection of SA-β-gal activity. The cells were fixed for 3 min with 4% formaldehyde, washed twice with PBS and incubated overnight with a staining solution (5 mM potassium ferricyanide, 5 mM potassium ferrocyanide, 150 mM NaCl, 2 mM $MgCl_2$, 1 mg/ml X-gal in citrate buffer pH 6). The next day, the cells were washed with PBS and stained with Hoechst 33342 to detect nuclei. The images were taken in the brightfield and fluorescence using a fluorescent microscope (Nikon).

Immunofluorescent staining. The cells were fixed for 8 min in 4% paraformaldehyde, permeabilized with 0.2% Triton X-100 in PBS for 20 min and blocked with 10% goat serum for 1 h. The cells were incubated with anti-PCNA antibody (Life Technologies) in 3% bovine serum albumin overnight at 4^{o}C. The next day, the cells were incubated with secondary Alexa Fluor 568-labelled anti-mouse antibody (Invitrogen) and DAPI to stain the nuclei.

Fibrin Bead Assay. For the assay, ~ 1 million of HAECs were added to the glass FACS tube containing 2 ml of EGM-2MV medium and ~1000 Cytodex 3 microcarrier beads (GE Healthcare Life Sciences). Then the tubes were incubated (37°C, 5% CO_2) for 6-8 h and gently agitated every hour. After the indicated time, the suspensions with beads were transferred to a T-25 flask with 3 ml of fresh EGM-2MV medium. The flask was then incubated overnight, allowing to attach the suspended cells at the bottom of the flask. Afterwards, fibrinogen solution (2 mg/ml) (Sigma-Aldrich) was prepared in EBM-2 basal medium containing 2% FBS. 15 µl of the thrombin (50 U/ml) (Sigma-Aldrich) solution and 0.5 ml of the fibrinogen-beads solution (~30 beads per solution) were added to each well of the 24-well plate. The fibrin gel was allowed to polymerize for 5 min under the hood and then incubated for 15 min at 37°C, 5% CO_2. 0.5 ml of EBM-2 medium or EGM-2MV medium was added to the top of the fibrin clot, and those were incubated for 3 days. On day 3, the pictures of HAECs-coated beads were taken using a Nikon Eclipse TE 2000-U microscope fitted with a camera.

Serum miRNA isolation. RNA was isolated by phenol-chloroform extraction and precipitation in 50% isopropanol. Reverse transcription reaction was carried out using Mistiq microRNA and cDNA Synthesis mix (Sigma-Aldrich) and following the vendor's instructions. Quantitative RT-PCR was performed in a StepOnePlus real-time PCR system (Applied Biosystems) using SYBR Green PCR Master Mix (Sigma). Primer sequences: miR-34a: 5'- GCCTGGCAGTGTCTTAGCTGGTTGT -3'; U6: 5'- CGCAA GGATGACACGCAAAT -3'.

Statistical analysis

The analysis was performed with GraphPad Prism 9 software. Data are presented as mean±SEM (standard error of the mean). Gaussian distribution of data was tested with the Shapiro-Wilk test. Analysis of variance (ANOVA), followed by Tukey's posthoc test, was used to compare more than two groups. Fisher's exact test was used to calculate the frequency of aneurysm appearance and rupture. To calculate correlations, Pearson's test was applied. Grubbs' test was used to calculate statistically significant outliers ($p<0.05$), which were not included in the statistical analysis of the results. $p<0.05$ was accepted as statistically significant. The tendencies ($p<0.1$) were depicted on the graphs with dashed lines.

Results

The NRF2 transcriptional deficiency leads to premature ageing of the aorta and predisposes to abdominal aortic aneurysm

Our previous data indicate that the loss of NRF2 transcription factor leads to the induction of p53-dependent premature senescence in primary human aortic endothelial cells (HAECs)[251], which is accompanied by massive protein S-nitrosation and aggregation (Kopacz et al., Redox Biology[243]; Kopacz et al., Redox Biology[222]). Molecularly, the triggering factor is the overabundance of unrestrained KEAP1, the NRF2 repressor. Premature ageing shares several features with physiological ageing and seemingly underlies many CVDs (reviewed in Kloska, Kopacz et al., Vasc Pharm[190]). However, the relevance of the observed phenotype *in vivo* and its impact on cardiovascular disease remain elusive.

To verify if disturbed NRF2 signalling drives the senescent phenotype of vascular cells *in vivo*, we stained the aortas of 8-week-old wild-type (WT) and NRF2 transcriptional knockout (tKO) mice for senescence-associated β-galactosidase (SA-β-gal) activity. NRF2 tKO aortas were characterised by a profound increase of SA-β-gal-positive, senescent cells present throughout the vessel length (Fig. R1A). Notably, the *en face* projection confirmed the existence of SA-β-gal positive cells at the luminal surface of the aorta. The senescent cells are scattered across the whole depth of the aortic wall, including *tunica media* and *tunica adventitia* (Fig. R1A,B).

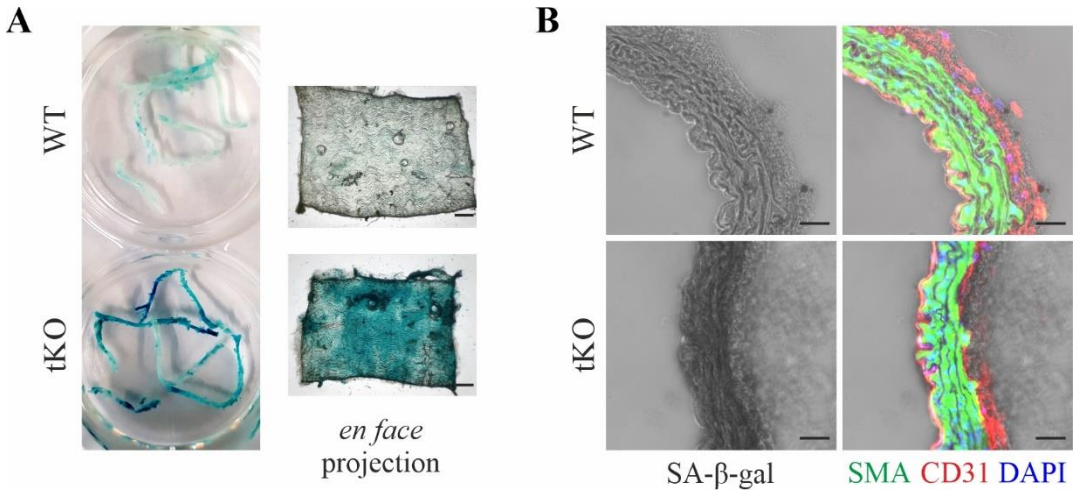

Figure R1. NRF2 transcriptional deficiency triggers aortic senescence *in vivo*. The staining for senescence-associated β-galactosidase activity (SA-β-gal) on **(A)** whole-mount aortas and in *en face* projection (scale bar = 500 μm), and **(B)** an abdominal aorta cross-section, followed by staining of intimal (CD31-red), medial (αSMA-green) layers; the nuclei are stained with DAPI (blue); scale bar = 25 μm; n=10; 2-3-month-old mice.

Consistently, there was a pronounced gain of senescent cells in all vascular layers, as proved in the transversal specimens of the abdominal aorta in tKO mice by SA-β-gal staining (Fig. R1B).

Senescence represents one of the substantial predisposing factors to cardiovascular diseases, including abdominal aortic aneurysm. Concomitantly, NRF2 is reported to be a crucial regulator of the aortic cell function (summarised in Kloska, Kopacz et al., Vasc Pharm[190]). Nevertheless, the involvement of NRF2 in AAA is vague, and the descriptive data relies primarily on NRF2-activating compounds. Therefore, the first aim of this thesis was to delineate the role of NRF2 in AAA using the genetic approach.

The reanalysis of published data, taking into account the AAA diameter[299] in relation to the expression of canonical NRF2-regulated genes *NQO1* and *GCLM*[300] in AAA, revealed a notable inverse correlation between these genes and AAA diameter – an indicator of the aneurysm severity and the rupture risk (Fig. R2). It outlined the plausible importance of NRF2 transcriptional activity in the regulation of AAA and the rationale for the transition to the mouse model.

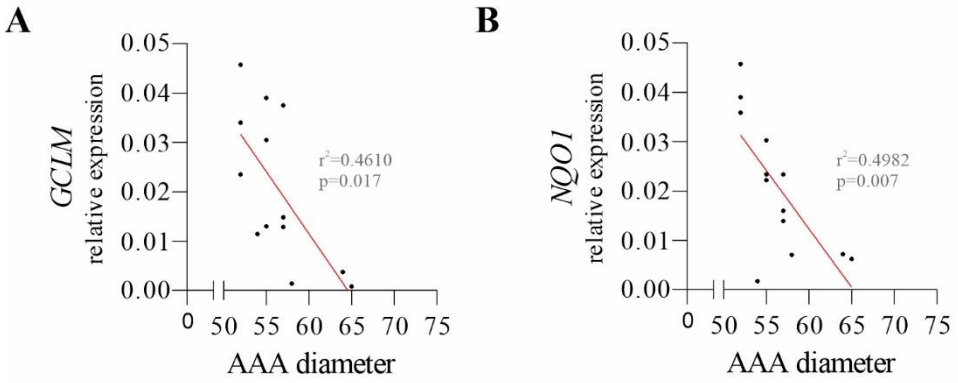

Figure R2. The aneurysm diameter correlates with the downregulation of canonical NRF2-regulated genes. (A-B) *GCLM* **(A)** and *NQO1* **(B)** mRNA levels plotted against aneurysm diameter in patients. *EEF2* was used as a reference gene; n=13.

The typical AAA induction model is based on angiotensin II (Ang II) infusion into hyperlipidaemic ApoE knockout mice[99], which provides approximately 4-fold higher aneurysm incidence compared to normolipidemic mice[301]. However, given the justifiable NRF2 deficiency-related promotion of AAA, we used a model of Ang II infusion combined with the fat-enriched diet (25% fat) in C57Bl6 mice. Control animals received Ang II-dissolving saline.

This AAA model relies on hypertension-inducing properties of Ang II, which, when combined with angiotensin II receptor 1-driven alteration of cellular signalling,

may lead to vascular damage and aortic dissection[110]. To corroborate the model functionality, we inspected the time course of blood pressure increase upon Ang II infusion. Ang II caused an abrupt elevation of systolic blood pressure within the first two days. The blood pressure stabilised till day 14 and revealed no differences between genotypes (Fig. R3).

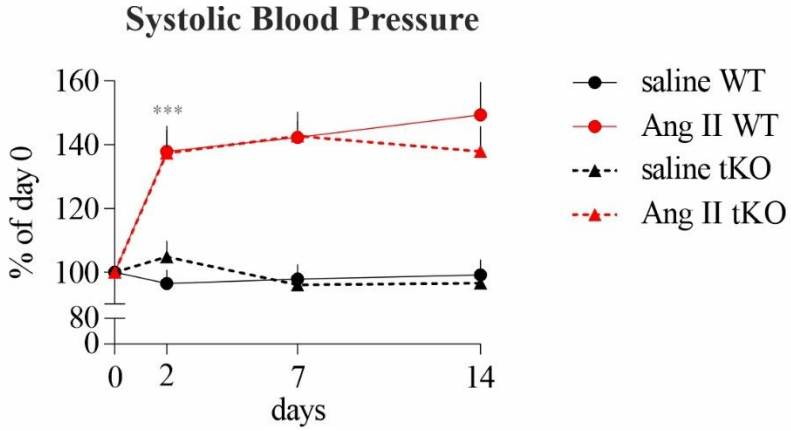

Figure R3. Ang II infusion triggers blood pressure elevation independently of the genotype. Time course of changes in systolic blood pressure (SBP) in WT and tKO, presented as a change of day 0. *** $p<0.001$ vs saline (relates to both genotypes); n=8-10; 6-month-old mice.

Yet, NRF2 transcriptional deficiency in mice rendered the aortas more susceptible to AAA formation and resulted in a 3-fold increase in the AAA frequency compared to WT counterparts (Fig. R4A). Importantly, Ang II infusion led to exclusive abdominal aortic enlargement, accompanied by thoracic or ascending part dilatation in some animals (Fig. R4B). Saline administration did not impact the aortic morphology (Suppl. Fig. 1). Ultrasound (US) imaging of the suprarenal aorta permitted tracing the formation of an aneurysm, which later was morphologically corroborated *post-mortem*. Moreover, the US evidenced a gradual increment of the maximal external aborting diameter in aneurysm-forming mice. The US captured the aortic dilatation in the longitudinal plane in these animals as early as day 7 in aneurysm-forming mice. Such dilatation preceded aortic dissection and stabilisation of the formed thrombus at day 28 (longitudinal and transverse plane; Fig. R4C,D).

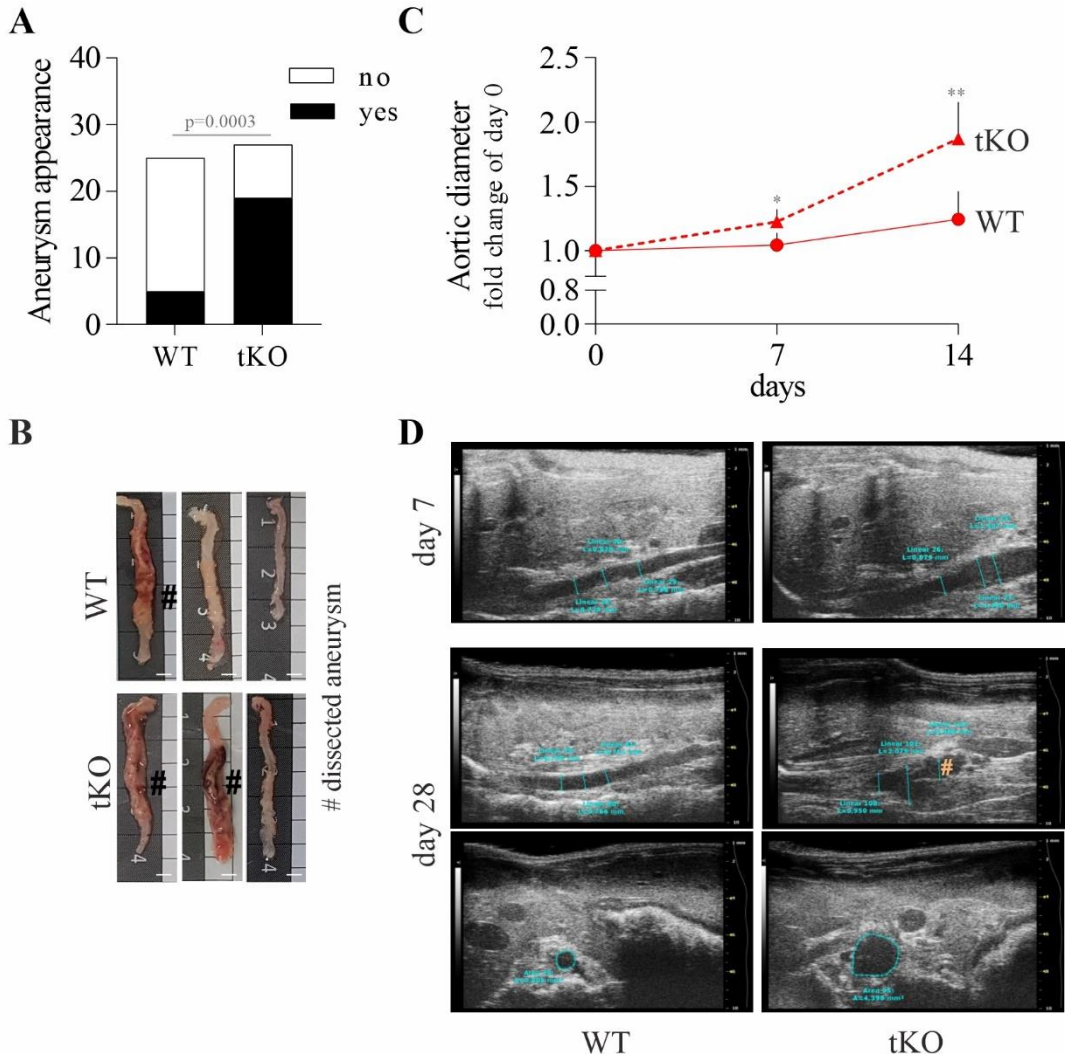

Figure R4. Lack of NRF2 transcriptional activity predisposes mice to abdominal aortic aneurysm upon Ang II infusion. (A) The frequency of aortic aneurysm appearance up to 28 days; **(B)** representative image of aortas isolated from WT and tKO mice. Hashtag indicates a dissected aneurysm, scale bar = 1 mm; **(C)** Time-dependent changes in the aortic outer diameter measured with ultrasound * $p<0.05$, ** $p<0.01$ vs WT Ang II; **(D)** Representative images of ultrasound images of aortic changes in WT and tKO mice upon Ang II infusion; # – stabilised thrombus; n=25-27; 6-month-old mice.

The recruitment and local tissue differentiation of the effector macrophages accompany the formation of Ang II-induced AAA[302]. Whereas 14-day Ang II infusion did not impact the level of blood leukocytes, including monocytes (Fig. R5A), it remarkably affected the expression of endothelial adhesion molecules.

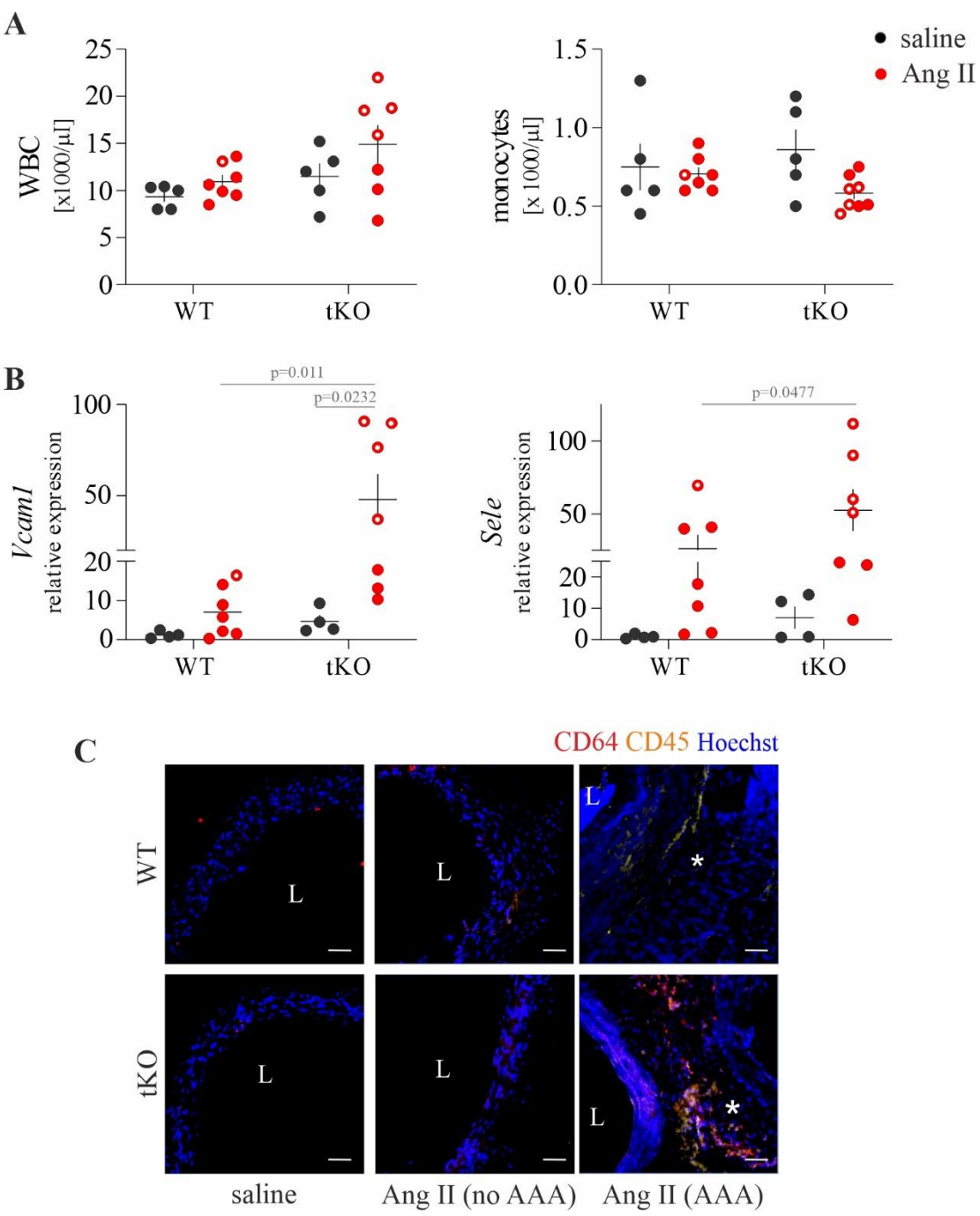

Figure R5. Immune cell infiltration and increased homing molecules level are associated with AAA formation in NRF2 tKO mice. (A) Quantification of circulating white blood cells and monocytes. **(B)** Relative expression of *Vcam1*, *Sele* in the aortic wall. *Eef2* was used as a reference gene. **(C)** Immunofluorescent staining of infiltrating $CD45^+$ and $CD64^+$ cells within the aortic wall. CD45 - yellow, CD64 - red, nuclei- blue. Scale bar = 50 µm. Open circles – mice which developed an aneurysm; n=4-7; 6-month-old mice.

Aneurysm formation was concomitant with a noticeable increase in *Vcam1*, encoding vascular cell adhesion molecule-1, and *Sele*, encoding E-selectin (Fig. R5B), which was even more pronounced in the case of NRF2 tKO mice. The expression of homing

molecules corresponded well to the infiltration of immune cells – mainly $CD64^+$ positive macrophages, into the aneurysmal area (Fig. R5C).

The formation of a stable aneurysm relies on complex aortic wall rearrangements. Physiologically, the mechanical properties of the aortic wall are submissive to elastin fibres. In contrast, upon Ang II-related disruption of elastin, the mechanical resistance of the vessel wall becomes highly reliant on the collagen network. Moreover, AAA progression and susceptibility to rupture are contingent on fine-tuned collagen turnover[4,195]. Elastin Van Gieson staining confirmed the appearance of elastin damage in mice treated with Ang II. However, whereas in the case of the non-AAA group, the destruction was mild and occurred in one of the elastin layers, in aneurysm-forming tKO, but not WT, animals, the break took the whole media layer (Fig. R6A). Then, we assessed the collagen status by trichrome staining, which unveiled an Ang II-, but not genotype-dependent, increase in total collagen content. Notably, there was an evident increase in collagen within the aneurysmal tissue (Fig. R6B).

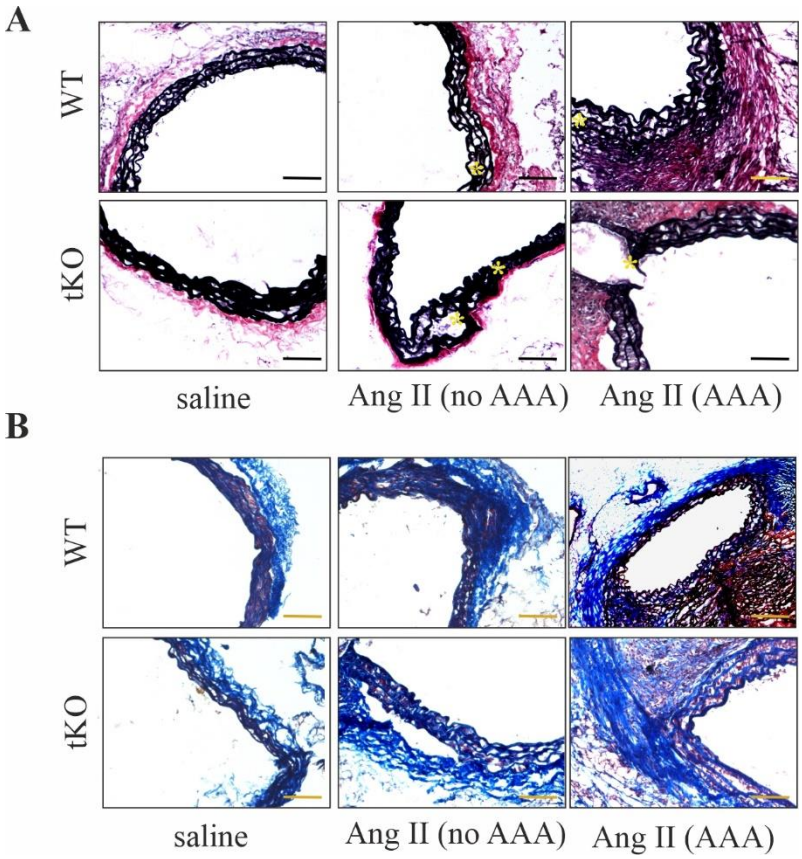

Figure R6. Ang II infusion triggers structural aortic wall rearrangements. (A) van Gieson elastin staining (elastin fibres – black), * elastin breaks; **(B)** trichrome staining depicting collagen level (blue). Representative images; scale bar = 50 μm; n=4-5; 6-month-old mice.

To further verify the collagen type present in the aneurysms, we examined the load-bearing collagens type I and III[95,303]. Even though Ang II infusion altered collagen I and III levels in the non-AAA group (Fig. R7A,B), the effect was significantly less pronounced than what we could imply from the transcript level (Suppl. Fig. 2). The effect for collagen I was genotype-independent. In contrast, for collagen III, the protein level was around 50% higher in tKO mice, which was more visible in saline-treated mice and less pronounced in Ang II-infused. Furthermore, the expression of collagen I and III was abrogated within aneurysmal tissue, indicating primarily that these collagens did not build up the thrombus and, secondly, suggesting enhanced degradation.

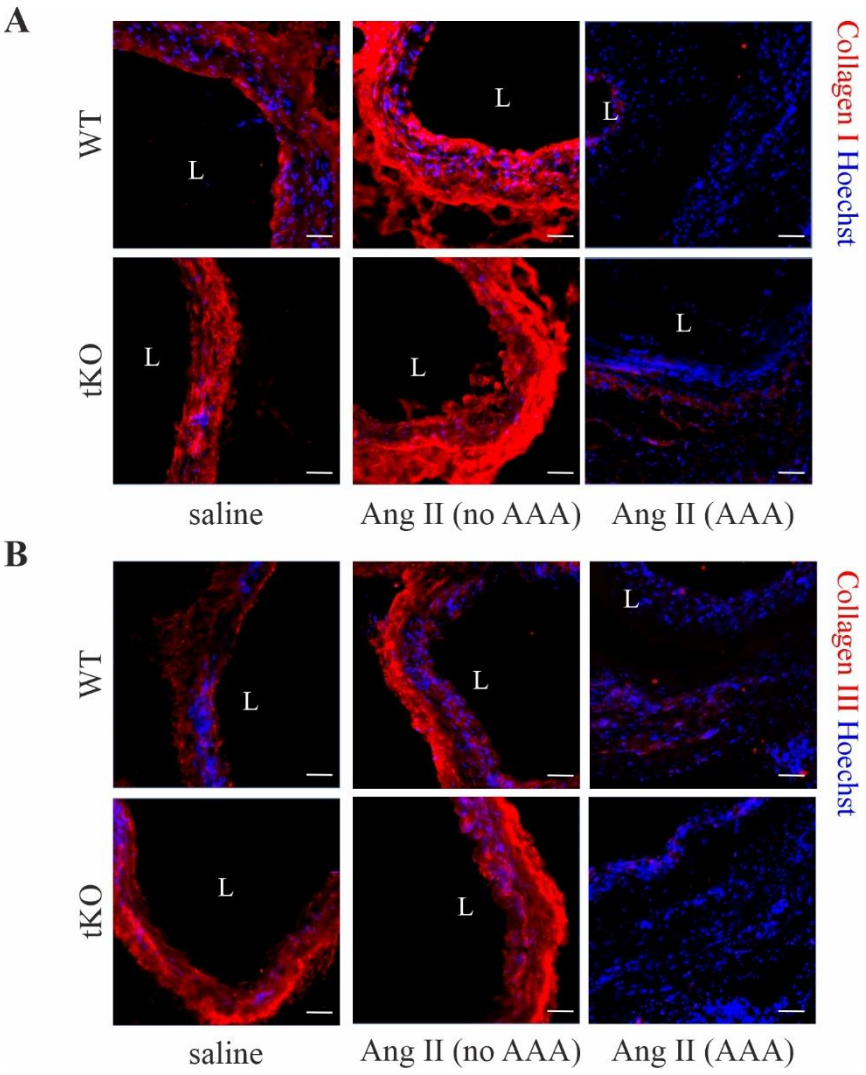

Figure R7. Collagen I and III are significantly decreased in formed AAAs. (A-B) Immunofluorescent staining of **(A)** collagen I and **(B)** collagen III within the aorta at magnification 200x. Collagen - red, nuclei - blue. Representative images; scale bar = 50 μm; n=4-5; 6-month-old mice.

The latter could be explained by enhanced metalloproteinase (MMP) activity. Hence, we performed *in situ* zymography (ISZ) with subsequent co-staining with MMP-9, one of the most expressed proteases in AAA tissue[304]. Ang II enhanced gelatinase activity to a striking level in the dissected aneurysm. Ang II promoted the expression of MMP-9, but its level and localisation did not correlate with proteolytic activity (Fig. R8).

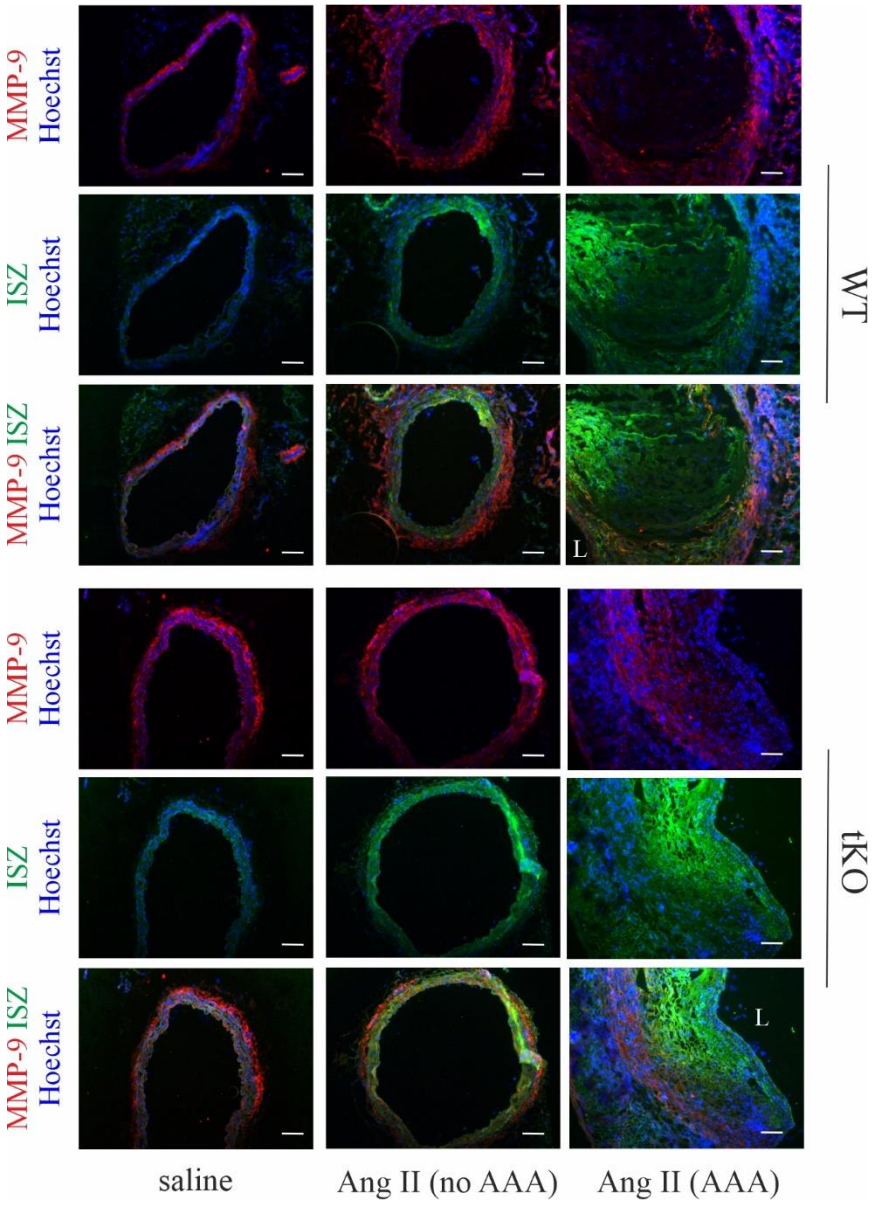

Figure R8. Enhanced metalloproteinase activity characterises formed AAA. The activity of gelatinases (green) and MMP-9 level (red) at a magnification of 100x. Blue - nuclei. The activity of gelatinases was assessed by *in situ* zymography. Representative images, scale bar = 0.1 mm; n=8-10; 6-month-old mice.

Such partial association was present in tKO mice without aneurysms, suggesting the potential role of other MMPs in aortic wall rearrangement. But it was not the case in a dissecting aneurysm (Fig. R8). Thus we inspected the expression of other MMPs,

known to play a role in aortic wall degradation during aneurysm formation[304]. Ang II infusion promoted the expression of both *MMP2* and *MMP3*, and this rise was much more marked in the case of NRF2 tKO mice and correlated with zymography results (Suppl. Fig. 3).

Ang II impacts cellular signalling by binding to AT1R, leading to subsequent activation of ERK[305]. Notably, this pathway has clinical relevance. The reanalysis of previously published data, taking into consideration AAA diameter[306], revealed that AAA size positively correlated with the level of activated p42 (ERK1) and activated p44 (ERK2) (Fig. R9A). Accordingly, pan-ERK activation correlated well with aneurysm susceptibility and incidence in the mouse model, as its level was pronouncedly higher in NRF2 tKO aortas (Fig. R9B).

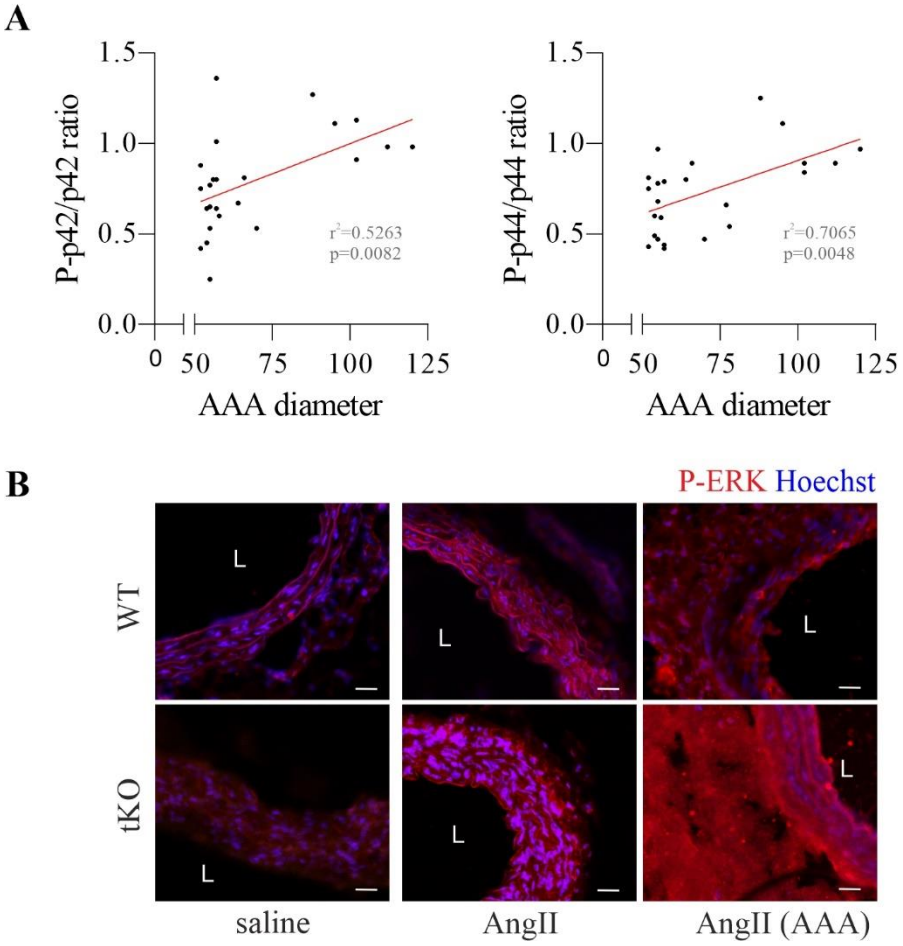

Figure R9. Activation of ERK signalling marks aneurysm formation. (A) Correlation of AAA diameter with P-p42/p42 and P-p44/p44 protein level ratio; **(B)** Immunofluorescent staining of P-ERK within the aortas at magnification 200x. L - aortic lumen. Representative images; scale bar = 50 μm; n=8-10; 6-month-old mice.

The analysis of aneurysmal features, presented in Fig. 4-9, was performed in 6-m.o. mice, which were subjected to a fat-enriched diet. On the other hand, young (3-m.o.) NRF2 tKO mice are prematurely senescent when kept on a regular chow diet (Fig. R1). To fully address the significance of diet and age on the NRF2 TA deficiency-related AAA, we compared the aneurysm incidence in younger against older animals and on regular chow vs fat-enriched diet. Significantly, aneurysms in NRF2 tKO mice happened with the same probability in young and older mice (Fig. R10A). Similarly, the diet did not affect aneurysm incidence (Fig. R10B).

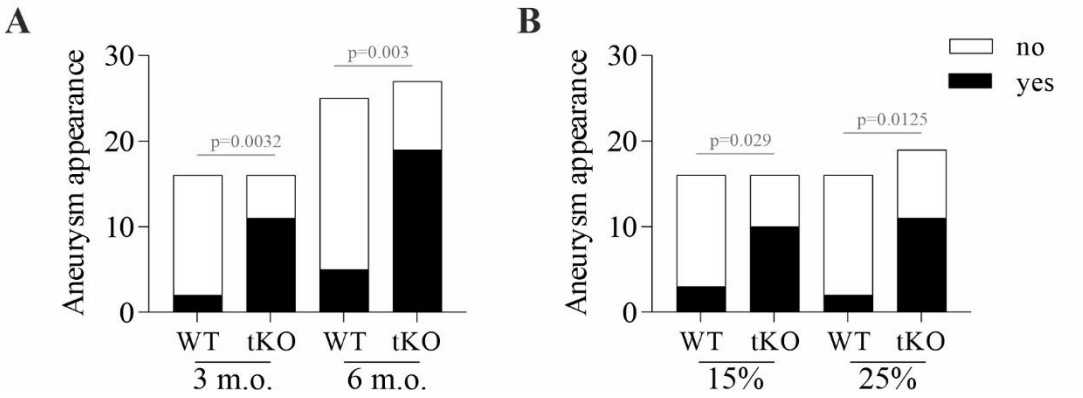

Figure R10. The formation of AAA in tKO mice upon Ang II infusion is independent of mice age and diet. The aneurysm incidence in relation to **(A)** mice age (animals kept on a chow diet), and **(B)** diet (3-month-old mice); n=16-27.

Oxidative stress often accompanies the malformation of the aortic wall[307], and it seems a relevant feature to be addressed in light of the oxidative stress harnessing properties of NRF2[180,181]. Therefore, we examined the redox status of aortas using a fluorescent probe. In saline-treated groups, the NRF2 tKO mice had a moderately increased reactive oxygen species (ROS) level than the wild-type counterparts. Ang II infusion elevated ROS level, more pronouncedly in animals that developed AAA. Notably, the influence of genotype was scarce (Fig. R11A). The distinctive ROS level was corroborated by mass spectrometry, where we observed a significant increase in oxidised peptides only in the AAA group (Fig. R11B) (WT AAA were not analysed).

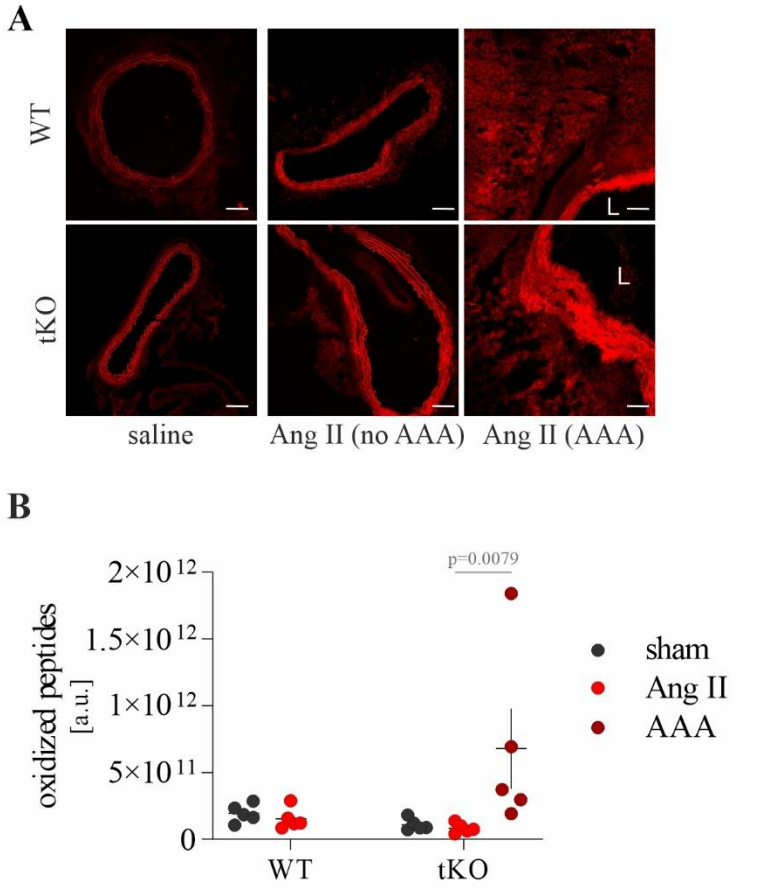

Figure R11. Decreased antioxidant capacity accompanies the formation of AAA. (A) Assessment of ROS level in the aortic tissue. Representative pictures. Magnification 100x. Scale bar = 0.1 mm. **(B)** The number of oxidized peptides in the aortas. The oxidation level was assessed by mass spectrometry in collaboration with Dr. Dominik Cysewski, Institute of Biochemistry and Biophysics, Polish Academy of Science; n=4-5; 6-month-old mice (A) and 3-month-old mice (B).

Then, we took a closer look at the pathways differentiating the NRF2 tKO animals without and with an aneurysm. For the analysis, we included only the Ang II–treated mice. The analysis of the pathways showed significant deregulation of the protein involved in the regulation of metabolism, immune response and, in general, signal transduction (Fig. R12). Peering closer, we could observe that aneurysmal aortas were characterised by enhanced glucose and lipid metabolism. Moreover, we outlined a strong protein signature suggesting a robust "O_2 and CO_2 exchange", which also could be related to the abundance of erythrocytes in AAAs. On the other hand, we depicted a general inhibition of the cellular processes (translation, nucleic acid processing) and a shift from oxygen-related metabolic pathways towards glycolysis (Table 11). Moreover, the proteome analysis clearly showed the gravity of the redox-related pathways switching between non- and proaneurysmal fate.

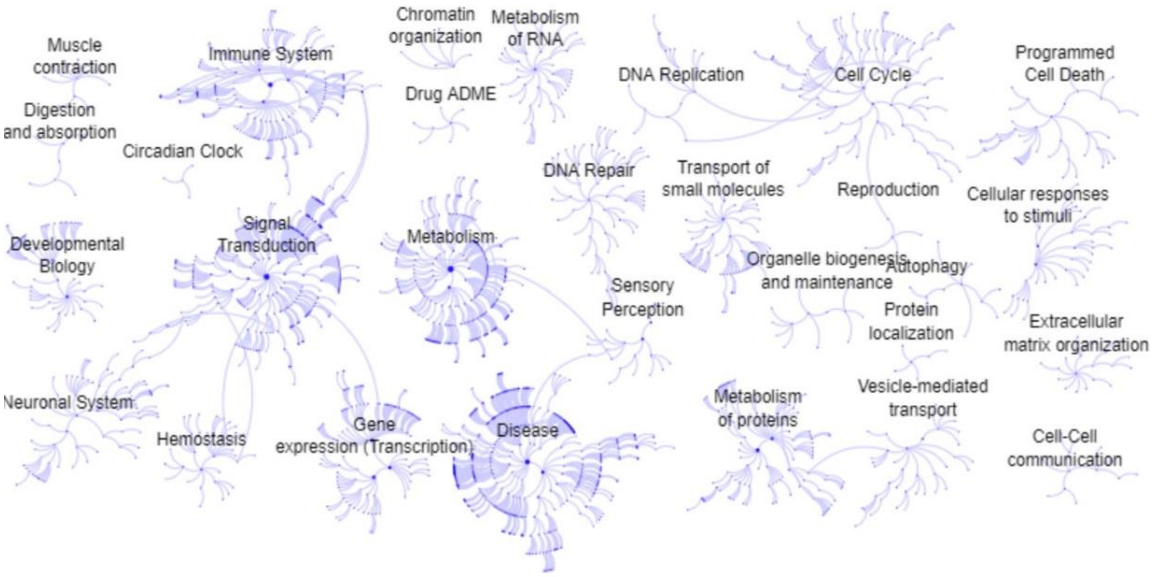

Figure R12. Genome-wide overview of the pathways significantly downregulated within the aneurysmal aortas. The relevant pathways are these with exiting bolded lines – outlining the differential expression proteins (metabolism, signal transduction, immune system and disease). The pathway analysis was performed with the Reactome database. The mass spectrometry analysis was performed in collaboration with Dr. Dominik Cysewski, Institute of Biochemistry and Biophysics, Polish Academy of Science; n=5; 3-month old mice.

Pathways upregulated in AAA vs no AAA	**Pathways downregulated in AAA vs no AAA**
CO_2/O_2 exchange and metabolism	translation
metabolism increased glucose synthesis and glycolysis	amino acid synthesis
glutathione conjugation and ROS metabolism	mRNA metabolism
lipoproteins turnover	respiratory electron transport
oxysterol metabolism	rRNA processing

Table 11. The most significantly altered pathways in the NRF2 tKO animals infused with Ang II, bearing an aneurysm or not. The pathway analysis was performed with the Reactome database.

To sum up, NRF2 transcriptional deficiency in mice leads to premature ageing of the aorta and predisposes to AAA. Aneurysms that are formed in both genotypes share similar features: increased immune cell infiltration and robust aortic wall rearrangement. Despite some intensification of the parameters mentioned above in NRF2 tKO, it does not seem to be the primary cause of the susceptibility of NRF2 tKO mice to AAA. Out of analysed parameters, Ang II-triggered ERK activation, significantly enhanced under NRF2 transcriptional deficiency even in the basal state, may partially explain the sensitivity to AAA. Furthermore, considering the significant increase in oxidation in AAA tissue and the importance of NRF2 transcriptional activity in harnessing oxidative stress[308],

it cannot be discarded that this is the susceptibility factor, rendering NRF2 tKO mice prone to AAA.

NRF2-related premature ageing leads to structural alterations, which resemble physiological ageing

The growing evidence points out Ang II-induced AAA as a highly mechanical model, inducing medial tear and aortic dissection rather than dilatation of the aorta[110]. The structural changes within the aortas could account for the increased susceptibility of NRF2 tKO mice to AAA. To visualize the structure of aortas, we performed haematoxylin and eosin stainings. While the aortas remained without signs of damage and occurring inflammation, there was a striking difference in media width. The histometric analysis confirmed a significant decrease in media size in NRF2 tKO mice, resembling features in aged WT animals. The effect was more pronounced in the thoracic aorta; however, the control animals' abdominal aortas were considerably thinner (Fig. R13A, B). One of the crucial structural proteins of *tunica media* is elastin, which accounts for the mechanical properties of the whole aorta, and its modification is a sign of progressing ageing[34,35]. Visualisation of elastin fibres confirmed findings of HE staining. Elastin fibres in NRF2 tKO and aged animals were considerably more packed than in young WT mice; however, they remained continuous, without signs of damage (Fig. R13C).

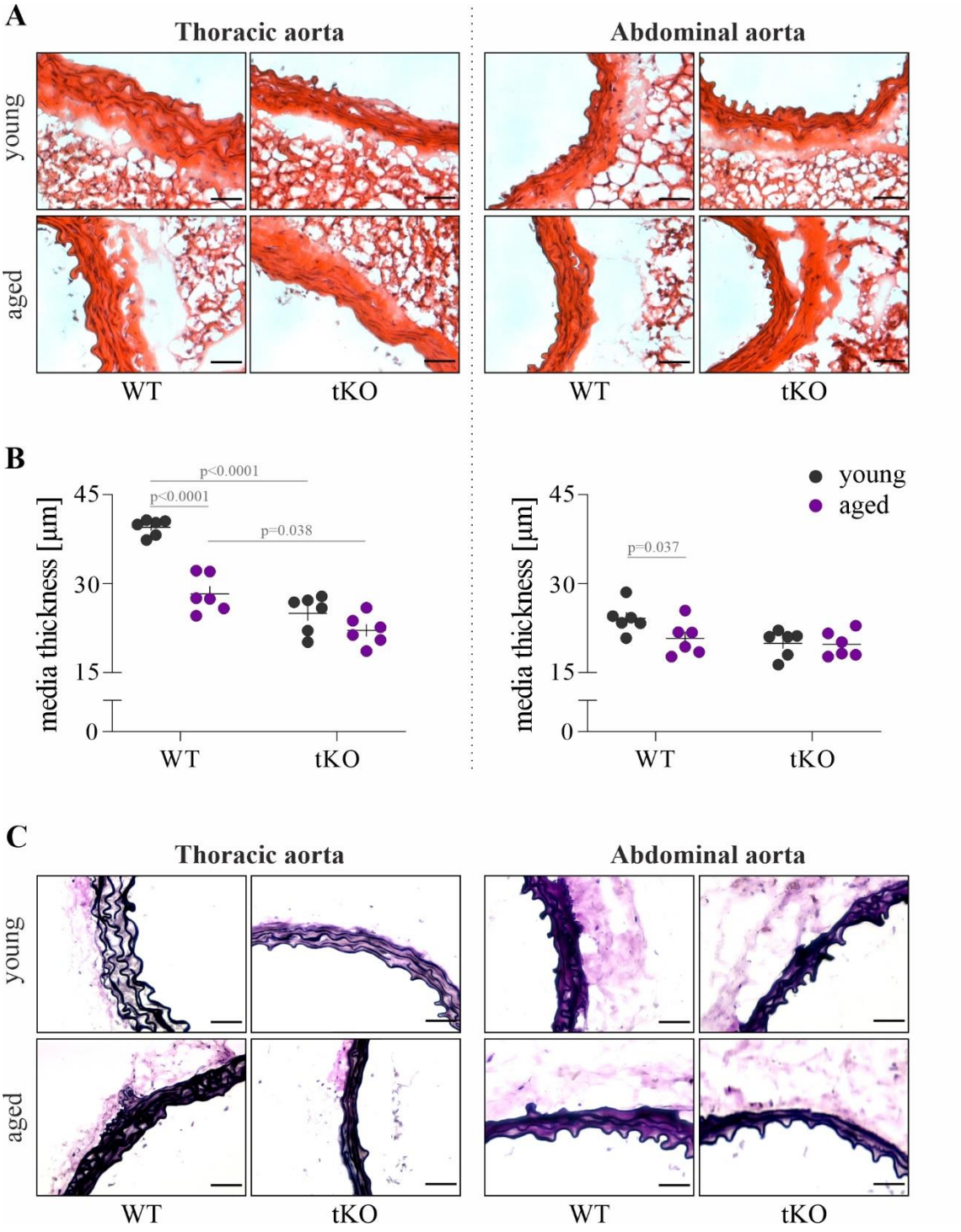

Figure R13. Young tKO mice show ageing-like abnormalities in the medial thickness. **(A)** Haematoxylin and eosin staining. Representative images. **(B)** Quantification of media width based on the H&E staining in both aortic parts. **(C)** Van Gieson elastin staining. Representative images; scale bar =50 µm; n=5-6; 2-3-(young) and 12-month-old mice (aged).

One plausible reason for such a dense elastin organisation is the reduced number of smooth muscle cells caused by increased death. Apoptosis is the primary cell death cause in the aortas, further intensified in the diseased vessel[309,310]. Thus, in the next step, we inspected apoptotic cells within the aortas by TUNEL staining, which revealed

the scarcity of dying cells in all analysed groups (Fig. R14 and positive control from aneurysmal tissue – Suppl. Fig. 4). Therefore, NRF2-related premature aortic ageing leads to thinning of the medial layer and tightly arranged elastin fibres, which is caused neither by elastin fibres damage nor by increased cellular apoptosis.

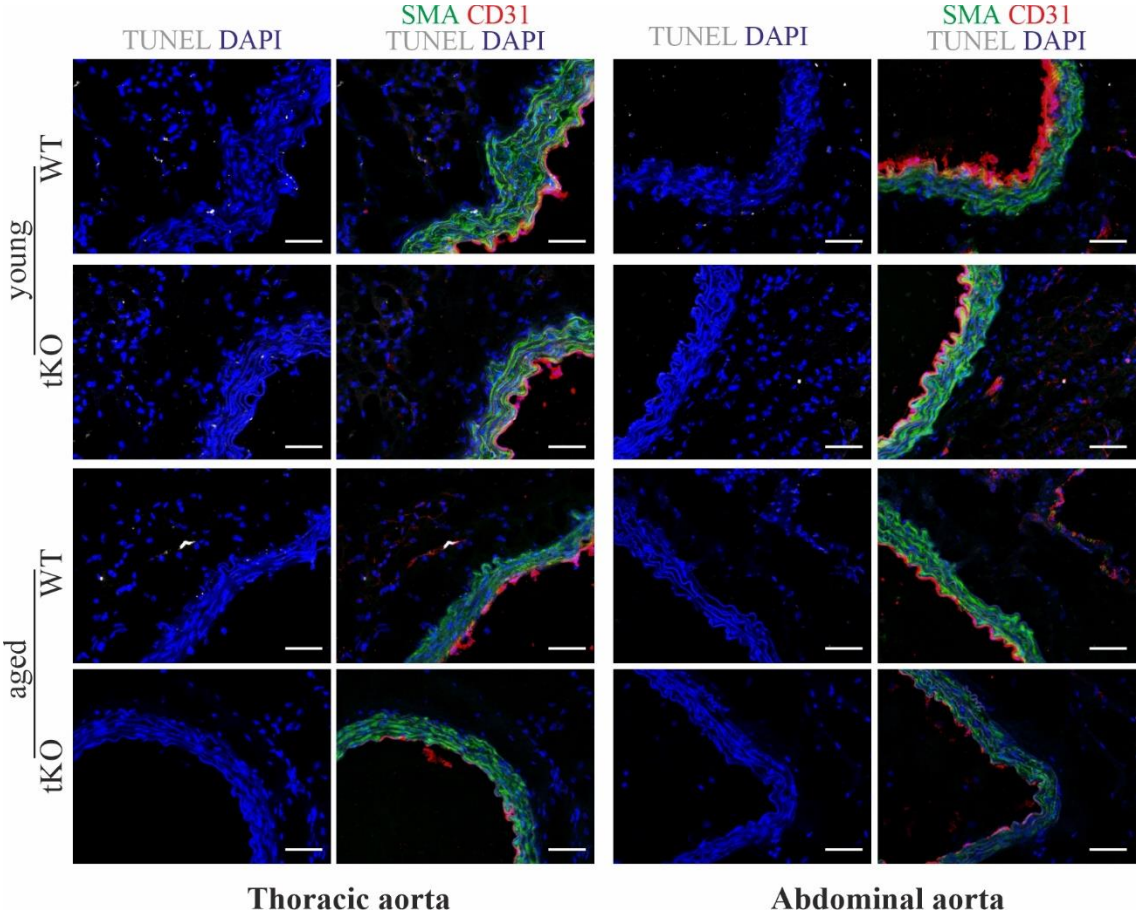

Figure R14. The lack of significant apoptosis in NRF2-related and physiological ageing. TUNEL – based detection of apoptotic cells (white) followed by co-staining of endothelial (CD31 – red) and smooth muscle cells (αSMA – green). The nuclei were stained with DAPI. Representative images; scale bar = 50 μm; n=5-6; 2-3-(young) and 12-month-old mice (aged).

Another sign of progressing ageing and AAA formation is vascular stiffening[311]. *Ex vivo* assessment of aortic stiffness using AFM nanoindentation revealed an appreciable age-dependent stiffening in the sub-EC layer in both genotypes. The effect in the EC layer was less pronounced yet still significant, especially in the thoracic part. NRF2 transcriptional deficiency prominently altered the elastic modulus of the sub-endothelial layer, and in the endothelial one, there was a tendency to increase (Fig. R15). Therefore, both physiological and NRF2-related premature ageing alter the mechanical properties of the aorta.

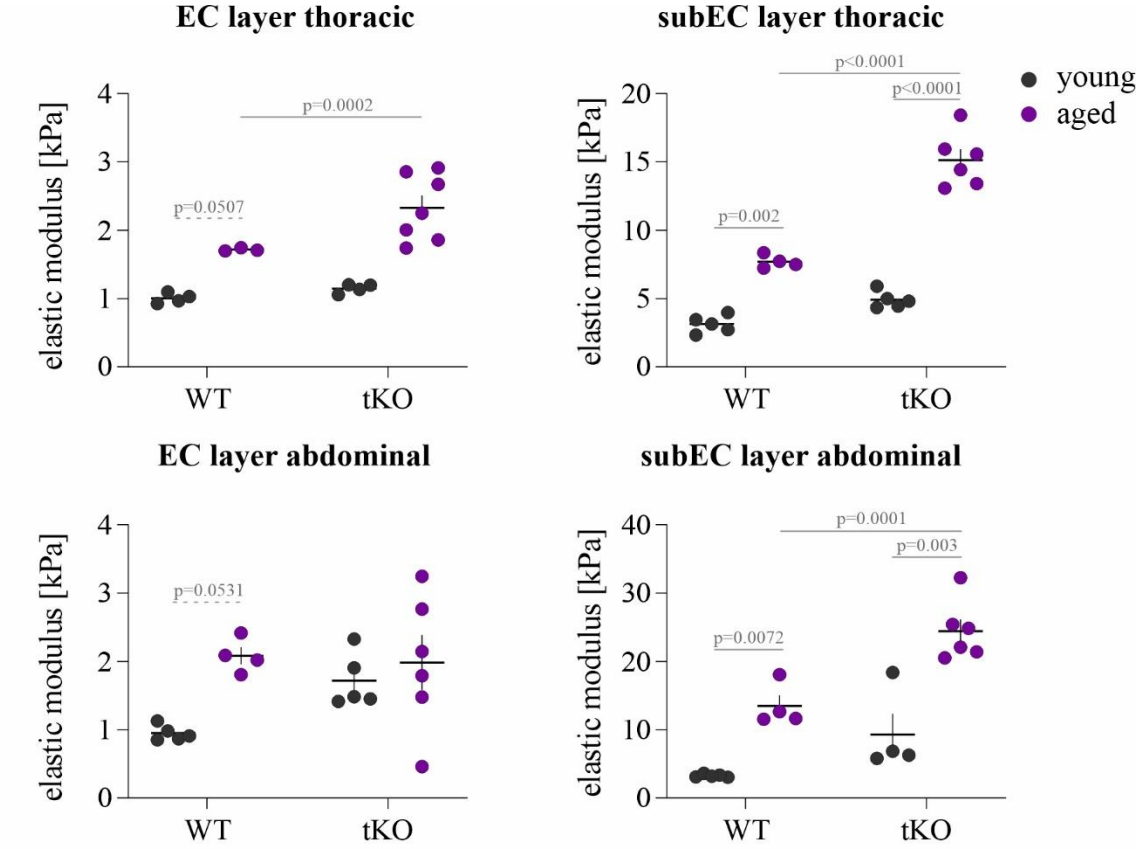

Figure R15. NRF2-related and physiological ageing leads to aortic stiffening. Atomic force microscopy-based assessment of Young elastic modulus of the endothelial and subendothelial layer of the thoracic and abdominal aorta. The results were obtained in collaboration with Dr. Marta Targosz-Korecka, Institute of Physics, Jagiellonian University; n=4-6; 2-3-(young) and 12-month-old mice (aged).

In the quest for the reason for observed changes, we assessed the collagen content by trichrome staining. There was an apparent age-dependent increase in collagen, even more pronounced in aged NRF2 tKO thoracic aortas; however, the degree of alteration did not correspond entirely to the AFM nanoindentation results, especially in young NRF2 tKO animals (Fig. R16).

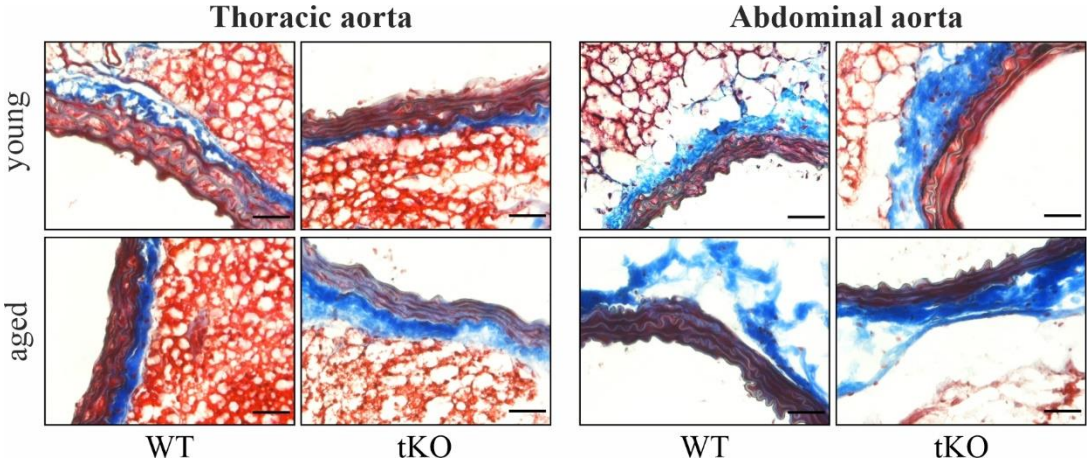

Figure R16. Alterations of collagen level in physiological and NRF2-related ageing. Trichrome staining. Representative images. Scale bar = 50 μm; n=5-6; 2-3- (young) and 12-month-old mice (aged).

As AFM senses well the actin cytoskeleton, which at the same time could alter cellular stiffness[312], the actin staining on the endothelial layer of the thoracoabdominal aorta was performed (Fig. R16A). NRF2 transcriptional deficiency triggers massive age-dependent actin polymerisation into stress fibres, which is substantially lower than in wild-type mice. These changes were maintained with age, especially in tKO animals. Based on these two analyses, collagen differences plausibly account for age-related stiffness, whereas the NRF2 transcriptional deficiency-related actin modifications amplify the stiffness (Fig. 17B).

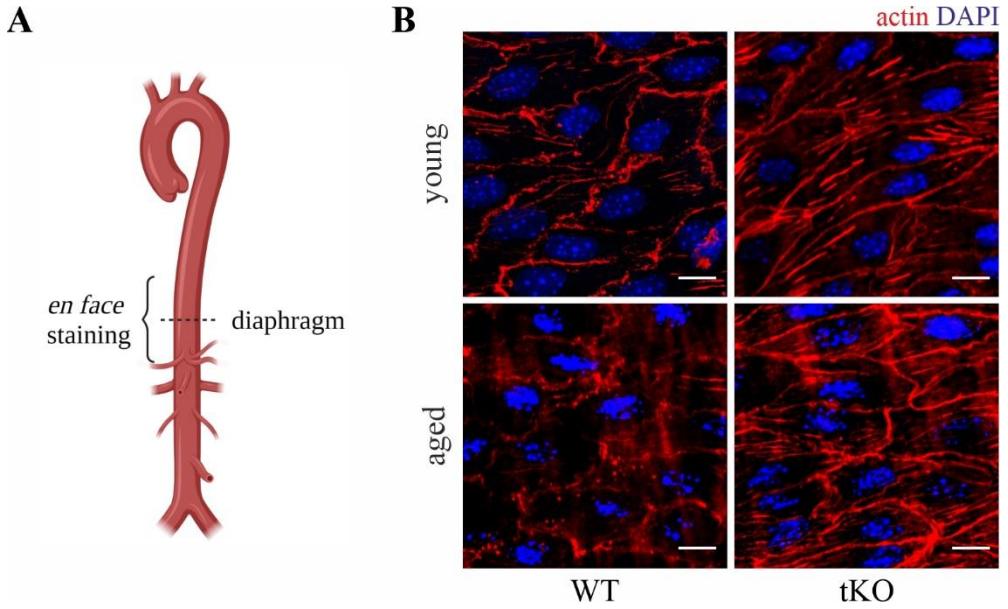

Figure R17. Visualization of the actin cytoskeleton in endothelial cells. (A) The thoracoabdominal fragment of the aorta was used for the staining. **(B)** Representative images of the *en face* actin staining. Red – actin, blue – nucleus. Scale bar = 10 μm; n=6; 2-3-(young) and 12-month-old mice (aged).

The aforementioned stiffness-related analyses were performed *ex vivo* and in an isolated model. To fully address vascular stiffness *in vivo*, measuring it in the living organism is pivotal. Aortic extensibility assessed in the suprarenal region of the abdominal aorta revealed no differences between inspected groups (Suppl. Fig. 5). The clinically relevant factor, pulse wave velocity, showed functional stiffening of aorta only in aged tKO mice (Fig. R18).

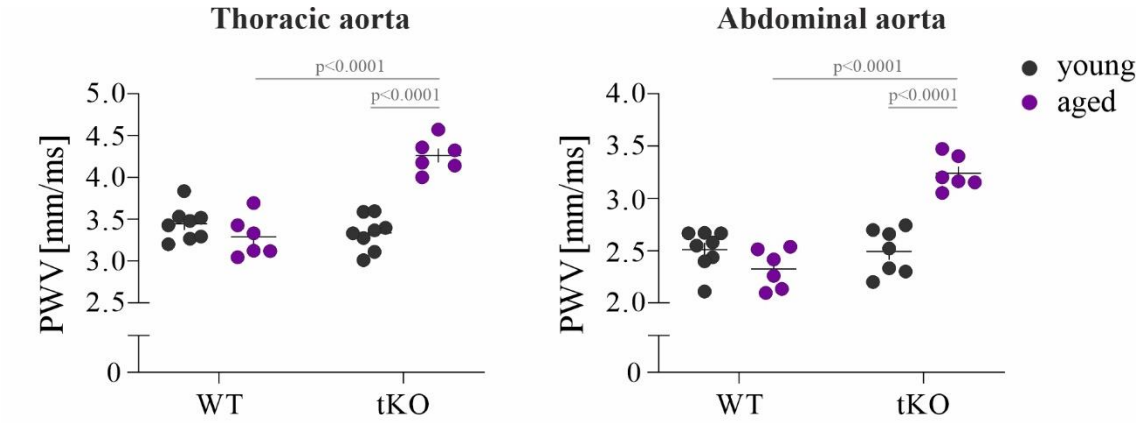

Figure R18. Assessment of arterial stiffness *in vivo* by pulse wave velocity (PWV) in the thoracic and abdominal aorta. Pulse wave velocity (PWV) was assessed by Doppler Flowmetry; results were obtained in collaboration with Dr. Anna Bar and Prof. Stefan Chłopicki, Jagiellonian Centre for Experimental Therapeutics; n=6-8; 2-3-(young) and 12-month-old mice (aged).

To sum up, NRF2 transcriptional deficiency-related premature ageing share some structural features with physiological ageing. In both cases, we observe medial thinning, however, not related to enhanced smooth muscle cell apoptosis. NRF2 transcriptional deficiency exacerbates the age-related stiffening of the aorta. Whereas increased collagen level may account for age-related changes, the more polymerized actin cytoskeleton seems to be the differentiating factor between the genotypes. Importantly, the alteration in the Young modulus does not fully translate to the changes in the functional arterial stiffness. Out of analysed parameters, the AFM-depicted stiffness could serve as a predilection factor to AAA.

The intimal ultrastructural changes, counteracted by simvastatin treatment, are associated with NRF2-deficiency related AAA

Ultrastructural changes in the media, mainly depicted as cavities, accompany the formation of AAA[313] and are associated with ageing[314]. Importantly, little is known about changes in the EC layer, which plausibly could facilitate intimal tear central to the onset of aortic dissection[315,316]. Therefore, we performed scanning electron microscopy (SEM) imaging of the aortas, focusing our attention on the intima structure. We observed prominent changes in aged tKO mice resembling such cavities (Fig. R19A). We evidenced similar, however much more robust, structures upon Ang II treatment, which were even more pronounced in the formed aneurysm. We could see the extensive alteration of the intimal layer with enormous hollows with exiting tears (Fig. R19B).

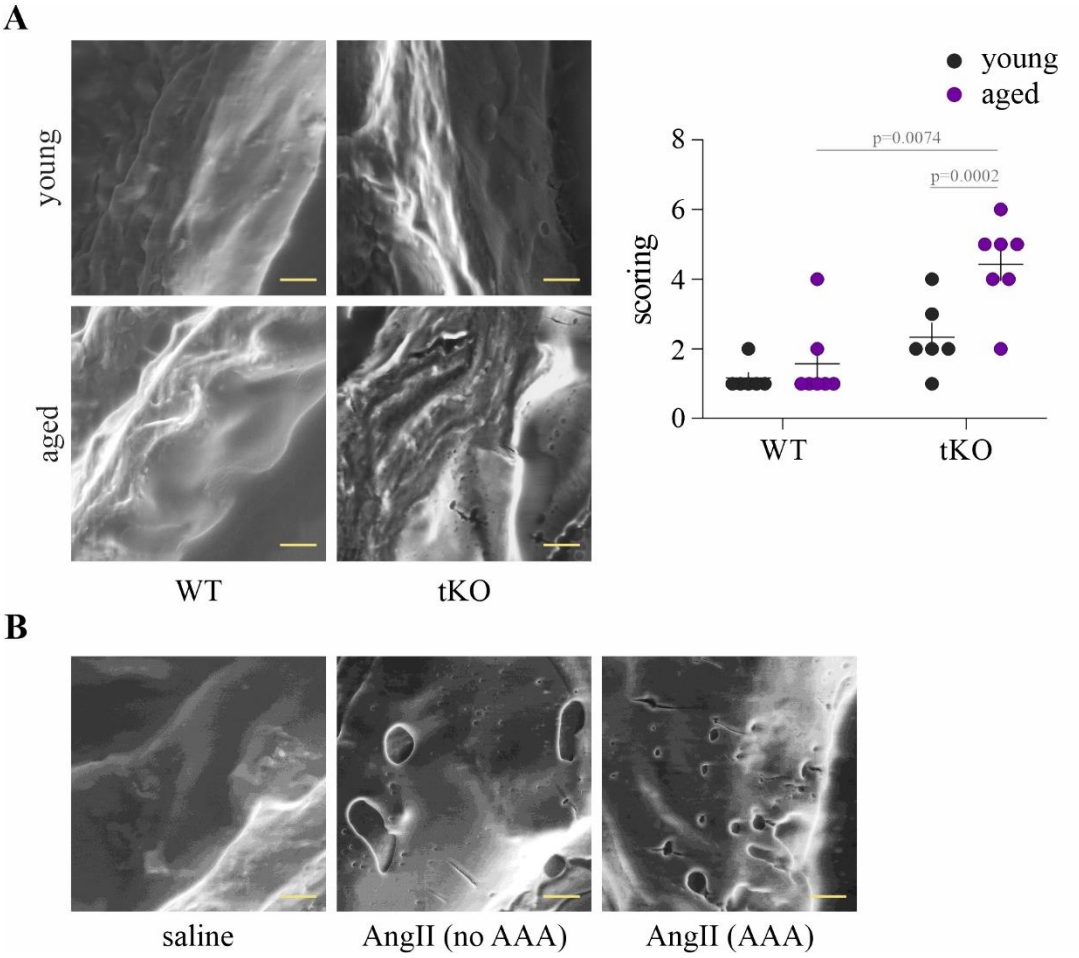

Figure R19. The significant SEM-depicted changes in the intimal ultrastructure in the aged NRF2 tKO mice and upon aneurysm formation. (A) representative images and quantification of the extent of intimal layer abnormalities, scale bar = 10 μm; **(B)** representative images of the endothelial cell layer in control animals and upon Ang II infusion in AAA- and not AAA-forming mice; scale bar = 10 μm; n=4-7; 2-3-(young) and 12-month-old mice (aged).

The intimal anomalies in aged tKO aortas resembled the exit of the vasa vasorum[317] or some vessels that could penetrate the arterial wall. Indeed, taking advantage of the fluorescent properties of gold particles, we showed that they penetrate the arterial wall till adventitia (PVAT) only in tKO animals when injected into the lumen (Fig. R20A). Moreover, these anomalies resembled vessels infiltrating the wall, further supported by IF staining (Fig. R20B), with small vessels spanning between the intima to the adventitia. However, based on the staining we cannot discard the presence of CD31-positive cell types different than ECs, as CD31 can also be present on ex. immune cells[318]. On the other hand, we did not observe high inflammation within the aortic wall (Fig. R13) and the stainings revealed vessel-like shape. Thus, the staining should rather depict the ECs but to address it we decided to perform the CD31 staining in parts richer in the capillaries.

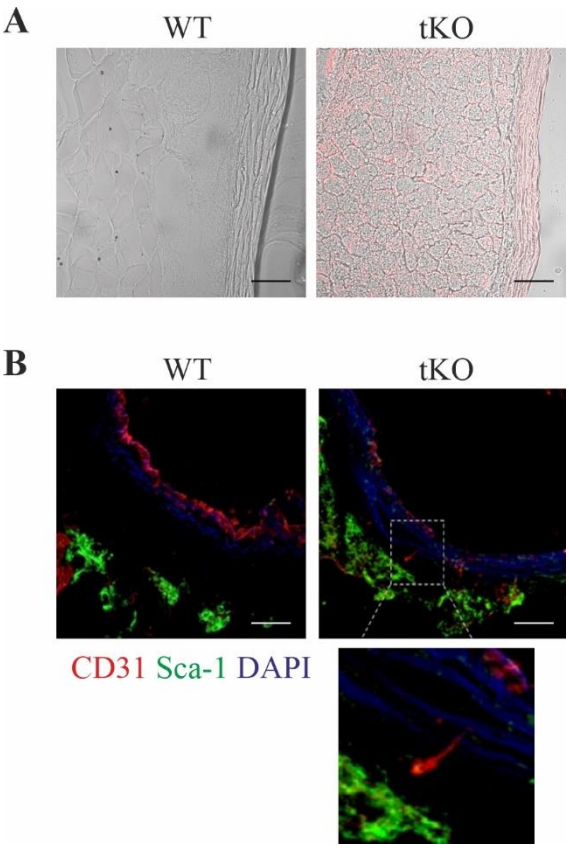

Figure R20. The structural anomalies in aged tKO are likely vessels or CD31-positive conduits spanning through the aorta to the adventitia. (A) Representative images of lumen-injected gold particles into aged aortas of both genotypes, n=5, scale bar = 100 μm. **(B)** Immunofluorescent staining of endothelial cells (CD31, red) and adventitia (Sca-1, green) in aged mice of both genotypes; DAPI was used to depict the nuclei. Scale bar = 20 μm; n=4-6; 12-month-old mice.

As one of the morphological features of tKO aortas was the tightness of adventitia and perivascular fat, we decided to inspect the PVAT vasculature. We observed age- and

NRF2 TA deficiency-related increase in CD31-positive vessels (Fig. R21) and CD31 seems a good marker to assess endothelial cells in the aorta. Furthermore, the angiogenic response seemed to be augmented in these mice, and such vessels could reach the intimal layer, as the *vasa vasorum* in the pathological cases can[319].

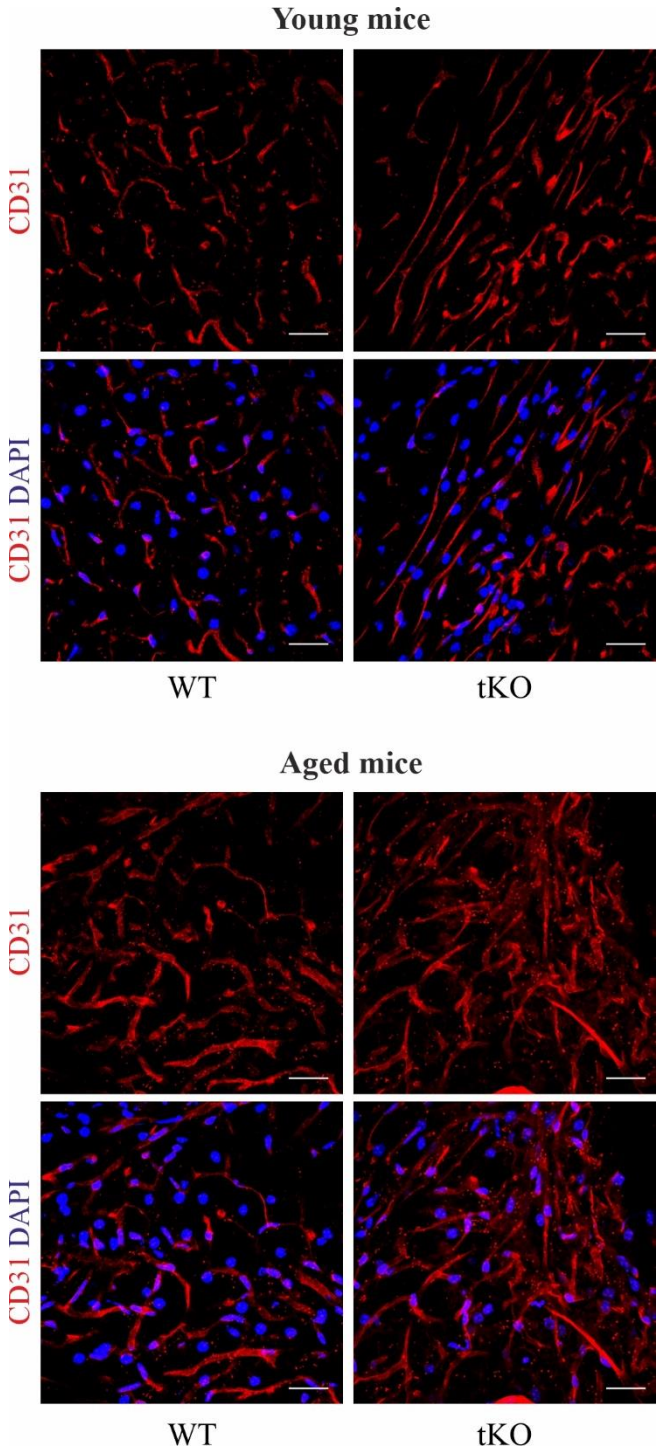

Figure R21. Significantly enhanced vascularisation of the PVAT upon lack of NRF2 transcriptional activity. Representative image of whole-mount CD31-positive microvessels (red), the nuclei are depicted with DAPI (blue); scale bar = 20 μm; n=5; 2-3- (young) and 12-month-old mice (aged).

Similarly, Ang II infusion promoted angiogenesis in the PVAT. Moreover, as evidenced by the exit of lectin from the vasculature, the newly formed vessels were leaky, which was intensified in the mice that developed the aneurysms (Fig. R22).

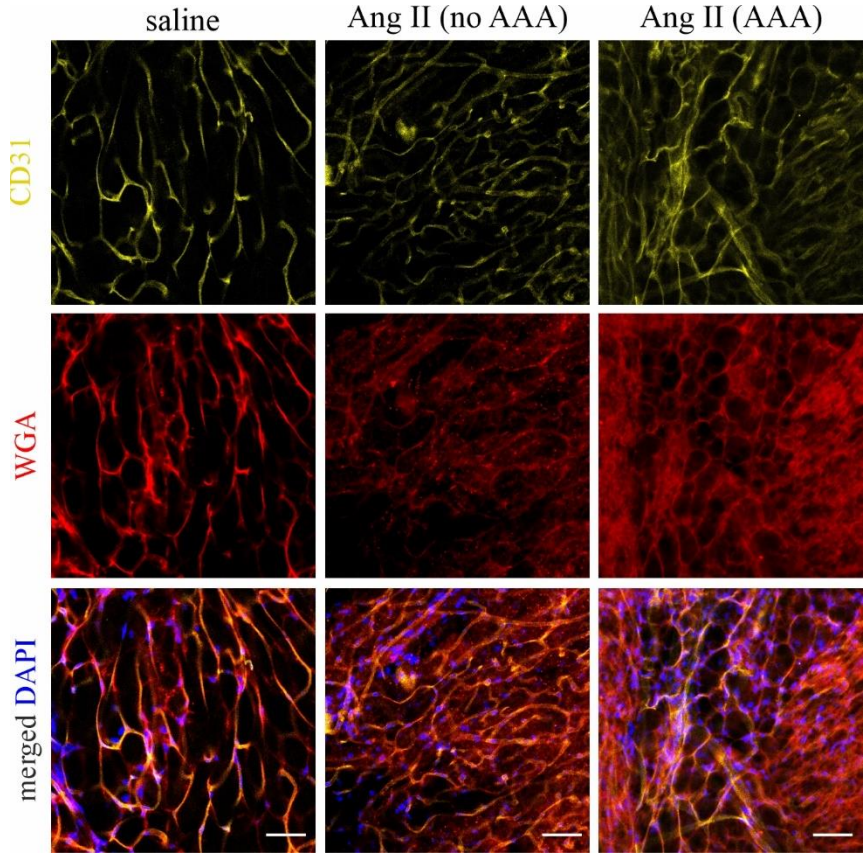

Figure R22. Ang II infusion promotes the formation of leaky neovessels. The whole-mount immunofluorescent staining of the PVAT vasculature upon Ang II infusion. EC marker CD31- yellow, WGA – red, nuclei – blue; scale bar = 50 μm; n=5-6; 3-month-old mice.

One of the proangiogenic and promigratory factors for the vascular cells is cholesterol[320]. Ultrastructural changes are evidenced in the mice with altered lipid profiles[321]. Moreover, aged tKO intimal abnormalities resemble cholesterol-containing 'endothelial breaches'[322]. Given that hypercholesterolemic mice are predilected to AAA[99], it is credible that the altered cholesterol distribution accounts for the susceptibility of NRF2 tKO mice to AAA and the incidence of intimal SEM-depicted changes. Then to further address the impact of cholesterol, we administered statin as pre- and cotreatment in the Ang II-induced AAA model, which fully abrogated Ang II-induced AAA formation in NRF2 tKO mice (Fig. R23A, Supp. Fig. 6). It was concomitant with the decrease in SEM-revealed intimal anomalies (Fig. R23B), suggesting a strong correlation between intimal ultrastructure and the susceptibility to AAA.

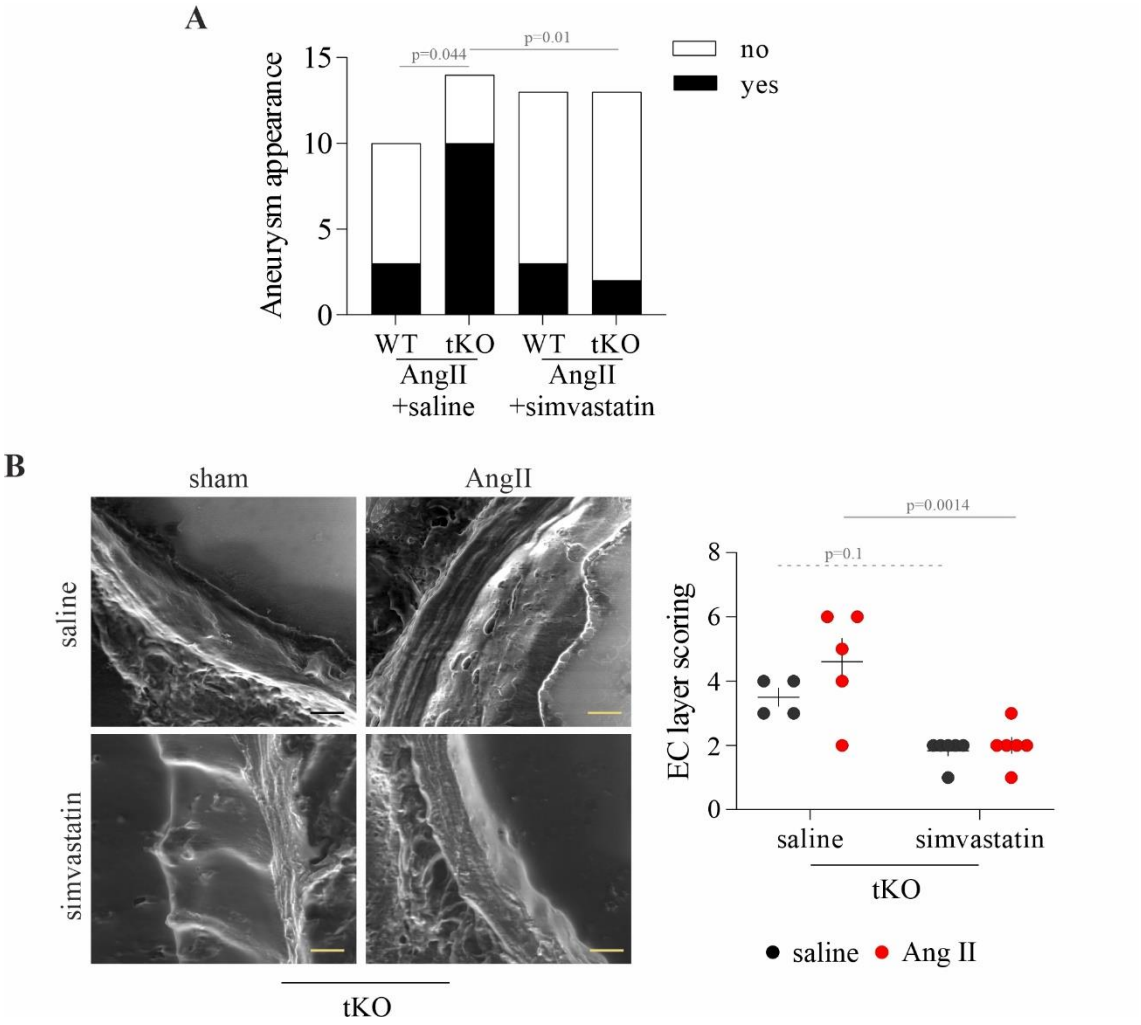

Figure R23. Simvastatin attenuates AAA formation favoured by lack of NRF2 transcriptional activity and abrogates endothelial anomalies. (A) Aneurysm incidence upon treatment with simvastatin or/and angiotensin II; n=10-14; 6-month-old mice. **(B)** Representative images and quantification of SEM-depicted changes of the EC layer in NRF2 tKO mice treated with simvastatin or/and angiotensin II; scale bar=10 μm; n=4-6; 6-month-old mice.

Then, we decided to use this correlation to establish further the link and credible origin of conduits we observed in aged NRF2 tKO mice. Upon simvastatin treatment, we evidenced a decrease in perivascular adipose tissue vascularisation (Fig. R24A) and significantly lower fluorescence of lumen-injected gold particles (Fig. R24B). That implied the link between PVAT vascularisation, aortic wall conduits and intimal ultrastructure changes. Furthermore, in the light of the enhanced Ang II-driven angiogenesis, the changes originating from the PVAT and aortic wall vascularisation were probably key to understanding the pathogenesis of AAA.

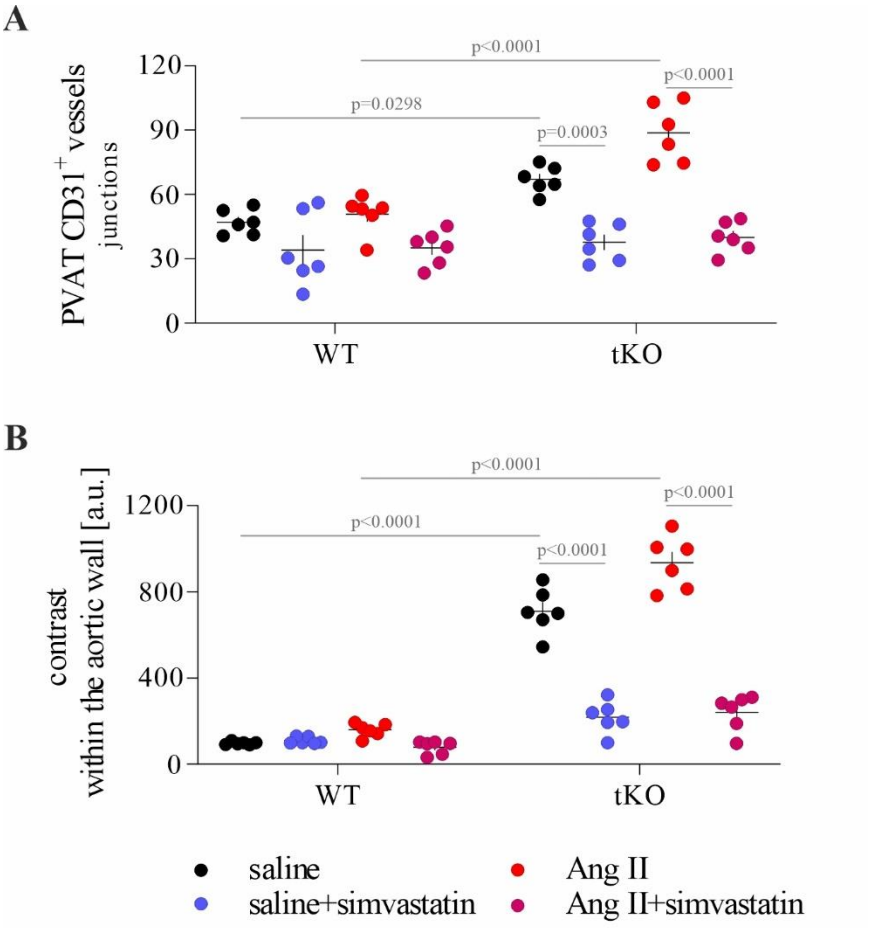

Figure R24. Simvastatin decreases the vascularisation of the PVAT and the permeability of the intimal ECs. (A) The quantification of the vascularisation of PVAT in mice upon administration of Ang II and/or simvastatin. **(B)** The quantification of the permeability of the intimal layer assessed by the intraluminal injection of gold particles; n=6; 3-month-old mice.

Still, an important question arose whether the observed protective impact of simvastatin was dependent on the lipid (cholesterol)-lowering capacities. To address that issue, we performed the Time of Flight – Secondary Ion Mass Spectrometry (TOF-SIMS) analysis of the cholesterol content within the aortic wall. The experimental setup permitted scanning and going deeper into the intimal layer. Still, supposingly, we could not reach the regions below 100 nm, and we mostly saw the membrane distribution of cholesterol. The analysis of the profile of cholesterol and its total content revealed that simvastatin treatment did not affect the cholesterol level. It implied that the AAA-protective action was independent of cholesterol-lowering capacities (Fig. R25).

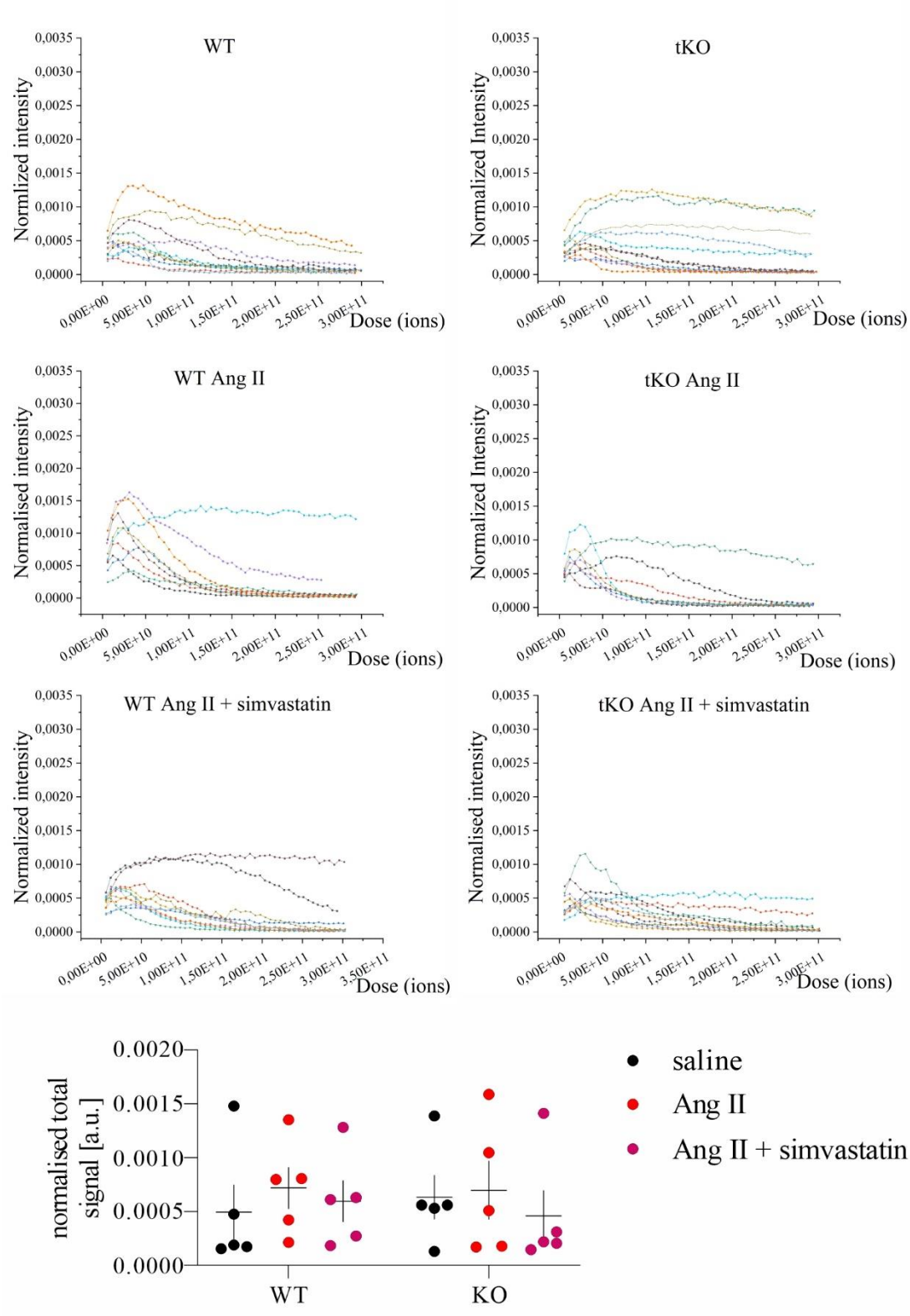

Figure R25. Simvastatin administration does not alter the EC cholesterol profile in mice infused with Ang II. The cholesterol profile in the intimal layer assessed by TOF-SIMS, the higher the dose of ions, the deeper in the cell is the signal localized and the total cholesterol signal in the analysed tissue. Each line on the plots show data recorded for at least once for different mice, the higher dose, the deeper the penetration within the arterial wall; for the final quantification the integral was calculated. The analysis was performed in collaboration with Dr. Kamil Awsiuk, Institute of Physics, Jagiellonian University; n=5; 3-month-old mice.

The performed analyses permitted delineating the sound role of intimal aortic structural changes and PVAT vascularization in the susceptibility to AAA formation. However, in this part of the research, we did not fully elucidate the involvement of ageing, especially of EC, in the proneness to AAA. Available data suggest that the most likely ageing-driven mechanism could rely on SIRT1[323] and miRNA-34a[282], the latter being a hallmark of ageing[266]. It is known that miRNA-34a inhibition counteracts ageing and AAA[282]. Based on that, we hypothesised that the depletion of miRNA-34a specifically from ECs would reverse their Nrf2 TA deficiency-driven senescence. Then such a model could be used to clarify the role of EC senescence in AAA.

The susceptibility of NRF2 tKO to AAA results from the overabundance of miRNA-34a in endothelial cells

Importantly, significant alterations in miRNA modulatory networks accompany the formation of Ang II-induced AAA, with miRNA-34a being significantly upregulated[324,325]. Also, in our hands, Ang II enhanced miRNA-34a levels in human aortic endothelial cells (HAEC) exposed to Ang II (Fig. R26A). Substantially, *in vivo*, Ang II infusion increases miRNA-34a level in serum (Fig. R26B) and the aortic tissue. Of note, in AAA, this miRNA was most abundantly present in endothelial cells (Fig. R26C), which coincided with strong miRNA-34a upregulation in serum.

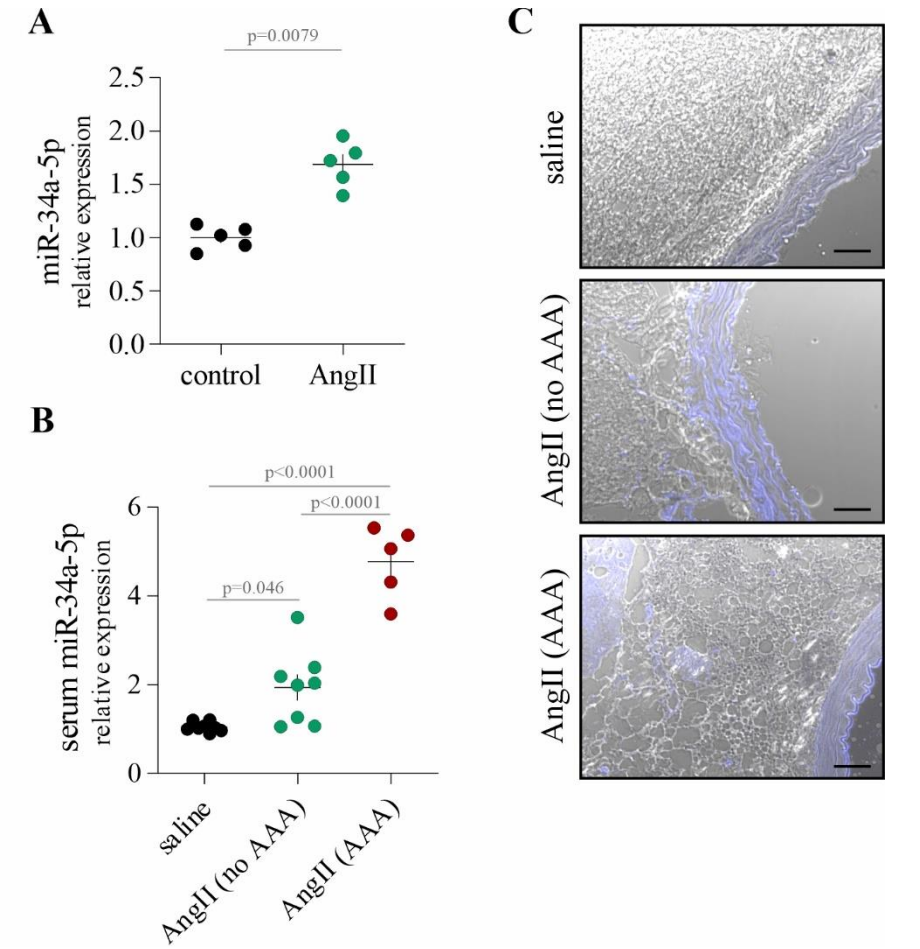

Figure R26. miRNA-34a-5p is increased upon Ang II treatment *in vitro* and *in vivo*. Relative expression of miR-34a in **(A)** HAECs incubated with 500 nM Ang II for 8h and **(B)** in serum of mice receiving control or Ang II (1000 ng/min/kg) for 7 days. Small nuclear U6 served as an internal control for qPCR; n=5. **(C)** Representative images of conventional RNA *in situ* hybridization-based detection of miRNA-34a-5p in control and Ang II-receiving animals, which formed or not the aneurysms, blue – miRNA-34a-5p; scale bar =50 μm; n=5-8; 3-month-old mice.

MiRNA-34a was significantly upregulated in senescent NRF2-deficient HAECs in a p53-dependent manner (Fig. R27A). As miR-34a is a known critical senescence-inducing agent[255,326,327], we hypothesised that its inhibition might result in the inversion of the senescent phenotype in NRF2-depleted HAECs. Indeed, concomitant silencing of NRF2 and miRNA-34a abrogated NRF2 deficiency-related senescence induction (Fig. R27B). Furthermore, *en face in situ* RNA hybridisation confirmed a pronounced increase of this miRNA in ECs of NRF2 transcriptional knockout mice (Fig. R27C).

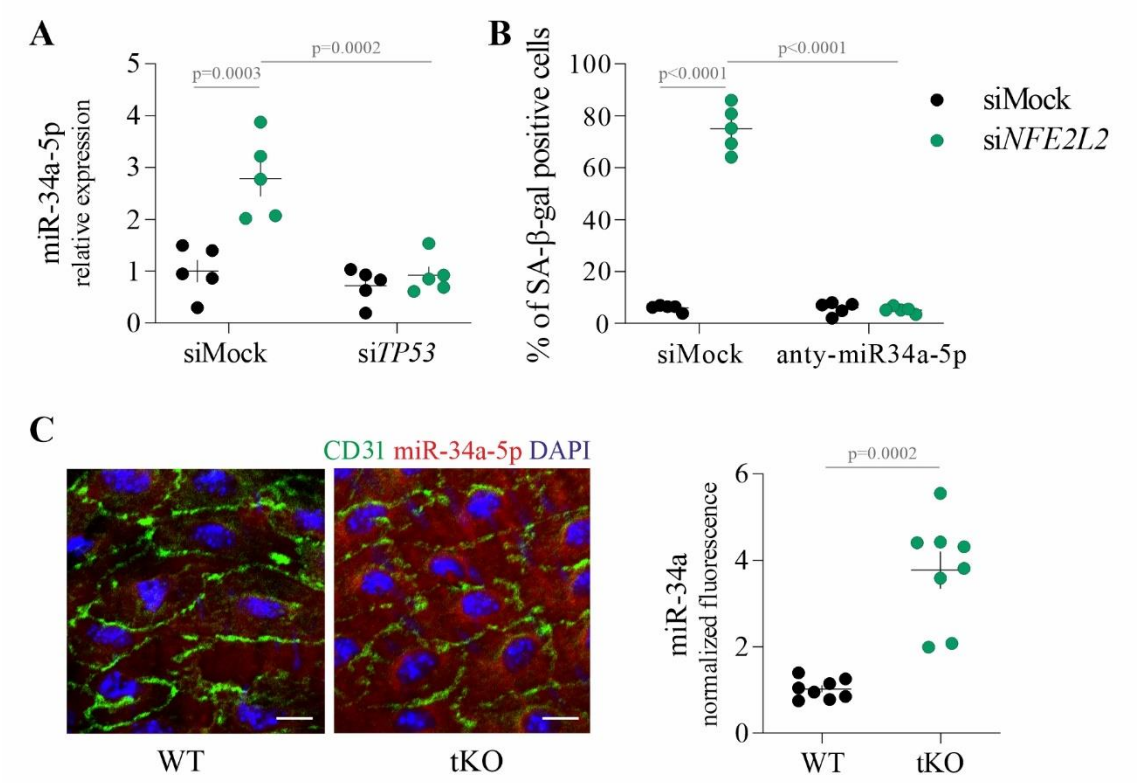

Figure R27. MiR-34a is upregulated in NRF2-related prematurely senescent endothelial cells. **(A)** Relative expression of miR-34a in HAECs deficient in NRF2 and p53. Small nuclear U6 served as an internal control for qPCR, n=5. **(B)** The level of senescence in HAECs devoid of NRF2 and miRNA-34a was assessed by SA-β-galactosidase staining, n=5. **(C)** Representative images and the quantification of the data of *en face in situ* hybridisation in the endothelial layer of WT and NRF2 tKO animals; the endothelial cells were visualised by CD31 (green) staining. DAPI was used for the depiction of the nuclei; scale bar = 15 μm; n=8; 3-month-old mice.

To address the significance of EC senescence in the susceptibility to aneurysm formation, we crossed NRF2 tKO with inducible EC-specific miRNA-34a knockout mice. It permitted the specific deletion of miRNA-34a in endothelial cells, and its level in VSMCs remained comparable (Fig. R28A). Furthermore, it reversed the senescent phenotype of ECs in NRF2 tKO mice (Fig. R28B).

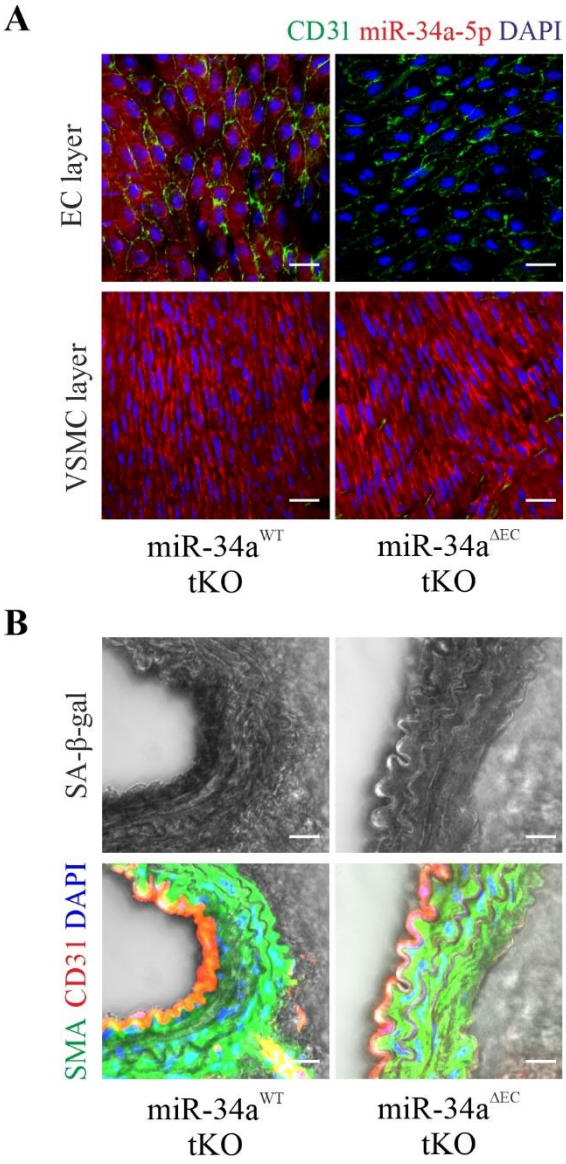

Figure R28. Efficient depletion of miRNA-34a from the aortic endothelium of tKO mice results in the inversion of the senescent phenotype. (A) Representative images of *in situ* hybridization detecting the miRNA-34a in EC and VSMC layer in tKO mice; the endothelial cells were visualised by CD31 (green) staining. DAPI was used to depict the nuclei; scale bar = 50 μm; n=5. **(B)** Senescence-associated β-galactosidase activity on the abdominal aorta cross-section, followed by staining of intimal (CD31-red) and medial (αSMA-green) layers. The nuclei are stained with DAPI (blue); scale bar = 25 μm; n=6; 3-month-old mice.

Moving to the Ang II-related AAA model, endothelial miRNA-34a deficiency hindered the formation of AAA in NRF2 tKO mice in 3-month-old mice (Fig. R29A), which was concomitant with the enhanced proliferation of ECs (Fig. R29B and representative pictures in Supp. Fig. 7).

To sum up, endothelial miRNA-34a is a pivotal regulator of Ang II-induced AAA in prematurely aged NRF2 tKO mice. The cessation of aneurysm incidence may be

related to the inversion of senescent phenotype and enhanced EC proliferation. Furthermore, endothelial cells are imperative regulators of AAA formation.

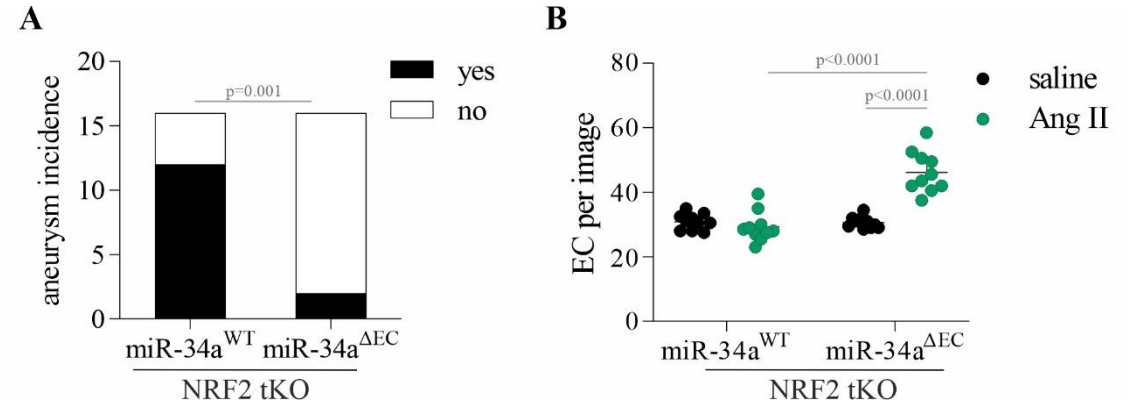

Figure R29. Deleting miRNA-34a from ECs of NRF2 tKO mice abrogates the AAA formation with a concomitant increase in the aortic EC proliferation. (A) The aneurysm incidence in miRNA-34a EC KO NRF2 tKO mice. The mice were infused with Ang II for up to 14 days; n=16. **(B)** Quantification of ECs visible on the EC monolayer images in mice infused with saline or Ang II for 7 days; n=10; 3-month-old mice.

miR-34a deficiency hampers Ang II-related AAA formation in other models independent of NRF2[282]. Therefore, to elucidate the mechanisms of miRNA-34a abrogation-related AAA cessation, we decided to use an inducible EC-specific knockout of miRNA-34a. Such an approach permitted delineating NRF2-independent mechanisms governing AAA formation and substantiating the pivotal role of EC in AAA formation.

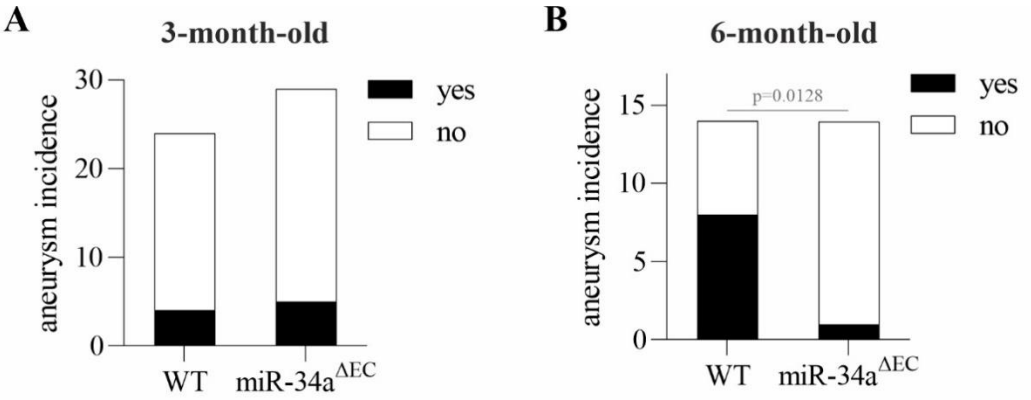

Figure R30. Deleting endothelial miRNA-34a results in the abrogation of AAA formation in older mice. (A-B) The incidence of AAA in **(A)** 3-month and **(B)** 6-month-old animals upon the infusion with Ang II for up to 14 days; n=14-29.

Upon subjecting to Ang II, we observed no impact on aneurysm incidence in younger mice and clear abrogation of aneurysm formation in older mice (Fig. R30). It confirmed our findings in NRF2 transcriptional knockout mice and available data from other groups.

miRNA-34a is a crucial regulator of endothelial cell phenotype

The protective role of ECs in cardiovascular diseases often interrelates with an enhancement of their function[328]. Moreover, if endothelial involvement is acknowledged in AAA, it is speculated it mainly relies on the endothelial function[117–119]. Therefore, the endothelial miRNA-34a deficiency may permit the maintenance of a healthy endothelial phenotype and thus impedes the formation of AAA. The rising evidence points to glycocalyx as an essential determinant of endothelial cell function and physiological response to mechanical stress[161,329]. Therefore, taking the first step, we inspected the glycocalyx length and endothelial stiffness by atomic force microscopy. It revealed that endothelial miRNA-34a deficiency led to a compelling decrease in glycocalyx length (Fig. R31A) with a concomitant increase in its stiffness (Fig. R32B). Moreover, *en face* staining of endothelial glycocalyx components N-acetyl-D-glucosamine and sialic acid detected with WGA lectin pointed out their considerable decrease under miRNA deficiency (Fig. R32C).

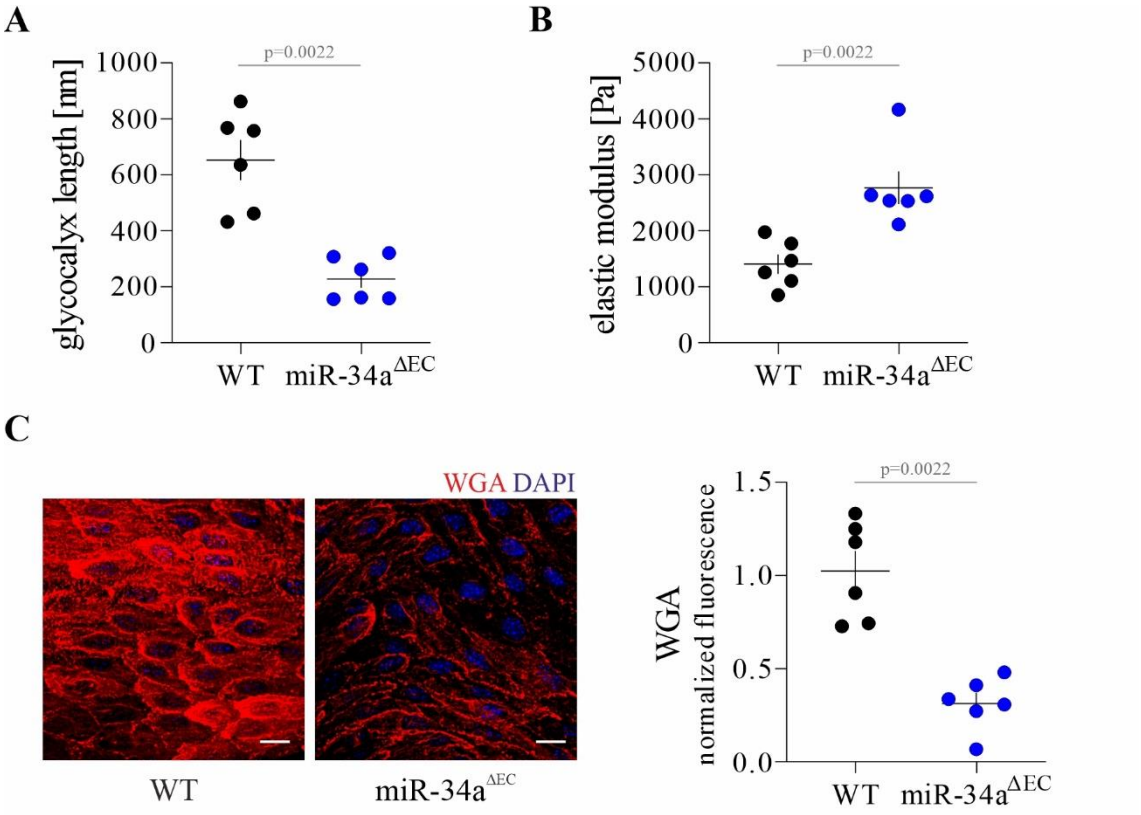

Figure R31. The endothelial deletion of miRNA-34a results in the shortening of the glycocalyx. (A-B) Assessment of endothelial cell glycocalyx **(A)** length and **(B)** EC stiffness assessed by atomic force microscopy. The data obtained in collaboration with Dr. Marta Targosz-Korecka; Institute of Physics, Jagiellonian University. **(C)** Representative images and the quantification of the staining of glycocalyx components by Wheat Germ Agglutinin (WGA, red); DAPI was used to depict the nuclei. scale bar = 30 μm; n=6; 3-month-old mice.

Such glycocalyx deterioration can significantly impair endothelial cell function, resulting in enhanced leukocyte rolling and diapedesis, prothrombotic phenotype, and impaired production of nitric oxide[330]. Therefore, to fully address the impact of miRNA-34a deficiency on endothelial function, we inspected these features of healthy endothelial phenotype. Intravital microscopy permitted life imaging of leukocyte adhesion to mesenteric venules, which was significantly higher in miR-34a$^{\Delta EC}$ and resulted in a notable decrease in leukocyte velocity (Fig. R32).

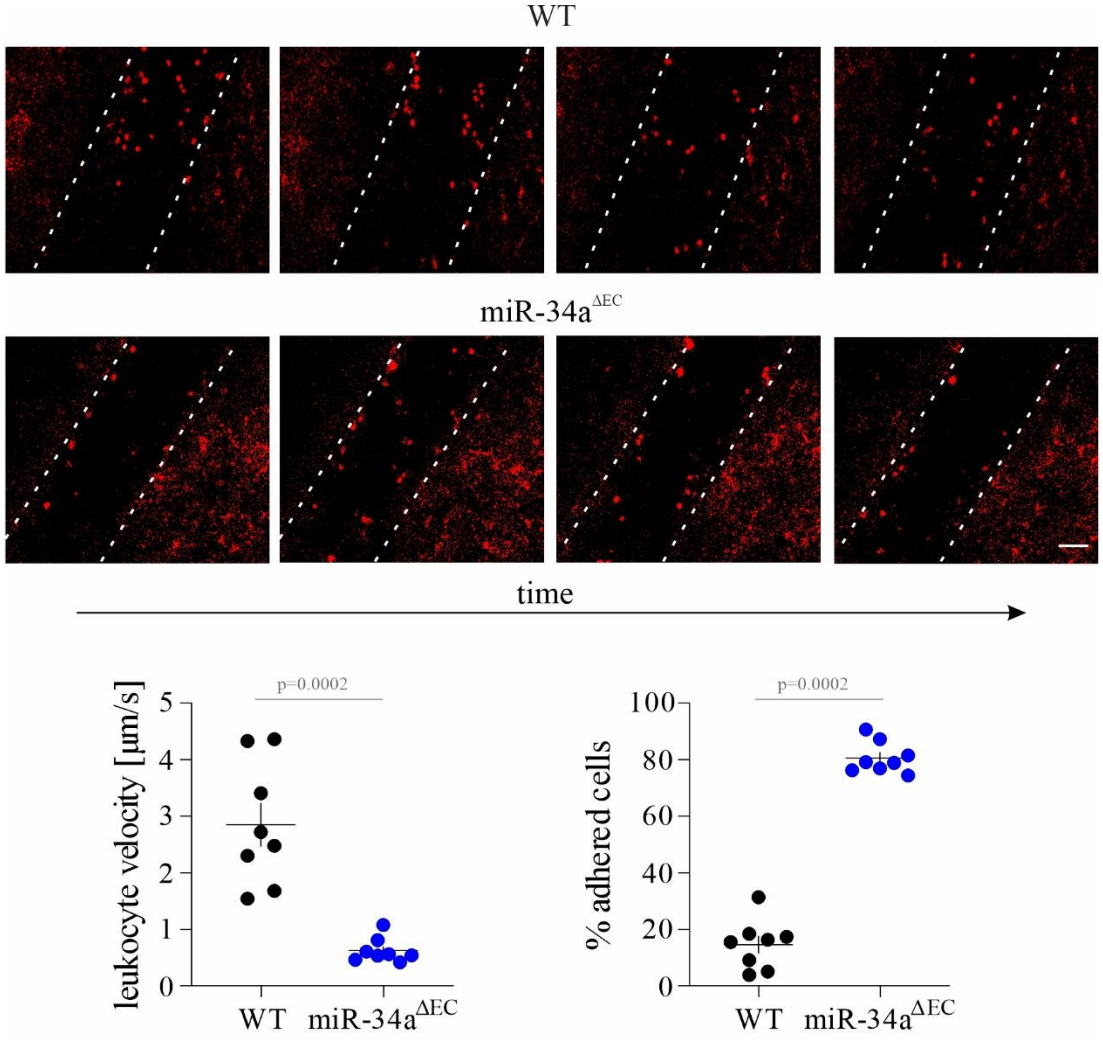

Figure R32. A significant pro-inflammatory phenotype of miRNA-34a deficient ECs *in vivo*. The representative images and the quantification of leukocyte velocity and adhesion to the mesenteric venules were assessed by intravital microscopy; scale bar = 200 µm; n=8; 3-month-old mice.

Then, we used two models to establish the impact of miRNA-34a deficiency on thrombosis. In the first one, low doses of collagen and epinephrine were used to trigger platelet activation and vasoconstriction. It led to pulmonary microembolisms and permitted the assessment of the prothrombotic phenotype of the endothelium[292]. The lack of miRNA-34a in endothelial cells induced a significantly higher pulmonary thrombosis. Of note, we observed spontaneous tonic and myoclonic movements, which substantiated the occurrence of robust thrombosis only in miRNA-34a$^{\Delta EC}$ mice (Fig. R33A). Accordingly, ferric chloride-induced carotid artery injury led to distinctively more extensive thrombus formation under miR-34a endothelial deficiency (Fig. R33B). However, in this model, the involvement of the sub-endothelial layer

could not be discarded. The prothrombotic phenotype did not depend on altered platelet features (Supp. Fig. 8).

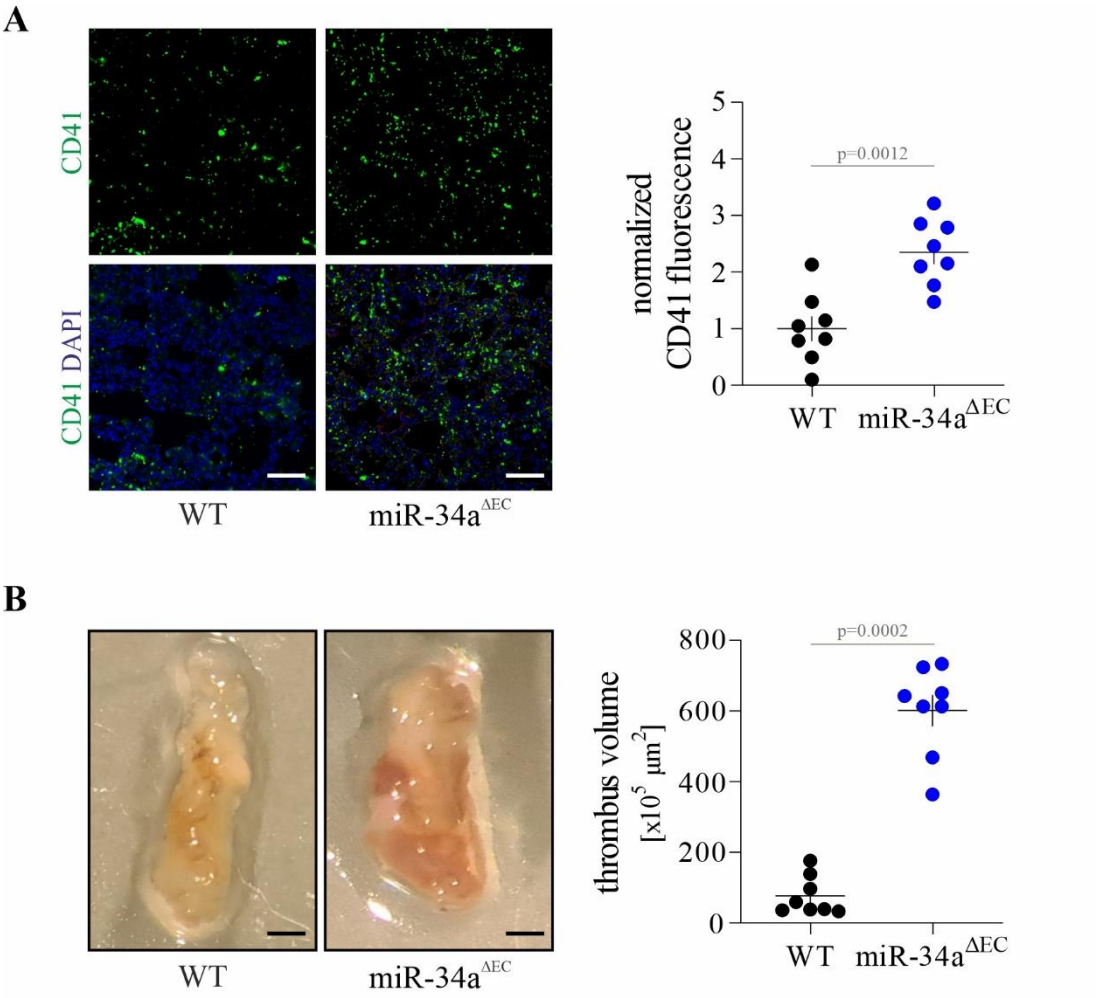

Figure R33. The lack of endothelial miRNA-34a results in the prothrombotic phenotype. (A) The representative images and the quantification of the pulmonary thrombosis induced by collagen and epinephrine injection. Platelets were stained *in vivo* with anti-CD41 antibody (green). DAPI (blue) was used to stain the nuclei. Scale bar =50 µm; n=8; 3-month-old mice. **(B)** The representative images of thrombus induced by $FeCl_3$ and the quantification of its volume. Scale bar = 500 µm, n=8; 3-month-old mice.

The production of nitric oxide by endothelial cells is a chief determinant of proper response to blood flow and the regulation of vascular tone. Its deregulation is a sign of EC dysfunction[328]. The lack of endothelial miR-34a diminished NO production (Fig. R34A). Such a decrease in NO production could mainly affect functional aortic stiffness. Supportively, pulse wave velocity measurements confirmed the significant stiffening of the aortas in miR-34a$^{\Delta EC}$ (Fig. R34B,C).

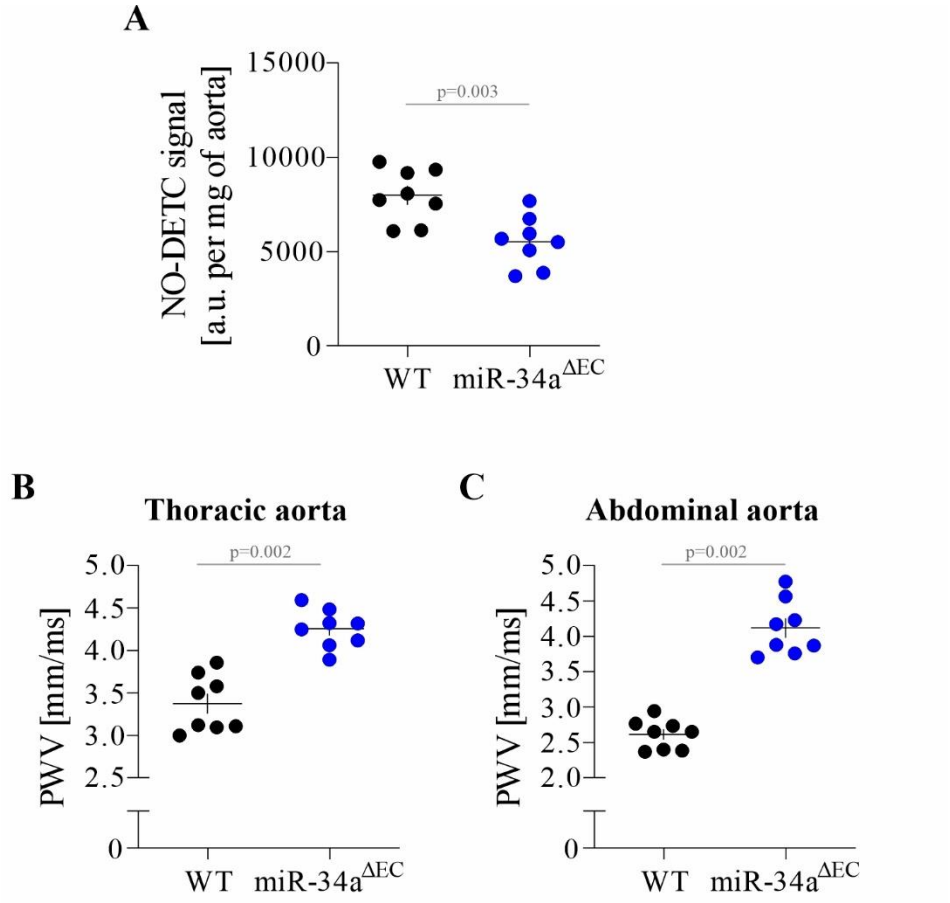

Figure R34. The abrogation of miRNA-34a in endothelial cells leads to significantly lower NO production and arterial stiffening. (A) NO production was assessed by Electron Paramagnetic Resonance. **(B-C)** Pulse wave velocity (PWV) in **(B)** thoracic and **(C)** abdominal aorta was assessed by Doppler Flowmetry. The results were obtained in collaboration with Dr. Anna Bar and Prof. Stefan Chłopicki. Jagiellonian Center for Experimental Therapeutics; n=8; 3-month-old mice (A-C).

Taking above, depletion of miRNA-34a in endothelium leads to a robust dysfunctional phenotype in young mice. As miRNA-34a is an age-dependent miRNA, we decided to address its significance in older – 6-month-old mice. Similarly to younger animals, increased leukocyte adhesion (Fig. R35A), thrombosis (Fig. R35B) and vascular stiffening were present in older miR-34a$^{\Delta EC}$ (Fig. R35C,D).

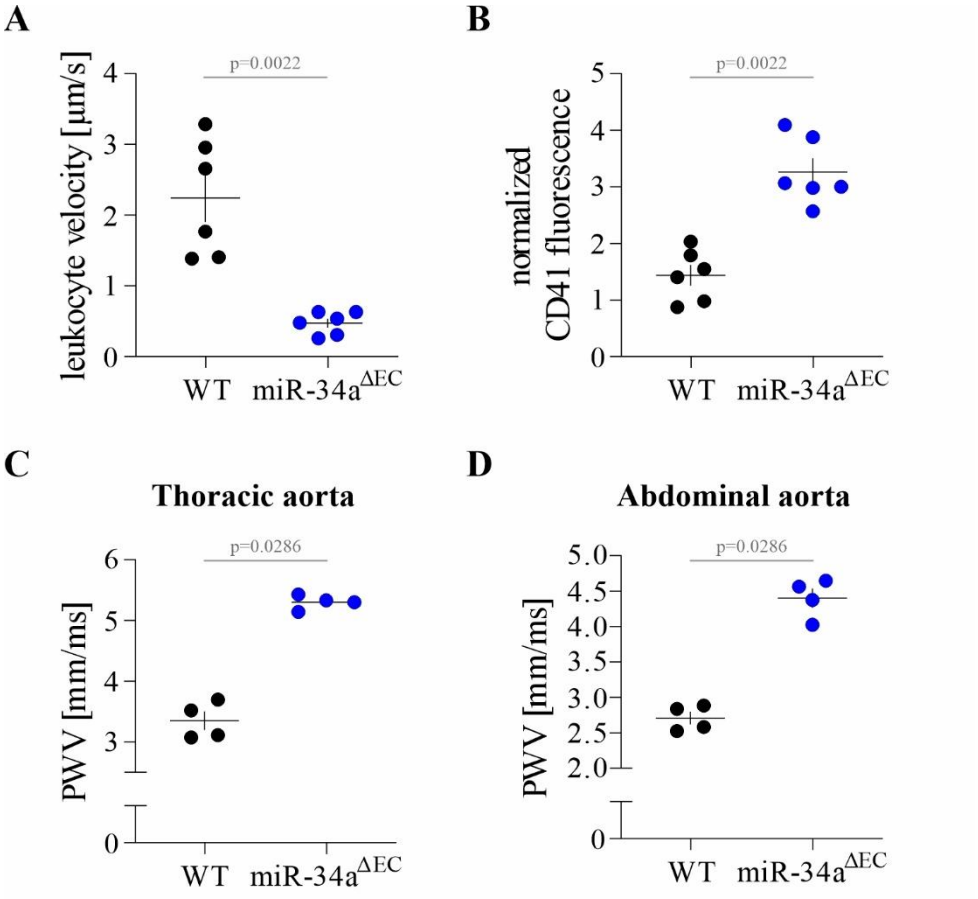

Figure R35. A significant deterioration of endothelial function upon the deletion of miRNA-34a *in vivo* in older mice. (A) Assessment of leukocyte velocity in the mesenteric venules by intravital microscopy; n=6. **(B)** assessment of thrombotic phenotype by collagen epinephrine-related model. Anti-CD41 antibody was used to stain the platelets; n=6. **(C-D)** Pulse wave velocity (PWV) in **(C)** thoracic and **(D)** abdominal aorta assessed by Doppler Flowmetry. The results were obtained in collaboration with Anna Bar, PhD and Prof. Stefan Chłopicki; n=4-5; 6-month-old mice (A-D).

Supportively, we observed significant glycocalyx shortening upon the depletion of endothelial miRNA-34a (Fig. R36A). However, in contrast to young animals (Fig. R31), the Young modulus of the ECs (Fig. R36B). Immunofluorescent staining corroborated the significant decrease in the glycocalyx size (Fig. R36C).

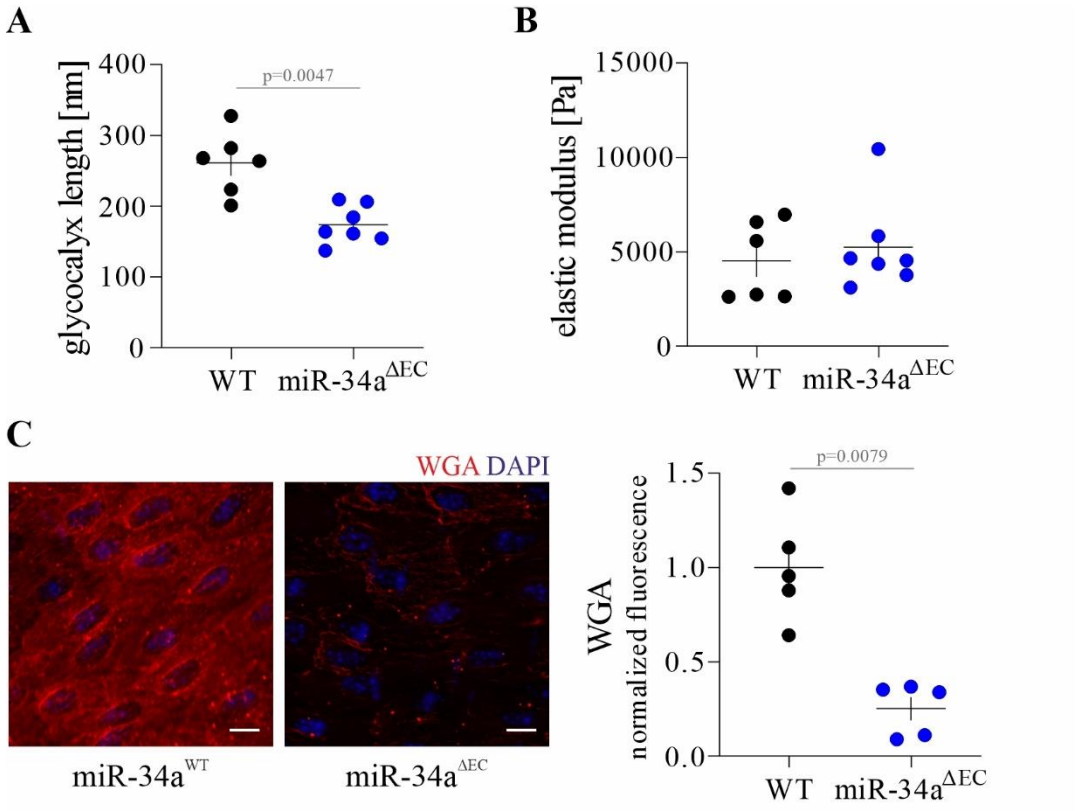

Figure R36. The endothelial deletion of miRNA-34a results in the shortening of the glycocalyx in older mice. (A-B) assessment of endothelial cell glycocalyx **(A)** length and **(B)** EC stiffness by atomic force microscopy; n=6. Data were obtained in collaboration with Dr. Marta Targosz-Korecka, Institute of Physics, Jagiellonian University. **(C)** Representative images and the quantification of the staining of glycocalyx components by Wheat Germ Agglutinin (WGA, red). DAPI was used to depict the nuclei; scale bar =15 μm; n=5; 6-month-old-mice (A-C).

To conclude, miRNA-34a is a vital regulator of endothelial cell function. Its deficiency *in vivo* leads to age-dependent EC dysfunction, as evidenced by a decreased length of the glycocalyx and reduced NO production, with a concurrent increase in arterial stiffness, leukocyte adhesion and prothrombotic phenotype. However, despite detrimental effects on EC function, deficiency of miR-34a in ECs does not result in higher aneurysm incidence and even abrogates AAA formation in older animals. Therefore, the endothelial function cannot be the primary determinant of aneurysm formation in the Ang II-based model.

Rapamycin reverses protective effect of EC miR-34a depletion on aneurysm formation

Ang II-triggered cellular signalling is central to the formation of aneurysms in this model[301]. Therefore, any alteration in this signalling pathway could affect AAA development and account for its abrogation in the older mice. Binding to Ang II receptor 1 (AT1R) permits the proaneurysmal action of Ang II[305]. Importantly, the AT1R level was augmented even in the saline-treated miR-34a$^{\Delta EC}$ mice and was more pronouncedly increased by Ang II (Fig. R37A). Of note, the protective Ang II receptor 2 (AT2R) level was barely detectable in any inspected group (data not shown). Moreover, we could observe a clear hypertensive action of Ang II infusion. However, there was no difference between the genotypes (Fig. R37B).

The product of Ang II degradation by ACE2, angiotensin 1-7 (Ang1-7), counteracts Ang II action and has a recognised protective effect on AAA[331]. Ang II infusion significantly enhanced the Ang1-7 level to a similar degree between genotypes (Fig. R37C). Taking the above, the analysis of Ang II-signalling determining factors revealed only a difference in the AT1R level. This proanuerysmal receptor was significantly upregulated upon endothelial miRNA-34a depletion. Therefore it is rather doubtful that the alterations in the Ang II signalling account for the abrogation of AAA formation in these mice.

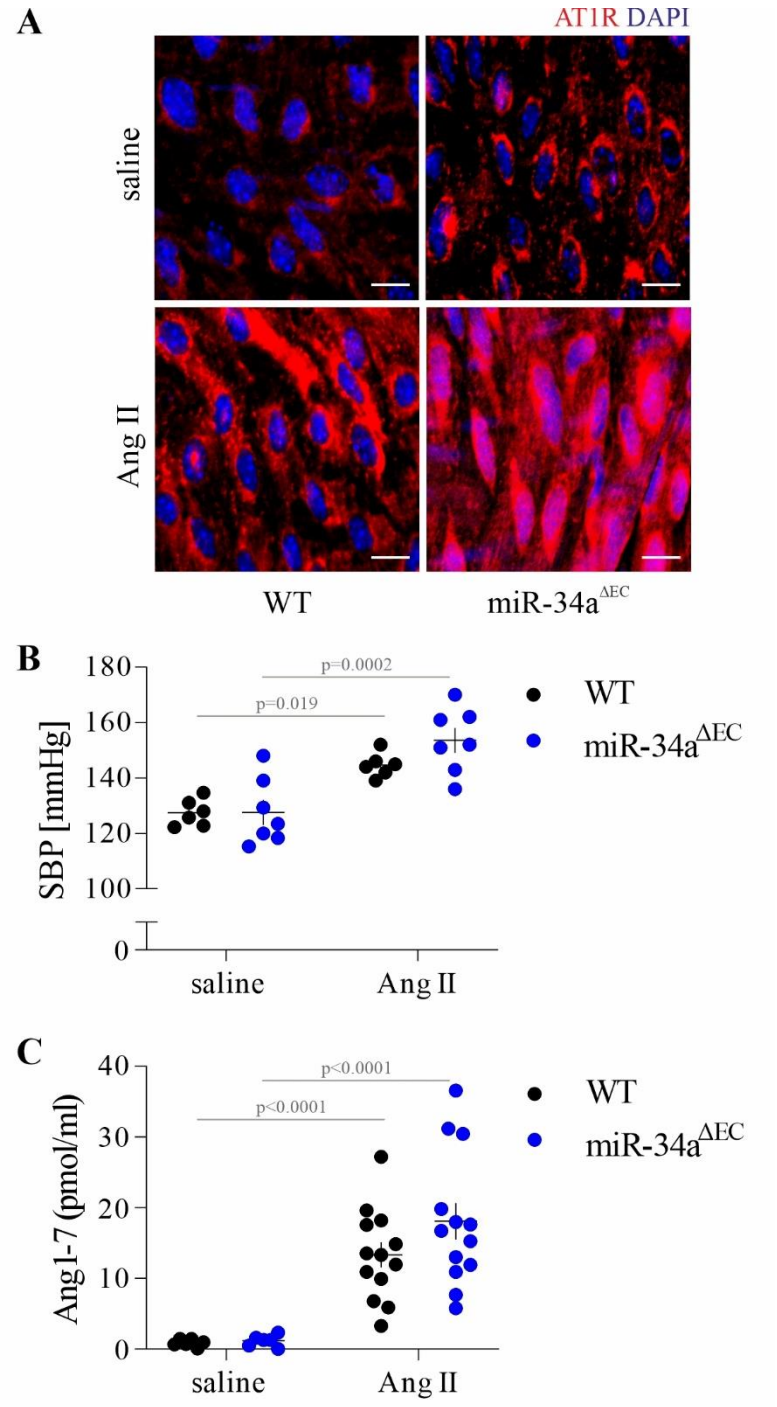

Figure R37. The miRNA-34a endothelial deficiency-related protection against AAA is not dependent on hypertensive and signalling features of Ang II. **(A)** Immunofluorescent *en face* staining of Ang II receptor 1 (AT1R, red); DAPI was used to depict the nuclei. Scale bar = 15 μm; n=7. **(B)** Systolic blood pressure (SBP), n=6-7. **(C)** Serum level of Ang II metabolite (Ang1-7); n=6-14; 6-month-old mice.

Similarly to the results obtained in the NRF2 tKO miR-34a$^{\Delta EC}$ (Fig. R29B), during this part of studies, we observed a higher number of ECs upon miR-34a deletion in endothelial cells. They even seemed to grow on each other, plausibly strengthening the EC layer. Also in this case, supporting our findings *in vitro*, we noticed significantly

higher intimal EC proliferation in Ang II-stimulated miRNA-34a-deficient endothelium, irrespectively of the age of the mice (Fig. R38).

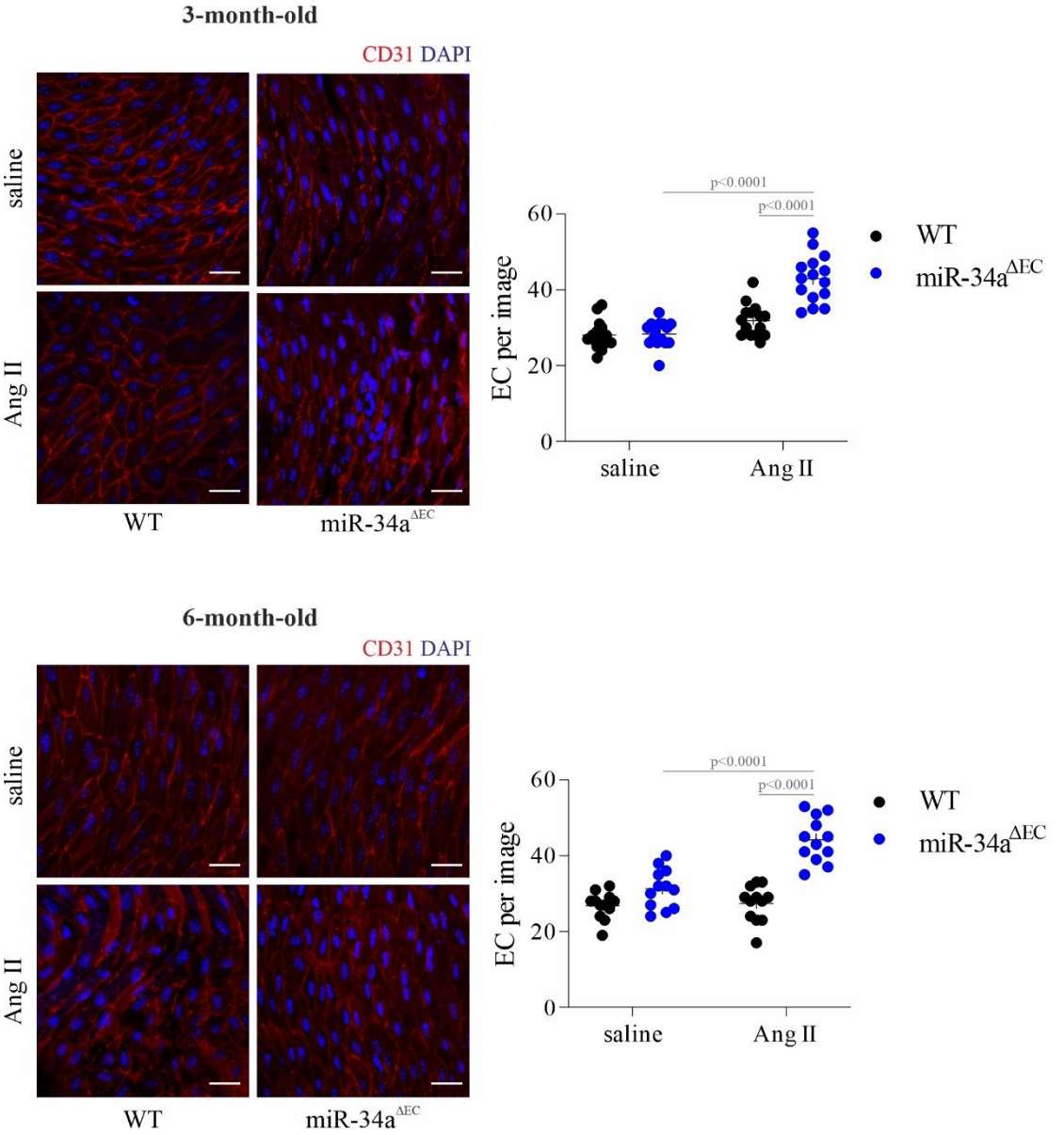

Figure R38. Endothelial miRNA-34a deficiency leads to enhanced intimal cell proliferation upon Ang II infusion. The level of proliferation was assessed by the number of intimal ECs per image upon miRNA-34a^{EC-KO} and infusion of Ang II in 3- and 6-month-old mice. DAPI was used to depict the nuclei. Scale bar = 50 μm; n=12-15.

In the next step, we decided to use rapamycin, which hampers proliferation in EC[332,333], to elucidate further the role of proliferation in the protection of dysfunctional aortas against AAA. Rapamycin administration efficiently decreased intimal cell proliferation (Fig. R39A) and resulted in robust induction of AAA only in miR-34a$^{\Delta EC}$ (Fig. R39B). Moreover, macroscopically, the formed AAA seemed rupture-prone (Fig. R39C). Therefore, in the miRNA-34a-based model, proliferation inversely

correlates with the AAA susceptibility. Consequently, it should be expected that proliferation confers protection against AAA. Still, we cannot discard the impact of other cellular processes, which could have also been affected by rapamycin[334].

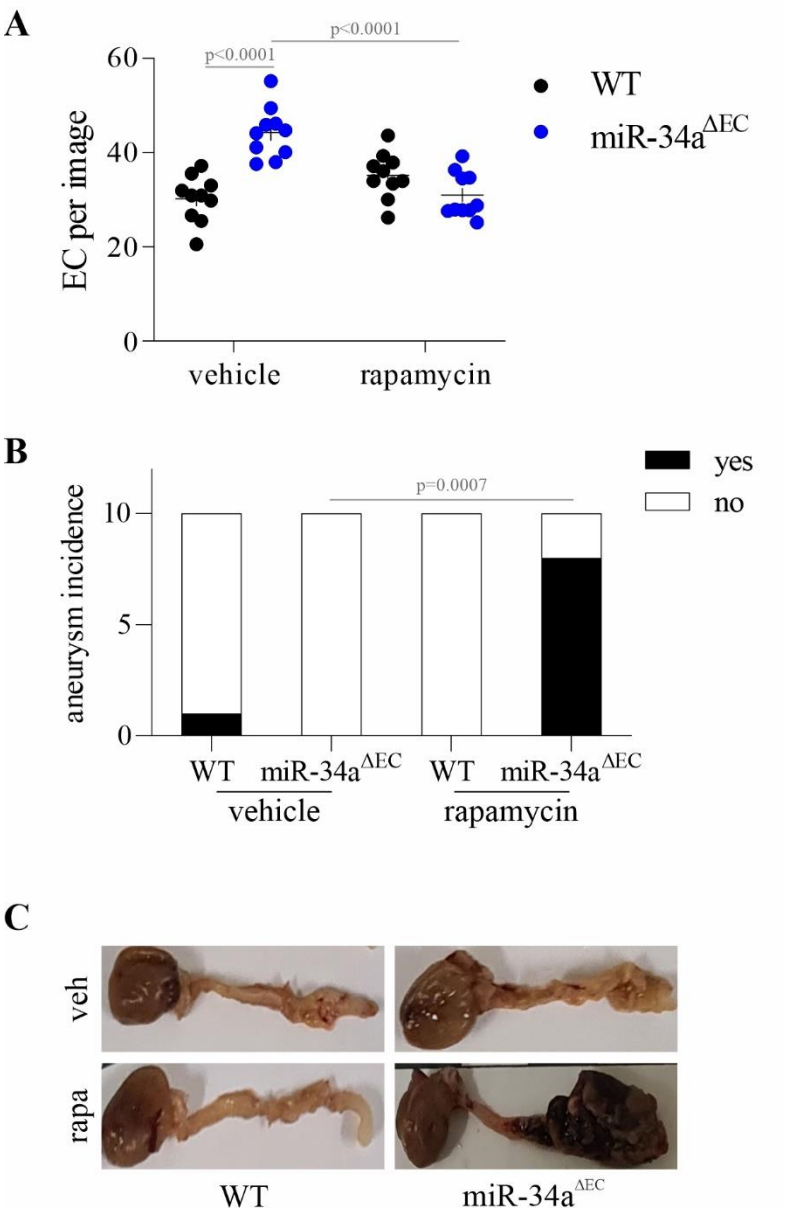

Figure R39. Endothelial cell proliferation confers the protection against AAA of EC-restricted miRNA-34a deficient mice. (A) Level of proliferation assessed by the number of intimal ECs per image upon rapamycin treatment and Ang II infusion. **(B)** The incidence of aneurysm upon rapamycin treatment and Ang II infusion. **(C)** The morphology of the aortas in the inspected groups revealed enormous, rupture-prone aneurysms in miRNA-34a$^{EC\text{-}KO}$ mice. Scale bar = 5 mm; n=10; 3-month-old mice.

Therefore, for further validation of the EC proliferation-associated mechanism, we decided to use EC-specific Rainbow mice. We aimed to detect and trace EC proliferation, substantiating its involvement in AAA. In accordance, we could observe the significant

enhancement of intimal cell proliferation. Whereas in saline-treated animals we noticed random recombination, upon Ang II we could observe neighbouring cells positive for the same reporter protein (Fig. R40A). Moreover, we could depict a link between the proliferative response and the stability of AAA. Only in firmly established AAA ECs were proliferating in the thrombus area (Fig. R40B). Interestingly, the area occupied by CD31-positive capillary-like structures decreased in time (Fig. R40C), which was concomitant with the presence of senescent cells at the borders of AAA (Fig. R40D). Therefore, we can suspect that there is a dynamic adjustment of proliferatory cellular state within the thrombus in the AAA.

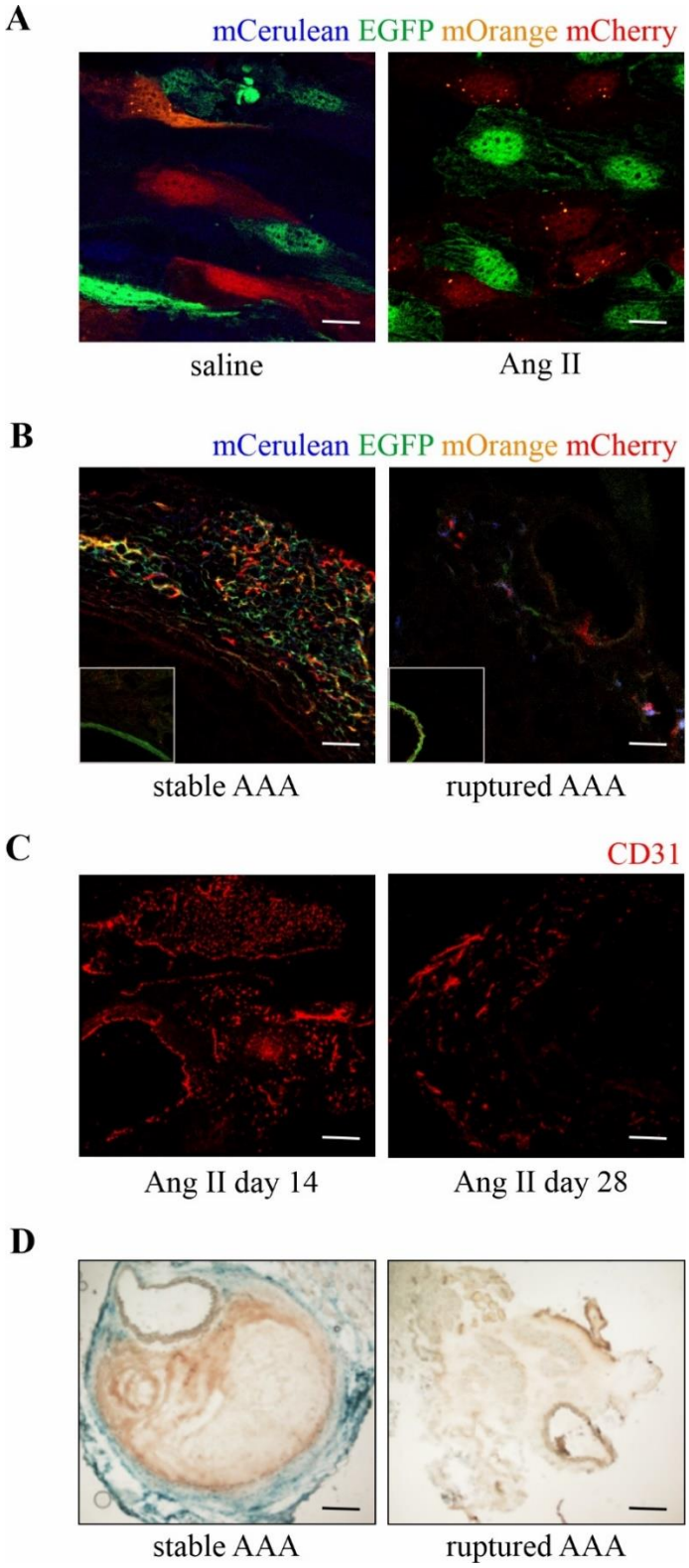

Figure R40. Fine-tuning of proliferation and senescence play a crucial role in the development and maintenance of AAA. (A) Tracing of intimal endothelial cell proliferation by *en face* detection of the reporter proteins. **(B)** Tracing of endothelial cells on the edges of aneurysmal tissue. The insets show the whole aorta with lumen. Scale bar = 20 μm (in A) or 50 μm (in B); n=8-10. **(C)** Immunofluorescent staining of CD31-positive endothelial cells (red) in the aneurysmal tissue of a growing aneurysm (day 14) and stabilised aneurysm (day 28), scale bar = 100 μ; n = 5-7. **(D)** Senescence-associated β-galactosidase staining of the stable and ruptured aneurysms, representative pictures; scale bar = 100 μm; n=8-10; 6-month-old mice.

Discussion

The vast majority of cells in the body lie within 100-150 μm of the next capillary due to the limited diffusion distance of oxygen in tissues. As a result, research in vascular biology impacts practically all medical disciplines – and is largely affected by ECs. On the other hand, it is still frequently overlooked that dysfunction of the inner lining of blood arteries is the single most important cause of human death. More than two-thirds of fatalities are caused by hypertensive, atherosclerotic, coagulation-related, and pathological angiogenesis-related disorders[131]. The ageing of endothelial cells is concomitant with the deterioration of their function, raising the significance of the research into mechanisms of ageing in the prevention of cardiovascular disorders. Furthermore, since cell dysfunction is triggered primarily by the impaired stress response, its regulators, such as the transcription factor NRF2, could represent a promising anti-ageing-related disease strategy[335].

In the last decade, NRF2 has become a sentinel of cellular homeostasis and a gatekeeper of longevity. Although it was fully acknowledged that the diminished NRF2 response occurs with ageing and, accordingly, that its inhibition triggers premature ageing in many types of cells, the related mechanisms were vague[190]. Most reports claim a decline in NRF2 activity and protein level with age (reviewed in Kloska, Kopacz et al., Vasc Pharm[190]). Recent data show that the NRF2 mRNA level is also affected by ageing[92], but the mechanisms behind it are not elucidated. C-Myc, a known NRF2 transcriptional regulator[336,337], appears a valid candidate, especially since its deletion in endothelial cells leads to the induction of senescence[338]. However, regardless of the origin, the decrease in NRF2 mRNA could further augment a decline in its activity. Importantly, NRF2 activity, not its protein level, correlates well with rodent longevity. On the other hand, the KEAP1 level was found to be strongly related to longevity[212]. Concordantly, our group identified KEAP1 as a central regulator of premature ageing upon NRF2 deficiency *in vitro* in endothelial cells (Kopacz et al. Redox Biology[243]).

However, it remains unknown what the regulator of NRF2-related ageing *in vivo* is. Here, we showed that all the aorta layers from young NRF2 transcriptional knockout mice are prematurely aged (Fig. R1). Premature endothelial senescence *in vivo* is concomitant with increased KEAP1 level (Kopacz et al., Redox Biology[243]). Unfortunately, in this part of the investigation, we did not attempt to rescue NRF2-related premature senescence *in vivo* by creating a double knockout of NRF2 / KEAP1 or RNA-mediated KEAP1 interference. However, given the *in vitro* phenotype and that the deletion of both

components of this duet regains the homeostasis perturbed by the deficiency of the other (reviewed by Kopacz et al., FRBM[230]), it is highly likely. Likewise, either overexpression of KEAP1 or NRF2 inactivation[339] triggers aneurysm formation, which confirms our results showing the predilection of NRF2 transcriptional knockout mice to AAA (Fig.R4) and outlines the possible impact of KEAP1 in the process. Furthermore, age-related mechanisms could not be excluded.

The associations between age and incidence of AAA are substantial. Age constitutes a major risk for aneurysm formation, as its incidence doubles every 5 years in men over 65 years of age[340]. Furthermore, AAA induction results in significantly larger aortic diameter in older mice[341]. As a mechanism, up to now, the age-related reduction of SIRT1, which eases the onset of senescence and increases vascular inflammation, was proposed[323]. However, in light of our results, the decrease in NRF2 activity could represent an additional mechanism. Notably, these two mechanisms do not exclude each other, as both proteins act in a positive feedback loop in the context of diabetic nephropathy[342], and SIRT1 induces NRF2 activation in lung microvascular endothelial cells[343].

In this thesis, the Ang II-based model of AAA was used. This is the most popular model; however, in most experimental settings, the hyperlipidaemic ApoE knockout mice are used and crossed with putative regulators of AAA formation[99,344]. In our case, given the presumed AAA-promoting impact of NRF2 transcriptional deficiency, we decided to use AAA-resistant normolipidemic mice. The maintenance of the physiological lipid profile was confirmed in our study, where we showed that the infusion of Ang II does not affect the lipid profile in normolipidemic mice (Kopacz et al., Cells[345]). Notably, another group evidenced that the cholesterol level remains unchanged in hyperlipidaemic ApoE KO mice on Ang II treatment, despite the exacerbation of atherosclerosis[344]. It rationalizes the heated debate about the role of hyperlipidaemia in the predisposition to AAA. Moreover, it substantiates the involvement of other crucial factors, such as plaque-driven blood hemodynamic alterations or different cellular compositions of the aortic wall. ApoE KO mice have much more immune cells, including macrophages, in the aorta compared to WT mice[346,347], which, owing to the presence of AT1R[348], could immediately respond to Ang II and induce aortic remodelling.

The relation between NRF2 and Ang II is vague and contradictory. Depending on experimental settings and concentration used, Ang II either up-[349] (100 nM) or downregulates NRF2 activity (2 μM)[350]. Such a dual action is also the case for other

processes like autophagy (reviewed in[305]), the NRF2-enhancing concentration seems to be more physiological, though. Ang II concentration in plasma in a physiological state is around 50 fmol/ml and rises to 100 fmol/ml in hypertension. In the kidney, it is approximately 2-3 times higher[351]. Doses commonly used in biomedical research far exceed these values. However, interestingly, Ang II-induced hypertension is characterized by an increase of only 2-fold in the plasma Ang II content[305]. Additionally, the application of angiotensin-converting enzyme inhibitors abrogates the induction of hypertension, implying that endogenous generation of Ang II is indispensable for the process[352]. Irrespectively of the dose (varying between 200-2500 ng/kg/min), Ang II infusion leads to around 40% increase in systolic blood pressure (Fig. R3)[290,346,347]. It substantiates that AAA formation is not solely dependent on hypertension. In accordance, if such blood pressure is induced by norepinephrine, it does not result in AAA formation[353,354]. The cellular effects and impact on angiotensin receptors shall have the most prominent effect on the observed changes in hypertension or AAA models.

The formed aneurysms share similar characteristics: increased immune cell infiltration and robust aortic wall rearrangement. We could observe some intensification of the parameters mentioned above in NRF2 tKO; however, it does not seem to be the primary cause of the susceptibility of NRF2 tKO mice to AAA. Of the parameters analysed, Ang II-triggered ERK activation, significantly enhanced under NRF2 transcriptional deficiency (Fig. R9), could partially explain the sensitivity to AAA (Fig. D1), suggesting the impact of cellular signalling changes on the predilection toward AAA. However, in this thesis, we did not explore them in detail.

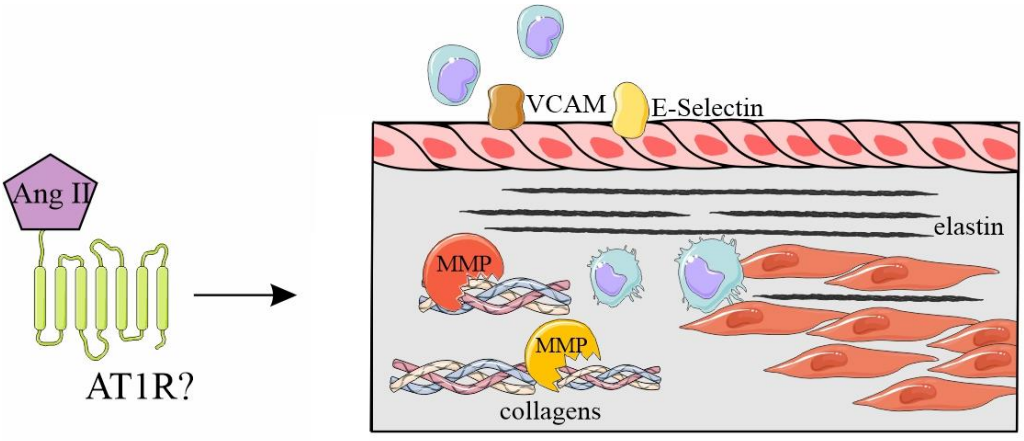

Figure D1. The schematic representation of the major features characterising the Ang II-induced AAA. The remodelling is likely exerted by the AT1R signalling. The image created using Servier Medical Art images.

For instance, the aortas of NRF2 transcriptional knockout mice are characterized by enhanced protein aggregation and S-nitrosation (Kopacz et al., Redox Biology[243]; Kopacz et al., Redox Biology[222]), both of which could enhance aneurysm formation. The protein aggregation occurs in the thoracic malformation and impacts VSMC death[355]. In terms of the abdominal aorta, increased endoplasmic reticulum stress and related protein aggregation occur in AAA[356], and its inhibition limits AAA[357]. The impact of S-nitrosation is granted mainly for thoracic aneurysms, as NO-related mechanisms trigger aortic disease in Marfan syndrome (MFS)[358] and plastin-3 S-nitrosation is responsible for the incidence of thoracic dilation[359]. Furthermore, S-nitrosation could promote ligand-independent activation of ERK, a crucial regulator of aortic malformation in MFS[360], a disease that could be mitigated by statins.

The coinciding impact of statins on the NRF2 deficiency-related AAA (Fig. R23) and MFS could imply some analogies between these two aortic diseases, and partially explain the predisposition of NRF2 tKO mice to AAA. Such speculations could be further corroborated by the presence of SEM-depicted altered endothelial layer (Fig. R19, and[361]), enhanced TGFβ signalling (Supp. Fig. 9, and[362]) and predilection to grade III, dissected aneurysm (Fig. R4 and[363]) in both situations. The above similarities could stem from altered cysteine status, modified by S-nitrosation in NRF2 tKO mice (Kopacz et al., Redox Biology[243]) and mutated in MFS[364]. On the other hand, MFS develops spontaneous aortic malformation, whereas such disease has not been reported or observed by us in NRF2 tKO mice till 18 months of age (data not shown).

It is widely accepted that NRF2 transcriptional knockout mice function well and do not get any specific disease unless challenged[183,190,230], for example, with oxidative stress-inducing agents[308]. Importantly, our team has already shown no detrimental oxidative imbalance in NRF2 tKO aortas at the basal state. But, we could indeed observe a shift towards a pro-oxidative environment, indicated by the increased level of superoxide anion in the aorta (Kopacz et al., Redox Biology[243]). Ang II is a known NADPH oxidase activating, pro-oxidative agent[365], and was previously reported to increase 4-hydroxynonenal presence-assessed oxidative stress significantly in the hearts of NRF2 tKO mice[366]. In contrast, in our experimental setting, a 14-day infusion of Ang II has a comparable effect on the induction of fluorescent probe-detected ROS between genotypes. Still, it was much more pronounced in the AAA than in the no AAA group. Mass spectrometry further corroborated these results, where we observed an approximately 10-fold increase in oxidized peptides in the tKO AAA group than in the

no AAA group (Fig. R11). Our results confirmed the already acknowledged notion that oxidative stress accompanies AAA formation[307,367–369]. However, the question remains if it is its cause or consequence. Given the predilection of oxidative-stress susceptible NRF2 tKO animals to AAA, it is seemingly the trigger. The levels of Ang II-induced ROS (in no-AAA and AAA group) are similar between the genotypes. However, it is important to bear in mind that the WT animals have high potential to hamper any detrimental oxidants-related effects, while tKO do not. Therefore, even with a similar ROS production, the cellular impact can be completely different. In accordance, ROS have already been shown to modulate the growth of cerebral aneurysms[365], and more importantly, ROS scavengers protected against AAA formation in elastase model[370]. Thus, it could likely be the trigger. Still, only performing a rescue experiment using ROS scavengers could give us the full answer.

Oxidative stress may forerun aortic rearrangement by increasing the inflammation and protease activity[367], and may affect the status of load-bearing components of the aortic wall. The presence of tropoelastin (amorphous monomeric precursor of elastin) is a hallmark of AAA[371]. It accumulates there as a result of oxidation of monomers, which prevents the further assembly into functional fibres[372]. The impact on aortic collagen is significantly less studied. However, based on the data from other organs, oxidative stress increases collagen level[373], while increasing its fragmentation and protease activity[374]. Interestingly, mechanical stress impacts biopolymers, such as collagen, and leads to the production of 'mechanoradicals'[375], which would close this vicious circle propelling oxidative stress. If these mechanisms were true also for the aortic wall, that could significantly alter the elastin:collagen ratio and shift towards aortic wall proteolysis, and subsequently weaken the aortic wall and result in the AAA.

Another possible mechanism triggering oxidative stress in the earliest stages of AAA formation[314] could stem from microinjuries. High-dose infusion of Ang II results in the erythrocyte-containing micro-ruptures in the aorta and surrounding vessels as early as on day 3, which either evolve in bigger tears or heal and disappear[110]. In such small 'wounds', erythrocytes could be trapped, damaged and release prooxidant haem. The latter may either induce cytoprotective haem oxygenase-1[114] or be non-enzymatically degraded and induce a pro-oxidative environment, which could be harnessed by many antioxidative enzymes, like catalase or glutathione pathway-related enzymes[376]. Given that oxidative stress is a known inhibitor of cellular healing[377], it is plausible that if the micro-rupture-driven oxidative stress is not hampered at this early stage,

it will propagate in another endless loop, resulting in the amplification of oxidative damage (Fig. D2). Importantly, these two possible oxidative stress-triggering mechanisms do not exclude each other, and the outcome could be a superposition of at least these two mechanisms.

A cytoprotective response may be crucial at these early steps to counteract the commencement of the oxidation-domino effect. Hopefully, the NRF2 transcriptional activity is not redundant. Its signature target genes, like *NQO1* or *HMOX1*, can be regulated by other transcription factors, mainly AP-1[378]. It also explains why the expression of these genes is not abrogated in NRF2 tKO mice (Kopacz et al., OMCL[290], Kopacz et al., FRBM[379]). On the other hand, upon oxidative challenge, NRF2 transcriptional action (minutes)[380] is significantly faster than that of AP-1 (few hours)[381], which renders NRF2 tKO mice in a losing position, making them more susceptible to oxidative damage and the causal nexus towards uncontrolled oxidative stress.

Importantly, when addressing the impact of oxidation, we should also consider some other post-translational modifications, such as protein carbamylation, which is a hallmark of oxidative stress[382] and ageing[383], affecting to a similar extent the load-bearing capacities of aortic structural proteins[383]. Therefore, the 'oxidative mechanism' governing the AAA formation can be related to many protein modifications, not only canonical cysteines. Indeed in the performed mass spectrometry analysis from the AAA tissue, we evidenced a plethora of oxidative modifications on different amino acids, and involving gaseous transmitters, such as nitric oxide (protein nitration). It implies a significant interrelation between signalling pathways and the complexity of the factors involved. However, as many of these post-translational modifications stem from ROS imbalance, it would be crucial to use ROS-scavenging molecules to fully delineate if the susceptibility of NRF2 tKO mice to AAA is driven by unharnessed oxidative stress. As such an approach was successful in elastase model[370], it is plausible that it could be the case.

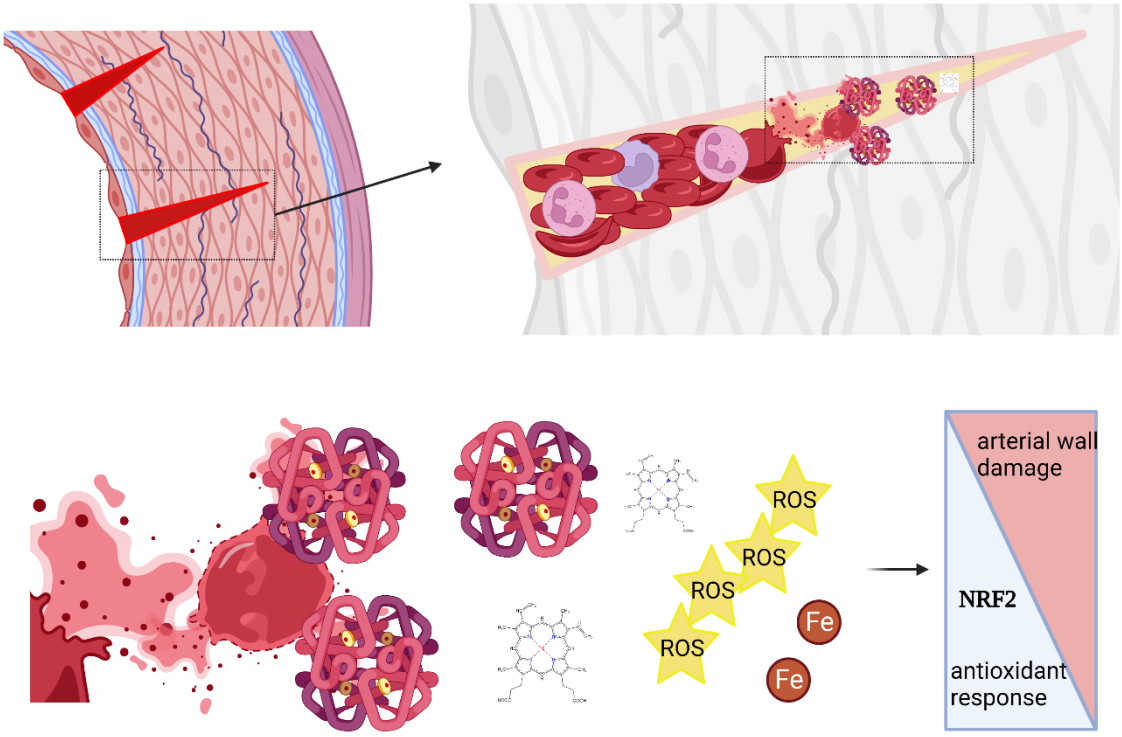

Figure D2. The schematic representation depicting the possible causal link between aortic wall damage and the increase in oxidative stress, underlining the role of NRF2 transcriptional activity in the process. Image created with BioRender.com, description in the text.

In fact, most mice models of AAA rely on damage to aortic wall components. In the elastase model, the protease is applied topically to the aorta and directly damages the structural protein, as it does in the calcium chloride model. Both models cause aortic dilatation formation of aneurysm[98,99]. Ang II infusions lead to a series of structural micro-ruptures in the aortic wall[96,110]. ECM organization is critical for sustaining aortic tensile strength and stiffness. Changes in the ECM composition, particularly collagen and elastin, might affect its normal function and lead to aneurysms or dissections[82]. Therefore, when addressing the mechanisms of AAA, it is pivotal to consider the impact of the aortic wall structure. Considering that AAA is an age-related disease[92], the age-oriented approach seems relevant.

In this study, we considered as aged 12-month-old mice. This choice is supported by a relatively low incidence of spontaneous diseases, including degenerative and neoplastic diseases, which may sometimes be asymptomatic. Usually, common conditions associated with age appear as early as 12 months of age and become more frequent in animals of 18-20 months[384,385]. They could affect whole organismal metabolism, thus perturbing the reliable interpretation of the data. Furthermore, we used the C57Bl6/J strain, which due to mutation in NNT, is significantly more prone to

oxidative stress, which affects ageing[386]. That could explain why we observe a mild occurrence of senescent cells in the young wild-type mice (Fig. R1). Importantly, significant changes in arterial function occur in humans around the third decade of life, thus supporting the use of such mice for ageing research[22,387]. Finally, the 12-month-old mice already have a 10-15% increase in blood pressure, mimicking the age-related changes in humans[388].

Nevertheless, even by using middle-aged mice, we could observe significant changes in the aortic histology and mechanical aortic stiffness, however, without impact on functional parameters (Fig. R13-18). Thus, it raises concerns about the inseparability and impact of age-related histological changes with functional impairment. Notably, such a relationship is also present in other organs. We observed no functional impairment in the colon despite pronounced differences in the microscopical features (Kopacz et al., after review). It implies the existence of some compensatory mechanisms ensuring the maintenance of homeostasis despite apparent changes in the histology.

Both NRF2 loss-related premature ageing and physiological one lead to significant thinning of the media layer (Fig. R13). This is a well-established, age-related degenerative change restricted to medial smooth muscle cells[60,62]. It was also observed in the premature ageing models[389]. Addressing its origin, we could exclude the enhanced cellular death detected by TUNEL assay[390] (Fig. R14). It instead suggests that the degenerative changes in the young tKO mice either stem from early development or it is an additive effect of senescence-related inhibition of proliferation with the gradual loss of SMCs. Importantly, these cells have a half-life of 270–400 days in the mouse aorta[391], so approximately a year. Thus, it could relate to the changes in aged wild-type mice, especially considering the strain-related premature onset of senescence (Fig. R1). In humans, the loss of SMCs leads to their replacement by proteoglycans (cystic medial necrosis), which weakens the aortic wall and results in aneurysms[392]. Therefore, we tried to assess the levels of proteoglycans by Alcian blue or pentachrome staining in the aortic wall of mice upon ageing; however, no positive signal was depictable (data not shown). On the other hand, it is plausible that the lack of detection of proteoglycans is caused by a significantly thinner aortic wall and the distance between elastic lamellae, rendering such deposits significantly less visible in the brightfield. Another possible approach could be high-resolution immunofluorescence and *in situ* mass spectrometry approaches. Importantly, the increased accumulation of proteoglycans contribute to nanomechanical stiffness, however to a lesser extent than the alterations in elastin and, mainly collagen[393].

Therefore, having observed significant age- and NRF2 transcriptional deficiency-related changes in AFM-limned mechanical stiffness (Fig. R15), we first focused on the collagen content. Whereas its level could partially explain the increase in stiffness in aged mice, it surely could not in the young NRF2 tKO mice. Moreover, collagen is significantly more abundant in the subendothelial layer[54] (Fig. R16). In the intimal cellular layer, its expression is concomitant with the endothelial to mesenchymal transition, which may occur during ageing or oxidative stress. Its hallmark is the acquisition of a fibroblast-like shape. However, as depicted by *en face* staining of the actin cytoskeleton, it does not happen in NRF2 tKO arterial ECs. At the same time, these images permitted the visualization of actin stress fibres. Alterations in the actin cytoskeleton are well sensed by AFM, especially in a topography mode, when a 25 nm tip is used. It stays in the same range as the actin fibre size (10 nm[394]). The actin cytoskeleton contributes to the cell mechanical stiffness[395] and could account for the observed changes differentiating WT from tKO mice, especially in the endothelial layer (Fig. R17). However, we cannot exclude that the actin cytoskeleton contributes to subendothelial layer stiffness. As the distinction between endothelial and subendothelial layer is made mainly based on the resistance points, it is hard to unequivocally assign which component constitutes the sub-endothelial layer. The strong actin cytoskeleton, more abundant than in ECs (Supp. Fig. 9), is present in SMCs, which could enhance the aorta stiffness[396]. However, it does not seem to be affected by the genotype (Supp. Fig. 10). The main differentiating factor is the presence of stress fibres only in tKO ECs (Fig. R17). So far, we have evidenced a moderate KEAP1-dependent increase of such structures in NRF2-deficient ECs[251]; however, the changes are much more pronounced *in vivo*. Plausibly it is related to sensing of shear forces or adhesion surface. To maintain homeostasis, arterial endothelium has to properly sense the blood forces and mechanotransduce them, which is largely dependent on nitric oxide[397]. Importantly, NRF2 transcriptional deficiency alters the NO metabolism, and the production of this gasotransmitter is significantly impaired (Kopacz et al., Redox Biology[243]). Interestingly, increased NO availability reduces the number of stress fibres[398]. Thus, it is possible that the NRF2 transcriptional deficiency-related altered NO metabolism could promote the actin cytoskeleton changes. Importantly, actin fibres polymerization is induced by Ang II in podocytes[399], which is required for the Ang II-induced signalling in VSMCs[400].

Moreover, surface stiffness predominantly affects the cytoskeleton organization and related cellular shape and phenotype. The altered nanomechanical stiffness could partially account for the AAA proneness, as the hypertensive features of Ang II promote collagen deposition and hence increase stiffness[88]. Here, we also confirmed the increase of collagen upon Ang II infusion (Fig. R7). It would be valuable to fully establish the exact ECM network by NaOH-mediated decellularization, followed by SEM imaging. Mainly to a prominent impact of matrix array on nanomechanical stiffness, which also explains the greater stiffness of abdominal than thoracic aorta[401], also showed by us (Fig. R15).

On the other hand, *ex vivo* measured arterial samples are not mechanically loaded. This factor plays a role in total arterial mechanics. Moreover, the samples are aligned, which is not a physiological state[402,403]. A potential limitation of the AFM analysis is also the scan size, which only measures a small tissue region. Most biological samples, including arteries and cells, are not topographically and biomechanically homogeneous. This heterogeneity can potentially result in artifactually significant variations of the elastic modulus depending on the smoothness of the indentation site, indentation depth, and the amount of force applied to the sample surface[26,27]. Therefore, complementing these analyses with the *in vivo* pulse wave velocity measurements gives a more comprehensive overview of the arterial function.

The functional measurements revealed that NRF2 tKO mice function well in the basal state. The increased arterial stiffness is present only in aged animals (Fig. R18). Outstandingly, the aged wild-type animals do not exhibit any changes in this parameter, despite pronounced differences in the nanomechanical stiffness (Fig. R15). Moreover, the main drawback of this study is that the analyses were not performed upon the Ang II challenge, especially the involvement of altered parameters such as AFM, actin cytoskeleton, and PWV. That would give more variables to understand the relation between the *in vivo* and *ex vivo* measurements and the significance in the disease progression.

An open question remains how despite such pronounced changes in stiffness, the pulse wave velocity remains unchanged. It could raise doubts about the relevance of *ex vivo* mechanical measurements with functional, *in vivo* ones. On the other hand, when considering Moen-Korteweg equation[404], to maintain the constant blood speed, the increase in Young modulus could be compensated by a decrease in the aortic wall thickness or by the rise in blood density or aortic diameter. As the latter remains unchanged by NRF2 transcriptional deficiency (Supp. Fig. 5), the aortic wall thickness or

blood density could be more relevant. Based on our results, the aortic wall thickening could be an adaptational change to maintain the constant pulse wave velocity (and wall shear stress) in young NRF2 tKO mice and aged wild-type (Fig. R13, Fig. R18). The 2-5 fold augmented mechanical stiffness in aged NRF2 tKO mice could barely be expiated by adapting the arterial dimensions. Thus, a threshold exists above which the mechanical stiffness translates to the functional one. To further corroborate such a hypothesis, it would be interesting to use mice of both genotypes older than 12-month-old or to add the stiffness-modulating factors exogenously[393].

If not accompanied by a change in the aortic diameter, blood velocity proportionally affects the wall shear stress, which is a major trigger for the formation of collaterals – junctional vessels between the two bigger ones[405]. The SEM-depicted intimal anomalies in aged NRF2 tKO mice resemble the entry or exit of a vessel. In fact, we could confirm the entry of plasma to the arterial wall using the gold particles, which we also corroborated with the immunofluorescent staining (Fig. R20). Thus, we can suppose that a junction between the arterial lumen and the perivascular adipose tissue (PVAT) is created. We also evidenced significantly higher vascularization of PVAT (Fig. R21). Therefore, an emerging issue is the interrelation of these phenomena, the trigger and the origin of the conduct. Given the abundance of PVAT vessels, with the number diminishing towards the arterial lumen, it seems that the vessels originate from the adventitia, which also happens in the atherosclerotic plaques[406]. Moreover, this inward angiogenesis hypothesis can be supported by observations made during aorta preparations and removal of PVAT, which is difficult even for young tKO mice and progresses with time. It correlates well with the increase in PVAT vascularization (Fig. R21) and the occurrence of intimal anomalies in aged NRF2 tKO mice (Fig. R19). Notably, the presence of any vessel in the abdominal aorta is abnormal. While in the thoracic aorta, the outer parts of the medial layer contain the *vasa vasorum*, which contrasts with the medial layer of the abdominal aorta, which is entirely avascular[407]. Since the absence of microcirculation limits the diapedesis of leukocytes through postcapillary venules, the media layer is physiologically an "immune-privileged" site, devoid of lymphoid and myeloid cells[408]. The appearance of such cells in the media of pathologically remodelled aortas is tightly linked to the process of inward neoangiogenesis within the vascular wall[409]. On the other hand, hypoperfusion of adventitial *vasa vasorum* triggers AAA in rats, implying possible interdependence of conduit presence and functionality[410]. Here, we could confirm that these CD31-positive tunnels span the vessel thickness from

the lumen (Fig. R20). However, for this assay, we used 15 nm gold particles. Therefore, verifying if even a red blood cell could enter is impossible. It is unlikely, given the size of intimal fenestrations and the scarcity of immune cells within the aortic wall (Agnieszka Moździerz, Master thesis). Still, we could address this issue in more detail by employing larger, few μm in diameter fluorescent beads or by labelling the red blood cells. Importantly, if unfunctional, these vessels would not carry the nutrients to the arterial wall sustaining the arterial functioning. They would mainly become the vulnerability points, which could facilitate the aortic dissection – the primary postulated mechanism for Ang II-induced changes[96,110]. Furthermore, in the light of the increased permeability of Ang II-driven neovessels, the basal enhanced hypervascularisation of the PVAT in NRF2 tKO animals could forerun the accumulation of red blood cells and the release of pro-oxidants (Fig. D2). Thus, we can be entitled to argue that the PVAT vascularisation, together with the presence of arterial conduits, could promote the formation of AAA.

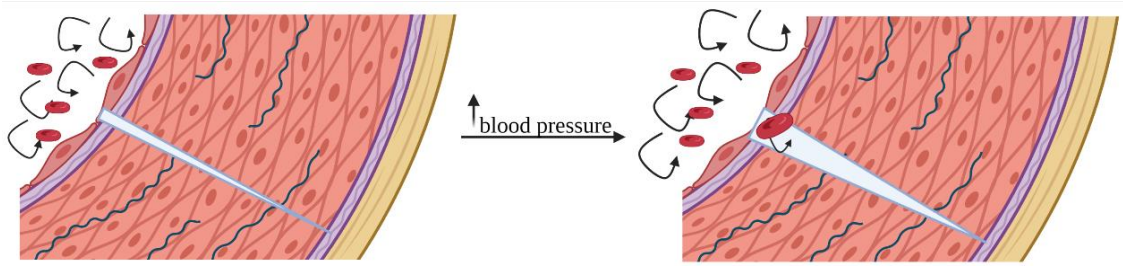

Figure D3. The schematic image portraying how the intimal anomalies or unfunctional conduits in the aortic wall could promote hypertension-induced arterial damage and the influx of red blood cells. Image created with BioRender.com.

Another possible mechanism explaining the existence of intimal anomalies is endothelial damage. In the 1980s, pioneering studies documented the occurrence of multiple small intimal lesions and arterial haemodynamic stress, termed 'endothelial breaches,' at areas of disturbed flow in human coronary arteries[411]. These lesions were characterized by localised EC desquamation and the build-up of blood in the subintimal region. Earlier observations were superseded by a focus on LDL-triggered EC dysfunction[322]. Notably, the endothelial breaches are filled with cholesterol, which is intriguing considering the statin administration-related abrogation of aneurysm formation in NRF2 tKO mice (Fig. R23). Moreover, simvastatin has already been proved protective in the elastase model of AAA formation[412]. In our hands, simvastatin also abrogates the increased vascularization and the permeability of the arterial wall (Fig. R24). In fact, cholesterol is a proangiogenic factor[413], which may be deposited extra

or intracellularly. For the latter, the key governor of cellular uptake is leptin[414]. Leptin promotes vascularization[415], and can be decreased by statins[416]. Therefore, it cannot be excluded that altered leptin signalling contributes to increased vascularization of PVAT. Still, based on the TOF-SIMS profiling of the intimal cholesterol level (Fig. R25), we can rather discard the link between the total cholesterol level and the aneurysm susceptibility, at least in the luminal layer. Supportively, the level of cholesterol in the diet had not impact on the AAA formation (Fig. R10B). That raises the question of the less intuitive mechanism of action of simvastatin. It may involve the modulation of cellular signalling. Importantly, cholesterol-driven protein modification (ex. prenylation) positively impacts the AT1R-originated signal transduction[417,418]. Our analysis was based on the total cholesterol content; we did not address the level of cholesterol metabolites. Therefore, we cannot discard such a mechanism. However, considering our claims that the presence of vascularisation-related intimal ultrastructural features is one of the main determinants of the susceptibility to AAA, the antiangiogenic and anti-inflammatory[419] mechanisms seem more probable.

Whereas the first part of the thesis associates the structural changes with the incidence of AAA and outlines uncontrolled oxidative stress as a plausible trigger for the disease, we could not clearly link the senescence with the AAA susceptibility. Of course, a possible way would be to compare the incidence of AAA in aged wild-type mice. However, such an approach would give only causative relations between age and the aneurysm. Therefore, we decided to take a different strategy, which permitted us to delineate the impact of endothelial cell senescence on NRF2 transcriptional deficiency-related AAA. The task was rather pertinent, as aortic EC are monolayer and constitute less than 5% of aortic wall cells[420,421], thus can be affected by every other cell subtype. Moreover, the inversion of the senescent phenotype is not easy. Senescence, contrary to quiescence, is known to be an irreversible phenomenon[155]. However, molecular biology techniques permit us to modulate the expression of crucial senescence regulators and, thus, define the mechanism behind it. Our group has already successfully reversed the senescent phenotype by depletion of senescence-inducing p53[251] or KEAP1 (Kopacz et al., Redox Biology[243]). In accordance, in this thesis, we identified miRNA-34a as a crucial regulator of the senescence of EC devoid of NRF2 (Fig. R27). Therefore, to understand the impact of endothelial cell senescence on AAA, we generated a triple mutant of NRF2 tKO, miRNA-34a floxed-, and inducible *Cdh5*-CreERT2-bearing mice, which permitted us to address this issue.

The choice of miRNA-34a was not random. First, it is a crucial regulator of senescence-inducing p53[422]. Thus, it was plausible it would reverse the senescent phenotype of NRF2-deficient ECs. Of note, the inversion of premature ageing has already been observed in endothelial cells[257], but also smooth muscle[278,423] and mesenchymal cells[424,425]. Secondly, it proved to have a protective impact on AAA[282]. However, its role in endothelial cells was not elucidated. And, last and foremost, short non-coding RNA are suitable disease biomarkers. They are often secreted to the bloodstream and permit a non-invasive assessment of the disease risk. Of note, up to now, miRNA-34a is considered a biomarker for several cardiovascular diseases, including insulin resistance, atherosclerosis and hypertension[266]. Its significance in endothelial cells in the governance of diseases and the resulting biomarker signature could be even more pronounced for ECs, which are in constant contact with the bloodstream. Based on our conventional *in situ* hybridization results, miRNA-34a was the most abundantly present in the intimal layer (Fig. R26C), which was concomitant with the increased level in the blood in the AAA group (Fig. R26B). However, we did not fully elucidate the origin of the circulating miRNA-34a. A plausible approach would be to use the inducible EC-knockout of miRNA-34a mice. However, these mice form rupture-prone aneurysms only upon rapamycin treatment (Fig. R39B). Thus, it would be impossible to conclude the involvement of ECs unequivocally. Another possible approach would be the generation of reporter miRNA-34a under Cre recombinase. However, the secretion of miRNA-34a could be altered by the accompanying protein.

Up to now, the impact of miRNA-34a was most directly studied in the recent paper by Zhong et al., where miRNA-34a mimic or inhibitor delivered by adeno-associated vector 9 (AAV9) were used in the Ang II model in ApoE KO mice. Increasing miRNA-34a enhanced AAA formation, and the contrary was observed for the inhibitory group. While the results regarding miRNA-34a-deficiency-related attenuation of AAA formation coincide with ours (Fig. R30), it is worth stressing that while we observe complete abrogation of the AAA formation, the authors observed only partial one. Secondly, the choice of AAV9 vectors as a delivery route is debatable, as they transduce aortic cells with low efficiency (Izabela Kraszewska, unpublished and[426]), and in C57Bl6 mice, AAV9 transduce mainly the liver and the heart (Kraszewska, Kopacz, et al., in preparation and[427]). Moreover, surprisingly, despite the delivery of the vectors a month before the infusion with Ang II, the miRNA-34a levels were only decreased after Ang II treatment. Therefore, it could be argued that the protective effect of antagomiR delivery

was related to the modulation of miRNA-34a in the aorta. It seems more plausible that the observed effect may stem from the altered lipid metabolism in these mice, which is also regulated by miRNA-34a[428]. However, we cannot exclude the impact on aortic cells, as the results coincide with ours (Fig. R29, Fig. R30). Still, in this work, the authors did not determine the cellular subset responsible for the miRNA-34a deficiency-related protection. Of note, the strategy of decreasing miRNA-34a level by the *in vivo* delivery of antagomiRs has been proved protective in many CVD settings, such as atherosclerosis[428,429] and diabetes[430,431].

In these papers and many others, the major protective impact of miRNA-34a deficiency is attributed to the increase in SIRT1, its hallmark target (exhaustively reviewed in[266]). Another considerable target could be the ERG transcription factor involved in the governance of endothelial fate[432]. Our mass spectrometry data from primary human aortic endothelial cells showed its significant upregulation in miRNA-34a-lacking cells (Kopacz et al., in preparation). Of note, ERG-reducing single nucleotide polymorphism correlated with AAA susceptibility in human[92,433], and its modulation was proposed as a possible strategy to prevent thoracic aortic aneurysm[434]. It would be essential to establish the role of these two putative players in the mechanisms of the protection against AAA conferred by miRNA-34a deficiency in endothelial cells. It could be achieved either by using inhibitors delivered with Ang II or, more specifically, by creating EC-specific double knockout mice.

When addressing the mechanism of the miRNA-34a-related protection, we decided to focus on the EC-specific knockout of miRNA-34a without the concomitant deficiency of NRF2 transcriptional activity. This choice was mainly driven by the need to establish the general mechanism that could relate not only to NRF2 deficiency-related premature senescence or the resulting impact on endothelial cell function. While in NRF2-related AAA research, our decision to use normolipidemic mice was mainly explained by the predilection towards AAA upon NRF2 transcriptional deficiency, we were not sure about the appropriateness of this model when addressing the impact of endothelial miRNA-34a alone. To our surprise, we observed that miRNA-34a^{WT} mice are prone to AAA (Fig. R30); however, the reason behind is not yet elucidated. We suspect it may be related to the significantly higher proinflammatory phenotype of the outbred strain, which could promote AAA formation. These mice more often develop rectal prolapse, the characteristic feature of IL-10 deficient mice[435], which of note, are prone to AAA formation[436]. We cannot renounce an altered thrombotic response upon Ang II infusion,

as in WT we observed the appearance of intraluminal thrombus, which is quite rare in the murine models of AAA[98]. The lack of intraluminal thrombus (ILT) is a significant flaw of almost every murine model of AAA and the putative cause of slow progress in the pharmacological treatment of AAA[437]. Given the significance of ILT in AAA formation in humans, which is the source of proteolytic enzymes and significantly alters the biomechanics of arterial blood flow[92], this may account for the higher susceptibility of this strain to AAA.

When addressing the role of ECs in any cardiovascular disease, it is always ascribed to EC function[438,439]. Consideration of endothelial cell proliferation is quite common in the settings of angiogenesis or reendothelialization, and it is not straightforward in the context of CVD or AAA. In fact, the involvement of the EC function was only proposed in some review papers[117–119]. What was supported by the research data was the protecting and stabilizing impact of the reendothelialization on AAA[120]. The exacerbation of aneurysm formation upon the lack of eNOS was mainly attributed to the changes in endothelial function[121,341]. In contrast, it went unnoticed that the lack of this enzyme significantly decreases the EC number by enhancing endothelial cell apoptosis[440]. Moreover, single-cell RNA sequencing of the arterial wall of a forming aneurysm did not reveal any canonical function-related transcriptome profile; it mainly indicated stimulation of proliferation, angiogenesis, and extracellular matrix production[124,125,434,441].

The data presented in this thesis sheds more light on the involvement of ECs in AAA, if it is related to their function. It has to be fully admitted that we did not assess the endothelial function upon Ang II infusion, which would be the most relevant experimental setting in this case. On the other hand, choosing the proper time-point for the analysis would be an arduous task and also hard to rationalize. With so little information about the involvement of ECs in AAA, it is hard to clearly outline when the EC function could be required. Therefore, we chose to assess the EC function at the basal state. It should be the moment when the intimal layer would face Ang II for the first time. As discussed above, presumably, these early time-points have the most prominent impact on the healing of aneurysm-causing micro-ruptures; thus, such a strategy seems relevant.

The detailed assessment of EC function revealed that miRNA-34a is its crucial regulator (Fig. R31-36). Such a multimodal approach to the comprehensive evaluation of endothelial phenotype *in vivo*, supplemented by *ex vivo* analyses, enabled an insight into

the alterations of healthy endothelial phenotype, including glycocalyx features and NO-dependent endothelial function. These observations were novel and previously attributed only to miRNA-34a increase[266]. Of note, in our hands, despite the miRNA-34a-deficiency-related loss of healthy endothelial features *in vivo*, the angiogenic capacity (a main functional characteristic *in vitro*) is preserved (Supp. Fig. R12). As the latter may be related to enhanced proliferation, it may suggest the separability of typical endothelial functional features and the angiogenic (reendothelialization) capacity (Supp. Fig. 12). We also confirmed the findings of the other groups, pointing out the onset of senescence upon miRNA-34a delivery (Supp. Fig. 13).

The detrimental effects of miRNA-34a deficiency on EC function have never been considered. However, upon scrutinized analyses, we may find that miRNA-34a downregulation in the diseased lung biopsies was concomitant with strong EC dysfunction[442]. The negative effect of miRNA-34a devoidness is not considered, given its protective effect in many disease settings[266]. However, our results clearly show the robust deterioration of EC function in miRNA-34a EC-KO, pointing to miRNA-34a as a crucial regulator of endothelial cell fate. At the same time, a significant increase of this ncRNA triggers EC dysfunction[266]. Therefore, we can conclude that fine-tuning the miRNA-34a level is crucial for maintaining cellular balance.

Despite pronounced EC dysfunction, the disease-protecting phenotype upon miRNA-34a deficiency raises serious doubts about almost, taken for granted, function-oriented protection. Still, the open question remains if there could be any defensive impact of the dysfunctional phenotype on AAA. Such a hypothesis was proposed in the 80s by Schwartz et al., but this topic was soon after dropped. The dysfunctional, prothrombotic phenotype of ECs could trigger the release of mitogenic factors, mainly platelet-derived growth factor (PDGF), and stimulate cellular proliferation[443]. Of note, PDGFR is a miRNA-34a target[444,445], PDGF is induced by Ang II[446], and both are expressed in ECs[447,448]. In accordance, we observed that silencing of both PDGFRs in HAECs completely abrogates the enhanced proliferation of miRNA-34a-lacking ECs (Supp. Fig. 14). However, we did not perform the PDGF neutralization to fully establish its role *in vitro* and *in vivo*. Moreover, it would be worth assessing other miRNA-34a targets in ECs to fully delineate the exact mechanisms of the proliferation regulation and possibly of the loss of healthy endothelial phenotype. However, the latter can be directly related to the proliferative (activated) phenotype of ECs[142]. If so, it would be very interesting to elucidate which one is the supreme regulator: proliferation or function.

In light of our results, this chicken-egg dilemma could be somehow solved. Given the major canonical proliferatory miRNA targets, it rather seems that the enhancement of cell division preceded the loss of function, at least basally *in vitro* (Supp. Fig. 12). Still, it is plausible that in the different experimental settings or upon stimulation, the order could be reversed.

Nevertheless, our results show a strong correlation between the proliferative capacity of ECs and the Ang II-induced aneurysm formation. Still, we must stress that we did not provide direct proof that endothelial cell proliferation is the main switch conferring the AAA protection. We cannot discard the plausible impact on other cell types, as rapamycin was delivered systemically. Importantly, in our previous paper, we could observe significant medial thickening and increased proliferation of SMCs in AAA-protected HO-1 deficient mice (Kopacz et al., Cells[345]). In the current experimental setting, we did not see such a pronounced increase in SMC number. However, it is impossible to exclude the impact of mild changes, especially in AAA. We observed the clonal proliferation of SMCs in AAA in the thrombus[449], and the decrease in this cell type within the aortic wall[450]. In accordance, we observed a polyclonal proliferation of ECs in the intimal layer and the aneurysmal area (Fig. R40A,B). Such an increase can be triggered by the more than 2-fold change in the aortic wall area and may have functional relevance. The increased arterial size by stretch is a known proliferatory factor of ECs[451]. At the same time, a functional pertinence cannot be excluded, given the resemblance of neovessels within the aneurysmal area to sinusoid bone marrow ECs. The sinusoid EC, contrary to other EC types, assist in mobilising immune cells and modulating their function[452]. Such a task could have relevance in the immune-cell-rich aneurysmal area and possibly, by such a mechanism, assist in the stability of aneurysms. The need for strong vascularisation of the aneurysmal site is transient (Fig. R40C), and it correlates with the degradation of RBC-derived haem to bilirubin (the aneurysm changes colour from red to yellow). We could hypothesise that the role of ECs throughout the AAA expansion is related to the fine-tuning of the macrophage activity to degrade haem. If so, we could reconcile protective EC proliferation (Fig. R40) with the detrimental Ang II-driven vascularisation of PVAT (Fig. R22). The latter occurs at the early timepoints and triggers hyperpermeability of the vessels, enabling the influx of immune and red blood cells and hence, provoking arterial dilatation. Still, at the later stages, the abundance of ECs could fine-tune the processes occurring in the aneurysmal tissue, ensuring its stability.

It is also intriguing why we observe senescence at the border of the stable aneurysms (Fig. R40D). It may be the sign of the increased deposition of collagen[453], which could fortify the aneurysm border, still triggering the cellular senescence. We cannot also exclude the physiological significance of this. Senescence could hamper the further expansion of the aneurysm. Undoubtedly, this study leaves many open questions and the inspiration for further research aimed at the detailed investigation of the role of EC proliferation in every stage of the AAA formation and verification if such mechanisms also translate to human disease.

Finalising the discussion, here we performed a comprehensive, EC-oriented analysis of the mechanisms of the formation of AAA. Although the NRF2- and miRNA-34a-centred stories at first glance could seem fairly separate entities, they are not. They complement each other and provide a broad perspective on the mechanisms of AAA, looking from the senescence/proliferation perspective, and integrating it with the structural features of AAA formation. Both are valid in the Ang II-based model and can be easily reconciled. The age-related abrogation of the proliferation can trigger the appearance of cavities in the intimal layer, fostering arterial damage and the formation of an aneurysm (Fig. D4).

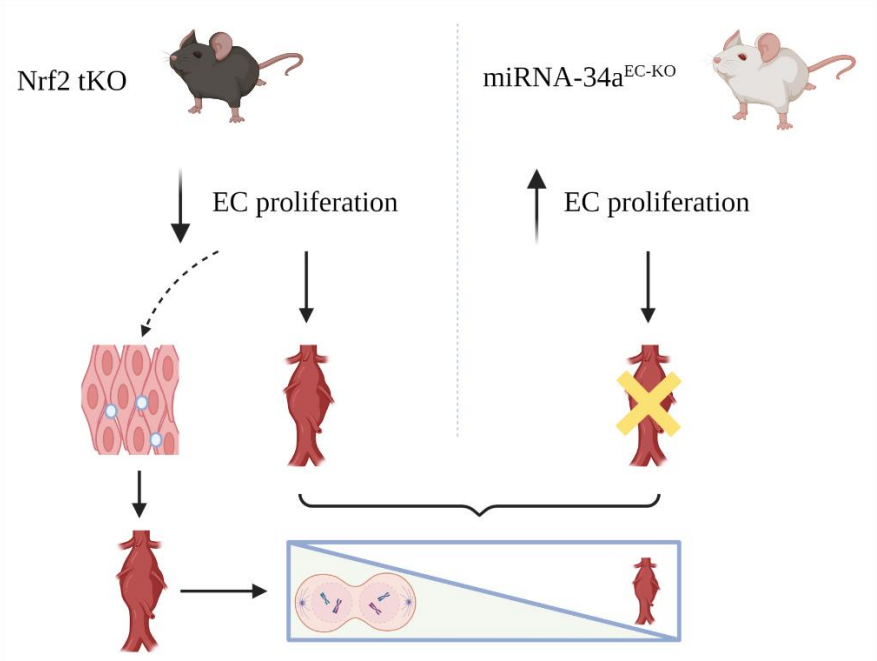

Figure D4. The schematic image showing the complementarity of used models in the elucidation of the predisposing mechanisms to AAA. Nrf2 transcriptional deficiency triggers premature ageing in all the layers of the aorta. Thus, it irreversibly inhibits EC proliferation. It may also result in the appearance of structural changes in the intimal layer, which correlate well with the aneurysm incidence. On the other hand, the endothelial deficiency of miRNA-34a enhances EC proliferation and impedes AAA formation. Taking into account the results from both models, we can conclude that the diminished proliferative capacity could be the main determinant of the susceptibility to AAA. Image created with BioRender.com.

Conclusions

In the frame of this doctoral thesis, I propose novel mechanisms for the regulation of EC biology and aortic pathology. I confirmed that both NRF2 and miRNA-34a are crucial regulators of arterial fate and emphasised the role of ECs in the regulation of the formation of AAA. In essence, the obtained results indicate that:

- The NRF2-related premature ageing leads to significant phenotypic and structural changes in the aorta but has a mild impact on the functional features;
- The lack of NRF2 transcriptional activity predisposes to the development of AAA, which can be attenuated by the administration of statins;
- Altered intimal ultrastructure correlates with AAA incidence;
- The susceptibility of NRF2 tKO to AAA results from the overabundance of miRNA-34a in ECs;
- Endothelial cells are imperative regulators of AAA formation;
- miRNA-34a is a crucial regulator of EC function;
- miR-34a abrogation prevents Ang II-induced AAA, which likely is not related to the enhancement of EC function;
- Endothelial cell proliferation outweighs their function in the prevention of Ang II-induced AAA formation in mice;
- Fine-tuning of proliferation and senescence plays a crucial role in the development and maintenance of AAA.

Considering the whole story described in this thesis, we can conclude that EC ability to proliferate and tighten the arterial wall is the main determinant of the onset of AAA. Therefore, contrary to current opinions, the age-dependent proneness to AAA does not rely on the functional EC features but could instead stem from the cessation of proliferation.

References

1. Keele, K. D. Movement of the Heart and Blood in Animals: An Anatomical Essay. *Med. Hist.* **1**, 371–372 (1957).
2. Earl, E. & Mohammadi, H. *Biomechanics of Human Blood*. *Biomechanics* (IntechOpen, 2018). doi:10.5772/intechopen.78305.
3. Evans, P. C. & Kwak, B. R. Biomechanical factors in cardiovascular disease. *Cardiovasc. Res.* **99**, 229–231 (2013).
4. Mazurek, R. *et al.* Vascular Cells in Blood Vessel Wall Development and Disease. *Adv. Pharmacol. San Diego Calif* **78**, 323–350 (2017).
5. Hadley, G. Basic Histology. *J. Anat.* **211**, 412–413 (2007).
6. Zakrzewicz, A., Secomb, T. W. & Pries, A. R. Angioadaptation: Keeping the Vascular System in Shape. *Physiology* **17**, 197–201 (2002).
7. Campinho, P., Vilfan, A. & Vermot, J. Blood Flow Forces in Shaping the Vascular System: A Focus on Endothelial Cell Behavior. *Front. Physiol.* **11**, 552 (2020).
8. Hoefer, I. E., den Adel, B. & Daemen, M. J. A. P. Biomechanical factors as triggers of vascular growth. *Cardiovasc. Res.* **99**, 276–283 (2013).
9. Jones, E. A. V., le Noble, F. & Eichmann, A. What Determines Blood Vessel Structure? Genetic Prespecification vs. Hemodynamics. *Physiology* **21**, 388–395 (2006).
10. Maringanti, R., Meijer, E., Brandt, M. M., Duncker, D. J. & Cheng, C. Contributions of Wall Stretch and Shear Stress to Vascular Regulation: Molecular Mechanisms of Homeostasis and Expansion. in *Vascular Mechanobiology in Physiology and Disease* (eds. Hecker, M. & Duncker, D. J.) 21–46 (Springer International Publishing, 2021). doi:10.1007/978-3-030-63164-2_2.
11. Huang, L., Korhonen, R. K., Turunen, M. J. & Finnilä, M. A. J. Experimental mechanical strain measurement of tissues. *PeerJ* **7**, e6545 (2019).
12. Yang, S., Gong, X., Qi, Y. & Jiang, Z. Comparative study of variations in mechanical stress and strain of human blood vessels: mechanical reference for vascular cell mechano-biology. *Biomech. Model. Mechanobiol.* **19**, 519–531 (2020).
13. Anwar, M. A., Shalhoub, J., Lim, C. S., Gohel, M. S. & Davies, A. H. The effect of pressure-induced mechanical stretch on vascular wall differential gene expression. *J. Vasc. Res.* **49**, 463–478 (2012).
14. Delli Gatti, C. *et al.* Pulsatile stretch induces release of angiotensin II and oxidative stress in human endothelial cells: effects of ACE inhibition and AT1 receptor antagonism. *Clin. Exp. Hypertens. N. Y. N 1993* **30**, 616–627 (2008).
15. Shin, H. Y., Gerritsen, M. E. & Bizios, R. Regulation of endothelial cell proliferation and apoptosis by cyclic pressure. *Ann. Biomed. Eng.* **30**, 297–304 (2002).
16. Kroll, M. H., Hellums, J. D., McIntire, L. V., Schafer, A. I. & Moake, J. L. Platelets and shear stress. *Blood* **88**, 1525–1541 (1996).
17. Roux, E., Bougaran, P., Dufourcq, P. & Couffinhal, T. Fluid Shear Stress Sensing by the Endothelial Layer. *Front. Physiol.* **11**, (2020).
18. Chatzizisis, Y. S. *et al.* Role of Endothelial Shear Stress in the Natural History of Coronary Atherosclerosis and Vascular Remodeling: Molecular, Cellular, and Vascular Behavior. *J. Am. Coll. Cardiol.* **49**, 2379–2393 (2007).
19. Morel, S. *et al.* Effects of Low and High Aneurysmal Wall Shear Stress on Endothelial Cell Behavior: Differences and Similarities. *Front. Physiol.* **12**, (2021).
20. Westerhof, N., Lankhaar, J.-W. & Westerhof, B. E. The arterial Windkessel. *Med. Biol. Eng. Comput.* **47**, 131–141 (2009).

21. Vera, J. *et al.* Mathematical Modelling in Biomedicine: A Primer for the Curious and the Skeptic. *Int. J. Mol. Sci.* **22**, 547 (2021).
22. O'Rourke, M. F. & Hashimoto, J. Mechanical factors in arterial aging: a clinical perspective. *J. Am. Coll. Cardiol.* **50**, 1–13 (2007).
23. O'Rourke, M. F. & Safar, M. E. Relationship between aortic stiffening and microvascular disease in brain and kidney: cause and logic of therapy. *Hypertens. Dallas Tex 1979* **46**, 200–204 (2005).
24. Butlin, M. & Avolio, A. P. Age-Related Changes in the Mechanical Properties of Large Arteries. in *Mechanical Properties of Aging Soft Tissues* (eds. Derby, B. & Akhtar, R.) 37–74 (Springer International Publishing, 2015). doi:10.1007/978-3-319-03970-1_3.
25. Wagenseil, J. E. & Mecham, R. P. Vascular Extracellular Matrix and Arterial Mechanics. *Physiol. Rev.* **89**, 957–989 (2009).
26. Vlachopoulos, C., O'Rourke, M. & Nichols, W. W. *McDonald's Blood Flow in Arteries: Theoretical, Experimental and Clinical Principles*. (CRC Press, 2012). doi:10.1201/b13568.
27. Boudoulas, K. D. *et al.* Aortic Function: From the Research Laboratory to the Clinic. *Cardiology* **121**, 31–42 (2012).
28. O'Connell, M. K. *et al.* The three-dimensional micro- and nanostructure of the aortic medial lamellar unit measured using 3D confocal and electron microscopy imaging. *Matrix Biol. J. Int. Soc. Matrix Biol.* **27**, 171–181 (2008).
29. Kohn, J. C., Lampi, M. C. & Reinhart-King, C. A. Age-related vascular stiffening: causes and consequences. *Front. Genet.* **6**, 112 (2015).
30. Schriefl, A. J., Zeindlinger, G., Pierce, D. M., Regitnig, P. & Holzapfel, G. A. Determination of the layer-specific distributed collagen fibre orientations in human thoracic and abdominal aortas and common iliac arteries. *J. R. Soc. Interface* **9**, 1275–1286 (2012).
31. Wagenseil, J. E. & Mecham, R. P. Elastin in large artery stiffness and hypertension. *J Cardiovasc. Transl. Res.* **5**, 264–273 (2012).
32. Matsumoto, T., Sugita, S. & Yaguchi, T. Biomechanics of Blood Vessels: Structure, Mechanics, and Adaptation. in *Advances in Metallic Biomaterials: Tissues, Materials and Biological Reactions* (eds. Niinomi, M., Narushima, T. & Nakai, M.) 71–98 (Springer, 2015). doi:10.1007/978-3-662-46836-4_4.
33. Huang, J. T. J. *et al.* Age-dependent elastin degradation is enhanced in chronic obstructive pulmonary disease. *Eur. Respir. J.* **48**, 1215–1218 (2016).
34. Duca, L. *et al.* Matrix ageing and vascular impacts: focus on elastin fragmentation. *Cardiovasc. Res.* **110**, 298–308 (2016).
35. Labella, F. S., Vivian, S. & Thornhill, D. P. Amino Acid Composition of Human Aortic Elastin as Influenced by Age. *J. Gerontol.* **21**, 550–555 (1966).
36. Wang, M. *et al.* Chronic matrix metalloproteinase inhibition retards age-associated arterial proinflammation and increase in blood pressure. *Hypertens. Dallas Tex 1979* **60**, 459–466 (2012).
37. Avolio, A., Jones, D. & Tafazzoli-Shadpour, M. Quantification of Alterations in Structure and Function of Elastin in the Arterial Media. *Hypertension* **32**, 170–175 (1998).
38. Greenwald, S. E. Ageing of the conduit arteries. *J. Pathol.* **211**, 157–172 (2007).
39. Atkinson, J. Age-related medial elastocalcinosis in arteries: mechanisms, animal models, and physiological consequences. *J. Appl. Physiol. Bethesda Md 1985* **105**, 1643–1651 (2008).
40. Wagenseil, J. E. *et al.* The importance of elastin to aortic development in mice. *Am. J. Physiol. Heart Circ. Physiol.* **299**, H257-264 (2010).

41. Li, D. Y. *et al.* Novel arterial pathology in mice and humans hemizygous for elastin. *J. Clin. Invest.* **102**, 1783–1787 (1998).
42. Kim, J., Cocciolone, A. J., Staiculescu, M. C., Mecham, R. P. & Wagenseil, J. E. Captopril treatment during development alleviates mechanically induced aortic remodeling in newborn elastin knockout mice. *Biomech. Model. Mechanobiol.* **19**, 99–112 (2020).
43. Fleenor, B. S., Marshall, K. D., Durrant, J. R., Lesniewski, L. A. & Seals, D. R. Arterial stiffening with ageing is associated with transforming growth factor-β1-related changes in adventitial collagen: reversal by aerobic exercise. *J. Physiol.* **588**, 3971–3982 (2010).
44. Rekhter, M. D. Collagen synthesis in atherosclerosis: too much and not enough. *Cardiovasc. Res.* **41**, 376–384 (1999).
45. Wang, X. *et al.* Increased Collagen Deposition and Elevated Expression of Connective Tissue Growth Factor in Human Thoracic Aortic Dissection. *Circulation* **114**, I200–I205 (2006).
46. Fleenor, B. S., Marshall, K. D., Rippe, C. & Seals, D. R. Replicative Aging Induces Endothelial to Mesenchymal Transition in Human Aortic Endothelial Cells: Potential Role of Inflammation. *J. Vasc. Res.* **49**, 59–64 (2012).
47. Schleicher, E. D., Wagner, E. & Nerlich, A. G. Increased accumulation of the glycoxidation product N(epsilon)-(carboxymethyl)lysine in human tissues in diabetes and aging. *J. Clin. Invest.* **99**, 457–468 (1997).
48. Cepas, V., Collino, M., Mayo, J. C. & Sainz, R. M. Redox Signaling and Advanced Glycation Endproducts (AGEs) in Diet-Related Diseases. *Antioxidants* **9**, 142 (2020).
49. Tsamis, A., Krawiec, J. T. & Vorp, D. A. Elastin and collagen fibre microstructure of the human aorta in ageing and disease: a review. *J. R. Soc. Interface* **10**, (2013).
50. Zulliger, M. A., Rachev, A. & Stergiopulos, N. A constitutive formulation of arterial mechanics including vascular smooth muscle tone. *Am. J. Physiol.-Heart Circ. Physiol.* **287**, H1335–H1343 (2004).
51. Holzapfel, G. A., Sommer, G., Gasser, C. T. & Regitnig, P. Determination of layer-specific mechanical properties of human coronary arteries with nonatherosclerotic intimal thickening and related constitutive modeling. *Am. J. Physiol. Heart Circ. Physiol.* **289**, H2048-2058 (2005).
52. Lu, X., Pandit, A. & Kassab, G. S. Biaxial incremental homeostatic elastic moduli of coronary artery: two-layer model. *Am. J. Physiol. Heart Circ. Physiol.* **287**, H1663-1669 (2004).
53. Pandit, A., Lu, X., Wang, C. & Kassab, G. S. Biaxial elastic material properties of porcine coronary media and adventitia. *Am. J. Physiol. Heart Circ. Physiol.* **288**, H2581-2587 (2005).
54. Gasser, T. C., Ogden, R. W. & Holzapfel, G. A. Hyperelastic modelling of arterial layers with distributed collagen fibre orientations. *J. R. Soc. Interface* **3**, 15–35 (2006).
55. Xu, X. *et al.* Age-related Impairment of Vascular Structure and Functions. *Aging Dis.* **8**, 590–610 (2017).
56. Akhtar, R., Sherratt, M., Cruickshank, J. K. & Derby, B. Characterizing the elastic properties of tissues. *Mater. Today Kidlington Engl.* **14**, 96–105 (2011).
57. Shadwick, R. E. Mechanical design in arteries. *J. Exp. Biol.* **202**, 3305–3313 (1999).
58. Milnor, W. R. *Hemodynamics*. (Williams & Wilkins, 1982).
59. Matsumoto, T. & Nagayama, K. Tensile properties of vascular smooth muscle cells: Bridging vascular and cellular biomechanics. *J. Biomech.* **45**, 745–755 (2012).
60. Lacolley, P., Regnault, V. & Avolio, A. P. Smooth muscle cell and arterial aging: basic and clinical aspects. *Cardiovasc. Res.* **114**, 513–528 (2018).

61. Hamczyk, M. R. & Andrés, V. Vascular smooth muscle cell loss underpins the accelerated atherosclerosis in Hutchinson-Gilford progeria syndrome. *Nucleus* **10**, 48–54 (2019).
62. Chi, C. *et al.* Vascular smooth muscle cell senescence and age-related diseases: State of the art. *Biochim. Biophys. Acta Mol. Basis Dis.* **1865**, 1810–1821 (2019).
63. Greenberg, S. R. The association of medial collagenous tissue with atheroma formation in the aging human aorta as revealed by a special technique. *Histol. Histopathol.* **1**, 323–326 (1986).
64. Schlatmann, T. J. M. & Becker, A. E. Histologic changes in the normal aging aorta: Implications for dissecting aortic aneurysm. *Am. J. Cardiol.* **39**, 13–20 (1977).
65. Ikeda, Y. Aortic Aneurysm: Etiopathogenesis and Clinicopathologic Correlations. *Ann. Vasc. Dis.* **9**, 73–79 (2016).
66. Mammoto, A., Matus, K. & Mammoto, T. Extracellular Matrix in Aging Aorta. *Front. Cell Dev. Biol.* **10**, (2022).
67. Ribeiro-Silva, J. C., Nolasco, P., Krieger, J. E. & Miyakawa, A. A. Dynamic Crosstalk between Vascular Smooth Muscle Cells and the Aged Extracellular Matrix. *Int. J. Mol. Sci.* **22**, 10175 (2021).
68. Pisano, C., Balistreri, C. R., Ricasoli, A. & Ruvolo, G. Cardiovascular Disease in Ageing: An Overview on Thoracic Aortic Aneurysm as an Emerging Inflammatory Disease. *Mediators Inflamm.* **2017**, e1274034 (2017).
69. Komutrattananont, P., Mahakkanukrauh, P. & Das, S. Morphology of the human aorta and age-related changes: anatomical facts. *Anat. Cell Biol.* **52**, 109–114 (2019).
70. Patel, D. J., Fry, D. L. & Janicki, J. S. The Elastic Symmetry of Arterial Segments in Dogs. *Circ. Res.* **24**, 1–8 (1969).
71. Humphrey, J. D. & Schwartz, M. A. Vascular Mechanobiology: Homeostasis, Adaptation, and Disease. *Annu. Rev. Biomed. Eng.* **23**, 1–27 (2021).
72. Bakker, E. N. T. P. & van Bavel, E. Biomechanics in Small Artery Remodeling. in *Vascular Mechanobiology in Physiology and Disease* (eds. Hecker, M. & Duncker, D. J.) 47–68 (Springer International Publishing, 2021). doi:10.1007/978-3-030-63164-2_3.
73. VanBavel, E. & Tuna, B. G. Integrative Modeling of Small Artery Structure and Function Uncovers Critical Parameters for Diameter Regulation. *PLOS ONE* **9**, e86901 (2014).
74. Herman, I. P. Cardiovascular System. in *Physics of the Human Body* (ed. Herman, I. P.) 533–621 (Springer International Publishing, 2016). doi:10.1007/978-3-319-23932-3_8.
75. Humphrey, J. D. & Taylor, C. A. Intracranial and Abdominal Aortic Aneurysms: Similarities, Differences, and Need for a New Class of Computational Models. *Annu. Rev. Biomed. Eng.* **10**, 221–246 (2008).
76. Miller, J. S. Pressure within a Bubble. *Am. J. Phys.* **20**, 115–115 (1952).
77. Gasser, T. C. Damage and Failure of the Vascular Wall. in *Encyclopedia of Continuum Mechanics* (eds. Altenbach, H. & Öchsner, A.) 1–12 (Springer, 2018). doi:10.1007/978-3-662-53605-6_243-1.
78. Humphrey, J. Vascular Adaptation and Mechanical Homeostasis at Tissue, Cellular, and Sub-cellular Levels. *Cell Biochem. Biophys.* **50**, 53–78 (2008).
79. Kulkarni, R., Andraska, E. & McEnaney, R. Structural Remodeling of the Extracellular Matrix in Arteriogenesis: A Review. *Front. Cardiovasc. Med.* **8**, (2021).
80. Ma, Z., Mao, C., Jia, Y., Fu, Y. & Kong, W. Extracellular matrix dynamics in vascular remodeling. *Am. J. Physiol.-Cell Physiol.* **319**, C481–C499 (2020).
81. Renna, N. F., de las Heras, N. & Miatello, R. M. Pathophysiology of Vascular Remodeling in Hypertension. *Int. J. Hypertens.* **2013**, 808353 (2013).

82. Jana, S., Hu, M., Shen, M. & Kassiri, Z. Extracellular matrix, regional heterogeneity of the aorta, and aortic aneurysm. *Exp. Mol. Med.* **51**, 1–15 (2019).
83. Perlstein, T. S. & Lee, R. T. Smoking, Metalloproteinases, and Vascular Disease. *Arterioscler. Thromb. Vasc. Biol.* **26**, 250–256 (2006).
84. Kehrer, J. P. Collagen synthesis and degradation in acutely damaged mouse lung tissue following treatment with prednisolone. *Biochem. Pharmacol.* **34**, 2519–2524 (1985).
85. Humphrey, J. D., Milewicz, D. M., Tellides, G. & Schwartz, M. A. Dysfunctional Mechanosensing in Aneurysms. *Science* **344**, 477–479 (2014).
86. Krings, T., Lasjaunias, P. L., Geibprasert, S., Pereira, V. & Hans, F. J. The Aneurysmal Wall. *Interv. Neuroradiol.* **14**, 39–47 (2008).
87. Raaz, U. *et al.* Segmental aortic stiffening contributes to experimental abdominal aortic aneurysm development. *Circulation* **131**, 1783–1795 (2015).
88. Qian, W. *et al.* Microskeletal stiffness promotes aortic aneurysm by sustaining pathological vascular smooth muscle cell mechanosensation via Piezo1. *Nat. Commun.* **13**, 512 (2022).
89. Milewicz, D. M. *et al.* Genetic basis of thoracic aortic aneurysms and dissections: focus on smooth muscle cell contractile dysfunction. *Annu. Rev. Genomics Hum. Genet.* **9**, 283–302 (2008).
90. Meng, H., Tutino, V. M., Xiang, J. & Siddiqui, A. High WSS or low WSS? Complex interactions of hemodynamics with intracranial aneurysm initiation, growth, and rupture: toward a unifying hypothesis. *AJNR Am. J. Neuroradiol.* **35**, 1254–1262 (2014).
91. Vollmar, J. F., Paes, E., Pauschinger, P., Henze, E. & Friesch, A. Aortic aneurysms as late sequelae of above-knee amputation. *Lancet Lond. Engl.* **2**, 834–835 (1989).
92. Sakalihasan, N. *et al.* Abdominal aortic aneurysms. *Nat. Rev. Dis. Primer* **4**, 34 (2018).
93. Golledge, J. Abdominal aortic aneurysm: update on pathogenesis and medical treatments. *Nat. Rev. Cardiol.* **16**, 225–242 (2019).
94. Polanczyk, A., Piechota-Polanczyk, A., Stefanczyk, L. & Strzelecki, M. Shape and Enhancement Analysis as a Useful Tool for the Presentation of Blood Hemodynamic Properties in the Area of Aortic Dissection. *J. Clin. Med.* **9**, (2020).
95. Thompson, R. W., Geraghty, P. J. & Lee, J. K. Abdominal aortic aneurysms: basic mechanisms and clinical implications. *Curr. Probl. Surg.* **39**, 110–230 (2002).
96. Trachet, B., Fraga-Silva, R. A., Piersigilli, A., Segers, P. & Stergiopulos, N. Dissecting abdominal aortic aneurysm in Angiotensin II-infused mice: the importance of imaging. *Curr. Pharm. Des.* **21**, 4049–4060 (2015).
97. Daugherty, A. & Cassis, L. A. Mouse models of abdominal aortic aneurysms. *Arterioscler. Thromb. Vasc. Biol.* **24**, 429–434 (2004).
98. Busch, A. *et al.* Translating mouse models of abdominal aortic aneurysm to the translational needs of vascular surgery. *JVS Vasc. Sci.* **2**, 219–234 (2021).
99. Lysgaard Poulsen, J., Stubbe, J. & Lindholt, J. S. Animal Models Used to Explore Abdominal Aortic Aneurysms: A Systematic Review. *Eur. J. Vasc. Endovasc. Surg. Off. J. Eur. Soc. Vasc. Surg.* **52**, 487–499 (2016).
100. Lu, H. *et al.* Vascular Smooth Muscle Cells in Aortic Aneurysm: From Genetics to Mechanisms. *J. Am. Heart Assoc.* **10**, e023601 (2021).
101. Paravicini, T. M. & Touyz, R. M. Redox signaling in hypertension. *Cardiovasc. Res.* **71**, 247–258 (2006).
102. Benigni, A., Cassis, P. & Remuzzi, G. Angiotensin II revisited: new roles in inflammation, immunology and aging. *EMBO Mol. Med.* **2**, 247–257 (2010).
103. Jiang, L. *et al.* Increased Aortic Calpain-1 Activity Mediates Age-Associated Angiotensin II Signaling of Vascular Smooth Muscle Cells. *PLOS ONE* **3**, e2231 (2008).

104. Korystova, A. F. *et al.* Distribution of the activity of the angiotensin-converting enzyme in the rat aorta and changes in the activity with aging and by the action of l-NAME. *Age* **34**, 821–830 (2012).
105. Basso, N. *et al.* Protective effect of long-term angiotensin II inhibition. *Am. J. Physiol. Heart Circ. Physiol.* **293**, H1351-1358 (2007).
106. Kansui, Y., Fujii, K., Goto, K., Abe, I. & Iida, M. Angiotensin II receptor antagonist improves age-related endothelial dysfunction. *J. Hypertens.* **20**, 439–446 (2002).
107. Mukai, Y. *et al.* Inhibition of Renin-Angiotensin System Ameliorates Endothelial Dysfunction Associated With Aging in Rats. *Arterioscler. Thromb. Vasc. Biol.* **22**, 1445–1450 (2002).
108. Quintana, R. A. & Taylor, W. R. Cellular Mechanisms of Aortic Aneurysm Formation. *Circ. Res.* **124**, 607–618 (2019).
109. Shen, Y. H. *et al.* Aortic Aneurysms and Dissections Series. *Arterioscler. Thromb. Vasc. Biol.* **40**, e37–e46 (2020).
110. Trachet, B. *et al.* Angiotensin II infusion into ApoE-/- mice: a model for aortic dissection rather than abdominal aortic aneurysm? *Cardiovasc. Res.* **113**, 1230–1242 (2017).
111. Chen, P.-Y. *et al.* Smooth Muscle Cell Reprogramming in Aortic Aneurysms. *Cell Stem Cell* **26**, 542-557.e11 (2020).
112. Joviliano, E. E., Ribeiro, M. S. & Tenorio, E. J. R. MicroRNAs and Current Concepts on the Pathogenesis of Abdominal Aortic Aneurysm. *Braz. J. Cardiovasc. Surg.* (2017) doi:10.21470/1678-9741-2016-0050.
113. Curci, J. A. & Thompson, R. W. Adaptive cellular immunity in aortic aneurysms: cause, consequence, or context? *J. Clin. Invest.* **114**, 168–171 (2004).
114. Piechota-Polanczyk, A. *et al.* The Abdominal Aortic Aneurysm and Intraluminal Thrombus: Current Concepts of Development and Treatment. *Front. Cardiovasc. Med.* **2**, 19 (2015).
115. Swedenborg, J. & Eriksson, P. The intraluminal thrombus as a source of proteolytic activity. *Ann. N. Y. Acad. Sci.* **1085**, 133–138 (2006).
116. Yau, J. W., Teoh, H. & Verma, S. Endothelial cell control of thrombosis. *BMC Cardiovasc. Disord.* **15**, 130 (2015).
117. DeRoo, E. *et al.* Endothelial Dysfunction in the Pathogenesis of Abdominal Aortic Aneurysm. *Biomolecules* **12**, 509 (2022).
118. Siasos, G. *et al.* The Role of Endothelial Dysfunction in Aortic Aneurysms. *Curr. Pharm. Des.* **21**, 4016–4034 (2015).
119. Sun, J., Deng, H., Zhou, Z., Xiong, X. & Gao, L. Endothelium as a Potential Target for Treatment of Abdominal Aortic Aneurysm. *Oxid. Med. Cell. Longev.* **2018**, 6306542 (2018).
120. Franck, G. *et al.* Reestablishment of the Endothelial Lining by Endothelial Cell Therapy Stabilizes Experimental Abdominal Aortic Aneurysms. *Circulation* **127**, 1877–1887 (2013).
121. Kuhlencordt, P. J. *et al.* Accelerated atherosclerosis, aortic aneurysm formation, and ischemic heart disease in apolipoprotein E/endothelial nitric oxide synthase double-knockout mice. *Circulation* **104**, 448–454 (2001).
122. Siu, K. L., Miao, X. N. & Cai, H. Recoupling of eNOS with Folic Acid Prevents Abdominal Aortic Aneurysm Formation in Angiotensin II-Infused Apolipoprotein E Null Mice. *PLOS ONE* **9**, e88899 (2014).
123. Zhao, G. *et al.* KLF11 protects against abdominal aortic aneurysm through inhibition of endothelial cell dysfunction. *JCI Insight* **6**, (2021).

124. Li, Y., LeMaire, S. A. & Shen, Y. H. Molecular and Cellular Dynamics of Aortic Aneurysms Revealed by Single-Cell Transcriptomics. *Arterioscler. Thromb. Vasc. Biol.* **41**, 2671–2680 (2021).
125. Kalluri, A. S. *et al.* Single-Cell Analysis of the Normal Mouse Aorta Reveals Functionally Distinct Endothelial Cell Populations. *Circulation* **140**, 147–163 (2019).
126. Tugal, D., Jain, M. K. & Simon, D. I. Endothelial KLF4: Crippling Vascular Injury? *J. Am. Heart Assoc.* **3**, e000769.
127. Matsushita, H. *et al.* eNOS Activity Is Reduced in Senescent Human Endothelial Cells. *Circ. Res.* **89**, 793–798 (2001).
128. Félétou, M. *Introduction. The Endothelium: Part 1: Multiple Functions of the Endothelial Cells—Focus on Endothelium-Derived Vasoactive Mediators* (Morgan & Claypool Life Sciences, 2011).
129. Predescu, S. A., Predescu, D. N. & Malik, A. B. Molecular determinants of endothelial transcytosis and their role in endothelial permeability. *Am. J. Physiol. Lung Cell. Mol. Physiol.* **293**, L823-842 (2007).
130. Stan, R. V. *Channels across Endothelial Cells*. *Madame Curie Bioscience Database [Internet]* (Landes Bioscience, 2013).
131. Augustin, H. G. & Koh, G. Y. Organotypic vasculature: From descriptive heterogeneity to functional pathophysiology. *Science* **357**, eaal2379 (2017).
132. Feng, W., Chen, L., Nguyen, P. K., Wu, S. M. & Li, G. Single Cell Analysis of Endothelial Cells Identified Organ-Specific Molecular Signatures and Heart-Specific Cell Populations and Molecular Features. *Front. Cardiovasc. Med.* **6**, (2019).
133. Mescher, A. *Junqueira's Basic Histology Text & Atlas (14th ed.)*. (2016).
134. Rafii, S., Butler, J. M. & Ding, B.-S. Angiocrine functions of organ-specific endothelial cells. *Nature* **529**, 316–325 (2016).
135. Davies, P. F. Flow-mediated endothelial mechanotransduction. *Physiol. Rev.* **75**, 519–560 (1995).
136. Malek, A. M. & Izumo, S. Control of endothelial cell gene expression by flow. *J. Biomech.* **28**, 1515–1528 (1995).
137. Tsata, V. & Beis, D. In Full Force. Mechanotransduction and Morphogenesis during Homeostasis and Tissue Regeneration. *J. Cardiovasc. Dev. Dis.* **7**, E40 (2020).
138. Allaire, E. & Clowes, A. W. Endothelial cell injury in cardiovascular surgery: the intimal hyperplastic response. *Ann. Thorac. Surg.* **63**, 582–591 (1997).
139. Nakakura, T. *et al.* Fibronectin is essential for formation of fenestrae in endothelial cells of the fenestrated capillary. *Cell Tissue Res.* **383**, 823–833 (2021).
140. Jalali, S. *et al.* Integrin-mediated mechanotransduction requires its dynamic interaction with specific extracellular matrix (ECM) ligands. *Proc. Natl. Acad. Sci.* **98**, 1042–1046 (2001).
141. Jambusaria, A. *et al.* Endothelial heterogeneity across distinct vascular beds during homeostasis and inflammation. *eLife* **9**, e51413 (2020).
142. Grochot-Przęczek, A., Kozakowska, M., Dulak, J. & Józkowicz, A. Endothelial Cell Origin, Differentiation, Heterogeneity and Function. in *Angiogenesis and Vascularisation: Cellular and Molecular Mechanisms in Health and Diseases* (eds. Dulak, J., Józkowicz, A. & Łoboda, A.) 3–26 (Springer, 2013). doi:10.1007/978-3-7091-1428-5_1.
143. Hogan, N. T. *et al.* Transcriptional networks specifying homeostatic and inflammatory programs of gene expression in human aortic endothelial cells. *eLife* **6**, e22536 (2017).
144. Chiu, J.-J. & Chien, S. Effects of Disturbed Flow on Vascular Endothelium: Pathophysiological Basis and Clinical Perspectives. *Physiol. Rev.* **91**, 10.1152/physrev.00047.2009 (2011).

145. Peng, Z., Shu, B., Zhang, Y. & Wang, M. Endothelial Response to Pathophysiological Stress. *Arterioscler. Thromb. Vasc. Biol.* **39**, e233–e243 (2019).
146. Gimbrone, M. A. & García-Cardeña, G. Vascular endothelium, hemodynamics, and the pathobiology of atherosclerosis. *Cardiovasc. Pathol. Off. J. Soc. Cardiovasc. Pathol.* **22**, 9–15 (2013).
147. Luft, J. H. Fine structures of capillary and endocapillary layer as revealed by ruthenium red. *Fed. Proc.* **25**, 1773–1783 (1966).
148. Villalba, N., Baby, S. & Yuan, S. Y. The Endothelial Glycocalyx as a Double-Edged Sword in Microvascular Homeostasis and Pathogenesis. *Front. Cell Dev. Biol.* **9**, (2021).
149. Uchimido, R., Schmidt, E. P. & Shapiro, N. I. The glycocalyx: a novel diagnostic and therapeutic target in sepsis. *Crit. Care* **23**, 16 (2019).
150. Fels, B. & Kusche-Vihrog, K. It takes more than two to tango: mechanosignaling of the endothelial surface. *Pflüg. Arch. - Eur. J. Physiol.* **472**, 419–433 (2020).
151. Wang, G. *et al.* Shear Stress Regulation of Endothelial Glycocalyx Structure Is Determined by Glucobiosynthesis. *Arterioscler. Thromb. Vasc. Biol.* **40**, 350–364 (2020).
152. Kim, Y.-H., Nijst, P., Kiefer, K. & Wilson Tang, W. H. Endothelial Glycocalyx as Biomarker for Cardiovascular Diseases: Mechanistic and Clinical Implications. *Curr. Heart Fail. Rep.* **14**, 117–126 (2017).
153. Machin, D. R., Phuong, T. T. T. & Donato, A. J. The Role of the Endothelial Glycocalyx in Advanced Age and Cardiovascular Disease. *Curr. Opin. Pharmacol.* **45**, 66–71 (2019).
154. Weinbaum, S., Tarbell, J. & Damiano, E. The Structure and Function of the Endothelial Glycocalyx Layer. *Annu. Rev. Biomed. Eng.* **9**, 121–67 (2007).
155. Ricard, N., Bailly, S., Guignabert, C. & Simons, M. The quiescent endothelium: signalling pathways regulating organ-specific endothelial normalcy. *Nat. Rev. Cardiol.* **18**, 565–580 (2021).
156. Adamson, R. *et al.* Oncotic pressures opposing filtration across non-fenestrated rat microvessels. *J. Physiol.* **557**, 889–907 (2004).
157. Arkill, K. P. A Reinterpretation of Evidence for the Endothelial Glycocalyx Filtration Structure. *Front. Cell Dev. Biol.* **9**, 734661 (2021).
158. Radeva, M. Y. & Waschke, J. Mind the gap: mechanisms regulating the endothelial barrier. *Acta Physiol.* **222**, e12860 (2018).
159. Flynn, K. M., Michaud, M., Canosa, S. & Madri, J. A. CD44 regulates vascular endothelial barrier integrity via a PECAM-1 dependent mechanism. *Angiogenesis* **16**, 689–705 (2013).
160. Delgadillo, L. F., Marsh, G. A. & Waugh, R. E. Endothelial Glycocalyx Layer Properties and Its Ability to Limit Leukocyte Adhesion. *Biophys. J.* **118**, 1564–1575 (2020).
161. Moore, K. H., Murphy, H. A. & George, E. M. The glycocalyx: a central regulator of vascular function. *Am. J. Physiol.-Regul. Integr. Comp. Physiol.* **320**, R508–R518 (2021).
162. Pahakis, M. Y., Kosky, J. R., Dull, R. O. & Tarbell, J. M. The Role of Endothelial Glycocalyx Components in Mechanotransduction of Fluid Shear Stress. *Biochem. Biophys. Res. Commun.* **355**, 228–233 (2007).
163. Fukai, T. & Ushio-Fukai, M. Superoxide dismutases: role in redox signaling, vascular function, and diseases. *Antioxid. Redox Signal.* **15**, 1583–1606 (2011).
164. Queisser, A., Seront, E., Boon, L. M. & Vikkula, M. Genetic Basis and Therapies for Vascular Anomalies. *Circ. Res.* **129**, 155–173 (2021).
165. Erusalimsky, J. D. & Kurz, D. J. Endothelial cell senescence. *Handb. Exp. Pharmacol.* 213–248 (2006) doi:10.1007/3-540-36028-x_7.

166. Sun, X. & Feinberg, M. W. Vascular Endothelial Senescence: Pathobiological Insights, Emerging Long Noncoding RNA Targets, Challenges and Therapeutic Opportunities. *Front. Physiol.* **12**, (2021).
167. Jia, G., Aroor, A. R., Jia, C. & Sowers, J. R. Endothelial cell senescence in aging-related vascular dysfunction. *Biochim. Biophys. Acta BBA - Mol. Basis Dis.* **1865**, 1802–1809 (2019).
168. Potente, M. & Mäkinen, T. Vascular heterogeneity and specialization in development and disease. *Nat. Rev. Mol. Cell Biol.* **18**, 477–494 (2017).
169. Dessalles, C. A., Leclech, C., Castagnino, A. & Barakat, A. I. Integration of substrate- and flow-derived stresses in endothelial cell mechanobiology. *Commun. Biol.* **4**, 1–15 (2021).
170. Dorland, Y. L. & Huveneers, S. Cell-cell junctional mechanotransduction in endothelial remodeling. *Cell. Mol. Life Sci. CMLS* **74**, 279–292 (2017).
171. Szymonski, M., Targosz-Korecka, M. & Malek-Zietek, K. E. Nano-mechanical model of endothelial dysfunction for AFM-based diagnostics at the cellular level. *Pharmacol. Rep. PR* **67**, 728–735 (2015).
172. Martino, F., Perestrelo, A. R., Vinarský, V., Pagliari, S. & Forte, G. Cellular Mechanotransduction: From Tension to Function. *Front. Physiol.* **9**, (2018).
173. Fz, M., K, B. & F, M. The Endothelium-Dependent Nitric Oxide-cGMP Pathway. *Adv. Pharmacol. San Diego Calif* **77**, (2016).
174. Zemskov, E. A. *et al.* Biomechanical Forces and Oxidative Stress: Implications for Pulmonary Vascular Disease. *Antioxid. Redox Signal.* **31**, 819–842 (2019).
175. Lang, F. Stiff endothelial cell syndrome in vascular inflammation and mineralocorticoid excess. *Hypertens. Dallas Tex 1979* **57**, 146–147 (2011).
176. Sverdlov, A. L., Ngo, D. T. M., Chan, W. P. A., Chirkov, Y. Y. & Horowitz, J. D. Aging of the Nitric Oxide System: Are We as Old as Our NO? *J. Am. Heart Assoc. Cardiovasc. Cerebrovasc. Dis.* **3**, e000973 (2014).
177. Lee, H.-Y., Zeeshan, H. M. A., Kim, H.-R. & Chae, H.-J. Nox4 regulates the eNOS uncoupling process in aging endothelial cells. *Free Radic. Biol. Med.* **113**, 26–35 (2017).
178. Hayashi, T. *et al.* Endothelial cellular senescence is inhibited by nitric oxide: Implications in atherosclerosis associated with menopause and diabetes. *Proc. Natl. Acad. Sci.* **103**, 17018–17023 (2006).
179. Harman, D. Aging: a theory based on free radical and radiation chemistry. *J. Gerontol.* **11**, 298–300 (1956).
180. Cuadrado, A. *et al.* Therapeutic targeting of the NRF2 and KEAP1 partnership in chronic diseases. *Nat. Rev. Drug Discov.* **18**, 295–317 (2019).
181. Dodson, M. *et al.* Modulating NRF2 in Disease: Timing Is Everything. *Annu. Rev. Pharmacol. Toxicol.* **59**, 555–575 (2019).
182. Pillai, R., Hayashi, M., Zavitsanou, A.-M. & Papagiannakopoulos, T. NRF2: KEAPing Tumors Protected. *Cancer Discov.* **12**, 625–643 (2022).
183. Itoh, K. *et al.* An Nrf2/small Maf heterodimer mediates the induction of phase II detoxifying enzyme genes through antioxidant response elements. *Biochem. Biophys. Res. Commun.* **236**, 313–322 (1997).
184. Malhotra, D. *et al.* Global mapping of binding sites for Nrf2 identifies novel targets in cell survival response through ChIP-Seq profiling and network analysis. *Nucleic Acids Res.* **38**, 5718 (2010).
185. Baird, L., Llères, D., Swift, S. & Dinkova-Kostova, A. T. Regulatory flexibility in the Nrf2-mediated stress response is conferred by conformational cycling of the Keap1-Nrf2 protein complex. *Proc. Natl. Acad. Sci. U. S. A.* **110**, 15259–15264 (2013).

186. Moi, P., Chan, K., Asunis, I., Cao, A. & Kan, Y. W. Isolation of NF-E2-related factor 2 (Nrf2), a NF-E2-like basic leucine zipper transcriptional activator that binds to the tandem NF-E2/AP1 repeat of the beta-globin locus control region. *Proc. Natl. Acad. Sci. U. S. A.* **91**, 9926–9930 (1994).
187. Sykiotis, G. P. & Bohmann, D. Stress-activated cap'n'collar transcription factors in aging and human disease. *Sci. Signal.* **3**, re3 (2010).
188. Li, W. & Kong, A.-N. Molecular mechanisms of Nrf2-mediated antioxidant response. *Mol. Carcinog.* **48**, 91–104 (2009).
189. Okazaki, K. *et al.* Enhancer remodeling promotes tumor-initiating activity in NRF2-activated non-small cell lung cancers. *Nat. Commun.* **11**, 5911 (2020).
190. Kloska, D. *et al.* Nrf2 in aging - Focus on the cardiovascular system. *Vascul. Pharmacol.* **112**, 42–53 (2019).
191. Tebay, L. E. *et al.* Mechanisms of activation of the transcription factor Nrf2 by redox stressors, nutrient cues, and energy status and the pathways through which it attenuates degenerative disease. *Free Radic. Biol. Med.* **88**, 108–146 (2015).
192. Tong, K. I. *et al.* Keap1 recruits Neh2 through binding to ETGE and DLG motifs: characterization of the two-site molecular recognition model. *Mol. Cell. Biol.* **26**, 2887–2900 (2006).
193. Canning, P., Sorrell, F. J. & Bullock, A. N. Structural basis of Keap1 interactions with Nrf2. *Free Radic. Biol. Med.* **88**, 101–107 (2015).
194. Nioi, P., Nguyen, T., Sherratt, P. J. & Pickett, C. B. The carboxy-terminal Neh3 domain of Nrf2 is required for transcriptional activation. *Mol. Cell. Biol.* **25**, 10895–10906 (2005).
195. Katoh, Y. *et al.* Two domains of Nrf2 cooperatively bind CBP, a CREB binding protein, and synergistically activate transcription. *Genes Cells Devoted Mol. Cell. Mech.* **6**, 857–868 (2001).
196. Zhang, J. *et al.* Nrf2 Neh5 domain is differentially utilized in the transactivation of cytoprotective genes. *Biochem. J.* **404**, 459–466 (2007).
197. Chowdhry, S. *et al.* Nrf2 is controlled by two distinct β-TrCP recognition motifs in its Neh6 domain, one of which can be modulated by GSK-3 activity. *Oncogene* **32**, 3765–3781 (2013).
198. Wang, H. *et al.* RXRα inhibits the NRF2-ARE signaling pathway through a direct interaction with the Neh7 domain of NRF2. *Cancer Res.* **73**, 3097–3108 (2013).
199. Ooi, B. K., Chan, K.-G., Goh, B. H. & Yap, W. H. The Role of Natural Products in Targeting Cardiovascular Diseases via Nrf2 Pathway: Novel Molecular Mechanisms and Therapeutic Approaches. *Front. Pharmacol.* **9**, (2018).
200. Liu, W. *et al.* Ursodeoxycholic Acid Attenuates Acute Aortic Dissection Formation in Angiotensin II-Infused Apolipoprotein E-Deficient Mice Associated with Reduced ROS and Increased Nrf2 Levels. *Cell. Physiol. Biochem.* **38**, 1391–1405 (2016).
201. Shi, Y. *et al.* Nrf-2 signaling inhibits intracranial aneurysm formation and progression by modulating vascular smooth muscle cell phenotype and function. *J. Neuroinflammation* **16**, 185 (2019).
202. McSweeney, S. R., Warabi, E. & Siow, R. C. M. Nrf2 as an Endothelial Mechanosensitive Transcription Factor: Going With the Flow. *Hypertens. Dallas Tex 1979* **67**, 20–29 (2016).
203. Hosoya, T. *et al.* Differential Responses of the Nrf2-Keap1 System to Laminar and Oscillatory Shear Stresses in Endothelial Cells. *J. Biol. Chem.* **280**, 27244–27250 (2005).
204. Gómez-Guzmán, M. *et al.* Epicatechin lowers blood pressure, restores endothelial function, and decreases oxidative stress and endothelin-1 and NADPH oxidase activity in DOCA-salt hypertension. *Free Radic. Biol. Med.* **52**, 70–79 (2012).

205. Smyrnias, I. *et al.* Nicotinamide Adenine Dinucleotide Phosphate Oxidase-4–Dependent Upregulation of Nuclear Factor Erythroid–Derived 2-Like 2 Protects the Heart During Chronic Pressure OverloadNovelty and Significance. *Hypertension* **65**, 547–553 (2015).
206. Li, J. *et al.* Nrf2 protects against maladaptive cardiac responses to hemodynamic stress. *Arterioscler. Thromb. Vasc. Biol.* **29**, 1843–1850 (2009).
207. Lopes, R. A., Neves, K. B., Tostes, R. C., Montezano, A. C. & Touyz, R. M. Downregulation of Nuclear Factor Erythroid 2-Related Factor and Associated Antioxidant Genes Contributes to Redox-Sensitive Vascular Dysfunction in Hypertension. *Hypertens. Dallas Tex 1979* **66**, 1240–1250 (2015).
208. Kobayashi, E. H. *et al.* Nrf2 suppresses macrophage inflammatory response by blocking proinflammatory cytokine transcription. *Nat. Commun.* **7**, 11624 (2016).
209. Olagnier, D. *et al.* Nrf2 negatively regulates STING indicating a link between antiviral sensing and metabolic reprogramming. *Nat. Commun.* **9**, 3506 (2018).
210. Luo, W. *et al.* Critical role of cytosolic DNA and its sensing adaptor STING in aortic degeneration, dissection, and rupture. *Circulation* **141**, 42–66 (2020).
211. Hiebert, P. The Nrf2 transcription factor: A multifaceted regulator of the extracellular matrix. *Matrix Biol. Plus* **10**, 100057 (2021).
212. Lewis, K. N. *et al.* Regulation of Nrf2 signaling and longevity in naturally long-lived rodents. *Proc. Natl. Acad. Sci. U. S. A.* **112**, 3722–3727 (2015).
213. Yu, C. *et al.* RNA Sequencing Reveals Differential Expression of Mitochondrial and Oxidation Reduction Genes in the Long-Lived Naked Mole-Rat When Compared to Mice. *PLoS ONE* **6**, (2011).
214. Blackwell, T. K., Steinbaugh, M. J., Hourihan, J. M., Ewald, C. Y. & Isik, M. SKN-1/Nrf, stress responses, and aging in Caenorhabditis elegans. *Free Radic. Biol. Med.* **88**, 290–301 (2015).
215. Gounder, S. S. *et al.* Impaired transcriptional activity of Nrf2 in age-related myocardial oxidative stress is reversible by moderate exercise training. *PloS One* **7**, e45697 (2012).
216. Safdar, A., deBeer, J. & Tarnopolsky, M. A. Dysfunctional Nrf2-Keap1 redox signaling in skeletal muscle of the sedentary old. *Free Radic. Biol. Med.* **49**, 1487–1493 (2010).
217. Shih, P.-H. & Yen, G.-C. Differential expressions of antioxidant status in aging rats: the role of transcriptional factor Nrf2 and MAPK signaling pathway. *Biogerontology* **8**, 71–80 (2007).
218. Sykiotis, G. P. & Bohmann, D. Keap1/Nrf2 signaling regulates oxidative stress tolerance and lifespan in Drosophila. *Dev. Cell* **14**, 76–85 (2008).
219. Tullet, J. M. A. *et al.* Direct inhibition of the longevity-promoting factor SKN-1 by insulin-like signaling in C. elegans. *Cell* **132**, 1025–1038 (2008).
220. Ungvari, Z. *et al.* Age-associated vascular oxidative stress, Nrf2 dysfunction, and NF-{kappa}B activation in the nonhuman primate Macaca mulatta. *J. Gerontol. A. Biol. Sci. Med. Sci.* **66**, 866–875 (2011).
221. Ungvari, Z. *et al.* Vascular oxidative stress in aging: a homeostatic failure due to dysregulation of NRF2-mediated antioxidant response. *Am. J. Physiol. Heart Circ. Physiol.* **301**, H363-372 (2011).
222. Kopacz, A. *et al.* Keap1 governs ageing-induced protein aggregation in endothelial cells. *Redox Biol.* **34**, 101572 (2020).
223. Itoh, K. *et al.* Keap1 represses nuclear activation of antioxidant responsive elements by Nrf2 through binding to the amino-terminal Neh2 domain. *Genes Dev.* **13**, 76–86 (1999).

224. Dinkova-Kostova, A. T., Kostov, R. V. & Canning, P. Keap1, the cysteine-based mammalian intracellular sensor for electrophiles and oxidants. *Arch. Biochem. Biophys.* **617**, 84–93 (2017).
225. Dinkova-Kostova, A. T., Massiah, M. A., Bozak, R. E., Hicks, R. J. & Talalay, P. Potency of Michael reaction acceptors as inducers of enzymes that protect against carcinogenesis depends on their reactivity with sulfhydryl groups. *Proc. Natl. Acad. Sci. U. S. A.* **98**, 3404–3409 (2001).
226. McMahon, M., Lamont, D. J., Beattie, K. A. & Hayes, J. D. Keap1 perceives stress via three sensors for the endogenous signaling molecules nitric oxide, zinc, and alkenals. *Proc. Natl. Acad. Sci. U. S. A.* **107**, 18838–18843 (2010).
227. Go, Y.-M., Chandler, J. D. & Jones, D. P. The cysteine proteome. *Free Radic. Biol. Med.* **84**, 227–245 (2015).
228. Dhanoa, B. S., Cogliati, T., Satish, A. G., Bruford, E. A. & Friedman, J. S. Update on the Kelch-like (KLHL) gene family. *Hum. Genomics* **7**, 13 (2013).
229. Prag, S. & Adams, J. C. Molecular phylogeny of the kelch-repeat superfamily reveals an expansion of BTB/kelch proteins in animals. *BMC Bioinformatics* **4**, 42 (2003).
230. Kopacz, A., Kloska, D., Forman, H. J., Jozkowicz, A. & Grochot-Przeczek, A. Beyond repression of Nrf2: An update on Keap1. *Free Radic. Biol. Med.* (2020) doi:10.1016/j.freeradbiomed.2020.03.023.
231. Canning, P., Sorrell, F. J. & Bullock, A. N. Structural basis of Keap1 interactions with Nrf2. *Free Radic. Biol. Med.* **88**, 101–107 (2015).
232. Cleasby, A. *et al.* Structure of the BTB domain of Keap1 and its interaction with the triterpenoid antagonist CDDO. *PloS One* **9**, e98896 (2014).
233. Li, X., Zhang, D., Hannink, M. & Beamer, L. J. Crystal structure of the Kelch domain of human Keap1. *J. Biol. Chem.* **279**, 54750–54758 (2004).
234. Padmanabhan, B. *et al.* Purification, crystallization and preliminary X-ray diffraction analysis of the Kelch-like motif region of mouse Keap1. *Acta Crystallograph. Sect. F Struct. Biol. Cryst. Commun.* **61**, 153–155 (2005).
235. Padmanabhan, B., Tong, K. I., Kobayashi, A., Yamamoto, M. & Yokoyama, S. Structural insights into the similar modes of Nrf2 transcription factor recognition by the cytoplasmic repressor Keap1. *J. Synchrotron Radiat.* **15**, 273–276 (2008).
236. Suzuki, T., Maher, J. & Yamamoto, M. Select heterozygous Keap1 mutations have a dominant-negative effect on wild-type Keap1 in vivo. *Cancer Res.* **71**, 1700–1709 (2011).
237. Wakabayashi, N. *et al.* Protection against electrophile and oxidant stress by induction of the phase 2 response: fate of cysteines of the Keap1 sensor modified by inducers. *Proc. Natl. Acad. Sci. U. S. A.* **101**, 2040–2045 (2004).
238. Zhang, D. D. & Hannink, M. Distinct cysteine residues in Keap1 are required for Keap1-dependent ubiquitination of Nrf2 and for stabilization of Nrf2 by chemopreventive agents and oxidative stress. *Mol. Cell. Biol.* **23**, 8137–8151 (2003).
239. Dinkova-Kostova, A. T. *et al.* Direct evidence that sulfhydryl groups of Keap1 are the sensors regulating induction of phase 2 enzymes that protect against carcinogens and oxidants. *Proc. Natl. Acad. Sci. U. S. A.* **99**, 11908–11913 (2002).
240. Jain, A. *et al.* p62/SQSTM1 Is a Target Gene for Transcription Factor NRF2 and Creates a Positive Feedback Loop by Inducing Antioxidant Response Element-driven Gene Transcription. *J. Biol. Chem.* **285**, 22576–22591 (2010).
241. Karapetian, R. N. *et al.* Nuclear oncoprotein prothymosin alpha is a partner of Keap1: implications for expression of oxidative stress-protecting genes. *Mol. Cell. Biol.* **25**, 1089–1099 (2005).

242. Watai, Y. *et al.* Subcellular localization and cytoplasmic complex status of endogenous Keap1. *Genes Cells Devoted Mol. Cell. Mech.* **12**, 1163–1178 (2007).
243. Kopacz, A. *et al.* Keap1 controls protein S-nitrosation and apoptosis-senescence switch in endothelial cells. *Redox Biol.* **28**, 101304 (2020).
244. Buckley, B. J., Li, S. & Whorton, A. R. KEAP1 MODIFICATION AND NUCLEAR ACCUMULATION IN RESPONSE TO S-NITROSOCYSTEINE. *Free Radic. Biol. Med.* **44**, 692–698 (2008).
245. Ratnayake, S., Dias, I. H. K., Lattman, E. & Griffiths, H. R. Stabilising cysteinyl thiol oxidation and nitrosation for proteomic analysis. *J. Proteomics* **92**, 160–170 (2013).
246. Um, H.-C., Jang, J.-H., Kim, D.-H., Lee, C. & Surh, Y.-J. Nitric oxide activates Nrf2 through S-nitrosylation of Keap1 in PC12 cells. *Nitric Oxide Biol. Chem.* **25**, 161–168 (2011).
247. Tong, K. I. *et al.* Different electrostatic potentials define ETGE and DLG motifs as hinge and latch in oxidative stress response. *Mol. Cell. Biol.* **27**, 7511–7521 (2007).
248. Tong, K. I., Kobayashi, A., Katsuoka, F. & Yamamoto, M. Two-site substrate recognition model for the Keap1-Nrf2 system: a hinge and latch mechanism. *Biol. Chem.* **387**, 1311–1320 (2006).
249. Hast, B. E. *et al.* Proteomic analysis of ubiquitin ligase KEAP1 reveals associated proteins that inhibit NRF2 ubiquitination. *Cancer Res.* **73**, 2199–2210 (2013).
250. Karttunen, M., Choy, W.-Y. & Cino, E. A. Prediction of Binding Energy of Keap1 Interaction Motifs in the Nrf2 Antioxidant Pathway and Design of Potential High-Affinity Peptides. *J. Phys. Chem. B* **122**, 5851–5859 (2018).
251. Kloska, D. *et al.* Nrf2 Sequesters Keap1 Preventing Podosome Disassembly: A Quintessential Duet Moonlights in Endothelium. *Antioxid. Redox Signal.* **30**, 1709–1730 (2019).
252. O'Mealey, G. B. *et al.* A PGAM5-KEAP1-Nrf2 complex is required for stress-induced mitochondrial retrograde trafficking. *J. Cell Sci.* **130**, 3467–3480 (2017).
253. Wakabayashi, N. *et al.* Keap1-null mutation leads to postnatal lethality due to constitutive Nrf2 activation. *Nat. Genet.* **35**, 238–245 (2003).
254. Wang, R. *et al.* Reduced NRF2 expression suppresses endothelial progenitor cell function and induces senescence during aging. *Aging* **11**, 7021–7035 (2019).
255. Disayabutr, S. *et al.* miR-34 miRNAs Regulate Cellular Senescence in Type II Alveolar Epithelial Cells of Patients with Idiopathic Pulmonary Fibrosis. *PloS One* **11**, e0158367 (2016).
256. Xu, X. *et al.* miR-34a induces cellular senescence via modulation of telomerase activity in human hepatocellular carcinoma by targeting FoxM1/c-Myc pathway. *Oncotarget* **6**, 3988–4004 (2015).
257. Ito, T., Yagi, S. & Yamakuchi, M. MicroRNA-34a regulation of endothelial senescence. *Biochem. Biophys. Res. Commun.* **398**, 735–740 (2010).
258. Badi, I. *et al.* MicroRNA-34a Induces Vascular Smooth Muscle Cells Senescence by SIRT1 Downregulation and Promotes the Expression of Age-Associated Pro-inflammatory Secretory Factors. *J. Gerontol. A. Biol. Sci. Med. Sci.* **70**, 1304–1311 (2015).
259. Truscott, M., Islam, A. B. M. M. K. & Frolov, M. V. Novel regulation and functional interaction of polycistronic miRNAs. *RNA* **22**, 129–138 (2016).
260. Medley, J. C., Panzade, G. & Zinovyeva, A. Y. microRNA strand selection: Unwinding the rules. *Wiley Interdiscip. Rev. RNA* **12**, e1627 (2021).

261. Córdova-Rivas, S. *et al.* 5p and 3p Strands of miR-34 Family Members Have Differential Effects in Cell Proliferation, Migration, and Invasion in Cervical Cancer Cells. *Int. J. Mol. Sci.* **20**, E545 (2019).
262. Chang, T.-C. *et al.* Transactivation of miR-34a by p53 Broadly Influences Gene Expression and Promotes Apoptosis. *Mol. Cell* **26**, 745–752 (2007).
263. Raver-Shapira, N. *et al.* Transcriptional Activation of miR-34a Contributes to p53-Mediated Apoptosis. *Mol. Cell* **26**, 731–743 (2007).
264. Suzuki, H. I. & Miyazono, K. Emerging complexity of microRNA generation cascades. *J. Biochem. (Tokyo)* **149**, 15–25 (2011).
265. He, L. *et al.* A microRNA component of the p53 tumour suppressor network. *Nature* **447**, 1130–1134 (2007).
266. Raucci, A. *et al.* MicroRNA-34a: the bad guy in age-related vascular diseases. *Cell. Mol. Life Sci.* **78**, 7355–7378 (2021).
267. Jang, S. *et al.* 1p36 Deletion Syndrome and Left Ventricular Non-compaction Cardiomyopathy—Two Cases Report. *Front. Pediatr.* **9**, (2021).
268. García-López, J. *et al.* Large 1p36 Deletions Affecting Arid1a Locus Facilitate Mycn-Driven Oncogenesis in Neuroblastoma. *Cell Rep.* **30**, 454-464.e5 (2020).
269. Slabáková, E., Culig, Z., Remšík, J. & Souček, K. Alternative mechanisms of miR-34a regulation in cancer. *Cell Death Dis.* **8**, e3100–e3100 (2017).
270. Bommer, G. T. *et al.* p53-Mediated Activation of miRNA34 Candidate Tumor-Suppressor Genes. *Curr. Biol.* **17**, 1298–1307 (2007).
271. Menghini, R. *et al.* MicroRNA 217 Modulates Endothelial Cell Senescence via Silent Information Regulator 1. *Circulation* **120**, 1524–1532 (2009).
272. Luo, X., Hu, R., Zheng, Y., Liu, S. & Zhou, Z. Metformin shows anti-inflammatory effects in murine macrophages through Dicer/microribonucleic acid-34a-5p and microribonucleic acid-125b-5p. *J. Diabetes Investig.* **11**, 101–109 (2020).
273. Zhang, S. *et al.* Metformin-Induced MicroRNA-34a-3p Downregulation Alleviates Senescence in Human Dental Pulp Stem Cells by Targeting CAB39 through the AMPK/mTOR Signaling Pathway. *Stem Cells Int.* **2021**, 6616240 (2021).
274. Tabuchi, T., Satoh, M., Itoh, T. & Nakamura, M. MicroRNA-34a regulates the longevity-associated protein SIRT1 in coronary artery disease: effect of statins on SIRT1 and microRNA-34a expression. *Clin. Sci. Lond. Engl. 1979* **123**, 161–171 (2012).
275. Fan, W. *et al.* Shear-sensitive microRNA-34a modulates flow-dependent regulation of endothelial inflammation. *J. Cell Sci.* **128**, 70–80 (2015).
276. Linna-Kuosmanen, S. *et al.* NRF2 is a key regulator of endothelial microRNA expression under proatherogenic stimuli. *Cardiovasc. Res.* **117**, 1339–1357 (2021).
277. Concepcion, C. P. *et al.* Intact p53-dependent responses in miR-34-deficient mice. *PLoS Genet.* **8**, e1002797 (2012).
278. Badi, I. *et al.* miR-34a Promotes Vascular Smooth Muscle Cell Calcification by Downregulating SIRT1 (Sirtuin 1) and Axl (AXL Receptor Tyrosine Kinase). *Arterioscler. Thromb. Vasc. Biol.* **38**, 2079–2090 (2018).
279. Ichimura, A., Ruike, Y., Terasawa, K. & Tsujimoto, G. miRNAs and regulation of cell signaling. *FEBS J.* **278**, 1610–1618 (2011).
280. Zalewski, D. *et al.* Dysregulation of microRNA Modulatory Network in Abdominal Aortic Aneurysm. *J. Clin. Med.* **9**, 1974 (2020).
281. Maegdefessel, L. *et al.* miR-24 limits aortic vascular inflammation and murine abdominal aneurysm development. *Nat. Commun.* **5**, 5214 (2014).

282. Zhong, L. *et al.* METTL3 Induces AAA Development and Progression by Modulating N6-Methyladenosine-Dependent Primary miR34a Processing. *Mol. Ther. Nucleic Acids* **21**, 394–411 (2020).
283. Yuan, X. *et al.* miR-34a regulates phenotypic modulation of vascular smooth muscle cells in intracranial aneurysm by targeting CXCR3 and MMP-2. *Genet. Mol. Biol.* **44**, e20200124.
284. Itoh, K., Mimura, J. & Yamamoto, M. Discovery of the negative regulator of Nrf2, Keap1: a historical overview. *Antioxid. Redox Signal.* **13**, 1665–1678 (2010).
285. Itoh, K. *et al.* Keap1 regulates both cytoplasmic-nuclear shuttling and degradation of Nrf2 in response to electrophiles. *Genes Cells* **8**, 379–391 (2003).
286. Sörensen, I., Adams, R. H. & Gossler, A. DLL1-mediated Notch activation regulates endothelial identity in mouse fetal arteries. *Blood* **113**, 5680–5688 (2009).
287. Red-Horse, K. & Siekmann, A. F. Veins and Arteries Build Hierarchical Branching Patterns Differently: Bottom-Up versus Top-Down. *BioEssays News Rev. Mol. Cell. Dev. Biol.* **41**, e1800198 (2019).
288. Yanai, H., Tanaka, T. & Ueno, H. Multicolor lineage tracing methods and intestinal tumors. *J. Gastroenterol.* **48**, (2013).
289. Zahreddine, R. *et al.* Tamoxifen Accelerates Endothelial Healing by Targeting ERα in Smooth Muscle Cells. *Circ. Res.* **127**, 1473–1487 (2020).
290. Kopacz, A. *et al.* Simvastatin Attenuates Abdominal Aortic Aneurysm Formation Favoured by Lack of Nrf2 Transcriptional Activity. *Oxid. Med. Cell. Longev.* **2020**, 6340190 (2020).
291. Herr, N., Mauler, M., Bode, C. & Duerschmied, D. Intravital Microscopy of Leukocyte-endothelial and Platelet-leukocyte Interactions in Mesenterial Veins in Mice. *JoVE J. Vis. Exp.* e53077 (2015) doi:10.3791/53077.
292. Beviglia, L. *et al.* Mouse antithrombotic assay. Inhibition of platelet thromboembolism by disintegrins. *Thromb. Res.* **71**, 301–315 (1993).
293. Guy, A. *et al.* Vascular endothelial cell expression of JAK2V617F is sufficient to promote a pro-thrombotic state due to increased P-selectin expression. *Haematologica* **104**, 70–81 (2019).
294. Bar, A. *et al.* In Vivo Magnetic Resonance Imaging-Based Detection of Heterogeneous Endothelial Response in Thoracic and Abdominal Aorta to Short-Term High-Fat Diet Ascribed to Differences in Perivascular Adipose Tissue in Mice. *J. Am. Heart Assoc.* **9**, (2020).
295. Gkantidis, N., Blumer, S., Katsaros, C., Graf, D. & Chiquet, M. Site-Specific Expression of Gelatinolytic Activity during Morphogenesis of the Secondary Palate in the Mouse Embryo. *PLOS ONE* **7**, e47762 (2012).
296. Targosz-Korecka, M. *et al.* AFM-based detection of glycocalyx degradation and endothelial stiffening in the db/db mouse model of diabetes. *Sci. Rep.* **7**, 15951 (2017).
297. Proniewski, B., Kij, A., Sitek, B., Kelley, E. E. & Chlopicki, S. Multiorgan Development of Oxidative and Nitrosative Stress in LPS-Induced Endotoxemia in C57Bl/6 Mice: DHE-Based In Vivo Approach. *Oxid. Med. Cell. Longev.* **2019**, 7838406 (2019).
298. Drazkowska, K. *et al.* 2′-O-Methylation of the second transcribed nucleotide within the mRNA 5′ cap impacts the protein production level in a cell-specific manner and contributes to RNA immune evasion. *Nucleic Acids Res.* **50**, 9051–9071 (2022).
299. Piechota-Polanczyk, A. *et al.* Simvastatin Treatment Upregulates HO-1 in Patients with Abdominal Aortic Aneurysm but Independently of Nrf2. *Oxid. Med. Cell. Longev.* **2018**, 2028936 (2018).

300. Tonelli, C., Chio, I. I. C. & Tuveson, D. A. Transcriptional Regulation by Nrf2. *Antioxid. Redox Signal.* **29**, 1727–1745 (2018).
301. Sawada, H. *et al.* Twenty Years of Studying AngII (Angiotensin II)-Induced Abdominal Aortic Pathologies in Mice: Continuing Questions and Challenges to Provide Insight Into the Human Disease. *Arterioscler. Thromb. Vasc. Biol.* **42**, 277–288 (2022).
302. Yuan, Z. *et al.* Abdominal Aortic Aneurysm: Roles of Inflammatory Cells. *Front. Immunol.* **11**, (2021).
303. Abdul-Hussien, H. *et al.* Collagen Degradation in the Abdominal Aneurysm. *Am. J. Pathol.* **170**, 809–817 (2007).
304. Maguire, E. M., Pearce, S. W. A., Xiao, R., Oo, A. Y. & Xiao, Q. Matrix Metalloproteinase in Abdominal Aortic Aneurysm and Aortic Dissection. *Pharm. Basel Switz.* **12**, (2019).
305. Forrester, S. J. *et al.* Angiotensin II Signal Transduction: An Update on Mechanisms of Physiology and Pathophysiology. *Physiol. Rev.* **98**, 1627–1738 (2018).
306. Piechota-Polanczyk, A. *et al.* Decreased tissue levels of cyclophilin A, a cyclosporine a target and phospho-ERK1/2 in simvastatin patients with abdominal aortic aneurysm. *Eur. J. Vasc. Endovasc. Surg. Off. J. Eur. Soc. Vasc. Surg.* **45**, 682–688 (2013).
307. Emeto, T. I., Moxon, J. V., Au, M. & Golledge, J. Oxidative stress and abdominal aortic aneurysm: potential treatment targets. *Clin. Sci.* **130**, 301–315 (2016).
308. Ma, Q. Role of Nrf2 in Oxidative Stress and Toxicity. *Annu. Rev. Pharmacol. Toxicol.* **53**, 401–426 (2013).
309. Henderson, E. L. *et al.* Death of smooth muscle cells and expression of mediators of apoptosis by T lymphocytes in human abdominal aortic aneurysms. *Circulation* **99**, 96–104 (1999).
310. Thompson, R. W., Liao, S. & Curci, J. A. Vascular smooth muscle cell apoptosis in abdominal aortic aneurysms. *Coron. Artery Dis.* **8**, 623–631 (1997).
311. Vatner, S. F. *et al.* Vascular Stiffness in Aging and Disease. *Front. Physiol.* **12**, (2021).
312. Haase, K. & Pelling, A. E. Investigating cell mechanics with atomic force microscopy. *J. R. Soc. Interface* **12**, 20140970 (2015).
313. Ferraraccio, F. *et al.* Scanning Electron Microscopy of Aortic Medial Changes in Aortic Ascending Dilatation. *Ultrastruct. Pathol.* **28**, 137–140 (2004).
314. Nakamura, H., Izumiyama, N., Nakamura, K. & Ohtsubo, K. Age-associated ultrastructural changes in the aortic intima of rats with diet-induced hypercholesterolemia. *Atherosclerosis* **79**, 101–111 (1989).
315. Chin, A. S. *et al.* Acute Limited Intimal Tears of the Thoracic Aorta. *J. Am. Coll. Cardiol.* **71**, 2773–2785 (2018).
316. Maldjian, P. D. & Partyka, L. Intimal Tears in Thoracic Aortic Dissection: Appearance on MDCT With Virtual Angioscopy. *Am. J. Roentgenol.* **198**, 955–961 (2012).
317. Loesch, A. & Dashwood, M. R. Vasa vasorum inside out/outside in communication: a potential role in the patency of saphenous vein coronary artery bypass grafts. *J. Cell Commun. Signal.* **12**, 631–643 (2018).
318. Liu, L. & Shi, G.-P. CD31: beyond a marker for endothelial cells. *Cardiovasc. Res.* **94**, 3–5 (2012).
319. Langheinrich, A. C., Kampschulte, M., Buch, T. & Bohle, R. M. Vasa vasorum and atherosclerosis - Quid novi? *Thromb. Haemost.* **97**, 873–879 (2007).
320. Sanyour, H. J. *et al.* Statin-mediated cholesterol depletion exerts coordinated effects on the alterations in rat vascular smooth muscle cell biomechanics and migration. *J. Physiol.* **598**, 1505–1522 (2020).

321. Cao, C. *et al.* IKKε Knockout Prevents High Fat Diet Induced Arterial Atherosclerosis and NF-κB Signaling in Mice. *PloS One* **8**, e64930 (2013).
322. Franck, G. *et al.* Haemodynamic stress-induced breaches of the arterial intima trigger inflammation and drive atherogenesis. *Eur. Heart J.* **40**, 928–937 (2019).
323. Chen, H.-Z. *et al.* Age-Associated Sirtuin 1 Reduction in Vascular Smooth Muscle Links Vascular Senescence and Inflammation to Abdominal Aortic Aneurysm. *Circ. Res.* **119**, 1076–1088 (2016).
324. Fu, X., Zhou, Y., Cheng, Z., Liao, X. & Zhou, X. MicroRNAs: Novel Players in Aortic Aneurysm. *BioMed Res. Int.* **2015**, e831641 (2015).
325. Kim, C. W. *et al.* Prevention of abdominal aortic aneurysm by anti-miRNA-712 or anti-miR-205 in Angiotensin II infused mice. *Arterioscler. Thromb. Vasc. Biol.* **34**, 1412–1421 (2014).
326. Ye, Z. *et al.* MicroRNA-34a induces a senescence-like change via the down-regulation of SIRT1 and up-regulation of p53 protein in human esophageal squamous cancer cells with a wild-type p53 gene background. *Cancer Lett.* **370**, 216–221 (2016).
327. Park, H. *et al.* miR-34a inhibits differentiation of human adipose tissue-derived stem cells by regulating cell cycle and senescence induction. *Differentiation* **90**, 91–100 (2015).
328. Alexander, Y. *et al.* Endothelial function in cardiovascular medicine: a consensus paper of the European Society of Cardiology Working Groups on Atherosclerosis and Vascular Biology, Aorta and Peripheral Vascular Diseases, Coronary Pathophysiology and Microcirculation, and Thrombosis. *Cardiovasc. Res.* **117**, 29–42 (2020).
329. Qu, J., Cheng, Y., Wu, W., Yuan, L. & Liu, X. Glycocalyx Impairment in Vascular Disease: Focus on Inflammation. *Front. Cell Dev. Biol.* **9**, (2021).
330. Potje, S. R., Paula, T. D.-C., Paulo, M. & Bendhack, L. M. The Role of Glycocalyx and Caveolae in Vascular Homeostasis and Diseases. *Front. Physiol.* **11**, (2021).
331. Thatcher, S. E. *et al.* ACE2 Decreases Formation and Severity of Angiotensin II-induced Abdominal Aortic Aneurysms. *Arterioscler. Thromb. Vasc. Biol.* **34**, 2617–2623 (2014).
332. Serruys, P. W., Regar, E. & Carter, A. J. Rapamycin eluting stent: the onset of a new era in interventional cardiology. *Heart* **87**, 305–307 (2002).
333. Si, Y. *et al.* Concentration-dependent effects of rapamycin on proliferation, migration and apoptosis of endothelial cells in human venous malformation. *Exp. Ther. Med.* **16**, 4595–4601 (2018).
334. Schmeisser, K. & Parker, J. A. Pleiotropic Effects of mTOR and Autophagy During Development and Aging. *Front. Cell Dev. Biol.* **7**, 192 (2019).
335. Cheng, Y., Pitoniak, A., Wang, J. & Bohmann, D. Preserving transcriptional stress responses as an anti-aging strategy. *Aging Cell* **20**, e13297 (2021).
336. Biroccio, A., Benassi, B., Fiorentino, F. & Zupi, G. Glutathione Depletion Induced by c-Myc Downregulation Triggers Apoptosis on Treatment with Alkylating Agents. *Neoplasia N. Y. N* **6**, 195–206 (2004).
337. Harder, B. *et al.* Molecular mechanisms of Nrf2 regulation and how these influence chemical modulation for disease intervention. *Biochem. Soc. Trans.* **43**, 680–686 (2015).
338. Florea, V. *et al.* c-Myc Is Essential to Prevent Endothelial Pro-Inflammatory Senescent Phenotype. *PLoS ONE* **8**, (2013).
339. Song, H. *et al.* Itaconate prevents abdominal aortic aneurysm formation through inhibiting inflammation via activation of Nrf2. *EBioMedicine* **57**, 102832 (2020).
340. Nordon, I. M., Hinchliffe, R. J., Loftus, I. M. & Thompson, M. M. Pathophysiology and epidemiology of abdominal aortic aneurysms. *Nat. Rev. Cardiol.* **8**, 92–102 (2011).

341. Pimiento, J. M. *et al.* Endothelial Nitric Oxide Synthase Stimulates Aneurysm Growth in Aged Mice. *J. Vasc. Res.* **45**, 251–258 (2008).
342. Huang, K., Gao, X. & Wei, W. The crosstalk between Sirt1 and Keap1/Nrf2/ARE anti-oxidative pathway forms a positive feedback loop to inhibit FN and TGF-β1 expressions in rat glomerular mesangial cells. *Exp. Cell Res.* **361**, 63–72 (2017).
343. Chai, D. *et al.* Nrf2 Activation Induced by Sirt1 Ameliorates Acute Lung Injury After Intestinal Ischemia/Reperfusion Through NOX4-Mediated Gene Regulation. *Cell. Physiol. Biochem. Int. J. Exp. Cell. Physiol. Biochem. Pharmacol.* **46**, 781–792 (2018).
344. Daugherty, A., Manning, M. W. & Cassis, L. A. Angiotensin II promotes atherosclerotic lesions and aneurysms in apolipoprotein E-deficient mice. *J. Clin. Invest.* **105**, 1605–1612 (2000).
345. Kopacz, A. *et al.* A Dual Role of Heme Oxygenase-1 in Angiotensin II-Induced Abdominal Aortic Aneurysm in the Normolipidemic Mice. *Cells* **10**, 163 (2021).
346. Guzik, T. J. *et al.* Role of the T cell in the genesis of angiotensin II induced hypertension and vascular dysfunction. *J. Exp. Med.* **204**, 2449–2460 (2007).
347. Moore, J. P. *et al.* A flow cytometric method for the analysis of macrophages in the vascular wall. *J. Immunol. Methods* **396**, 33–43 (2013).
348. Wang, X. *et al.* AT1R Regulates Macrophage Polarization Through YAP and Regulates Aortic Dissection Incidence. *Front. Physiol.* **12**, 644903 (2021).
349. Parga, J. A., Rodriguez-Perez, A. I., Garcia-Garrote, M., Rodriguez-Pallares, J. & Labandeira-Garcia, J. L. Angiotensin II induces oxidative stress and upregulates neuroprotective signaling from the NRF2 and KLF9 pathway in dopaminergic cells. *Free Radic. Biol. Med.* **129**, 394–406 (2018).
350. Kang, S. J., You, A. & Kwak, M.-K. Suppression of Nrf2 signaling by angiotensin II in murine renal epithelial cells. *Arch. Pharm. Res.* **34**, 829–836 (2011).
351. Navar, L. G., Mitchell, K. D., Harrison-Bernard, L. M., Kobori, H. & Nishiyama, A. Review: Intrarenal angiotensin II levels in normal and hypertensive states. *J. Renin-Angiotensin-Aldosterone Syst. JRAAS* **2**, S176–S184 (2001).
352. Gonzalez-Villalobos, R. A. *et al.* Angiotensin-converting enzyme-derived angiotensin II formation during angiotensin II-induced hypertension. *Hypertens. Dallas Tex 1979* **53**, 351–355 (2009).
353. Cassis, L. A. *et al.* ANG II infusion promotes abdominal aortic aneurysms independent of increased blood pressure in hypercholesterolemic mice. *Am. J. Physiol. Heart Circ. Physiol.* **296**, H1660-1665 (2009).
354. Gavazzi, G. *et al.* NOX1 Deficiency Protects From Aortic Dissection in Response to Angiotensin II. *Hypertension* **50**, 189–196 (2007).
355. Peng, S. *et al.* Role of aggregated medin in the pathogenesis of thoracic aortic aneurysm and dissection. *Lab. Investig. J. Tech. Methods Pathol.* **87**, 1195–1205 (2007).
356. Navas-Madroñal, M. *et al.* Enhanced endoplasmic reticulum and mitochondrial stress in abdominal aortic aneurysm. *Clin. Sci. Lond. Engl. 1979* **133**, 1421–1438 (2019).
357. Pérez, M. C., Navas-Madroñal, M., Martínez-González, J., Rodríguez, C. & Galán, M. Inhibition Of Endoplasmic Reticulum Stress As A Potential Therapy To Limit The Progression Of Aaa And Hypertensive Heart Disease. *Atherosclerosis* **287**, e19 (2019).
358. de la Fuente-Alonso, A. *et al.* Aortic disease in Marfan syndrome is caused by overactivation of sGC-PRKG signaling by NO. *Nat. Commun.* **12**, 2628 (2021).
359. Pan, L. *et al.* S-Nitrosylation of Plastin-3 Exacerbates Thoracic Aortic Dissection Formation via Endothelial Barrier Dysfunction. *Arterioscler. Thromb. Vasc. Biol.* **40**, 175–188 (2020).

360. Tashima, Y. *et al.* Androgens Accentuate TGF-β Dependent Erk/Smad Activation During Thoracic Aortic Aneurysm Formation in Marfan Syndrome Male Mice. *J. Am. Heart Assoc.* **9**, e015773 (2020).
361. López-Guimet, J., Andilla, J., Loza-Alvarez, P. & Egea, G. High-Resolution Morphological Approach to Analyse Elastic Laminae Injuries of the Ascending Aorta in a Murine Model of Marfan Syndrome. *Sci. Rep.* **7**, 1505 (2017).
362. Benke, K. *et al.* The role of transforming growth factor-beta in Marfan syndrome. *Cardiol. J.* **20**, 227–234 (2013).
363. de Beaufort, H. W. L. *et al.* Aortic dissection in patients with Marfan syndrome based on the IRAD data. *Ann. Cardiothorac. Surg.* **6**, 633–641 (2017).
364. Schrijver, I., Liu, W., Brenn, T., Furthmayr, H. & Francke, U. Cysteine substitutions in epidermal growth factor-like domains of fibrillin-1: distinct effects on biochemical and clinical phenotypes. *Am. J. Hum. Genet.* **65**, 1007–1020 (1999).
365. Aoki, T. *et al.* Reactive oxygen species modulate growth of cerebral aneurysms: a study using the free radical scavenger edaravone and p47phox−/− mice. *Lab. Invest.* **89**, 730–741 (2009).
366. Li, J. *et al.* Up-regulation of p27kip1 contributes to Nrf2-mediated protection against angiotensin II-induced cardiac hypertrophy. *Cardiovasc. Res.* **90**, 315–324 (2011).
367. McCormick, M. L., Gavrila, D. & Weintraub, N. L. Role of Oxidative Stress in the Pathogenesis of Abdominal Aortic Aneurysms. *Arterioscler. Thromb. Vasc. Biol.* **27**, 461–469 (2007).
368. Portelli, S. S., Hambly, B. D., Jeremy, R. W. & Robertson, E. N. Oxidative stress in genetically triggered thoracic aortic aneurysm: role in pathogenesis and therapeutic opportunities. *Redox Rep.* **26**, 45–52 (2021).
369. Guzik, B. *et al.* Mechanisms of oxidative stress in human aortic aneurysms — Association with clinical risk factors for atherosclerosis and disease severity. *Int. J. Cardiol.* **168**, 2389–2396 (2013).
370. Morimoto, K. *et al.* Free-radical scavenger edaravone inhibits both formation and development of abdominal aortic aneurysm in rats. *J. Vasc. Surg.* **55**, 1749–1758 (2012).
371. Lavin, B. *et al.* Tropoelastin: an in vivo imaging marker of dysfunctional matrix turnover during abdominal aortic dilation. *Cardiovasc. Res.* **116**, 995–1005 (2020).
372. Akhtar, K. *et al.* Oxidative Modifications of the C-terminal Domain of Tropoelastin Prevent Cell Binding. *J. Biol. Chem.* **286**, 13574–13582 (2011).
373. Siwik, D. A., Pagano, P. J. & Colucci, W. S. Oxidative stress regulates collagen synthesis and matrix metalloproteinase activity in cardiac fibroblasts. *Am. J. Physiol. Cell Physiol.* **280**, C53-60 (2001).
374. Fisher, G. J. *et al.* Collagen fragmentation promotes oxidative stress and elevates matrix metalloproteinase-1 in fibroblasts in aged human skin. *Am. J. Pathol.* **174**, 101–114 (2009).
375. Zapp, C. *et al.* Mechanoradicals in tensed tendon collagen as a source of oxidative stress. *Nat. Commun.* **11**, 2315 (2020).
376. Nagababu, E. & Rifkind, J. M. Heme degradation by reactive oxygen species. *Antioxid. Redox Signal.* **6**, 967–978 (2004).
377. Rosenbaum, M. A., Miyazaki, K. & Graham, L. M. Hypercholesterolemia and oxidative stress inhibit endothelial cell healing after arterial injury. *J. Vasc. Surg.* **55**, 489–496 (2012).
378. Wang, B. & Williamson, G. Transcriptional regulation of the human NAD(P)H:quinone oxidoreductase (NQO1) gene by monofunctional inducers. *Biochim. Biophys. Acta* **1307**, 104–110 (1996).

379. Kopacz, A. *et al.* Overlooked and valuable facts to know in the NRF2/KEAP1 field. *Free Radic. Biol. Med.* (2022) doi:10.1016/j.freeradbiomed.2022.08.044.
380. Xue, M. *et al.* Frequency Modulated Translocational Oscillations of Nrf2 Mediate the Antioxidant Response Element Cytoprotective Transcriptional Response. *Antioxid. Redox Signal.* **23**, 613–629 (2015).
381. Chaum, E., Yin, J., Yang, H., Thomas, F. & Lang, J. C. Quantitative AP-1 gene regulation by oxidative stress in the human retinal pigment epithelium. *J. Cell. Biochem.* **108**, 1280–1291 (2009).
382. Carracedo, J. *et al.* Protein Carbamylation: A Marker Reflecting Increased Age-Related Cell Oxidation. *Int. J. Mol. Sci.* **19**, 1495 (2018).
383. Gorisse, L. *et al.* Protein carbamylation is a hallmark of aging. *Proc. Natl. Acad. Sci.* **113**, 1191–1196 (2016).
384. Brayton, C. Spontaneous Diseases in Commonly Used Mouse Strains. *Mouse Biomed. Res.* 623–717 (2007) doi:10.1016/B978-012369454-6/50053-4.
385. Pettan-Brewer, C. & Treuting, P. M. Practical pathology of aging mice. *Pathobiol. Aging Age Relat. Dis.* **1**, (2011).
386. Ronchi, J. A. *et al.* A spontaneous mutation in the nicotinamide nucleotide transhydrogenase gene of C57BL/6J mice results in mitochondrial redox abnormalities. *Free Radic. Biol. Med.* **63**, 446–456 (2013).
387. Guinea, G. V. *et al.* Factors influencing the mechanical behaviour of healthy human descending thoracic aorta. *Physiol. Meas.* **31**, 1553–1565 (2010).
388. Wirth, A. *et al.* Age-dependent blood pressure elevation is due to increased vascular smooth muscle tone mediated by G-protein signalling. *Cardiovasc. Res.* **109**, 131–140 (2016).
389. Varga, R. *et al.* Progressive vascular smooth muscle cell defects in a mouse model of Hutchinson–Gilford progeria syndrome. *Proc. Natl. Acad. Sci.* **103**, 3250–3255 (2006).
390. Grasl-Kraupp, B. *et al.* In situ detection of fragmented DNA (TUNEL assay) fails to discriminate among apoptosis, necrosis, and autolytic cell death: a cautionary note. *Hepatol. Baltim. Md* **21**, 1465–1468 (1995).
391. Roostalu, U. & Wong, J. K. Arterial smooth muscle dynamics in development and repair. *Dev. Biol.* **435**, 109–121 (2018).
392. Yamada, M., Ohno, M., Itagaki, T., Takaba, T. & Matsuyama, T. Coexistence of cystic medial necrosis and segmental arterial mediolysis in a patient with aneurysms of the abdominal aorta and the iliac artery. *J. Vasc. Surg.* **39**, 246–249 (2004).
393. Beenakker, J.-W. M., Ashcroft, B. A., Lindeman, J. H. N. & Oosterkamp, T. H. Mechanical Properties of the Extracellular Matrix of the Aorta Studied by Enzymatic Treatments. *Biophys. J.* **102**, 1731–1737 (2012).
394. Grazi, E. What is the diameter of the actin filament? *FEBS Lett.* **405**, 249–252 (1997).
395. Gavara, N. & Chadwick, R. S. Relationship between cell stiffness and stress fiber amount, assessed by simultaneous atomic force microscopy and live-cell fluorescence imaging. *Biomech. Model. Mechanobiol.* **15**, 511–523 (2016).
396. Tang, D. D. Chapter One - The Dynamic Actin Cytoskeleton in Smooth Muscle. in *Advances in Pharmacology* (ed. Khalil, R. A.) vol. 81 1–38 (Academic Press, 2018).
397. Chatterjee, S. Endothelial Mechanotransduction, Redox Signaling and the Regulation of Vascular Inflammatory Pathways. *Front. Physiol.* **9**, 524 (2018).
398. Atkinson, L. *et al.* Reversal of stress fibre formation by Nitric Oxide mediated RhoA inhibition leads to reduction in the height of preformed thrombi. *Sci. Rep.* **8**, 3032 (2018).
399. Schenk, L. K. *et al.* Angiotensin II regulates phosphorylation of actin-associated proteins in human podocytes. *FASEB J.* **31**, 5019–5035 (2017).

400. Touyz, R. M., Yao, G. & Schiffrin, E. L. Role of the actin cytoskeleton in angiotensin II signaling in human vascular smooth muscle cells. *Can. J. Physiol. Pharmacol.* **83**, 91–97 (2005).
401. Zhang, J. *et al.* Extracellular Matrix Disarray as a Mechanism for Greater Abdominal Versus Thoracic Aortic Stiffness With Aging in Primates. *Arterioscler. Thromb. Vasc. Biol.* **36**, 700–706 (2016).
402. Heinemeier, K. & Kjaer, M. In vivo investigation of tendon responses to mechanical loading. *J. Musculoskelet. Neuronal Interact.* **11**, 115–23 (2011).
403. Wang, Y., Zeinali-Davarani, S. & Zhang, Y. Arterial mechanics considering the structural and mechanical contributions of ECM constituents. *J. Biomech.* **49**, 2358–2365 (2016).
404. Lawence-Brown, M. M., Liffman, K., Semmens, J. B. & Sutalo, I. D. Vascular Arterial Haemodynamics. in *Mechanisms of Vascular Disease: A Reference Book for Vascular Specialists* (eds. Fitridge, R. & Thompson, M.) (University of Adelaide Press, 2011).
405. Korshunov, V. "Slava" A. Arteriogenesis and Collateral Formation. in *PanVascular Medicine* (ed. Lanzer, P.) 1–26 (Springer, 2013). doi:10.1007/978-3-642-37393-0_7-1.
406. Kawabe, J. & Hasebe, N. Role of the Vasa Vasorum and Vascular Resident Stem Cells in Atherosclerosis. *BioMed Res. Int.* **2014**, 701571 (2014).
407. Wolinsky, H. Comparison of Medial Growth of Human Thoracic and Abdominal Aortas. *Circ. Res.* **27**, 531–538 (1970).
408. Tellides, G. & Pober, J. S. Inflammatory and Immune Responses in the Arterial Media. *Circ. Res.* **116**, 312–322 (2015).
409. Phillippi, J. A. On vasa vasorum: A history of advances in understanding the vessels of vessels. *Sci. Adv.* **8**, eabl6364 (2022).
410. Tanaka, H. *et al.* Hypoperfusion of the Adventitial Vasa Vasorum Develops an Abdominal Aortic Aneurysm. *PLOS ONE* **10**, e0134386 (2015).
411. Davies, M. J., Woolf, N., Rowles, P. M. & Pepper, J. Morphology of the endothelium over atherosclerotic plaques in human coronary arteries. *Br. Heart J.* **60**, 459 (1988).
412. Steinmetz, E. F. *et al.* Treatment with simvastatin suppresses the development of experimental abdominal aortic aneurysms in normal and hypercholesterolemic mice. *Ann. Surg.* **241**, 92–101 (2005).
413. Samson, F. P. *et al.* Oleic Acid, Cholesterol, and Linoleic Acid as Angiogenesis Initiators. *ACS Omega* **5**, 20575–20585 (2020).
414. Koh, K. K., Park, S. M. & Quon, M. J. Leptin and Cardiovascular Disease. *Circulation* **117**, 3238–3249 (2008).
415. Qi, X.-Y. *et al.* Perivascular adipose tissue (PVAT) in atherosclerosis: a double-edged sword. *Cardiovasc. Diabetol.* **17**, 134 (2018).
416. Singh, P. *et al.* Statins decrease leptin expression in human white adipocytes. *Physiol. Rep.* **6**, (2018).
417. Zeng, L. *et al.* Simvastatin Modulates Angiotensin II Signaling Pathway by Preventing Rac1-Mediated Upregulation of p27. *J. Am. Soc. Nephrol.* **15**, 1711–1720 (2004).
418. Rodríguez-Peña, A. B. *et al.* Effect of Angiotensin II and Small GTPase Ras Signaling Pathway Inhibition on Early Renal Changes in a Murine Model of Obstructive Nephropathy. *BioMed Res. Int.* **2014**, 124902 (2014).
419. Szade, A., Grochot-Przeczek, A., Florczyk, U., Jozkowicz, A. & Dulak, J. Cellular and molecular mechanisms of inflammation-induced angiogenesis. *IUBMB Life* **67**, 145–159 (2015).
420. Haas, T. L. & Duling, B. R. Morphology favors an endothelial cell pathway for longitudinal conduction within arterioles. *Microvasc. Res.* **53**, 113–120 (1997).

421. Dora, K. A., Doyle, M. P. & Duling, B. R. Elevation of intracellular calcium in smooth muscle causes endothelial cell generation of NO in arterioles. *Proc. Natl. Acad. Sci.* **94**, 6529–6534 (1997).
422. Hua, C.-C., Liu, X.-M., Liang, L.-R., Wang, L.-F. & Zhong, J.-C. Targeting the microRNA-34a as a Novel Therapeutic Strategy for Cardiovascular Diseases. *Front. Cardiovasc. Med.* **8**, (2022).
423. Zuccolo, E. *et al.* The microRNA-34a-Induced Senescence-Associated Secretory Phenotype (SASP) Favors Vascular Smooth Muscle Cells Calcification. *Int. J. Mol. Sci.* **21**, 4454 (2020).
424. Mokhberian, N. *et al.* Inhibition of miR-34a reduces cellular senescence in human adipose tissue-derived mesenchymal stem cells through the activation of SIRT1. *Life Sci.* **257**, 118055 (2020).
425. Pi, C. *et al.* MiR-34a suppression targets Nampt to ameliorate bone marrow mesenchymal stem cell senescence by regulating NAD+-Sirt1 pathway. *Stem Cell Res. Ther.* **12**, 271 (2021).
426. Ellis, B. L. *et al.* A survey of ex vivo/in vitro transduction efficiency of mammalian primary cells and cell lines with Nine natural adeno-associated virus (AAV1-9) and one engineered adeno-associated virus serotype. *Virol. J.* **10**, 74 (2013).
427. Nathwani, A. C. *et al.* Enhancing transduction of the liver by adeno-associated viral vectors. *Gene Ther.* **16**, 60–69 (2009).
428. Xu, Y. *et al.* Macrophage miR-34a Is a Key Regulator of Cholesterol Efflux and Atherosclerosis. *Mol. Ther.* **28**, 202–216 (2020).
429. Su, G., Sun, G., Liu, H., Shu, L. & Liang, Z. Downregulation of miR-34a promotes endothelial cell growth and suppresses apoptosis in atherosclerosis by regulating Bcl-2. *Heart Vessels* **33**, 1185–1194 (2018).
430. Wu, J. *et al.* Inhibition of P53/miR-34a improves diabetic endothelial dysfunction via activation of SIRT1. *J. Cell. Mol. Med.* **23**, 3538–3548 (2019).
431. Li, Q. *et al.* P66Shc-Induced MicroRNA-34a Causes Diabetic Endothelial Dysfunction by Downregulating Sirtuin1. *Arterioscler. Thromb. Vasc. Biol.* **36**, 2394–2403 (2016).
432. Shah, A. V., Birdsey, G. M. & Randi, A. M. Regulation of endothelial homeostasis, vascular development and angiogenesis by the transcription factor ERG. *Vascul. Pharmacol.* **86**, 3–13 (2016).
433. Marsman, J., Gimenez, G., Day, R. C., Horsfield, J. A. & Jones, G. T. A non-coding genetic variant associated with abdominal aortic aneurysm alters ERG gene regulation. *Hum. Mol. Genet.* **29**, 554–565 (2020).
434. Li, Y. *et al.* Single-Cell Transcriptome Analysis Reveals Dynamic Cell Populations and Differential Gene Expression Patterns in Control and Aneurysmal Human Aortic Tissue. *Circulation* **142**, 1374–1388 (2020).
435. Berg, D. J. *et al.* Enterocolitis and colon cancer in interleukin-10-deficient mice are associated with aberrant cytokine production and CD4(+) TH1-like responses. *J. Clin. Invest.* **98**, 1010–1020 (1996).
436. Ait-Oufella, H. *et al.* Natural regulatory T cells limit angiotensin II-induced aneurysm formation and rupture in mice. *Arterioscler. Thromb. Vasc. Biol.* **33**, 2374–2379 (2013).
437. Lareyre, F. *et al.* TGFβ (Transforming Growth Factor-β) Blockade Induces a Human-Like Disease in a Nondissecting Mouse Model of Abdominal Aortic Aneurysm. *Arterioscler. Thromb. Vasc. Biol.* **37**, 2171–2181 (2017).

438. Biswas, I. & Khan, G. A. *Endothelial Dysfunction in Cardiovascular Diseases*. *Basic and Clinical Understanding of Microcirculation* (IntechOpen, 2019). doi:10.5772/intechopen.89365.
439. Gao, Y. & Galis, Z. S. Exploring the Role of Endothelial Cell Resilience in Cardiovascular Health and Disease. *Arterioscler. Thromb. Vasc. Biol.* **41**, 179–185 (2021).
440. Hoffmann, J. *et al.* Aging enhances the sensitivity of endothelial cells toward apoptotic stimuli: important role of nitric oxide. *Circ. Res.* **89**, 709–715 (2001).
441. Lukowski, S. W. *et al.* Single-Cell Transcriptional Profiling of Aortic Endothelium Identifies a Hierarchy from Endovascular Progenitors to Differentiated Cells. *Cell Rep.* **27**, 2748-2758.e3 (2019).
442. Centa, A. *et al.* Deregulated miRNA expression is associated with endothelial dysfunction in post-mortem lung biopsies of COVID-19 patients. *Am. J. Physiol. - Lung Cell. Mol. Physiol.* **320**, L405–L412 (2021).
443. Schwartz, S. M., Reidy, A. & Hansson, G. Role of Endothelial Dysfunction in Vivo in Smooth Muscle Proliferation. in *Atherosclerosis VI* (eds. Schettler, F. G., Gotto, A. M., Middelhoff, G., Habenicht, A. J. R. & Jurutka, K. R.) 343–349 (Springer, 1983). doi:10.1007/978-3-642-81817-2_66.
444. Peng, Y., Guo, J.-J., Liu, Y.-M. & Wu, X.-L. MicroRNA-34A inhibits the growth, invasion and metastasis of gastric cancer by targeting PDGFR and MET expression. *Biosci. Rep.* **34**, e00112 (2014).
445. Ruiz-Camp, J. *et al.* Targeting miR-34a/Pdgfra interactions partially corrects alveologenesis in experimental bronchopulmonary dysplasia. *EMBO Mol. Med.* **11**, e9448 (2019).
446. Deguchi, J., Makuuchi, M., Nakaoka, T., Collins, T. & Takuwa, Y. Angiotensin II stimulates platelet-derived growth factor-B chain expression in newborn rat vascular smooth muscle cells and neointimal cells through Ras, extracellular signal-regulated protein kinase, and c-Jun N-terminal protein kinase mechanisms. *Circ. Res.* **85**, 565–574 (1999).
447. Beitz, J. G., Kim, I. S., Calabresi, P. & Frackelton, A. R. Human microvascular endothelial cells express receptors for platelet-derived growth factor. *Proc. Natl. Acad. Sci. U. S. A.* **88**, 2021–2025 (1991).
448. Erickson, C. B. & Payne, K. A. Inductive Signals and Progenitor Fates During Osteogenesis. in *Encyclopedia of Tissue Engineering and Regenerative Medicine* (ed. Reis, R. L.) 395–404 (Academic Press, 2019). doi:10.1016/B978-0-12-801238-3.65483-1.
449. Clément, M. *et al.* Vascular Smooth Muscle Cell Plasticity and Autophagy in Dissecting Aortic Aneurysms. *Arterioscler. Thromb. Vasc. Biol.* **39**, 1149–1159 (2019).
450. Rombouts, K. B. *et al.* The role of vascular smooth muscle cells in the development of aortic aneurysms and dissections. *Eur. J. Clin. Invest.* **52**, e13697 (2022).
451. Masuda, H. *et al.* Increase in endothelial cell density before artery enlargement in flow-loaded canine carotid artery. *Arterioscler. Dallas Tex* **9**, 812–823 (1989).
452. Itkin, T. *et al.* Distinct bone marrow blood vessels differentially regulate haematopoiesis. *Nature* **532**, 323–328 (2016).
453. Blokland, K. E. C., Pouwels, S. D., Schuliga, M., Knight, D. A. & Burgess, J. K. Regulation of cellular senescence by extracellular matrix during chronic fibrotic diseases. *Clin. Sci. Lond. Engl. 1979* **134**, 2681–2706 (2020).

PhD candidate scientific contributions

Original research publications:

Kopacz, A.; Klóska, D.; Klimczyk, D.; Kopec, M.; Jozkowicz, A.; Piechota-Polanczyk, A.. *NRF2 transcriptional activity governs the intestinal development.* International Journal of Molecular Sciences 2021, ID:6175, doi: 10.3390/ijms23116175 (IF_{2021}=6.208)

Targosz-Korecka, M.; Kubisiak, A.;, Klóska, D.;, **Kopacz, A.;** Grochot-Przęczek, A.; Szymoński, M. *Endothelial glycocalyx shields the interaction of SARS-CoV-2 spike protein with ACE2 receptors*. Scientific Reports 2021; 12157; doi: 10.1038/s41598-021-91231 (IF_{2021}=4.379)

Kopacz, A.; Klóska, D.; Werner, E., Hajduk, K.; Grochot-Przęczek, A.; Jozkowicz, A.; Piechota-Polanczyk, A.. *A Dual Role of Heme Oxygenase-1 in Angiotensin II- Induced Adominal Aortic Aneurysm in the Normolipidemic Mice;* Cells 2021, doi: 10.3390/cells10010163 (IF_{2021}=7.666)

Kopacz, A., Werner, E., Grochot-Przeczek, A., Klóska, D., Hajduk, K., Neumayer, C., Jozkowicz, A., Piechota-Polanczyk, A. *Simvastatin attenuates abdominal aortic aneurysm formation favoured by lack of NRF2 transcriptional activity.* Oxidative Medicine & Cellular Longevity 2020; ID:6340190; doi: 10.1155/2020/6340190 (IF_{2020} =6.543)

Kopacz, A., Werner, E., Klóska, D., Nesterak, S., Hajduk, K., Fichna, J., Jozkowicz, A., Piechota-Polanczyk, A. *NRF2 transcriptional activity in the mouse affects the physiological response to tribromoethanol.* Biomedicine&Pharmacotherapy 128 (2020) 110317 doi: 10.1016/j.biopha.2020.111020 (IF_{2020}=6.529)

Kopacz, A., Klóska, D., Targosz-Korecka, M., Zapotoczny, B., Cysewski, D., Personnic, N., Werner, E., Hajduk, K., Jozkowicz, A., Grochot-Przeczek, A. *KEAP1 governs ageing-induced protein aggregation in endothelial cells.* Redox Biology 2020, Jul ;34:101572. doi: 10.1016/j.redox.2020.101572 (IF_{2020} =11.799)

Kopacz, A.; Klóska, D.; Cysewski, D., Proniewski, B.; Personnic, N.; Piechota-Polanczyk, A.; Kaczara, P.; Zakrzewska, A.; Forman, HJ; Dulak, J.; Jozkowicz, A.; Grochot-Przeczek, A. *KEAP1 controls protein S-nitrosylation and apoptosis-senescence switch in endothelial cells*. Redox Biology . 2020 Jan;28:101304. doi: 10.1016/j.redox.2019.101304 (IF_{2020} =11.799)

Rozga, P.; Kloska,D.;, Pawlak, S.; Teska-Kaminska, M.; Galazka, M.; Bukato, K.; Pieczykolan, A; Jaworski, A.; Molga, A.; **Kopacz, A.;** Badyra, B.; Kachamakova-Trojanowska, N.; Zolnierkiewicz, O.; Targosz-Korecka, M.; Poleszak, K.; Szymanik, M.; Zerek, B.; Pieczykolan, J.; Jozkowicz, A., Grochot-Przeczek, A.; *Novel engineered TRAIL-based chimeric molecule forcefully inhibits tumor growth and bypasses TRAIL resistance*. International Journal of Cancer 2019 Dec 21. doi: 10.1002/ijc.32845 (IF_{2019} =5.145)

Kloska, D.; **Kopacz, A.;** Piechota-Polanczyk, A.; Neumayer, C.; Huk, I.; Dulak, J.; Jozkowicz, A.; Grochot-Przeczek, A. *Biliverdin reductase deficiency triggers an endothelial-to-mesenchymal transition in human endothelial cells*. Archives of Biochemistry and Biophysics 2019 Dec 15; 678: 108182, doi: 10.1016/j.abb.2019.108182 (IF_{2019} =3.391)

Klóska, D.; **Kopacz, A.**; Cysewski, D.; Aepfelbacher, M.; Dulak, J.; Jozkowicz, A.; Grochot-Przeczek, A. *NRF2 sequesters KEAP1 preventing podosome disassembly: a quintessential duet moonlights in endothelium*. Antioxid. Redox Signal. 2019 May 10; 30 (14): 1709-1730, doi:10.1089/ars.2018.7505 (IF_{2019} =6.323)

Nowak, W.N., Taha, H., Kachamakova-Trojanowska, N., Stępniewski, J., Markiewicz, J.A., Kusienicka, A., Szade, K., Szade, A., Bukowska-Strakova, K., Hajduk, K., Klóska, D., **Kopacz, A.**, Grochot-Przęczek, A., Barthenheier, K., Cauvin, C., Dulak, J., Józkowicz, A., 2018. *Murine Bone Marrow Mesenchymal Stromal Cells Respond Efficiently to Oxidative Stress Despite the Low Level of Heme Oxygenases 1 and 2*. Antioxid. Redox Signal 2018 Jul 10; 29(2):111-127; doi: 10.1089/ars.2017.7097 (IF_{2018} =5.828)

Piechota-Polańczyk, A., **Kopacz, A.**, Kloska, D., Zagrapan, B., Neumayer, C., Grochot-Przęczek, A., Huk, I., Brostjan, C., Dulak, J., Jozkowicz, A., 2018. *Simvastatin treatment up-regulates HO-1 in patients with abdominal aortic aneurysm but independently of NRF2*. Oxid. Med. Cell. Longevity. 2018, ID: 2028936, doi:10.1155/2018/2028936 (IF_{2018} =4.936)

Reviews:

Kopacz, A.; Rojo, A.; Patibandla, C.; Lastra-Martinez, D.; Piechota-Polanczyk, A.; Kloska, D.; Jozkowicz, A.; Suterland, C.; Cuadrado, A.; Grochot-Przeczek, A. *Overlooked and valuable* facts *to know in the NRF2/KEAP1 field*, Free Radical Biology & Medicine 2022, accepted (IF_{2021} =8.101)

Kopacz, A.; Klóska, D.; Forman, HJ; Jozkowicz, A.; Grochot-Przeczek, A. *Beyond repression of NRF2: an update on KEAP1*. Free Radical Biology & Medicine 2020 Mar 28:S0891-5849(19)32525-0. doi: 10.1016/j.freeradbiomed.2020.03.023 (IF_{2020} =7.376)

Kloska, D.*; **Kopacz, A.*;** Piechota-Polanczyk, A.; Nowak, W.; Dulak, J.; Jozkowicz, A.; Grochot-Przeczek, A. *NRF2 in aging - Focus on the cardiovascular system*. Vascular Pharmacol. 2018, 112:42-53; doi: 10.1016/j.vph.2018.08.009 (IF_{2018} =3.607)

Supplementary information

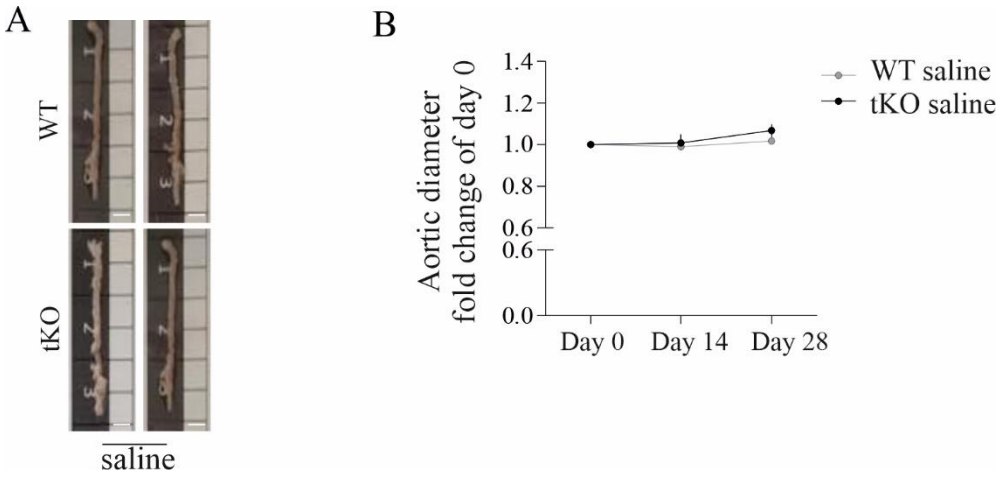

Supp. Fig. 1. Saline infusion does not affect the aortic morphology and diameter. (A) Representative images of the aortas. **(B)** Aortic diameter changes depicted by ultrasound; n=10; 6-month-old mice.

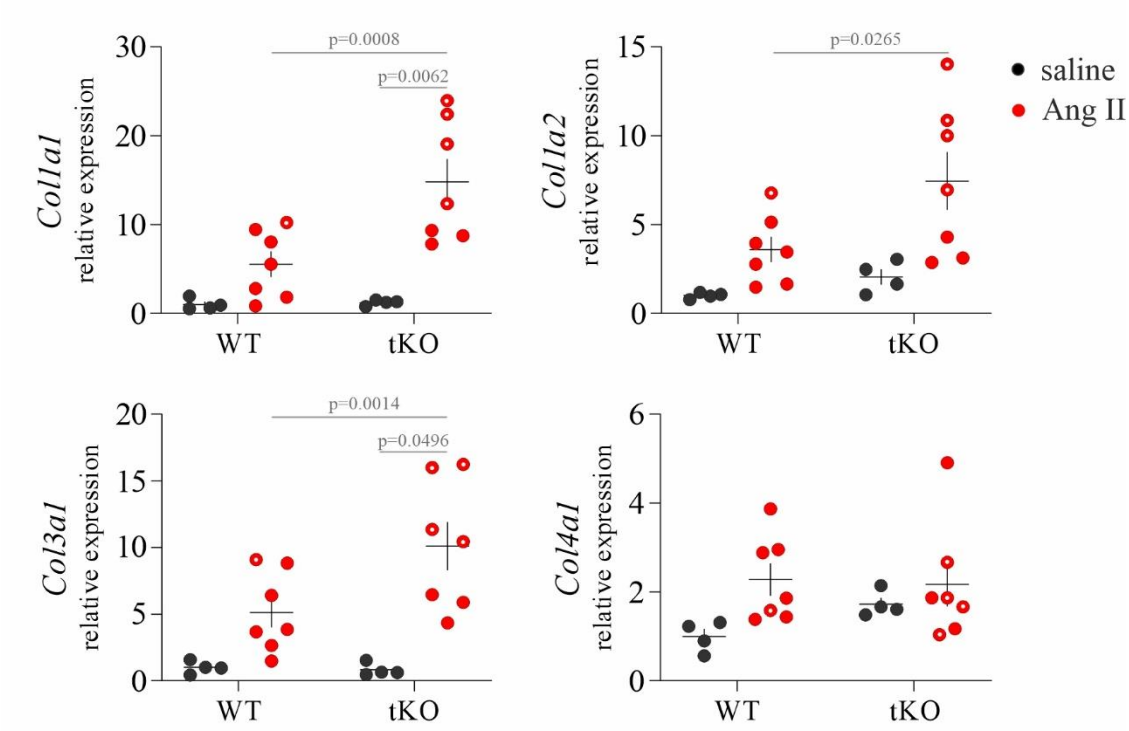

Supp. Fig. 2. Relative expression of *COL1A1*, *COL1A2*, *COL3A1* and *COL4A1* in the aortic wall. *Eef2* was used as a reference gene, open circles – mice with AAA; n=4-7; 6-month-old mice.

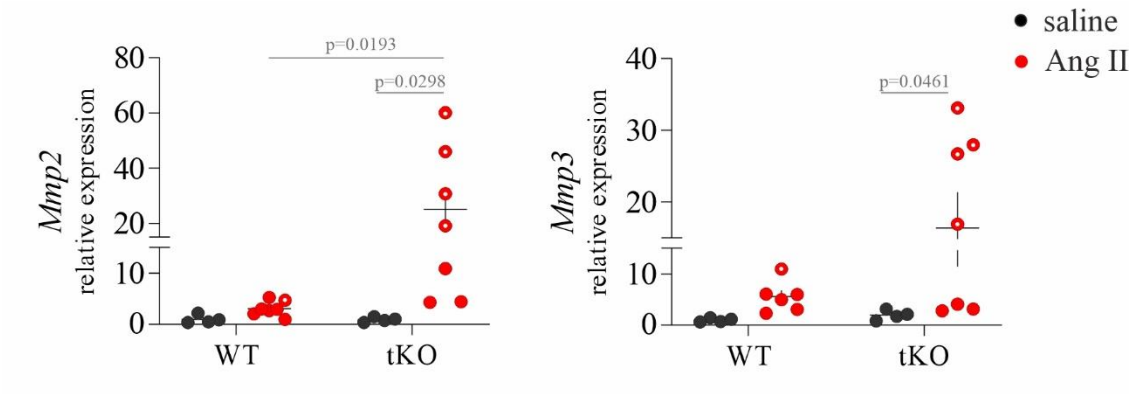

Supp. Fig. 3. Relative expression of *MMP2* and *MMP3* in the aortic wall. *Eef2* was used as a reference gene, open circles – mice with AAA; n=4-7; 6-month-old mice.

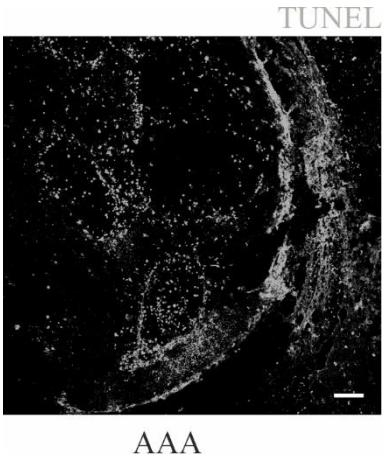

Supp. Fig. 4. Positive control for TUNEL staining (aneurysmal tissue). Scale bar=50 μm.

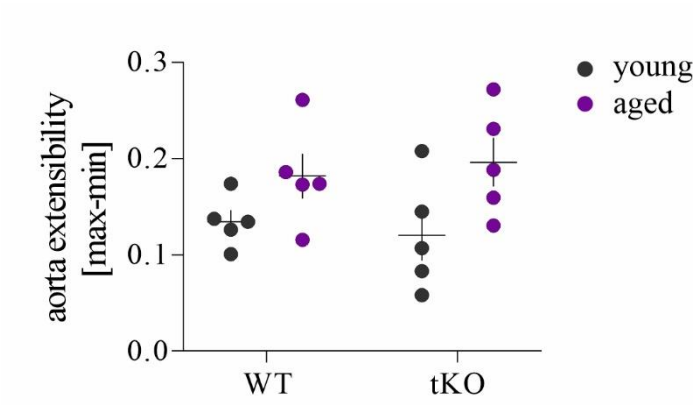

Supp. Fig. 5. The aorta extensibility assessed by *in vivo* ultrasound. n=5; 2-3-(young) and 12-month-old mice (aged).

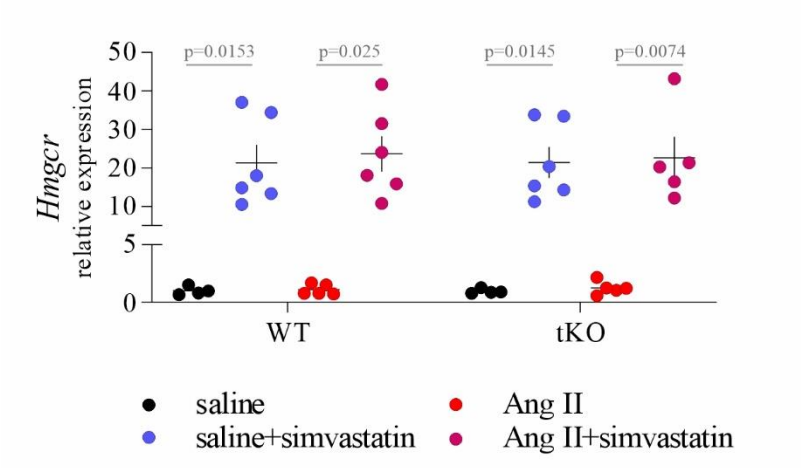

Supp. Fig. 6. Relative expression of *HMGCR* in the liver. The increase in its expression confirms the efficient action of simvastatin. *Eef2* was used as a reference gene; n=4-6; 6-month-old mice.

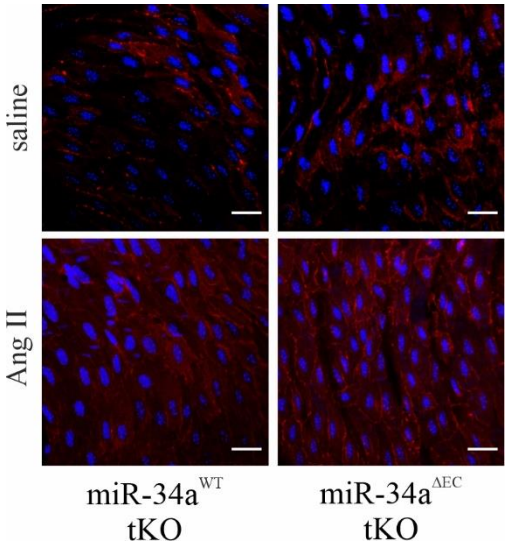

Supp. Fig. 7. MiRNA-34a deficiency in endothelial cells triggers pronounced proliferation of intimal cells, representative images. Scale bar=50 μm; n=10; 3-month-old mice.

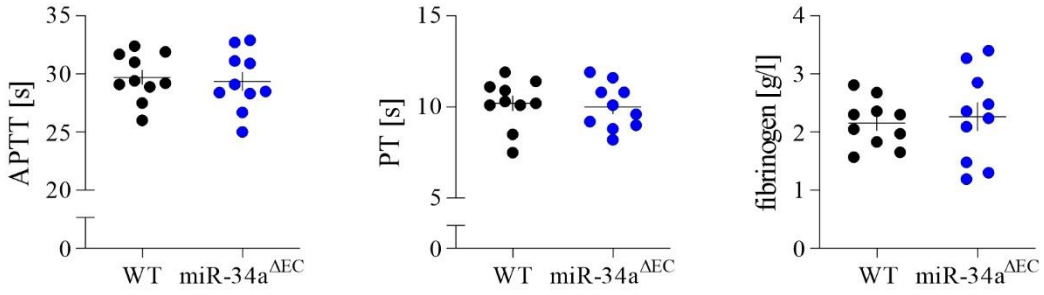

Supp. Fig. 8. The deletion of miRNA-34a does not affect the platelet coagulation features. Activated partial thromboplastin time (aPTT), prothrombin time (PT) and fibrinogen level, n=10; 3-month-old mice.

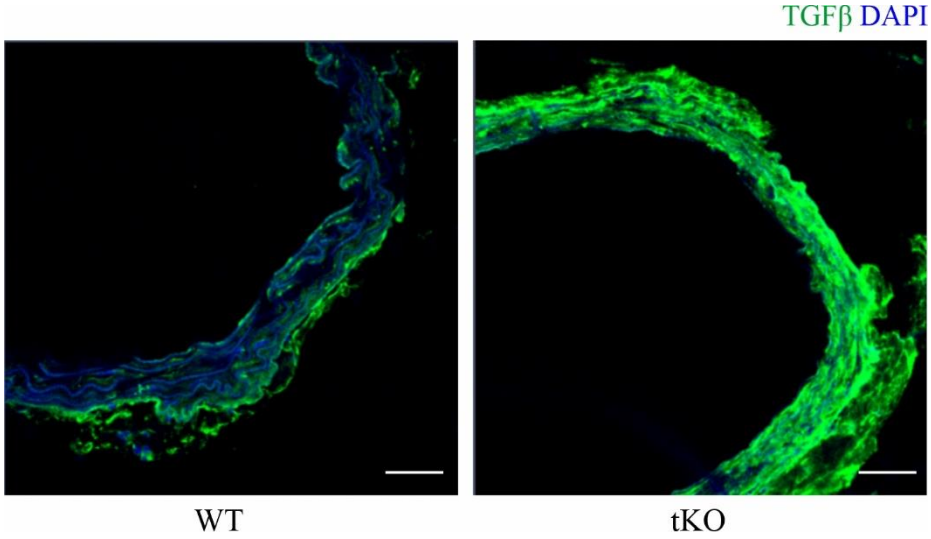

Supp. Fig. 9. NRF2 transcriptional deficiency leads to the enhanced level of TGFβ. Scale bar = 50 μm; n=6; 12-month-old mice.

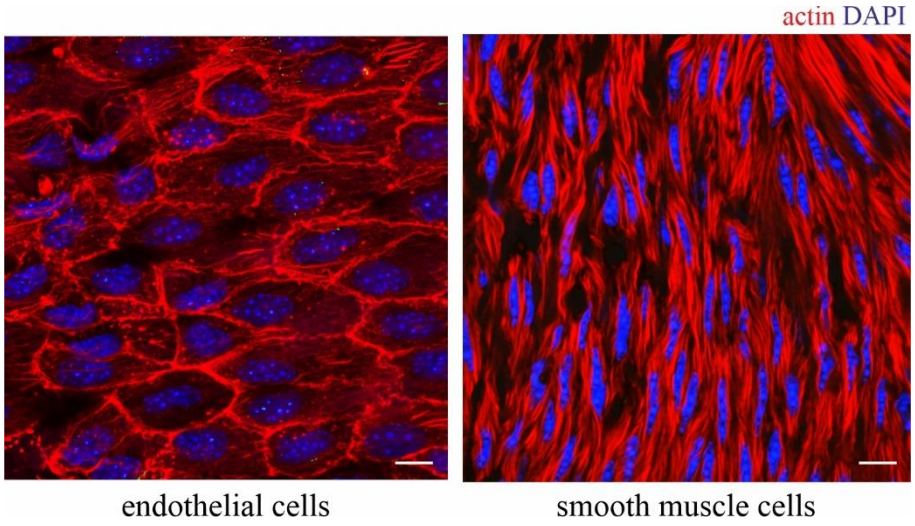

Supp. Fig. 10. Aortic smooth muscle cells have a more abundant actin cytoskeleton than endothelial cells. Scale bar = 10 μm; n=5; 2-3-month-old mice.

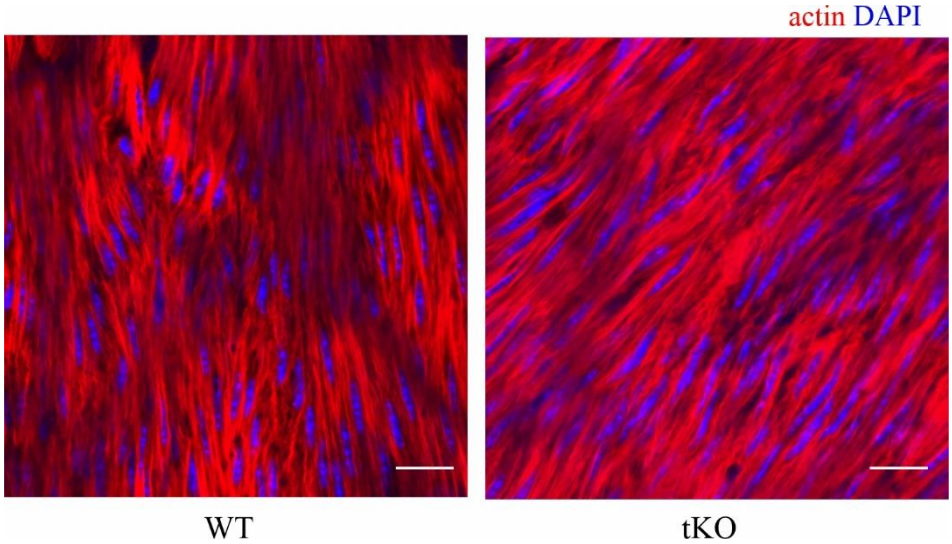

Supp. Fig. 11. NRF2 transcriptional deficiency does not affect the actin cytoskeleton in SMCs. Scale bar = 10 μm; n=5; 2-3-month-old mice.

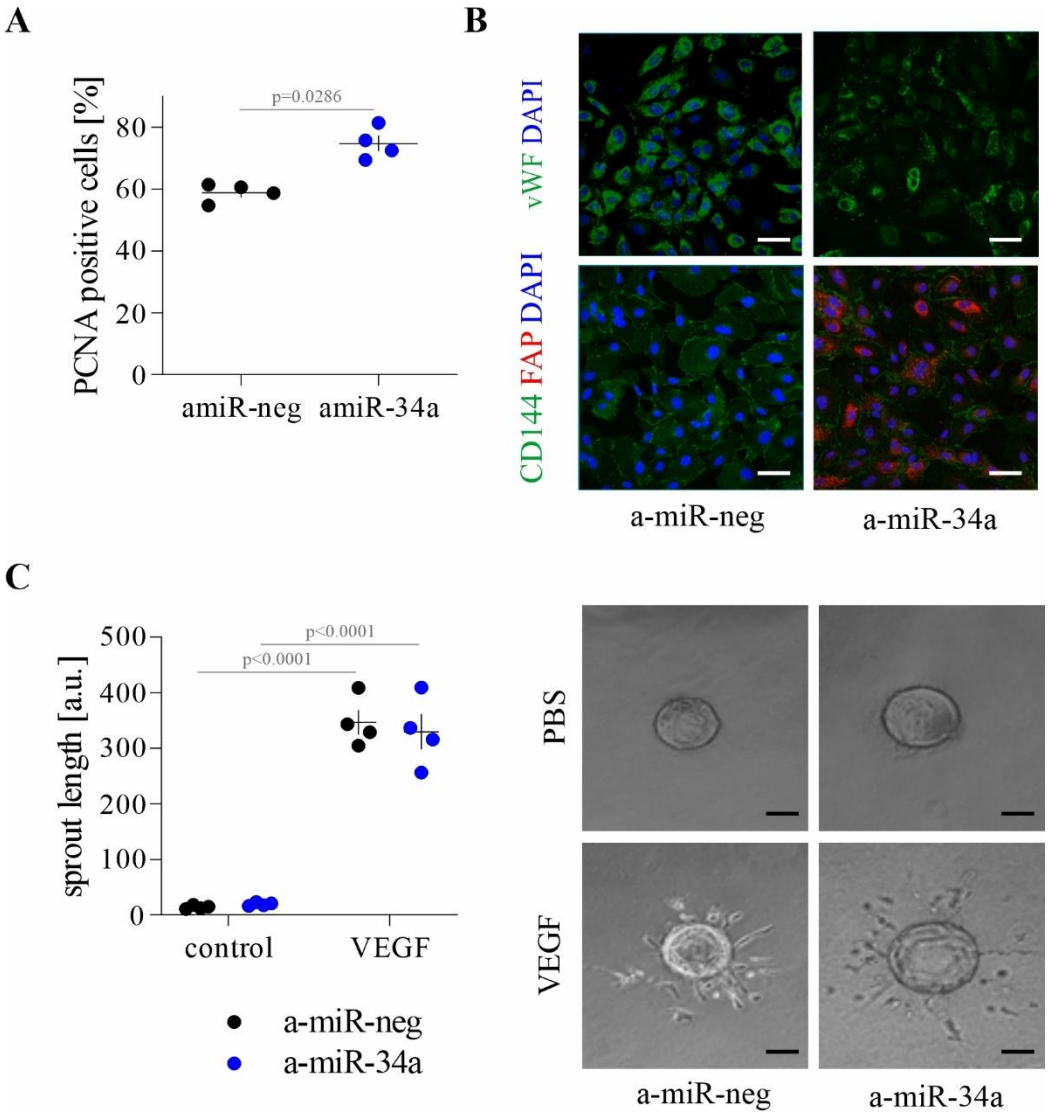

Supp. Fig. 12. The inhibition of miRNA-34a in HAECs enhances their proliferation, however, they lose the endothelial markers. Still, the VEGF-induced angiogenic function is preserved. (A) HAEC proliferation assessed by PCNA proliferative marker staining. **(B)** Immunofluorescent staining of endothelial cells marker (von Willebrand Factor, vWF, green) and mesenchymal (fibroblast activated protein, FAP, red). Nuclei were counterstained with DAPI (blue). **(C)** 3D angiogenesis in fibrin gel upon VEGF-stimulation, quantification, and representative images. n=4

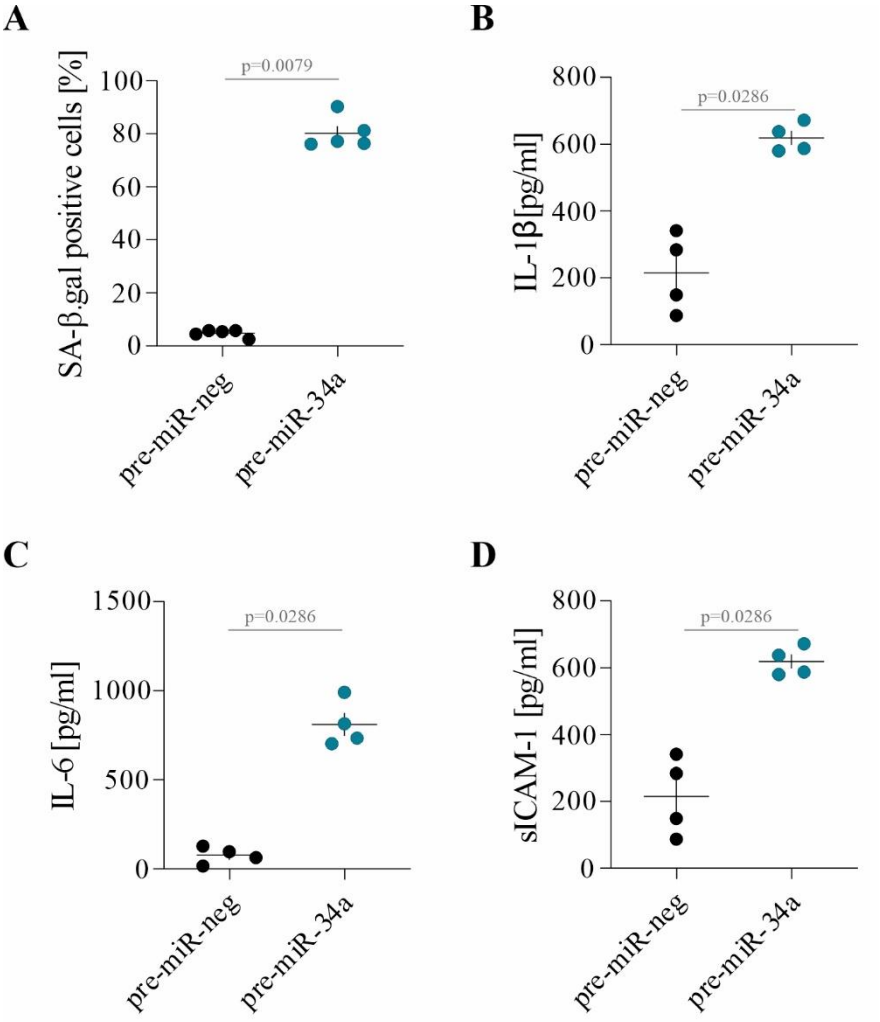

Supp. Fig. 13. Exogenous delivery of miRNA-34a triggers premature senescence of HAECs, with a concomitant increase in SASP factors. **(A)** Level of senescence in HAECs upon miRNA-34a mimic transfection, assessed by SA-β-galactosidase staining; **(B-D)** Level of IL-6, IL-1β and soluble ICAM-1 (sICAM-1) in the conditioned medium assessed by ELISA.

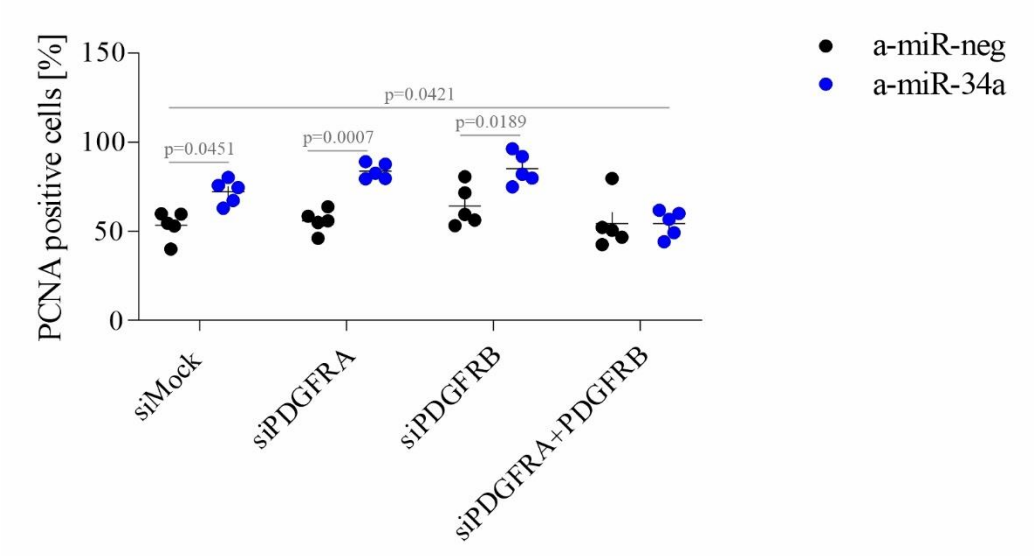

Supp. Fig. 14. The inhibition of both PDGF receptors abrogates miRNA-deficiency associated enhancement of proliferation. HAEC proliferation assessed by PCNA proliferative marker staining, n=5.

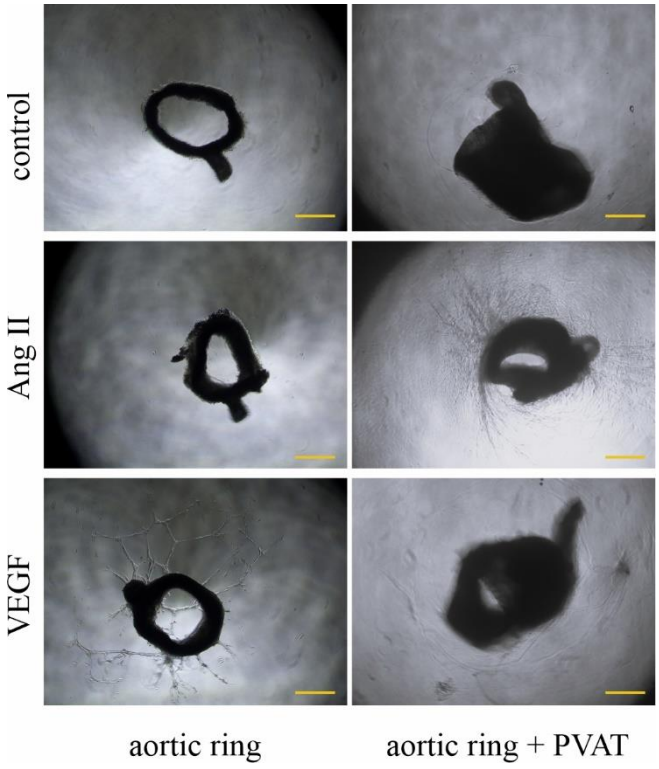

Supp. Fig. 15. The perivascular fat ECs, not the intimal ECs, respond to Ang II. Fibrin gel angiogenic assay from aortic rings (intima+media+adventitia) or together with perivascular fat stimulated with Ang II or VEGF; scale bar=1 mm; n=5.